



HAL
open science

Modélisation du transfert de charge dans les piles à combustible

Giuseppe Mangiatordi

► **To cite this version:**

Giuseppe Mangiatordi. Modélisation du transfert de charge dans les piles à combustible. Theoretical and/or physical chemistry. Université Pierre et Marie Curie - Paris VI, 2012. English. NNT : 2012PAO66526 . tel-00833250

HAL Id: tel-00833250

<https://theses.hal.science/tel-00833250>

Submitted on 12 Jun 2013

HAL is a multi-disciplinary open access archive for the deposit and dissemination of scientific research documents, whether they are published or not. The documents may come from teaching and research institutions in France or abroad, or from public or private research centers.

L'archive ouverte pluridisciplinaire **HAL**, est destinée au dépôt et à la diffusion de documents scientifiques de niveau recherche, publiés ou non, émanant des établissements d'enseignement et de recherche français ou étrangers, des laboratoires publics ou privés.

THÈSE DE DOCTORAT DE L'UNIVERSITÉ PIERRE ET MARIE CURIE

Présentée le 10 décembre 2012 par

Giuseppe Mangiatordi

Pour obtenir le grade de

DOCTEUR de l'UNIVERSITÉ PIERRE ET MARIE CURIE

École Doctorale Chimie Physique et Analytique de Paris VI
Spécialité Chimie Informatique et Théorique

**Modélisation du transfert de charge dans les piles à
combustible**

devant le jury composé de :

M. Nicolas Ferré	Rapporteur
M. Thomas Heine	Rapporteur
M. Esmail Alikhani	Examineur
M. Damien Laage	Examineur
Mme Emilia Sicilia	Examineur
M. Carlo Adamo	Directeur de thèse



*"More than machinery we need humanity;
more than cleverness we need kindness and gentleness.
Without these qualities, life will be violent and all will be lost."
Charlie Chaplin*

Remerciements

Tout d'abord, je tiens à remercier mon directeur de thèse M. Carlo Adamo qui m'a donné la possibilité de travailler dans son groupe de *Modélisation des Systèmes Complexes*. Il a eu confiance en mes capacités et il m'a permis de grandir beaucoup pendant ces années en me permettant de travailler de façon autonome.

Je remercie les rapporteurs M. Nicolas Ferré et M. Thomas Heine ainsi que les examinateurs M. Esmail Alikhani, M. Damien Laage et Mme. Emilia Sicilia pour avoir accepté de faire partie de mon jury.

Je vais garder un précieux souvenir de tous ces années et je vais me rappeler surtout des personnes que j'ai eu la grande chance de rencontrer à partir de tous ceux avec qui j'ai partagé la vie du laboratoire, établissement, souvent, une relation au-delà du domaine professionnel. Des remerciements particuliers vont à Ilaria et à Fred, pour leur disponibilité et leurs précieux conseils.

Je remercie vivement Valentina, non seulement pour notre amitié précieuse, mais aussi pour le soutien qu'elle m'a donné surtout dans la première partie de cette expérience. Je ne sais pas comment j'aurais pu affronter tous les problèmes initiaux sans son aide.

Je remercie aussi: Mario and son Renault Magnum 500CV, Giuseppe et ses *ammantint fort*, Felix, Alessandro, Angela, Valeria, Violena, Simonetta, Pietro, Massimiliano, Daniele, Viviane et Marion avec qui j'ai partagé de nombreux moments pendant ces trois dernières années.

Enfin, les remerciements les plus importants: à mes parents et à ma sœur, parce qu'ils n'ont jamais cessé de soutenir mes choix malgré les nombreux kilomètres qui nous séparent; et à Pia qui est tout simplement la meilleure chose qui me soit jamais arrivée.

Acknowledgments

First, I would like to thank my supervisor Prof. Carlo Adamo who has given me the opportunity to work in his group *Modélisation des Systèmes Complexes*. He has believed in my abilities and he has permitted me to grow during these years by allowing me to work independently.

I would also like to thank the *rapporteurs* Nicolas Ferré and Thomas Heine as well as the *examineurs* Esmail Alikhani, Damien Laage and Emilia Sicilia for agreeing to be a part of my thesis committee.

I will remember with pleasure these years especially because of the people I have had the great fortune to meet, including all with whom I shared laboratory life often establishing a relationship beyond the professional field. Special thanks go to Ilaria and Fred, for their availability and their valuable advice.

I deeply thank Valentina, not only for our precious friendship, but also for the support she gave me in the first part of this experience. I do not know how I could have faced all the teething problems without her help.

I also want to thank: Mario and his Renault Magnum 500CV, Giuseppe and his *ammantint fort*, Felix, Alessandro, Angela, Valeria, Violena, Simonetta, Pietro, Massimiliano, Daniele, Viviane and Marion with whom I shared many moments worth remembering during these last three years.

Finally, the most important thanks: to my parents and my sister, because they never stopped supporting my choices despite those which put distance between us; and to Pia, simply the best thing that ever happened to me.

Ringraziamenti

Un primo doveroso ringraziamento va al mio direttore di tesi, Prof. Carlo Adamo che mi ha dato la possibilità di lavorare nel suo gruppo di *Modélisation des Systèmes Complexes*. Ha creduto nelle mie capacità e mi ha permesso di crescere molto in questi anni consentendomi di lavorare autonomamente.

Ringrazio i *rapporteurs* Nicolas Ferré e Thomas Heine e gli *examineurs* Esmail Alikhani, Damien Laage ed Emilia Sicilia per aver accettato di far parte della mia commissione di tesi.

Ricorderò con piacere questi anni soprattutto per le persone che ho avuto la fortuna di incontrare a partire da tutti coloro con cui ho condiviso la vita di laboratorio instaurando, spesso, un rapporto che è andato al di là dell'ambito professionale. Un ringraziamento speciale va ad Ilaria e a Fred per la loro disponibilità e i loro preziosi consigli.

Ringrazio profondamente Valentina non solo per la nostra preziosa amicizia ma anche per il supporto che mi ha dato soprattutto nella prima parte di questa esperienza. Non so come avrei potuto affrontare tutte le difficoltà iniziali senza il suo aiuto.

Ringrazio inoltre: Mario e il suo Renault Magnum 500CV, Giuseppe e i suoi *ammantint fort*, Felix, Alessandro, Angela, Valeria, Violena, Simonetta, Pietro, Massimiliano, Daniele, Viviane e Marion con cui ho condiviso molti dei momenti cui vale la pena ricordare durante questi ultimi tre anni.

Infine i ringraziamenti più importanti: ai miei genitori e a mia sorella, per non aver mai smesso di sostenere le mie scelte nonostante queste portassero alla mia lontananza da loro; e a Pia, semplicemente ciò che di più bello mi sia mai capitato.

CHAPTER I: BACKGROUND AND OBJECTIVES.....	1
1. The Hydrogen Economy.....	1
1.1. Hydrogen production.....	2
1.2. Hydrogen storage	4
1.3. Hydrogen use.....	5
2. Fuel cells: working principle	5
2.1. High temperature fuel cells	7
SOFC.....	7
MCFC	9
2.2. An example of low temperature fuel cell: the proton exchange membrane fuel cell (PEMFC) 10	
Working principle and applications.....	10
Reducing catalyst poisoning.....	13
Increasing the catalyst activity	13
Increasing operative temperature	13
A PEMFC subcategory: DMFC.....	14
2.3. Other low temperature fuel cells	15
AFC	15
PAFC	16
3. The key component of PEMFCs: the Proton Exchange Membrane.....	17
3.1. Mechanisms of proton transport in PEMs	17
3.2. Other desired properties of the membrane	18
3.3. The PEM state of the art: Nafion	19
Limitations	21
3.4. Alternatives PEMs for high temperature PEMFCs	22
3.5. Azoles and azole-based polymers as proton conductors.....	23
Azoles as liquid solvents.....	23
Azole-based polymers as anhydrous proton conductors	24
4. Objectives	26
5. References.....	29
CHAPTER II: THEORETICAL BACKGROUND	41
1. Quantum Mechanics (QM)	41
1.1. The Schrödinger equation.....	41
1.2. The Born-Oppenheimer approximation	42
1.3. Molecular orbital (MO) approximation and basis functions	42
1.4. The Hartree-Fock Theory.....	44
The Hartree-Fock Equations.....	44
1.5. The correlation energy.....	46
1.6. The Møller-Plesset (MP) perturbation theory	47

1.7.	The Coupled-Cluster (CC) theory	49
1.8.	The Density Functional Theory	50
	The Hohenberg-Kohn theorems	51
	The Kohn-Sham method	52
	Exchange-correlation Functionals	53
1.9.	Statistical thermodynamics and partition function.....	55
	Electronic partition function	56
	Translational partition function	56
	Rotational partition function.....	56
	Vibrational partition function.....	57
2.	Molecular Mechanics (MM)	57
2.1.	Force Field.....	58
2.2.	Molecular Dynamic simulations	60
	Basic principle	60
	The Verlet integration algorithm.....	61
	Choosing the time step	62
	The thermodynamic ensembles.....	62
	Molecular Dynamics at constant temperature.....	63
2.3.	Free energy calculations: the umbrella sampling technique.....	63
3.	References	66
CHAPTER III: DFT STUDY OF PROTON TRANSFER REACTIONS		71
1.	Modeling proton transfer in imidazole-like dimers.....	71
1.1.	Introduction	71
1.2.	Methodological details.....	72
1.3.	Identification of the PT reaction mechanisms	73
1.4.	Basis Set selection.....	74
1.5.	The reference energy values.....	76
1.6.	PT in imidazolium-imidazole complex.....	77
1.7.	PT in 1,2,3-triazolium-1,2,3-triazole complex	79
1.8.	PT in tetrazolium-tetrazole complex	80
1.9.	Comments	84
1.10.	The BMK/B3LYP model	87
2.	PT reactions: a benchmark study.....	88
2.1.	Introduction	88
2.2.	Methodological details.....	88
2.3.	Results and discussion.....	90
	Proton transfer barriers at given structure.....	91
	Standard energy barrier evaluations on the DBH24/08 database	92

Optimized structures: PT barriers & H-bond structural parameters	93
Comments	94
3. Conclusions	96
4. References	97
CHAPTER IV: STUDY OF PROTON TRANSPORT IN P4VI	105
1. Introduction	105
1.1. Poly-(4-vinyl-imidazole).....	105
1.2. The Brédas mechanism	106
2. Methodological details.....	108
3. Results and discussion.....	108
3.1. Conduction mechanism in small models: DFT investigation	108
Protonated dimers.....	108
Protonated trimer	111
3.2. Conduction mechanism in large models: molecular dynamics simulations.....	113
Force field parametrization	113
Analysis of the trajectory	114
3.3. A new charge-transport mechanism.....	119
3.4. Support from experimental evidences	123
3.5. Charges and electrostatic potential: support to the MD simulation quality.....	124
4. Conclusions	125
5. References	126
CHAPTER V: PROTON CONDUCTION OF H₃PO₄-DOPED P4VI.....	131
1. Introduction.....	131
2. Results and discussion.....	132
2.1. Identification of a Gotthuss chain in the starting complex.....	133
2.2. Proton transfer reactions in the protonated model	134
2.3. Investigation of the rate-limiting step.....	136
2.4. Comments	138
3. Conclusions	140
4. References	141
CHAPTER VI: PROTON TRANSPORT IN 2-TETHERED SYSTEMS.....	145
1. Introduction.....	145
2. Methodological details.....	147
3. Results and discussion.....	148
3.1. Conduction mechanism in small models: DFT investigation	148
PT in protonated dimers.....	148

Cooperative reorientation in a trimeric model.....	150
3.2. Conduction mechanism in large models: Molecular Dynamics simulations	152
Force Field calibration.....	153
Analysis of trajectory	154
4. Comments and experimental evidences.....	157
5. Conclusions	159
6. References	161
GENERAL CONCLUSIONS.....	163
References.....	168
ANNEXES	171
ANNEX I: Supplementary information for chapter III	172
ANNEX II: Supplementary information for chapter IV	185
ANNEX III: Supplementary information for chapter VI.....	190
Synthèse générale	197
1. Contexte et objectifs.....	197
1.1. Les piles à combustible	197
La membrane d'échange de protons (PEM).....	198
1.2. Les azoles et les polymères à base d'azoles comme conducteurs de protons	199
1.3. Objectifs de la thèse	200
2. Étude DFT des réactions de transfert de proton dans les azoles.....	201
2.1. Le modèle BMK/B3LYP.....	204
3. Une étude de référence de réactions PT.....	205
4. Étude du transport de protons dans P4VI.....	207
4.1. Étude DFT du mécanisme de conduction dans les petits modèles	208
4.2. Étude MD du mécanisme de conduction dans les grands modèles	210
4.3. Un nouveau mécanisme de transport de charge.....	211
5. Conduction protonique des P4VI dopés avec du H₃PO₄.....	212
6. Transport des protons dans les systèmes avec attache en position 2.....	213
6.1. Étude DFT du mécanisme de conduction dans les petits modèles	214
6.2. Étude MD du mécanisme de conduction dans les grands modèles	215
7. Conclusion générale.....	216
8. Références	218
Abstract.....	229
Résumé.....	231

CHAPTER I: BACKGROUND AND OBJECTIVES

This chapter is devoted to the scientific and economic context of this thesis. In the first part, the main aspects related to the increasing use of Hydrogen as energy carrier will be presented. A general overview of the fuel cell technologies will be given in the second section while the last part will be focused on a detailed description of the design issues related to the Proton Exchange Membrane (PEM), key component of the Proton Exchange membrane Fuel Cells (PEMFCs) and object of the present theoretical study.

1. The Hydrogen Economy

Most of the environmental issues such as acid rain, stratospheric ozone depletion and global climate change are related to the production, transformation and use of energy. For instance, the global warming magnitude is strongly dependant on emissions of the so-called greenhouse gases (GHG)¹ such as carbon dioxide, methane and nitrous oxide. Furthermore, it is expected that the increasing of population with the consequent augmented request of food and energy could lead to an even increased dependency of the European Union and the US on oil imports. Notably, according to US Energy Information Administration's International Energy Outlook 2011,² the global market for Energy consumption is estimate to grow almost 55% by 2035 (figure I-1).

In the last years, these aspects have led to an increasing interest in renewable energies. In particular, one of the most promising alternatives to fossil fuel is Hydrogen. Indeed, Hydrogen energy systems are emerging as the one of the most successful solutions which can play a significant role in providing better sustainability and environment. Importantly, the use of Hydrogen to create the so called *Hydrogen Economy* (a future energy system based on Hydrogen and electricity) only requires technology, not political access. However, although hydrogen atoms are abundant and widely distributed throughout the world, they do not occur in nature as fuel H_2 but in chemical compounds like water or hydrocarbons that must be chemically transformed to produce it. Obviously, the hydrogen production from fossil fuels would deprive the hydrogen economy of much of its "*raison d'être*": it does not reduce the use of fossil fuels but rather shifts them from end use to an earlier production step still releasing carbon to the environment in the form of CO_2 . However, when made from non-fossil resources like water or using other renewable energy sources, Hydrogen is definable a "*forever fuel*" as called by Peter

Hoffman in his book "*Tomorrow's Energy: Hydrogen, Fuel Cells and the Prospects for a Cleanest Planet*".³

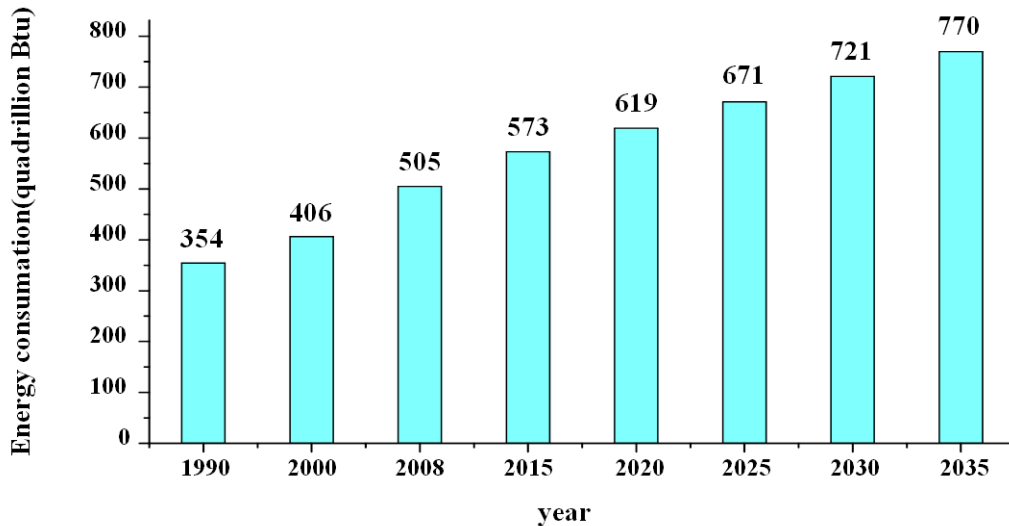


Figure I-1: World marketed energy consumption, history (1990-2008) and projections (2015-2035). All data are in quadrillion Btu (British thermal unit). Source: US Energy Information Administration, International Energy Outlook 2011.

As depicted in the figure I-2, the *Hydrogen economy* relies on a network composed of three functional steps: production, storage and use.⁴ Despite the great effort devoted in the last few years, none of the several technical means used to achieve these steps can yet compete with fossil fuel in performance, cost and reliability. In this context, the possible future conversion of the world economy to the hydrogen will be possible only if a more and more in-depth basic research will be done in the next years.

1.1. Hydrogen production

Molecular hydrogen is an energy carrier but not an energy resource, and therefore it must be produced first. Hydrogen can be produced using different methods. Currently the most widely used concern the electrolysis of water and the steam reforming of methane and other natural gasses.⁵ Biological production of H₂ (biohydrogen) using microorganisms is an area of technology development that offers the potential production of renewable H₂ from biomass.⁶ Nevertheless, at the present about 50% of the global demand for H₂ is produced by steam reforming of natural gas, a process that is not considered sustainable since it leads to emissions of GHG. On the contrary, only a low percentage is made through *green methods*.⁷ Since this limit depends on the low-efficiency and high-cost of the low-emission methodologies, a great effort has been made by both academic and industrial research to increase the rule of the green

hydrogen production. In this context, some examples are represented by recent methodologies such as water electrolysis plus concentrated solar power (CSP), Ocean Thermal Energy Conversion (OTEC) power or wind power.⁸

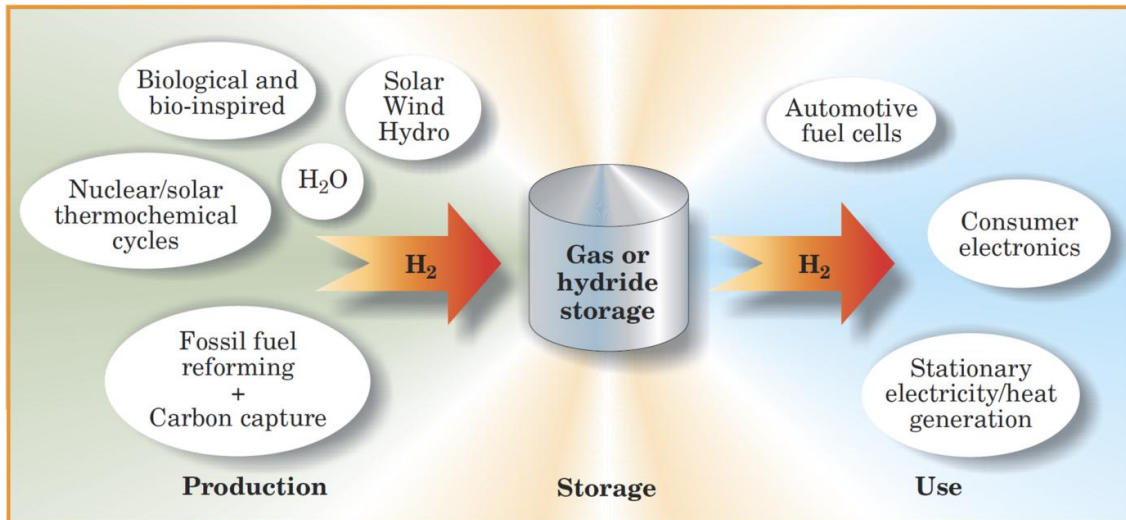
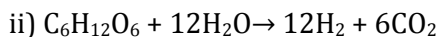
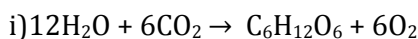


Figure I-2: The Hydrogen Economy as a system of primary energy sources linked to multiple uses (adapted from ⁴).

Despite these efforts, the most promising and fascinating strategy to produce hydrogen seems to reside in biological methods which are able to produce H_2 miming biochemical reactions performed by plants or microorganisms and without any emission of *GHG*. For instance, some green algae convert sunlight into water, hydrogen and oxygen while through microorganisms such as some Cyanobacteria, H_2 is made by two photosynthesis reactions:



Even though these attractive technologies are still far to be competitive due to their high cost, a great progress has been achieved in the last few years. For instance, a molecular biodevice capable to use an enzyme to produce adenosine tri-phosphate (ATP, which is able to produce hydrogen directly from the substrate) through an artificial photosynthetic membrane (Figure I-3) has been developed at the Arizona State University⁹ whereas Levin and Chanine in a recent review¹⁰ evidence the importance of methods mainly based on fermentation, such as photo and dark-fermentations, pointing out that "although biohydrogen technologies are still in their infancy, developing technologies offer potential for practical application".

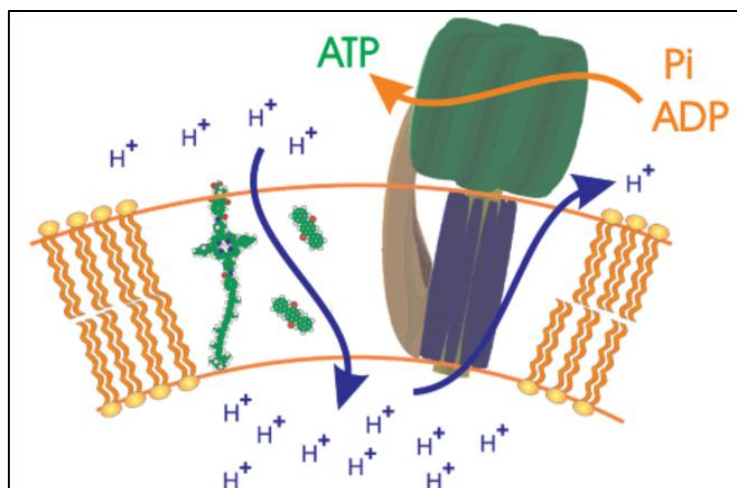


Figure I-3: Schematic representation of an artificial photosynthetic membrane obtained in a liposome vesicle (adapted from⁹).

1.2. Hydrogen storage

Obtaining a safe technology for hydrogen storage at room temperature is nowadays considered one of the major obstacles in the Hydrogen Economy, especially for the development of fuel cells for automobiles. Although different methods of hydrogen storage have been applied in the last years, none of them have completely satisfied the indicated standard of the US Department of energy considering economic as well as environmental parameters.¹¹

Today the available technologies permit directly to store hydrogen through chemical or physical combination with several materials or by modifying its physical state in gaseous (pressurized gas) or liquid (cryogenic liquid). Nevertheless, these last two methods are hindered by the H_2 physico-chemical properties. Indeed, because of the low boiling point (20.28 K) liquid hydrogen requires addition of a refrigeration unit to maintain a cryogenic state, a process which is very expensive. Concerning the storage in gaseous phase, the very low density (0.08988 g/L at 1 atm) makes necessary the use of high-pressures, a process complicated by the weight of the canisters and the possible leaks. For these reasons, a great effort has been done in the last years to develop methods able to store hydrogen through the combination with other materials so that today different methodologies can be used: 1) adsorption on materials with a large specific surface area,¹² 2) adsorption in interstitial sites in a host metal,¹³ 3) bonding in covalent and ionic compounds¹⁴ and 4) oxidation of reactive metals (Zn, Li, Mg, Al, Na) with water.^{15,16} This last method allows for the highest densities of hydrogen and offers a very safe and efficient way to store it. For instance, 6.5 H atoms are stored in each cm^3 of MgH_2 ¹⁶ in spite of 0.99 in hydrogen gas and 4.2 in liquid hydrogen.¹⁷ It is believed that further scientific research and technical developments will lead to new materials with values of hydrogen density close to 300 kg/m^3 which is almost two times the best materials known till date (Mg_2FeH_6 and $Al(BH_4)_3$).

1.3. Hydrogen use

After being produced and properly stored, Hydrogen is ready to be utilized. Notably, it can provide energy in two different ways: i) combustion ii) through fuel cells.^{18,19}

The combustion is mainly used for transport applications. Hydrogen can be, in fact, burned in an internal combustion engine in the same way as non-renewable fuels such as petrol or diesel in order to power vehicles. This process produces water as the main byproduct, but also small amounts of oxides of nitrogen which is an air pollutant.

In contrast, fuel cells are suitable for a wide range of applications going from stationary power generators to laptops and mobile phones. Furthermore they assure higher efficiency with respect to combustion based devices (45% vs 25%¹⁹). This technology is, therefore, considered of choice for a possible future Hydrogen Economy.

2. Fuel cells: working principle

The fuel cells are devices used to produce electricity from different fuels. In spite of their recent development, they represent one of the oldest electrical energy conversion system known to man. Their invention is attributed, indeed, to Sir William Grove, a Professor at the university of Brasle who in 1852 summarized the fuel cell principle in the following famous words: *“Every chemical synthetic action may by a proper disposition of the constituents be made to produce a voltaic current”*.

All fuel cells have the same basic operating principle and their core consists of two electrodes and one electrolyte. At the negative anode the fuel is oxidized while at the positive cathode the oxygen is reduced and ions are transported from one side to the other through the electrolyte (Figure I-4). In other words, a fuel cell operates as a galvanic cell in which the free energy of a chemical reaction is converted into electrical energy. Notably, if we consider n electrons involved in the reaction, the Gibbs free energy change is related to the cell voltage via:

$$\Delta G = -nF\Delta U_o \quad (I-1)$$

where F is the Faraday constant and ΔU_o is the voltage of the cell for thermodynamic equilibrium in the absence of a current flow.

The electrochemical reactions occurring in a fuel cell (oxidation at the anode and reduction at the cathode) would occur very slowly in absence of a catalyst which is therefore critical to ensure the correct operation of these devices.²⁰ Such a catalyst, which covers each of the electrodes, is usually made of platinum powder very thinly coated onto carbon paper or cloth. Furthermore, in order to have the maximum surface area of the platinum exposed to the hydrogen or oxygen, the catalyst is porous and rough.²¹ However, the efficiency of a catalyst in a fuel cell can be strongly affected by the low degree of purity of the fuel.²² This can arise some

problems especially when the fuel is hydrogen since high levels of purity are obtained only after very expensive and difficult processes.

The key component of a fuel cell is the electrolyte which determines the temperature window of operation. Consequently fuel cells are named after their electrolyte material and are commonly classified into two main groups depending on the temperature operation:

- Low-temperature fuel cells operating at temperatures $< 250^{\circ}\text{C}$ such as alkaline (AFCs), polymer electrolyte membrane (PEMFCs) and phosphoric acid (PAFCs) fuel cells.
- High-temperature fuel cells operating at $> 500^{\circ}\text{C}$ such as solid oxide (SOFCs) and molten carbonate (MCFCs).

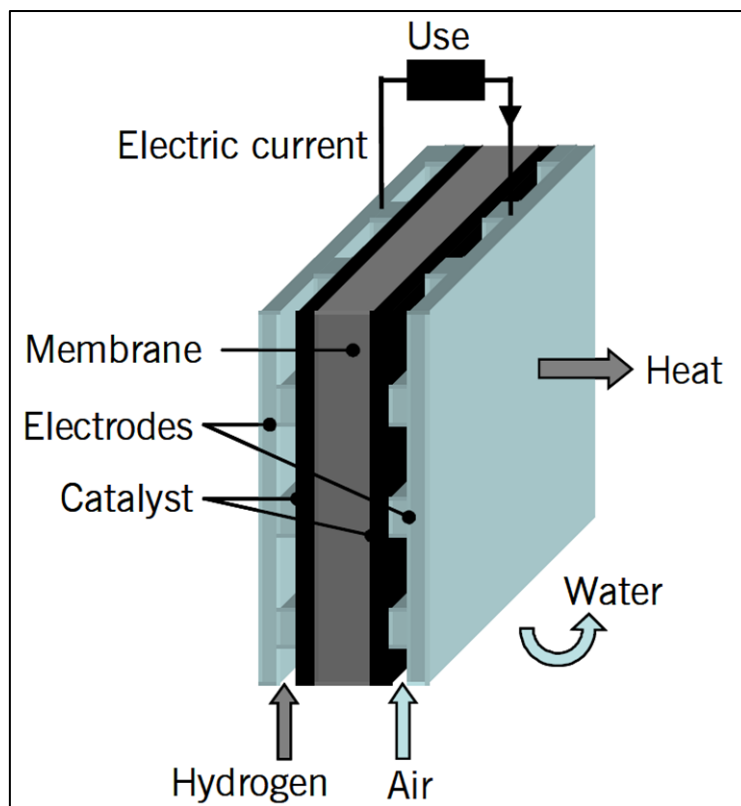


Figure I-4: Working principle of a generic fuel cell (the solid electrolyte is here represented by a membrane).

As shown in table I-1, all fuel cells operate through reactions in which ion species migrate through the electrolyte membrane: protons (H^+) in PEMFC and PAFC, hydroxyl ions (OH^-) in AFC, oxide ions (O^{2-}) in SOFC and carbonate ions (CO_3^{2-}) in MCFC.

The growing interest of the last few years in these devices has been due to their capacity to convert Hydrogen in electricity without any GHG emission and producing only water as by-product. Nevertheless, after more than 150 years from their invention, a strong technical progress able to reduce the cost is still necessary for a large scale commercialization which can

be optimistically obtained in the near future. Obviously, the high cost can be reduced only if substantial investments and strong research effort in fuel cell development will be made in the next years.

Table I-1: Electrolyte, operative temperature and transferred ion for each of the different types of fuel cells (Adapted from²³).

fuel cell	electrolyte	operative temperature, °C	transferred ions
PEMFC	polymer membrane	70-110	H ⁺
PAFC	phosphoric acid	150-250	H ⁺
AFC	alkaline	100-250	OH ⁻
SOFC	solid oxide	700-1000	O ²⁻
MCFC	molten carbonate	500-700	CO ₃ ²⁻

The different suitability for particular applications depends on different characteristics mainly due to the operative temperatures. PEMFC and PAFC are well matched to transport and mobile applications thanks to the fast start-up, whereas high-temperatures fuel cells are better suited as stationary power generators because of the longer time to arrive at operating temperature. A brief overview of the different fuel cells technologies will be given in the following with particular attention devoted to advantages and disadvantages relative to each other as well as on their different suitability.

2.1. High temperature fuel cells

SOFC

The solid oxide fuel cells (SOFCs) are the oldest devices of the family. The solid oxide electrolyte, basic component from which they were conceived, was discovered in 1899 by Nernst who reported the different conductivity between pure metal oxides (very low even at high temperatures) and the mixtures of metal oxides which can possess dramatically higher conductivity.²⁴ Notably, he pointed out the coherence of these results with the behavior of liquid electrolyte where the conductivities of aqueous salt solutions are much higher than pure water and pure common salt. Mixed oxides which exhibit high conductivity at elevated temperatures were therefore identified including the composition 85% zirconium oxide and 15% yttrium oxide, particularly favorable as patented by Nernst himself. Only six years later the first patent on fuel cells with a solid electrolyte (using porcelain and glass) was filed by Haber.²⁵

In the following years, the development of SOFC was significantly hampered by serious materials problems especially related to the high operating temperature and to the reducing nature of the fuel gas. A renewed interest in this technology is evident only after 1960 due to various factors such as the progress in preparation and production of ceramic materials and the general interest in fuel cell technology as "environmental friendly".

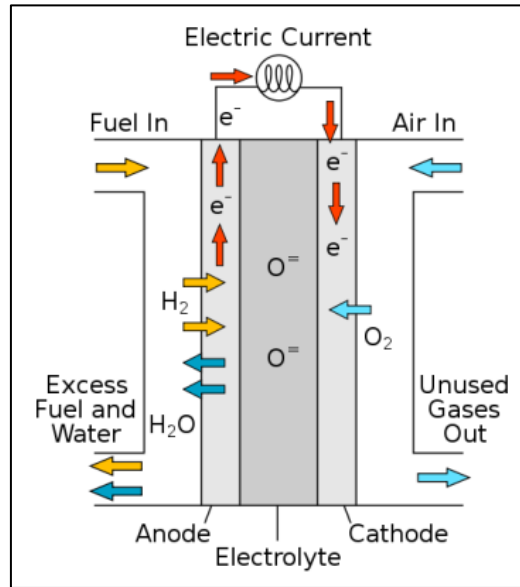


Figure I-5: Concept diagram of SOFC (adapted from²⁶).

SOFC are also the only fuel cell in which the charge transport in the electrolyte involves negatively oxygen ions (O²⁻) (Figure I-5). Notably, in the case of pure H₂ as fuel, the chemical reactions occurring during the operation are the following:

- i) Anode reaction: $2\text{H}_2 + 2\text{O}^{2-} \rightarrow 2\text{H}_2\text{O} + 4\text{e}^-$
- ii) Cathode reaction: $\text{O}_2 + 4\text{e}^- \rightarrow 2\text{O}^{2-}$
- iii) Overall cell reaction: $2\text{H}_2 + \text{O}_2 \rightarrow 2\text{H}_2\text{O}$

At the cathode the oxygen gas reacts with electrons to create oxygen ions which then cross the electrolyte to react with hydrogen gas at the anode where electricity and water is produced. It is worth to underline that also carbon dioxide (CO₂) can be a product of SOFC for instance using hydrocarbons which are converted into carbon monoxide (CO) and hydrogen (H₂) at the anode. In this case the reactions can be expressed as in the following:

- i) Anode reaction: $\text{CO} + \text{H}_2 + 2\text{O}^{2-} \rightarrow \text{CO}_2 + \text{H}_2\text{O} + 4\text{e}^-$
- ii) Cathode reaction: $\text{O}_2 + 4\text{e}^- \rightarrow 2\text{O}^{2-}$
- iii) Overall cell reaction: $\text{H}_2 + \text{CO} + \text{O}_2 \rightarrow \text{H}_2\text{O} + \text{CO}_2$

Nevertheless, the carbon emissions from an SOFC system are less than those from a fossil fuel combustion.²⁷

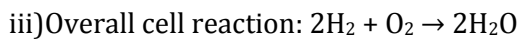
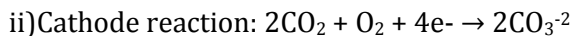
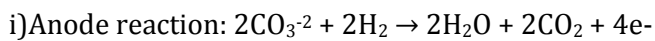
Concerning the technological aspects of this device, the peculiarity is represented by the high temperatures used (conventionally between 700-1000°C) which leads to several effects. For instance, in case of using hydrocarbon fuel, thanks to the high temperatures, an internal reforming of the fuel is possible so that the hydrocarbon is catalytically converted to carbon monoxide and hydrogen within SOFC. This reduces the costs and the complexity of the system. The tolerance to carbon monoxide and in general to impurities represent another advantage of SOFC which markedly contrasts with other types of fuel cells like PEMFC which for instance requires expensive and complex systems to contrast the CO poisoning (for a short discussion on that see section 3.3).

Despite these advantages, since high temperatures are necessary, SOFCs are not suitable for a large range of applications where a rapid start up and cool down is essential such as mobile devices and transportation. In contrast, they represent the most suitable fuel cells for applications in the distributed generation market (stationary power) because of their high conversion efficiency.^{28,29}

MCFC

Like SOFCs, the molten carbonate fuel cells (MOFCs) are high-temperature fuel cells, with an operative temperature of about 600°C. In such devices the electrolyte is a molten lithium potassium carbonate salt suspended in a ceramic matrix of beta-alumina solid (*BASE*) which is porous and chemically inert. Figure I-6 illustrates the working principle of a MOFC.

The molten state of the electrolyte allows for the movement of the negative carbonate ions within the cell. Notably, the chemical reactions occurring during the operation are the following:



The hydrogen fuel reacts with the carbonate ions available in the electrolyte to give carbon dioxide, water and electrons while the reduction happening at the cathode produce new carbonate ions which are then transferred to the anode. As in SOFCs, since the high operating temperature dramatically improves reaction kinetics, a non-expensive catalyst can be used. The elevated operative temperature also makes the cell less prone to carbon monoxide poisoning than other fuel cells systems and prevent the need for an external reformer. One disadvantage associated with MCFCs concerns the necessity to inject carbon dioxide at the cathode as carbonate ions are consumed in reactions occurring at the anode. Furthermore, the presence of carbonate ions together with the high temperatures lead to a fast corrosion at the MCFC components and to a consequent very short cell life, considered one of the mayor limits of these devices.³⁰ Regarding the applications, like SOFCs, MCFCs are used in large stationary power

generation whereas they are not suitable for mobile applications because of the high operative temperature.²⁹

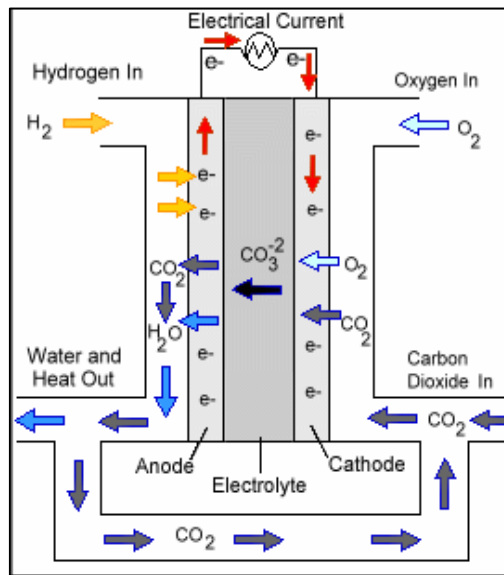


Figure I-6: Concept diagram of MOFC (adapted from²⁶).

2.2. An example of low temperature fuel cell: the proton exchange membrane fuel cell (PEMFC)

Working principle and applications

The distinguish features of a PEMFC are the use of a polymer membrane (PEM) as electrolyte and the low operative temperature range (50-100°C). The occurring reactions can be expressed as in the following:

- i) Anode reaction: $2\text{H}_2 \rightarrow 4\text{H}^+ + 4\text{e}^-$
- ii) Cathode reaction: $\text{O}_2 + 4\text{H}^+ + 4\text{e}^- \rightarrow 2\text{H}_2\text{O}$
- iii) Overall reaction: $2\text{H}_2 + \text{O}_2 \rightarrow 2\text{H}_2\text{O}$

The Hydrogen is activated by a catalyst to form electrons and protons. These last are the charge carriers of the system: they permeate through the polymer membrane from the anode to the cathode side. Here they react with the liberated stream of oxygen and the electrons arriving through the external circuit to give water as product (figure I-7)

Basically the PEMFC is comprised of (i) electrode-bipolar plates (ii) catalyst and (iii) PEM (figure I-8). The electrode-bipolar plates act as anode for one cell and as cathode for the adjacent cell and can be made by different materials such as metal, graphite, carbon-polymer composites and others.³¹ Moreover they usually incorporate flow channels for the fluids feeds. The core of the system is represented by the so called membrane electrolyte assembly (MEA) which consist of the proton conducting membrane between two carbon papers coated with the

catalyst. Thanks to the presence of a immobilized electrolyte these devices are shock and vibration tolerant. This feature together with the fast startup and the instantaneous response to changes in demand for power make them the most promising type of fuel cell for transportation and mobile applications.³²

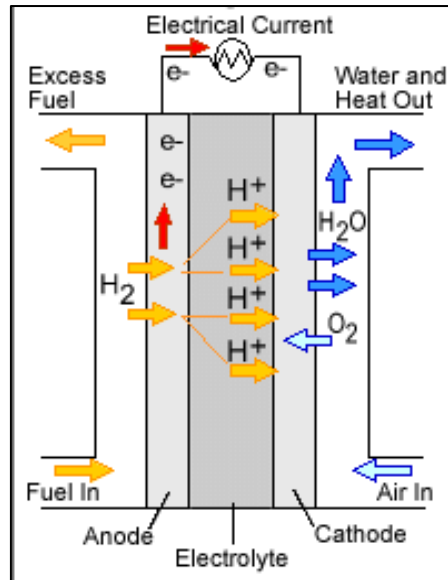


Figure I-7: Concept diagram of PEMFCs (adapted from²⁶)

Nowadays most of the motor companies using fuel cells technology use solely PEMFC. Notably, automakers such as General Motors (GM), Hyundai, Honda, Daimler and Toyota, have proclaimed plans for commercializing their PEMFC vehicles by 2015.³⁴ Figure I-9 shows some prototypes using PEMFC technology. Considering the fast-growing energy demand of the modern portable electric devices such as laptops or cell phones as well as the limited energy capacity of the current batteries, another promising area for PEMFCs is the portable electronics. Major electronics companies, such as Toshiba, Sony, Motorola, LG, and Samsung, have set up research units for portable fuel cells. The main advantage in this field concerns the ability of PEMFCs to provide continuous power as long as hydrogen fuel efficiency loss.³²

Despite these efforts, barriers to their world-wide commercialization still exist mainly because of the low durability and the high cost.³⁴ Further scientific breakthroughs in the field are therefore required mainly in material development and in improved understanding of PEMFC operation principles. Much of the current research topics in PEMFCs can be classified following few objectives:

- reducing the poisoning of the catalyst by impurities gas.
- obtaining materials with higher catalyst activity than the standard platinum particle catalyst.

- obtaining high temperature PEMFCs (HT-PEMFCs).

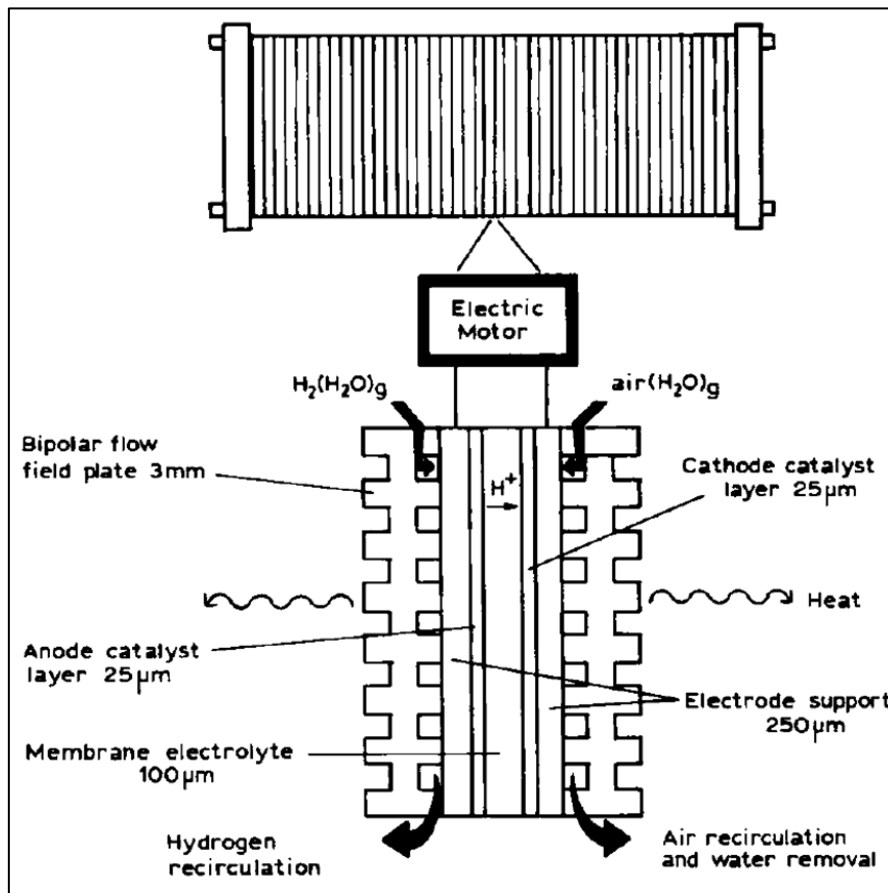


Figure I-8: The PEMFC components (adapted from³³)

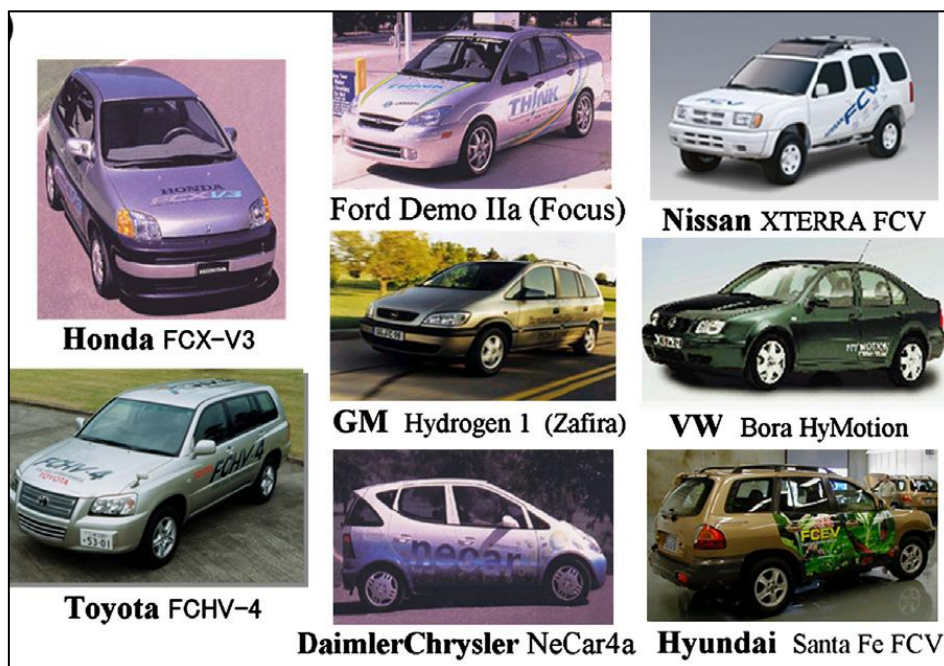


Figure I-9: Fuel cell vehicles by various automakers (adapted from³²)

Reducing catalyst poisoning

As above mentioned, the hydrogen gas is produced mainly using steam reforming light hydrocarbons. This makes a mixture which also contains CO (1–3%), CO₂ (19–25%), and N₂ (25%)³⁵. Since they combine both activity and stability in the fuel cell environment, Platinum-based electrocatalysts are still the only used catalyst materials. Nevertheless, the sensitivity of the platinum to the impurities (especially to carbon monoxide) strongly reduce the catalyst performance during the operation.³⁶ Therefore, reduction of the concentration of CO in the fuel and development of CO-tolerant electrocatalysts are considered among the most important factors to improve the performance of PEMFCs. Notably, current research is focusing on few ways to overcome the CO poisoning such as the use of CO tolerant catalysts, the oxidant bleeding into the fuel feed stream and the develop of membranes for the CO separation.^{37,38}

Increasing the catalyst activity

Because of his high cost, the large amount of platinum needed for a PEMFCs is today considered one of the reasons for which PEMFCs are excluded from commercialization. As a consequence, one of the main aims of catalyst design consist of improving his catalytic activity. In this sense, one of the most investigated strategy consist of modifying the size and the shape of the platinum particles in order to maximize the available surface to participate in reactions.³⁹ Another strategy concerns the synthesis of platinum nanocrystals with high-index planes which exhibit much higher catalytic activity than that of the most common stable planes.²¹

Increasing operative temperature

Several technical advantages can be obtained working at temperatures beyond the typical temperature range (50-100 °C).⁴⁰ Indeed, It has been shown that the catalyst poisoning effect strongly depends on the operative temperature.⁴¹ For instance, at CO concentration of 100 ppm, a cell temperature of at least 100 °C is required for having CO tolerance while an operative temperature of 140°C makes the poisoning effect almost negligible.⁴² This dependence has been explained considering the strong temperature reliance of the adsorption equilibrium constant of CO on the catalyst since this interaction is associated with high negative entropy.

Advantages related to heat management can also be obtained. The 40-50% of the energy produced by a PEMFC, in fact, is heat that must be removed quickly to avoid overheating problems.⁴³ For PEMFCs operating at low temperatures the heat rejection velocity of the conventional automotive radiators is insufficient to reject continuous full power waste heat so that a complex, weight and very large system is required. On the contrary, the cooling systems utilized for internal combustion engine (ICE) vehicles are sufficient for PEMFCs working at high temperatures so obtaining an improvement in terms of weight- and mass-specific energy densities of the system.⁴⁴ Furthermore the produced excess heat can be recovered as steam

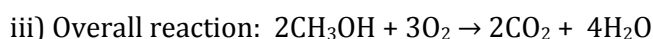
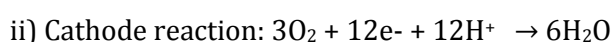
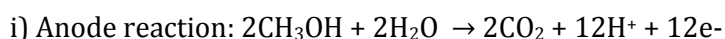
which can be used for direct heating or for pressurized operations. For instance, it has been shown that under an operating temperature of about 200 °C, the fuel cell stack can produce a water steam of up to 15 atm⁴⁴ leading to a significantly increased efficiency.

In addition to the heat management, also a carefully and often difficult water management is necessary during the operation of a low-temperature PEMFC.⁴⁴ Indeed, since in a low temperatures scenario a dual-phase water system is involved (liquid water/ vapor water), in high humidity conditions the electrodes can be flooded thus effecting the durability of the system.^{45,46} Under temperatures above the boiling point of water, the flooding problem is avoided and therefore the water management significantly simplified. Finally, thanks to the elimination or reduction of liquid water, an increasing of exposed surface area of the electrocatalysts is obtained as well as a better diffusion of the reactants in the reaction layer.⁴⁷

Another technical advantages of the high temperatures PEMFCs concerns the electrode reaction kinetics. Indeed, working at high temperatures the reaction kinetics of both hydrogen oxidation and oxygen reduction reactions can be enhanced.^{40,48} Especially the latter is considered crucial to improve the performance of a PEMFC since, being slow, it determines the overall electrochemical kinetics of the systems. It is believed^{49,50} that thanks to the enhanced kinetic obtained working at higher temperatures, the necessity of using platinum catalyst (one of the mayor obstacle which makes PEMFCs non competitive) could be overcome with a consequent significant reducing of the system total cost.

A PEMFC subcategory: DMFC

A particular type of PEMFC is the direct methanol fuel cell (DMFC). This device uses methanol instead of hydrogen as power source:



The main advantage respect to classical PEMFCs concerns the easy transportation of methanol which is stable at all the environmental conditions. Furthermore, these devices do not have many of the fuel storage problems typical of fuel cells because methanol has a higher energy density than hydrogen. Nevertheless, because of the so-called methanol cross-over (methanol diffusion through the membrane without any reaction), the fuel is fed as a weak solution so that the efficiency of these systems is very low.⁵¹ This disadvantage makes them targeted only to a restricted range of portable applications where power and energy density are more important than efficiency.⁵²

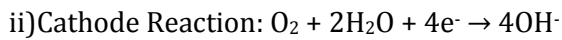
2.3. Other low temperature fuel cells

AFC

The Alkaline Fuel Cells (AFC) are devices typically performing at temperatures between 60 and 90 °C. The electric power is generated utilizing as electrolyte a porous matrix saturated with an aqueous alkaline solution such as potassium hydroxide (KOH). As depicted in figure I-10, the ions travelling across the electrolyte are the hydroxyl ions which react at the anode with two molecules of hydrogen to release 4 water molecules and 4 electrons:



The electrons flow through the external circuit and react with water to produce new OH⁻ ions:



The overall reaction is given by:

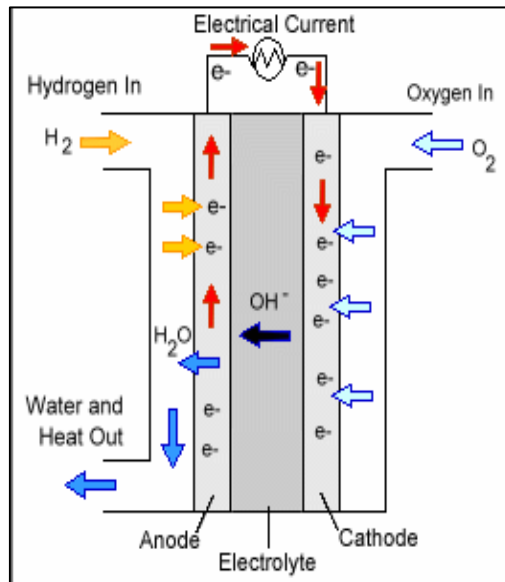
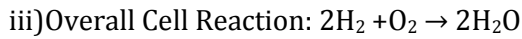


Figure I-10: Concept diagram of AFCs (adapted from²⁶)

Several advantages characterize such device with respect to the other fuel cells. Since the used electrolyte is potassium hydroxide, a very cheap chemical standard, AFCs are the most cost efficient type of fuel cells. Furthermore they have no GHG emissions and the potential efficiency is the highest among the others fuel cells technologies (estimated at 60%).⁵³ Despite these advantages, the use of AFCs is still very limited. Indeed, differently from the other types of fuel cells, in AFC only pure hydrogen can be used as a fuel. Furthermore, the alkaline solution (KOH) used as electrolyte is able to absorb carbon dioxide (conversion of KOH to potassium carbonate K₂CO₃) with the consequent poisoning of the cell. During the operation, therefore, air needs to be cleaned from CO₂ by incorporating a “scrubber” which significantly increases the cost of the

whole system.⁵⁴ Consequently, current research is focusing on finding a substitute of KOH.⁵³ Because of this poisoning effect, AFCs are mainly used for spatial applications, where purifying air is not necessary.⁵⁵

PAFC

The phosphoric acid fuel cells (PAFCs) have an operative range that is about 150°C-210°C. They use liquid phosphoric acid (H₃PO₄) saturated in a silicon carbon matrix as electrolyte whereas the carbon paper is used to make the electrodes which are covered by platinum catalyst. As shown in the figure I-11, the hydrogen at the anode splits into 4 protons and 4 electrons which at the cathode combine with oxygen to form water. In this case the charge carrier is the proton H⁺:

- i) Anode reaction: $2H_2 \rightarrow 4H^+ + 4e^-$
- ii) Cathode reaction: $O_2 + 4H^+ + 4e^- \rightarrow 2H_2O$
- iii) Overall reaction: $2H_2 + O_2 \rightarrow 2H_2O$

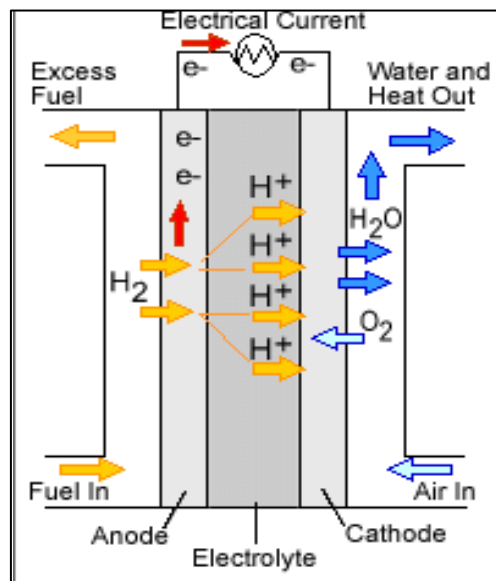


Figure I-11: Concept diagram of PAFCs (adapted from²⁶)

The expelled water is usually used in heating applications by conversion to steam thus increasing the efficiency of the system. Differently from AFCs, for which only pure H₂ can be used as fuel, PAFCs can operate with a larger choice of fuels. Indeed, CO₂ does not affect the electrolyte. However, the applicability of these devices is limited by the short range of operative temperature (150-210 °C). Indeed, at temperatures lower than 150°C phosphoric acid is a poor proton conductor and the poisoning of the platinum catalyst at the anode became severe. On the other hand, high temperatures create structural design problems, particularly for joints,

supporting pumps, and sensors mainly due to the aggressive hot phosphate. Their characteristics are therefore compatible only with a limited scale of on-site stationary applications.⁵⁶

3. The key component of PEMFCs: the Proton Exchange Membrane

It is commonly accepted that the commercialization and competitiveness of PEMFCs will depend on continuous innovation and improvement of its key component: the proton exchange membrane (PEM).^{40,57,58} Notably, the basic requirements for a PEM are the absence of an electronic conductivity and the presence of an high proton conductivity. Little concern is devoted to electronic conductivity because the polymer electrolytes typically employed are inherently electrically insulating. On the contrary, the proton conductivity is a very important tool for determining the performance or utility of a membrane as a candidate for PEMFCs. Notably, levels of conductivity at least above 0.01 S/cm are required. In a fuel cell system, such a value is measured using the following equation:

$$\sigma = L / Rdw \tag{I-2}$$

where L is the distance between the electrodes, R is the measured resistance and d and w are respectively the thickness and width of the membrane. Obviously, high levels of proton conductivity can be achieved only if the membrane is able to efficiently transport the protons from the anode to the cathode side, a process which can occur by means of different mechanisms.

3.1. Mechanisms of proton transport in PEMs

Proton transport in PEMs can be carried out either by a vehicle mechanism diffusion⁵⁹ or by a structural diffusion (also named Grotthuss mechanism^{60,61}).

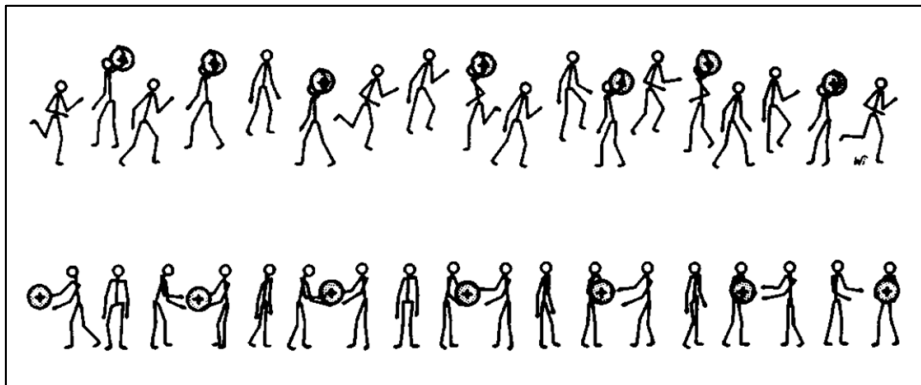


Figure I-12: Models of proton conduction. Top: Vehicle Mechanism; the protons transfer through a moving vehicle. Bottom: Grotthuss mechanism; the protons are passed through the cooperation of neighboring molecules. Adapted from.⁵⁹

The former takes place with the aid of a moving "vehicle" (Figure I-12, top). In other words, the excess protons migrate through the membrane carrying small molecules with them. An example is given by the migration of H_3O^+ in hydrated membranes.

With the Grotthuss mechanism (Figure I-12, bottom), the proton diffuses through proton displacement (also termed proton "hopping") and molecular reorientation. Notably, the proton conduction occurs through the formation and cleavage of H-bonds between neighboring molecules. Such a mechanism is named Grotthuss mechanism, since it was firstly proposed in 1806 by Theodor Grotthuss⁶⁰ who described the passing of protons in water as a cooperation of neighboring water molecules (Figure I-13).

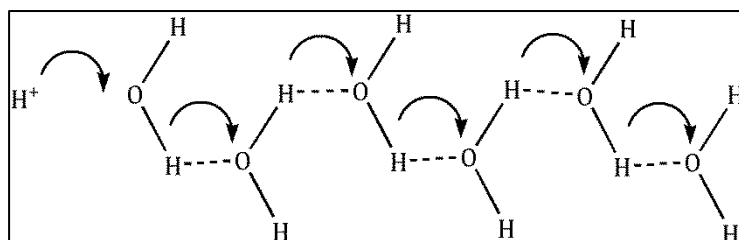


Figure I-13: Schematic representation of Grotthuss mechanism in water.

If proton conductivity through vehicle mechanism is mainly affected by the mobility of the used vehicle (e. g. H_2O or NH_3 as complexes H_3O^+ or NH_4^+), the major aspects governing the proton conductivity in the Grotthuss mechanism are still unclear even if it is commonly accepted that dynamic hydrogen bonds are desired in order to enhance the local mobility which is crucial to reach high level of proton conductivity through structural diffusion.⁵⁷

3.2. Other desired properties of the membrane

Together with an high proton conductivity, also chemical and mechanical stability are considered vital for PEMs. Indeed, they are closely related to the PEM durability which is still one of the critical issue impeding the commercialization of PEMFC. Notably, membrane degradation can be classified into three categories: mechanical, thermal and chemical/electrochemical.⁶² The early life failure is mainly due to the mechanical degradation which can be, for instance, the effect of the overall dimensional change occurring during the operation and due to the resulting non-humidification or low humidification of the membrane.^{63,64} Furthermore, the PEM mechanical strength can be negatively affected by the migration and accumulation of the catalysts and by the decomposition of the seal into the membrane. Since a rapid start-up and an efficient cooling system are essential for automotive and portable applications, the membrane must tolerate freezing temperatures as well as thermal cycling. Several studies⁶⁵⁻⁶⁷ have evidenced as the thermal stability issue of some PEMs is directly related

to the presence of water in the membrane. Indeed, the PEM's lifetime can be strongly affected by the volume change of water due to freeze/thaw cycles occurring during the operation.

The lifetime of the membrane can be also affected by the chemical/electrochemical instability. Indeed, the chemical reactions on the anode and cathode catalyst can produce peroxide and hydroperoxide radicals which are responsible of a chemical attack to the membrane whereas the rate of hydrogen and air crossover to opposite sides of the membrane causes only the 1-3% loss in fuel cell efficiency.⁶⁸ Together with the tolerability to radicals, also the reactant permeability is an important property for PEMs. Indeed, although the hydrogen and oxygen permeability in polymer electrolyte materials are typically low, they can affect the lifetime especially of ultra-thin membranes. Furthermore, as mentioned describing a subcategory of PEMFCs (DMFCs), also the PEM methanol permeability can represent a significant problem. It is much higher than reactant gas permeability and leads to significant performance losses due to the decrease of the overall fuel efficiency and to the impact on the cathode kinetics.⁵¹

Even though the membranes currently used fulfill many of the required properties, the projected PEMs cost has to be reduced drastically before having PEMFCs commercially feasible. Indeed, the strong PEMFC cost reduction of the last years (more than 35% from 2007 to 2009⁶⁹) is mainly due to the auxiliary facilities and catalyst while the membrane cost is nearly unchanged because of the widely employing of expensive perfluorinated polymers, still today considered the only marketable PEMs for use in PEMFCs. Nafion (Dupont de Nemours⁷⁰), Dow (Dow Chemical⁷¹), Flemion (Asahi Chemical) or Aciplex-S (Asahi Glass⁷²) are examples of perfluorinated polymers marketed as PEMs. In spite of a great number of alternative polymer membranes developed,^{58,69} including nonfluorinated types, Nafion is still considered the benchmark material against which most results are compared.

3.3. The PEM state of the art: Nafion

The development of Nafion, a sulfonated tetrafluorethylene copolymer, began in the early 1960s when the DuPont Company's Plastics Exploration Research Group was expanding on fluorine technology.⁷³ It is the progenitor of a class of synthetic polymers called ionomers and represents the first perfluorosulfonic acid (PFSA) membrane used as PEM. As shown in figure I-14, it consists of flexible side chains terminated with hydrophilic sulfonic acid groups and a chemically durable hydrophobic backbone. Ion content can be varied by changing the ratio of the two components (x and y in figure I-14).

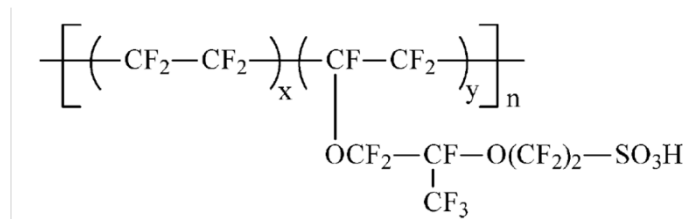


Figure I-14: Chemical structures of Nafion, (adapted from⁵⁸).

Because of the ionic nature of the SO₃H groups, the ends of the sides tend to cluster within the overall structure of the membrane. In 1977 Gierke and coworkers⁷⁴ proposed a Cluster-Channel Model for Nafion in which the neighboring ionic clusters are assumed to be connected by short narrow (Figure I-15). According to this model, the formed micelles, characterized by a 40 Å diameter, distribute continuous fluorocarbon matrix interconnected by narrow channels of about 10 Å in diameter. It is believed that this specific morphology and chemical structure is responsible of both the better proton conductivity and the higher lifetime compared to other materials.⁷⁵

Notably, Nafion is commercially available in different weights. Among them, Nafion 117, characterized by a weight of 1100 EW and a thickness of 7 mil (1 mil equals 25.4 μm), is currently the most widely used. Note that an equivalent weight (EW) corresponds to the weight of Nafion (in molecular mass) per mole of sulfonic acid group.⁷⁶ The combination of weight and thickness of Nafion 117 provides high proton conductivity (7.8 × 10⁻² S/cm at ambient temperature⁷⁷) and moderate swelling in water. Like other PFSA, Nafion is quite resistant to chemical attack whereas at high temperature (> 80°) the mechanical strength is very low.

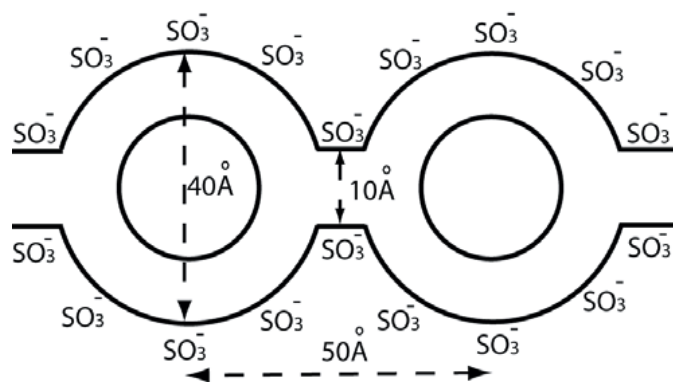


Figure I-15: Cluster-Channel Model of Nafion (Adapted from⁷⁸)

Like in the other PFSA membranes, the degree of hydration is the main factor which governs the proton conductivity in Nafion.⁷⁷ At high humidity condition, the membrane can be described as a two-phase system consisting of a network of water surrounded by a hydrophobic backbone (Figure I-16). This last provides the structural and thermal stability of the membrane

and it is also responsible for the immobilization of the dissociated sulfonic acid groups which are solvated in the interfacial region. During the process, catalytically produced protons act as defects and migrate through the membrane from the anode to the cathode carrying water molecules with them (H_3O^+ diffusion). Therefore the presence of this double-phase (hydrophobic matrix and hydrophilic channel) is necessary to transport protons since the proton transport mechanism is basically conduction through water. However, the hydronium diffusion alone (vehicle mechanism) can't explain the mobility of protons in water which is much higher if compared with other ions of a size similar to H_3O^+ . Such a difference can be explained in terms of contribution by the so-called Grotthuss mechanism⁶¹ in which, as above mentioned, the transport of protons is determined by forming and breaking process of hydrogen bonds between the neighboring molecules, in this case water molecules. In short, the conductivity of Nafion relies on the proton mobility in the hydrophilic channel where protons are carried through both Grotthuss and vehicle mechanisms.

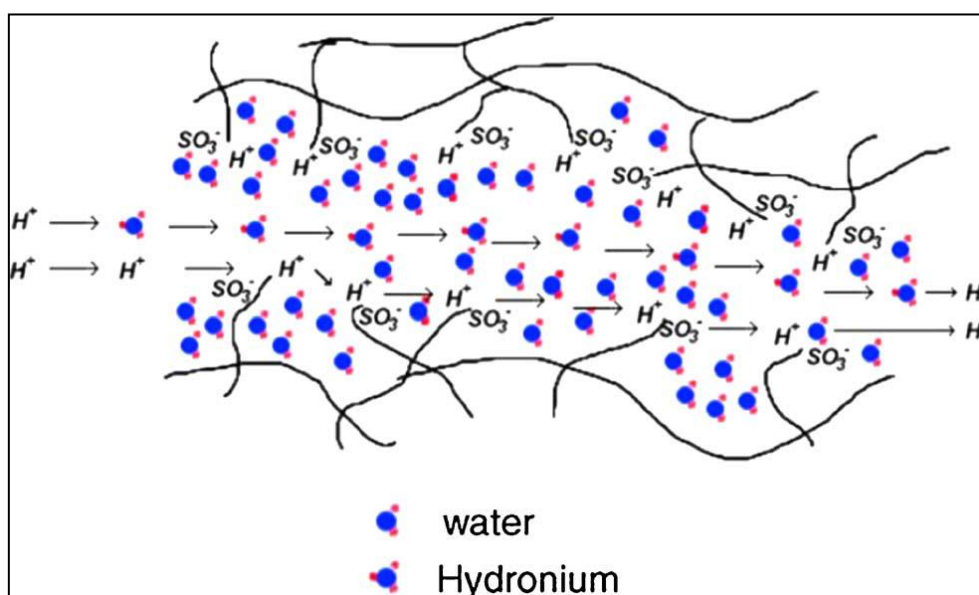


Figure I-16: Proton transport in Nafion (Adapted from⁴⁷)

Limitations

One disadvantage of Nafion consist of the high cost (amounting to US\$ 700 per square meter) so that it is commonly accepted that some sacrifice in material lifetime as well as in mechanical properties may be acceptable in order to develop materials having commercially realistic costs.

79

However, the major drawback of Nafion (and of the other PFSA membranes) is nowadays considered its inability to satisfy the requirements for the latest development of the PEMFC technology which consist of obtaining PEMs working at high temperatures (above 100 °C) which

allow for some important technical advantages (see section 2.2). Indeed, while this membrane performs very well in a water saturated environment, proton conductivity decreases considerably at low relative humidity because of its reliance on water for proton conduction.^{77,80} Obviously, as the temperature increases, the water uptake decreases considerably with a consequent strong decline of the cell voltage and efficiency. This makes impossible an operation temperature above 80°C. Furthermore, the adsorbed water affects the mechanical properties of the membrane by acting as a plasticizer so that a careful control of water uptake is critical during the operation for reducing adverse effects of swelling and degradation.

3.4. Alternatives PEMs for high temperature PEMFCs

There are various strategies for obtaining membranes working at low humidity and high temperatures.^{58,69} They can be divided in two main subcategories: i) Use of modified Nafion, ii) Use of different starting materials. For instance, an improved performance of PEMFCs under low humidity conditions can be obtained incorporating into Nafion membrane mesoporous silica spheres⁸¹. Furthermore, Nafion can be modified incorporating diversified additives such as functionalized silica^{82,83}, modified carbon nanotubes,⁸⁴ treated clays,⁸⁵ zeolite,⁸⁶ zirconia nanoparticles,⁸⁷ zirconium hydrogen phosphate⁸⁸ and ionic liquids.⁸⁹ Other strategies consist in impregnating nanofibers of polyvinyl alcohol with Nafion solution,^{90,91} blending Nafion with different polymers,⁹² or the use of electrospinning to produce Nafion nanofibers.⁹³ Although all these modifications allow for an enhanced performances respect to pure Nafion, they cannot reduce the final PEM cost since a high content of Nafion is still used for their production. In this sense, the use of alternatives and cheaper starting materials is more attractive. Notably, enhanced performance at elevated temperatures can be obtained using different aromatic polymers which are produced incorporating aromatic moieties into several hydrocarbon backbones. Examples of efforts in this directions are represented by sulfonated polymers containing diarylsulfone units,⁹⁴⁻⁹⁶ sulfonated polybenzimidazoles,⁹⁷ poly(aryloxyphosphazene)s functionalized with sulfonimide acid units and phenyl phosphonic units,⁹⁸ sulfonated polyimides.⁹⁹ Acid-base complexes are another viable alternative for having membranes maintaining high conductivity at elevated temperatures. These systems are characterized by an acid component which is incorporated into an alkaline polymer base for promoting proton conductivity. Examples are represented by polybenzimidazoles blended with phosphoric acid¹⁰⁰ or sulfuric acid,⁶⁶ amorphous polyamide with phosphoric acid,¹⁰¹ sulfonated arylene main-chain polymers with poly(4-vinylpyridine) and polybenzimidazoles,¹⁰² phosphoric acid blended polyvinyl alcohol,¹⁰³ blends of sulfonated polysulfones and polybenzimidazoles doped with phosphoric acid.^{104,105}

Among the various compounds utilized and investigated in this context, the mayor rule has been played by nitrogen containing heterocycles such as imidazole and 1,2,3-triazole. These azoles have been utilized to replace water in Nafion (liquid solvents) and as basic components of several aromatic polymers and acid-base complexes able to conduct protons at high temperatures and under anhydrous conditions.

3.5. Azoles and azole-based polymers as proton conductors

Azoles as liquid solvents

As described in section 3.2, the major drawback with the use of Nafion and other PFSA membranes is that their conduction mechanism relies on water-assisted proton transport involving both the vehicular motion of hydronium ions and the Grotthuss mechanism.

In this scenario, the replacement of water with imidazole and other N-heterocycles has generated much excitement in the last years.^{106,107,108} Indeed, charge migration in these compounds occurs, as in water, by protons mobility but their boiling points (bp) are higher so allowing for operative temperatures above 100°C. Notably, imidazole (bp: 257 °C) shows a proton conductivity of 10^{-3} S/cm in the range of 90–120 °C¹⁰⁶ and 1,2,3-triazole (bp: 203 °C) has a proton conductivity of about 1.3×10^{-4} S/cm in the anhydrous state at room temperature.¹⁰⁹ Kreuer et al.¹⁰⁶ have shown that in sulfonated polyetherketone membranes water can be replaced by imidazole allowing for high conductivity at temperature above 100°C.

Although details of the conduction mechanism in imidazole remain still obscure, the presence of a structural diffusion has been established experimentally.¹⁰⁶ A Grotthuss-type diffusion mechanism in imidazole was first proposed by Daycock in 1968¹¹⁰ and Kawada in 1970¹¹¹ (Figure I-17). It involves two steps: i) intermolecular proton transfer (PT) reactions along the chain, ii) reorientation of the scaffold for restoring the starting conformation and having subsequent PT reactions. The difference between the two models concerns the PT step which takes place as a cooperative process (Figure I-17, a) or by migration charged defects (Figure I-17, b). On the contrary, the reorientation step in both models involves a cooperative rotation of all the imidazoles in the hydrogen-bonded chain. This second step is expected being the rate limiting step since it involves the breaking of strong hydrogen bonds.^{107,110}

Even though imidazole and imidazole-like compounds can offer the opportunity of having PEMs working at high temperatures and low humidity conditions avoiding water dependent conductivity, they have a major drawback. Indeed, being small molecules, they can leach out gradually during the process leading to a long-term decline in the performance of PEMFCs.¹¹² The most efficient approach for solving this leaching issue consist of incorporating covalently these heterocyclic compounds into polymeric membranes. Indeed, if covalently

bonded, the azoles cannot be dragged out of the membrane while their local mobility is retained. In other words, instead of using them as alternative liquid solvents, these heterocycles became part of new alternative membranes, namely azole-based polymers.

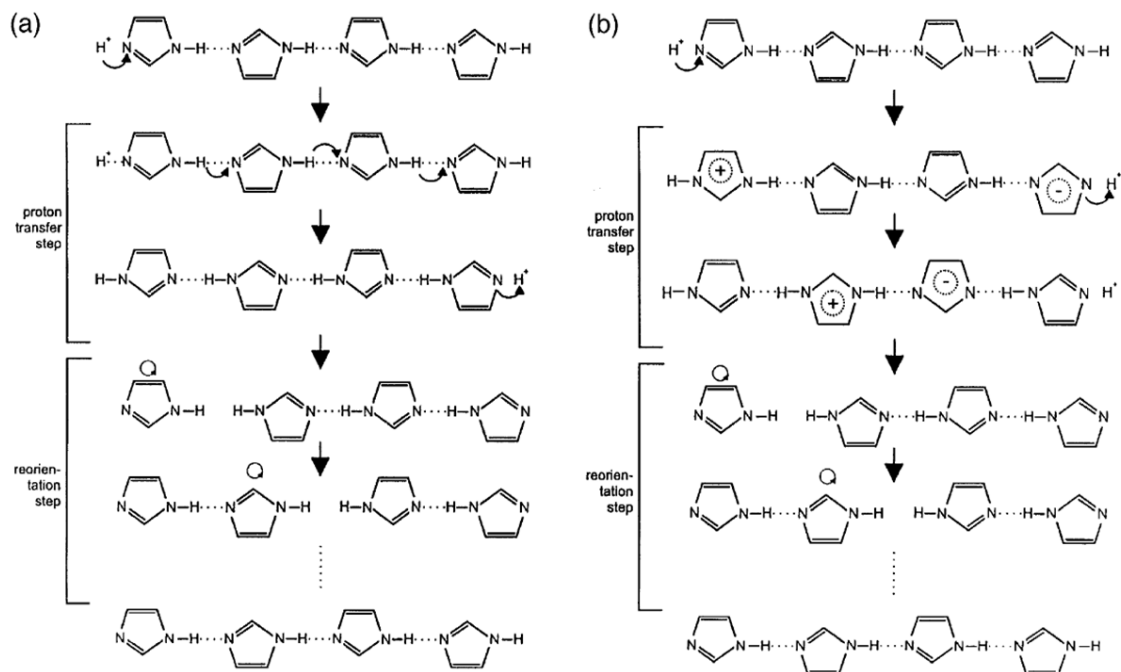


Figure I-17: Proton conduction mechanism in imidazole proposed b a) Daycock¹¹⁰ and b) Kawada¹¹¹ (adapted from¹⁰⁷).

Azole-based polymers as anhydrous proton conductors

The poly(benzimidazole) (PBI) (figure I-18) is considered the precursor of the azole-based polymers electrolytes. In 2000 Kawanara et al.¹¹³ shown that PBI films and strong acid (phosforic and solforic acid) form polymer complexes thermally stable up to 500°C and able to reach high conductivity in anhydrous conditions (10^{-5} S/cm at 160°C). The formation of the polymeric complex was explained as the result of acid-base interactions between imidazole moieties of PBI and acid molecules whereas the proton conduction as the result of Grotthuss mechanism involving the acid (i.e. exchange of protons between H_3PO_4 and $H_2PO_4^-$).

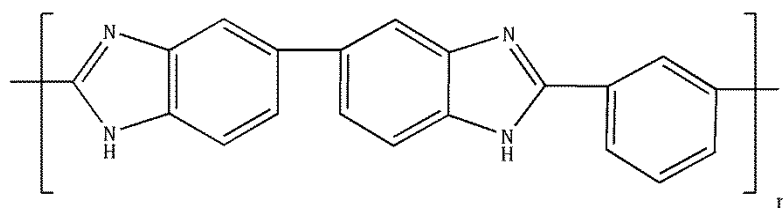


Figure I-18: Structure of PBI.

One year later Schuster et al¹¹⁴ laid the foundations of the basic concept according to which the immobilized azole moieties can directly participate in the proton conduction mechanism. Indeed, a series of compounds with imidazole tethered to the chain ends of oligo(ethylene oxide)s (named Imi-*n*EO, figure I-19) reached high conductivity at 120 °C in anhydrous conditions.

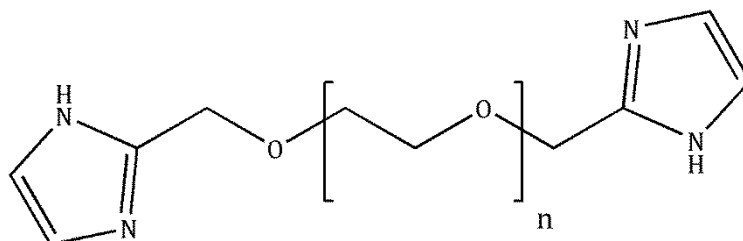


Figure I-19: Structure of the Imi-*n*EO (*n*=2,3,5) compounds investigated by Schuster and al.¹¹⁴

Since the vehicle mechanism cannot take place after heterocycles immobilization, the authors also suggested that the proton conductivity of these systems should be the result of a concerted (Grotthuss) proton transport in which a rapid long range transport of the "excess" protons occurs involving PT reactions between protonated imidazoles and their neutral neighbors followed by a conformational reorganization through rings rotation (figure I-20). Although these systems are much smaller than a fully polymeric system, their successful synthesis and characterization as well as their high conductivity demonstrated that the idea of reach high proton mobility in condensate phase through a fast N-heterocycle mediated proton transport was a viable strategy. Based on these evidences, several azole-based proton conducting polymers have been synthesized in the last few years^{109,115-120} Among them, systems having a backbone structure of polyethylene (table I-2) have been extensively studied both as pure polymers or as blends with strong acids such as H₃PO₄ or H₂SO₄. Notably, concerning the acid blending, two different strategies can be envisaged:

- doping with small amount of acid (< 15 mol % with respect to the azole units)
- blending with molar excess of acid

In the first case the increasing of the acid content plasticizes the materials shifting the temperature of glass transition (*T_g*) to lower values. The resulting higher polymer backbone mobility is consider the reason of the increased proton conductivity with respect to the pure polymer. On the contrary, it is commonly accepted that in systems where a molar excess of acid is used, the conductivity of the blends is mainly based on proton transfer between acid moieties as well as on their self diffusion.

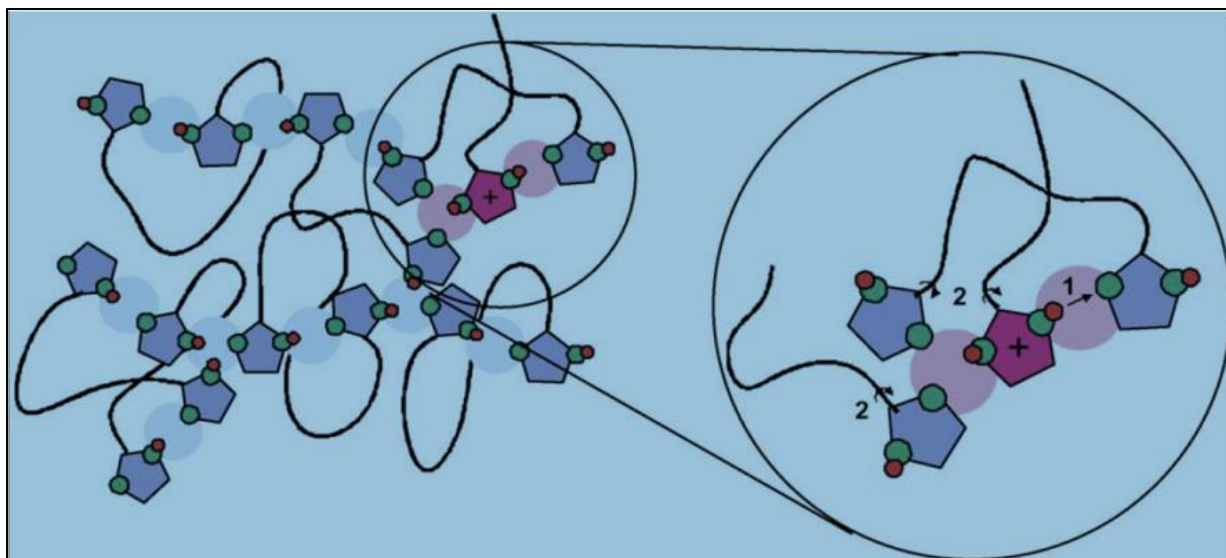


Figure I-20: Proton conduction mechanism hypothesized by Schuster et al¹¹⁴ for Imi-nEo compounds: 1) PT between heterocycles, 2) rings rotation (Adapted from¹¹⁴).

4. Objectives

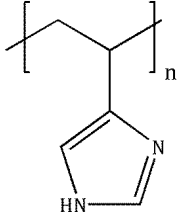
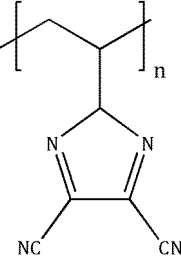
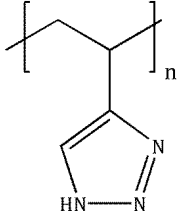
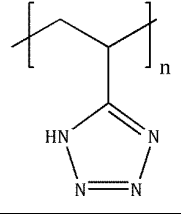
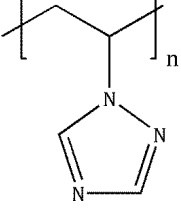
Despite the advances obtained in the last years, the conductivity exhibited by azole-based polymers (maximum values in the range 10^{-5} to 10^{-4} S/cm) is still order of magnitudes lower than that provided by fluorosulfonic acid membranes (10^{-1} S/cm). This is mainly due to the poor understanding of the mechanistic aspects involved in the charge transport. The necessary guidelines to pave the way for the design of more efficient materials can be obtained gaining insights into the structural underpinning that control the proton conduction mechanism.

Notably, several challenges must be addressed before these polymers can provide effective alternative to fluorosulfonic membranes:

- Obtaining a better understanding of the structural and energetic aspects of the proton transfer reactions occurring during the conduction.
- Shedding light on the effect of the plasticizer on the backbone mobility and understanding how it is related to the proton conduction.
- Obtaining new findings on the mechanism of conduction undertaking the complex interactions and the structural details of the polymeric systems.

In this context, an important role can be played by theoretical and computational chemistry. Indeed, the theoretical methods based on the density functional theory (DFT) allow to perform an in-depth investigation of the proton transfer reactions through a quantum approach while molecular dynamics simulations, which are based on a classical force field description of the system, enable the study of the complex dynamic processes occurring in polymeric systems.

Table I-2: Azole-based proton conductors having a backbone structure of polyethylene.

polymer	structure	reference	Year
a) poly-(4-vinyl-imidazole)		Bozkurt et al. ¹¹⁶	2001
b) poly-(2-vinyl-4,5-dicyanoimidazole)		Densmore et al. ¹²⁰	2004
c) poly-(4-vinyl-1,2,3-triazole)		Zhou et al. ¹⁰⁹	2005
d) poly-(5-vinyl-1,2,3,4-tetrazole)		Pu at al. ¹¹⁸	2008
e) poly-(1-vinyl-1,2,4-triazole)		Çelik et al. ¹¹⁹	2008

Based on these evidences and background, the present PhD thesis proposes an in-depth theoretical investigation of the processes related to the proton conductivity in azole-based polymeric systems in order to provide new relevant insights for a rational design of new and better performing materials. This study is performed through a combined approach based on both density functional theory and classical molecular dynamics.

In the **chapter II** of this manuscript the theoretical basis of the tools used in the present research are presented. The first part proposes a descriptions of the quantum chemistry based methods while the second part is devoted to the presentation of the classical molecular dynamics.

The **chapter III** is devoted to the investigation of proton transfer reaction in protonated imidazole, 1,2,3-triazole and tetrazole dimers, basic components of azole-based PEMs. The outcomes obtained using several approaches based on density functional theory will be compared with those provided by accurate reference values obtained using post-Hartree Fock methods in order to select the best performing model able to catch both the energetic and structural features of the investigated systems. Furthermore, based on this investigation and with the aim of select the best functional(s) from a more broad-spectrum point of view, a benchmark study involving a set of chosen systems in which different kinds of PT reactions occur will be briefly presented.

In the **chapter IV** a detailed study of the charge transport mechanism on Poly(4-vinly-imidazole) (table I-2, a)) is presented. The density functional theory results obtained for small systems are discussed in the first part while the simulations of molecular dynamics performed on a large oligomer are described in the second section. Finally, based on the obtained outcomes a mechanism of conduction for this system will be proposed.

The **chapter V** will be focused on a density functional theory based study of the rule of phosphoric acid in the conduction mechanism of Poly(4-vinly-imidazole). Notably, a molecular model characterized by a protonated trimer of P4VI and two molecules of phosphoric acid will be taken into account and the obtained results compared with those obtained with the acid-free model (chapter IV).

Starting from the conclusions drawn out in chapter IV, in the **chapter VI** the effect of a different wire tethering with respect to P4VI (position 2 instead of 4) will be explored by means of an investigation on a different polymeric system, namely poly (2-vinyl-imidazole). Such an investigation will be performed following the same theoretical protocol used for the first polymeric system and characterized by a combined used of methods rooted in density functional theory and molecular dynamics simulations.

5. References

- (1) Eckaus, R. S. Comparing the Effects of Greenhouse Gas Emissions on Global Warming. *The Energy Journal* **1992**, *13*, 25–36.
- (2) International energy outlook 2011, *U.S. Energy Information Administration*, **2011**.
- (3) Hoffmann, P. *Tomorrow's energy: hydrogen, fuel cells, and the prospects for a cleaner planet*; MIT Press, **2002**
- (4) Crabtree, G. W.; Dresselhaus, M. S.; Buchanan, M. V. The Hydrogen Economy. *Physics Today* **2004**, *57*, 39–44.
- (5) Turner, J. A. Sustainable Hydrogen Production. *Science* **2004**, *305*, 972–974.
- (6) Ni, M.; Leung, D. Y. C.; Leung, M. K. H.; Sumathy, K. An overview of hydrogen production from biomass. *Fuel Processing Technology* **2006**, *87*, 461–472.
- (7) Muradov, N. Z.; Veziroğlu, T. N. From hydrocarbon to hydrogen–carbon to hydrogen economy. *International Journal of Hydrogen Energy* **2005**, *30*, 225–237.
- (8) Lemus, R. G.; Martínez Duart, J. M. Updated hydrogen production costs and parities for conventional and renewable technologies. *International Journal of Hydrogen Energy* **2010**, *35*, 3929–3936.
- (9) Gust, D.; Moore, T. A.; Moore, A. L. Mimicking Photosynthetic Solar Energy Transduction. *Accounts of Chemical Research* **2000**, *34*, 40–48.
- (10) Levin, D. B.; Chahine, R. Challenges for renewable hydrogen production from biomass. *International Journal of Hydrogen Energy* **2010**, *35*, 4962–4969.
- (11) Ströbel, R.; Garche, J.; Moseley, P. T.; Jörissen, L.; Wolf, G. Hydrogen storage by carbon materials. *Journal of Power Sources* **2006**, *159*, 781–801.
- (12) Darkrim, F. L.; Malbrunot, P.; Tartaglia, G. P. Review of hydrogen storage by adsorption in carbon nanotubes. *International Journal of Hydrogen Energy* **2002**, *27*, 193–202.
- (13) Züttel, A. Materials for hydrogen storage. *Materials Today* **2003**, *6*, 24–33.
- (14) Züttel, A. Hydrogen storage methods. *Naturwissenschaften* **2004**, *91*, 157–172.

CHAPTER I: Background and objectives

- (15) Pinkerton, F. E.; Meyer, M. S.; Meisner, G. P.; Balogh, M. P.; Vajo, J. J. Phase Boundaries and Reversibility of LiBH₄/MgH₂ Hydrogen Storage Material. *Journal of Physical Chemistry C* **2007**, *111*, 12881–12885.
- (16) Jain, I. P.; Lal, C.; Jain, A. Hydrogen storage in Mg: A most promising material. *International Journal of Hydrogen Energy* **2010**, *35*, 5133–5144.
- (17) Weast R. C.; Astle, M. J.; Beyer W. H. *Handbook of chemistry and physics. 64th ed.*; **1983**, CRC Press, Boca Taton, FL..
- (18) Schäfer, A.; Heywood, J. B.; Weiss, M. A. Future fuel cell and internal combustion engine automobile technologies: A 25-year life cycle and fleet impact assessment. *Energy* **2006**, *31*, 2064–2087.
- (19) Prospects for a hydrogen economy, *Parliamentary Office of Science and Technology* **2002**, number 186.
- (20) Carrette, L.; Friedrich, K. A.; Stimming, U. Fuel Cells – Fundamentals and Applications. *Fuel Cells* **2001**, *1*, 5–39.
- (21) Tian, N.; Zhou, Z.-Y.; Sun, S.-G.; Ding, Y.; Wang, Z. L. Synthesis of Tetrahedral Platinum Nanocrystals with High-Index Facets and High Electro-Oxidation Activity. *Science* **2007**, *316*, 732–735.
- (22) Zhang, J.; Wang, H.; Wilkinson, D. P.; Song, D.; Shen, J.; Liu, Z.-S. Model for the contamination of fuel cell anode catalyst in the presence of fuel stream impurities. *Journal of Power Sources* **2005**, *147*, 58–71.
- (23) Haile, S. M. Fuel cell materials and components. *Acta Materialia* **2003**, *51*, 5981–6000.
- (24) Nernst Z. Über die elektrolytische Leitung fester Körper bei sehr hohen Temperaturen , *Elektrochem* **1899**, 41-43.
- (25) Haber F. Verfahren zur Erzeugung von elektrischer Energie aus Kohle und gasformigen Brennstoffen. *Austrian Patent* **1905**.
- (26) US Department of energy, Types of fuel cells, http://www1.eere.energy.gov/hydrogenandfuelcells/fuelcells/fc_types.html (accessed May 13, 2012).

CHAPTER I: Background and objectives

- (27) Stambouli, A. B.; Traversa, E. Solid oxide fuel cells (SOFCs): a review of an environmentally clean and efficient source of energy. *Renewable and Sustainable Energy Reviews* **2002**, *6*, 433–455.
- (28) Minh, N. Q. Solid oxide fuel cell technology—features and applications. *Solid State Ionics* **2004**, *174*, 271–277.
- (29) de Bruijn, F. The current status of fuel cell technology for mobile and stationary applications. *Green Chemistry* **2005**, *7*, 132.
- (30) Selman, J. R. Molten-salt fuel cells: Technical and economic challenges. *Journal of Power Sources* **2006**, *160*, 852–857.
- (31) Kakati, B.; Deka, D. Differences in physico-mechanical behaviors of resol(e) and novolac type phenolic resin based composite bipolar plate for proton exchange membrane (PEM) fuel cell. *Electrochimica Acta* **2007**, *52*, 7330–7336.
- (32) Wang, Y.; Chen, K. S.; Mishler, J.; Cho, S. C.; Adroher, X. C. A review of polymer electrolyte membrane fuel cells: Technology, applications, and needs on fundamental research. *Applied Energy* **2011**, *88*, 981–1007.
- (33) Ralph, T. R. Proton Exchange Membrane Fuel Cells. *Platinum Metals Review* **1997**, *41*, 102-113.
- (34) Gittleman C.; Masten D.; Jorgensen S. Automotive fuel cell R&D needs. DOE Fuel Cell Pre-Solicitation Workshop March 16, **2010**.
- (35) Hoogers G.; Editor Fuel Cell Technology Handbook, **2003**, CRC Press, Boca Raton, FL.
- (36) Oetjen, H.F.; Schmidt, V. M.; Stimming, U.; Trila, F. Performance Data of a Proton Exchange Membrane Fuel Cell Using H₂/CO as Fuel Gas. *Journal of The Electrochemical Society* **1996**, *143*, 3838–3842.
- (37) Adams, W. A.; Blair, J.; Bullock, K. R.; Gardner, C. L. Enhancement of the performance and reliability of CO poisoned PEM fuel cells. *Journal of Power Sources* **2005**, *145*, 55–61.
- (38) Ioroi, T.; Oku, T.; Yasuda, K.; Kumagai, N.; Mivazaki, Y. Influence of PTFE coating on gas diffusion backing for unitized regenerative polymer electrolyte fuel cells. *Journal of power sources* **2003**, *124*, 385–389.

CHAPTER I: Background and objectives

- (39) Wang, C.; Daimon, H.; Onodera, T.; Koda, T.; Sun, S. A General Approach to the Size- and Shape-Controlled Synthesis of Platinum Nanoparticles and Their Catalytic Reduction of Oxygen. *Angewandte Chemie International Edition* **2008**, *47*, 3588–3591.
- (40) Zhang, J.; Xie, Z.; Zhang, J.; Tang, Y.; Song, C.; Navessin, T.; Shi, Z.; Song, D.; Wang, H.; Wilkinson, D. P.; Liu, Z.-S.; Holdcroft, S. High temperature PEM fuel cells. *Journal of Power Sources* **2006**, *160*, 872–891.
- (41) Baschuk, J. J.; Li, X. Carbon monoxide poisoning of proton exchange membrane fuel cells. *International Journal of Energy Research* **2001**, *25*, 695–713.
- (42) Zawodzinski TA, Karuppaiah C, Uribe F, Gottesfeld S. **1997**. Aspects of CO tolerance in polymer electrolyte fuel cells: some experimental findings. *Electrode Materials and Processes for Energy Conversion and Storage IV*, Srinivasan S, McBreen J, Khandkar AC, Tilak VC (eds); Proceedings of the Electrochemical Society, vol. 97-13. The Electrochemical Society, Inc.: Pennington, 139-146.
- (43) Yi, J. S.; Nguyen, T. V. An Along-the-Channel Model for Proton Exchange Membrane Fuel Cells. *Journal of The Electrochemical Society* **1998**, *145*, 1149–1159.
- (44) Li, Q.; He, R.; Jensen, J. O.; Bjerrum, N. J. Approaches and Recent Development of Polymer Electrolyte Membranes for Fuel Cells Operating above 100 °C. *Chemistry of Materials* **2003**, *15*, 4896–4915.
- (45) Weber, A. Z.; Newman, J. Coupled Thermal and Water Management in Polymer Electrolyte Fuel Cells. *Journal of The Electrochemical Society* **2006**, *153*, A2205–A2214.
- (46) Berg, P.; Promislow, K.; Pierre, J. S.; Stumper, J.; Wetton, B. Water Management in PEM Fuel Cells. *Journal of The Electrochemical Society* **2004**, *151*, A341–A353.
- (47) Hogarth, W. H. J.; Diniz da Costa, J. C.; Lu, G. Q. (Max). Solid acid membranes for high temperature (> 140 °C) proton exchange membrane fuel cells. *Journal of Power Sources* **2005**, *142*, 223–237.
- (48) Parthasarathy, A.; Srinivasan, S.; Appleby, A. J.; Martin, C. R. Temperature Dependence of the Electrode Kinetics of Oxygen Reduction at the Platinum/Nafion interface - A Microelectrode Investigation. *Journal of The Electrochemical Society* **1992**, *139*, 2530–2537.
- (49) Zhang, L.; Zhang, J.; Wilkinson, D. P.; Wang, H. Progress in preparation of non-noble electrocatalysts for PEM fuel cell reactions. *Journal of Power Sources* **2006**, *156*, 171–182.

CHAPTER I: Background and objectives

- (50) Wang, B. Recent development of non-platinum catalysts for oxygen reduction reaction. *Journal of Power Sources* **2005**, *152*, 1–15.
- (51) Scott, K.; Taama, W. .; Argyropoulos, P.; Sundmacher, K. The impact of mass transport and methanol crossover on the direct methanol fuel cell. *Journal of Power Sources* **1999**, *83*, 204–216.
- (52) Rashidi, R.; Dincer, I.; Naterer, G. F.; Berg, P. Performance evaluation of direct methanol fuel cells for portable applications. *Journal of Power Sources* **2009**, *187*, 509–516.
- (53) Crawley G. Fuel Cell Today. Johnson Metthey Plc. 04241894; March **2006**, available online at: <http://www.fuelcelltoday.com>.
- (54) Wallace, J. S. Development of a Carbon Dioxide Continuous Scrubber (CDOCS) System for Alkaline Fuel Cells (<http://hdl.handle.net/10092/1077>), **2006**.
- (55) Kordesch, K.; Hacker, V.; Gsellmann, J.; Cifrain, M.; Faleschini, G.; Enzinger, P.; Fankhauser, R.; Ortner, M.; Muhr, M.; Aronson, R. R. Alkaline fuel cells applications. *Journal of Power Sources* **2000**, *86*, 162–165.
- (56) Sammes, N.; Bove, R.; Stahl, K. Phosphoric acid fuel cells: Fundamentals and applications. *Current Opinion in Solid State and Materials Science* **2004**, *8*, 372–378.
- (57) Bose, S.; Kuila, T.; Nguyen, T. X. H.; Kim, N. H.; Lau, K.; Lee, J. H. Polymer membranes for high temperature proton exchange membrane fuel cell: Recent advances and challenges. *Progress in Polymer Science* **2011**, *36*, 813–843.
- (58) Hickner, M. A.; Ghassemi, H.; Kim, Y. S.; Einsla, B. R.; McGrath, J. E. Alternative Polymer Systems for Proton Exchange Membranes (PEMs). *Chemical Review* **2004**, *104*, 4587–4612.
- (59) Kreuer, K. D.; Rabenau, A.; Weppner, W. Vehicle Mechanism, A New Model for the Interpretation of the Conductivity of Fast Proton Conductors. *Angewandte Chemie International Edition in English* **1982**, *21*, 208–209.
- (60) De Grotthuss, C. J. Memoir upon the decomposition of water, and of the bodies which it holds in solution, by means of galvanic electricity. *Philosophical Magazine Series 1* **1806**, *25*, 330–339.
- (61) Agmon, N. The Grotthuss mechanism. *Chemical Physics Letters* **1995**, *244*, 456–462.

CHAPTER I: Background and objectives

- (62) Collier, A.; Wang, H.; Ziyuan, X.; Zhang, J.; Wilkinson, D. Degradation of polymer electrolyte membranes. *International Journal of Hydrogen Energy* **2006**, *31*, 1838–1854.
- (63) Buchi, F. N.; Srinivasan, S. Operating Proton Exchange Membrane Fuel Cells Without External Humidification of the Reactant Gases. *Journal of The Electrochemical Society* **1997**, *144*, 2767–2772.
- (64) Yu, J.; Matsuura, T.; Yoshikawa, Y.; Nazrul Islam, M.; Hori, M. Lifetime behavior of a PEM fuel cell with low humidification of feed stream. *Physical Chemistry Chemical Physics* **2005**, *7*, 373–378.
- (65) Kim, Y. S.; Dong, L.; Hickner, M. A.; Glass, T. E.; Webb, V.; McGrath, J. E. State of Water in Disulfonated Poly(arylene ether sulfone) Copolymers and a Perfluorosulfonic Acid Copolymer (Nafion) and Its Effect on Physical and Electrochemical Properties. *Macromolecules* **2003**, *36*, 6281–6285.
- (66) Samms, S. R.; Wasmus, S.; Savinell, R. F. Thermal Stability of Proton Conducting Acid Doped Polybenzimidazole in Simulated Fuel Cell Environments. *Journal of The Electrochemical Society* **1996**, *143*, 1225–1232.
- (67) Sivashinsky, N.; Tanny, G. B. The state of water in swollen ionomers containing sulfonic acid salts. *Journal of Applied Polymer Science* **1981**, *26*, 2625–2637.
- (68) Inaba, M.; Kinumoto, T.; Kiriake, M.; Umabayashi, R.; Tasaka, A.; Ogumi, Z. Gas crossover and membrane degradation in polymer electrolyte fuel cells. *Electrochimica Acta* **2006**, *51*, 5746–5753.
- (69) Zhang, H.; Shen, P. K. Advances in the high performance polymer electrolyte membranes for fuel cells. *Chemical Society Reviews* **2012**, *41*, 2382–2394.
- (70) Steck A. E. New Materials for Fuel Cell Systems. *Proc. 1st Inter. Symp. Montreal* **1995**, 74.
- (71) Wakizoe, M.; Velev, O. A.; Srinivasan, S. Analysis of proton exchange membrane fuel cell performance with alternate membranes. *Electrochimica Acta* **1995**, *40*, 335–344.
- (72) Yoshida, N.; Ishisaki, T.; Watakabe, A.; Yoshitake, M. Characterization of Flemion membranes for PEFC. *Electrochimica Acta* **1998**, *43*, 3749–3754.
- (73) Hounshell D. A.; Smith Jr. J. K. Science and Corporate Strategy. *DuPont R&D*, **1988**, 1902–1980.

CHAPTER I: Background and objectives

- (74) Gierke, T. D.; Munn, G. E.; Wilson, F. C. The morphology in nafion perfluorinated membrane products, as determined by wide- and small-angle x-ray studies. *Journal of Polymer Science: Polymer Physics Edition* **1981**, *19*, 1687–1704.
- (75) Smitha, B.; Sridhar, S.; Khan, A. A. Solid polymer electrolyte membranes for fuel cell applications—a review. *Journal of Membrane Science* **2005**, *259*, 10–26.
- (76) Mauritz, K. A.; Moore, R. B. State of Understanding of Nafion. *Chemical Reviews* **2004**, *104*, 4535–4585.
- (77) Sone, Y.; Ekdunge, P.; Simonsson, D. Proton Conductivity of Nafion 117 as Measured by a Four-Electrode AC Impedance Method. *Journal of The Electrochemical Society* **1996**, *143*, 1254–1259.
- (78) Heitner-Wirguin, C. Recent advances in perfluorinated ionomer membranes: structure, properties and applications. *Journal of Membrane Science* **1996**, *120*, 1–33.
- (79) Rikukawa, M.; Sanui, K. Proton-conducting polymer electrolyte membranes based on hydrocarbon polymers. *Progress in Polymer Science* **2000**, *25*, 1463–1502.
- (80) Casciola, M.; Alberti, G.; Sganappa, M.; Narducci, R. On the decay of Nafion proton conductivity at high temperature and relative humidity. *Journal of Power Sources* **2006**, *162*, 141–145.
- (81) Choi, Y.; Kim, Y.; Kim, H. K.; Lee, J. S. Direct synthesis of sulfonated mesoporous silica as inorganic fillers of proton-conducting organic-inorganic composite membranes. *Journal of Membrane Science* **2010**, *357*, 199–205.
- (82) Pereira, F.; Vallé, K.; Belleville, P.; Morin, A.; Lambert, S.; Sanchez, C. Advanced Mesostructured Hybrid Silica–Nafion Membranes for High-Performance PEM Fuel Cell. *Chemistry of Materials* **2008**, *20*, 1710–1718.
- (83) Lin, Y.-F.; Yen, C.-Y.; Ma, C.-C. M.; Liao, S.-H.; Lee, C.-H.; Hsiao, Y.-H.; Lin, H.-P. High proton-conducting Nafion®/–SO₃H functionalized mesoporous silica composite membranes. *Journal of Power Sources* **2007**, *171*, 388–395.
- (84) Thomassin, J.-M.; Kollar, J.; Caldarella, G.; Germain, A.; Jérôme, R.; Detrembleur, C. Beneficial effect of carbon nanotubes on the performances of Nafion membranes in fuel cell applications. *Journal of Membrane Science* **2007**, *303*, 252–257.

CHAPTER I: Background and objectives

- (85) Bébin, P.; Caravanier, M.; Galiano, H. Nafion®/clay-SO₃H membrane for proton exchange membrane fuel cell application. *Journal of Membrane Science* **2006**, *278*, 35–42.
- (86) Baglio, V.; Arico, A. S.; Blasi, A. D.; Antonucci, P. L.; Nannetti, F.; Tricoli, V.; Antonucci, V. Zeolite-based composite membranes for high temperature direct methanol fuel cells. *Journal of Applied Electrochemistry* **2005**, *35*, 207–212.
- (87) Alberti, G.; Casciola, M.; Donnadio, A.; Narducci, R.; Pica, M.; Sganappa, M. Preparation and properties of nafion membranes containing nanoparticles of zirconium phosphate. *Desalination* **2006**, *199*, 280–282.
- (88) Chalkova, E.; Fedkin, M. V.; Komarneni, S.; Lvov, S. N. Nafion/Zirconium Phosphate Composite Membranes for PEMFC Operating at up to 120 °C and down to 13% RH. *Journal of The Electrochemical Society* **2007**, *154*, B288–B295.
- (89) Schmidt, C.; Glück, T.; Schmidt-Naake, G. Modification of Nafion Membranes by Impregnation with Ionic Liquids. *Chemical Engineering & Technology* **2008**, *31*, 13–22.
- (90) Mollá, S.; Compañ, V. Performance of composite Nafion/PVA membranes for direct methanol fuel cells. *Journal of Power Sources* **2011**, *196*, 2699–2708.
- (91) Lin, H.-L.; Wang, S.-H.; Chiu, C.-K.; Yu, T. L.; Chen, L.-C.; Huang, C.-C.; Cheng, T.-H.; Lin, J.-M. Preparation of Nafion/poly(vinyl alcohol) electro-spun fiber composite membranes for direct methanol fuel cells. *Journal of Membrane Science* **2010**, *365*, 114–122.
- (92) Sen, U.; Bozkurt, A.; Ata, A. Nafion/poly(1-vinyl-1,2,4-triazole) blends as proton conducting membranes for polymer electrolyte membrane fuel cells. *Journal of Power Sources* **2010**, *195*, 7720–7726.
- (93) Dong, B.; Gwee, L.; Salas-de la Cruz, D.; Winey, K. I.; Elabd, Y. A. Super Proton Conductive High-Purity Nafion Nanofibers. *Nano Letters* **2010**, *10*, 3785–3790.
- (94) Wang, F.; Hickner, M.; Kim, Y. S.; Zawodzinski, T. A.; Mcgrath, J. E. Direct polymerization of sulfonated poly(arylene ether sulfone) random (statistical) copolymers: candidates for new proton exchange membranes. *Journal of Membrane Science* **2002**, *197*, 231–242.
- (95) Poppe, D.; Frey, H.; Kreuer, K. D.; Heinzl, A.; Mülhaupt, R. Carboxylated and Sulfonated Poly(arylene-co-arylene sulfone)s: Thermostable Polyelectrolytes for Fuel Cell Applications. *Macromolecules* **2002**, *35*, 7936–7941.

CHAPTER I: Background and objectives

- (96) Lafitte, B.; Karlsson, L. E.; Jannasch, P. Sulfophenylation of Polysulfones for Proton-Conducting Fuel Cell Membranes. *Macromolecular Rapid Communications* **2002**, *23*, 896–900.
- (97) Asensio, J. A.; Borros, S.; Gomez-Romero, P. Proton-conducting polymers based on benzimidazoles and sulfonated benzimidazoles. *Journal of polymer science. Part A. Polymer chemistry* **2002**, *40*, 3703–3710.
- (98) Hofmann, M. A.; Ambler, C. M.; Maher, A. E.; Chalkova, E.; Zhou, X. Y.; Lvov, S. N.; Allcock, H. R. Synthesis of polyphosphazenes with sulfonimide side groups. *Macromolecules* **2002**, *35*, 6490–6493.
- (99) Fang, J.; Guo, X.; Harada, S.; Watari, T.; Tanaka, K.; Kita, H.; Okamoto, K. Novel Sulfonated Polyimides as Polyelectrolytes for Fuel Cell Application. 1. Synthesis, Proton Conductivity, and Water Stability of Polyimides from 4,4'-Diaminodiphenyl Ether-2,2'-disulfonic Acid. *Macromolecules* **2002**, *35*, 9022–9028.
- (100) Qingfeng, L.; Hjuler, H. A.; Bjerrum, N. J. Phosphoric acid doped polybenzimidazole membranes: Physicochemical characterization and fuel cell applications. *Journal of Applied Electrochemistry* **2001**, *31*, 773–779.
- (101) Lassègues, J.; Grondin, J.; Hernandez, M.; Marée, B. Proton conducting polymer blends and hybrid organic inorganic materials. *Solid State Ionics* **2001**, *145*, 37–45.
- (102) Jörissen, L.; Gogel, V.; Kerres, J.; Garche, J. New membranes for direct methanol fuel cells. *Journal of Power Sources* **2002**, *105*, 267–273.
- (103) Vargas, M. A.; Vargas, R. A.; Mellander, B.-E. New proton conducting membranes based on PVAL/H₃PO₂/H₂O. *Electrochimica Acta* **1999**, *44*, 4227–4232.
- (104) Hasiotis, C.; Deimede, V.; Kontoyannis, C. New polymer electrolytes based on blends of sulfonated polysulfones with polybenzimidazole. *Electrochimica Acta* **2001**, *46*, 2401–2406.
- (105) Hasiotis, C.; Qingfeng, L.; Deimede, V.; Kallitsis, J. K.; Kontoyannis, C. G.; Bjerrum, N. J. Development and Characterization of Acid-Doped Polybenzimidazole/Sulfonated Polysulfone Blend Polymer Electrolytes for Fuel Cells. *Journal of The Electrochemical Society* **2001**, *148*, A513–A519.
- (106) Kreuer, K. D.; Fuchs, A.; Ise, M.; Spaeth, M.; Maier, J. Imidazole and pyrazole-based proton conducting polymers and liquids. *Electrochimica Acta* **1998**, *43*, 1281–1288.

CHAPTER I: Background and objectives

- (107) Münch, W.; Kreuer, K.-D.; Silvestri, W.; Maier, J.; Seifert, G. The diffusion mechanism of an excess proton in imidazole molecule chains: first results of an ab initio molecular dynamics study. *Solid State Ionics* **2001**, *145*, 437–443.
- (108) Noda, A.; Susan, M. A. B. H.; Kudo, K.; Mitsushima, S.; Hayamizu, K.; Watanabe, M. Brønsted Acid–Base Ionic Liquids as Proton-Conducting Nonaqueous Electrolytes. *Journal of Physical Chemistry B* **2003**, *107*, 4024–4033.
- (109) Zhou, Z.; Li, S.; Zhang, Y.; Liu, M.; Li, W. Promotion of Proton Conduction in Polymer Electrolyte Membranes by 1H-1,2,3-Triazole. *Journal of the American Chemical Society* **2005**, *127*, 10824–10825.
- (110) Daycock, J. T.; Jones, G. P.; Evans, J. R. N.; Thomas, J. M. Rotation of Imidazole in the Solid State and its Significance in deciding the Nature of Charge Migration in Biological Materials. , *Nature* **1968**, *218*, 672–673.
- (111) Kawada, A.; McGhie, A. R.; Labes, M. M. Protonic Conductivity in Imidazole Single Crystal. *The Journal of Chemical Physics* **1970**, *52*, 3121–3125.
- (112) Fernicola, A.; Panero, S.; Scrosati, B. Proton-conducting membranes based on protic ionic liquids. *Journal of Power Sources* **2008**, *178*, 591–595.
- (113) Kawahara, M.; Morita, J.; Rikukawa, M.; Sanui, K.; Ogata, N. Synthesis and proton conductivity of thermally stable polymer electrolyte: poly(benzimidazole) complexes with strong acid molecules. *Electrochimica Acta* **2000**, *45*, 1395–1398.
- (114) Schuster, M.; Meyer, W. .; Wegner, G.; Herz, H. .; Ise, M.; Schuster, M.; Kreuer, K. .; Maier, J. Proton mobility in oligomer-bound proton solvents: imidazole immobilization via flexible spacers. *Solid State Ionics* **2001**, *145*, 85–92.
- (115) Pu, H.; Meyer, W. H.; Wegner, G. Proton Conductivity in Acid-Blended Poly(4-vinylimidazole). *Macromolecular Chemistry and Physics* **2001**, *202*, 1478–1482.
- (116) Bozkurt, A.; Meyer, W. . Proton conducting blends of poly(4-vinylimidazole) with phosphoric acid. *Solid State Ionics* **2001**, *138*, 259–265.
- (117) Martwiset, S.; Woudenberg, R. C.; Granados-Focil, S.; Yavuzcetin, O.; Tuominen, M. T.; Coughlin, E. B. Intrinsically conducting polymers and copolymers containing triazole moieties. *Solid State Ionics* **2007**, *178*, 1398–1403.

CHAPTER I: Background and objectives

- (118) Pu, H.; Wu, J.; Wan, D.; Chang, Z. Synthesis and anhydrous proton conductivity of poly(5-vinyltetrazole) prepared by free radical polymerization. *Journal of Membrane Science* **2008**, *322*, 392–399.
- (119) Çelik, S. Ü.; Aslan, A.; Bozkurt, A. Phosphoric acid-doped poly(1-vinyl-1,2,4-triazole) as water-free proton conducting polymer electrolytes. *Solid State Ionics* **2008**, *179*, 683–688.
- (120) Densmore, C. G.; Rasmussen, P. G.; Goward, G. R. Probing Hydrogen Bonding and Proton Mobility in Dicyanoimidazole Monomers and Polymers. *Macromolecules* **2004**, *38*, 416–421.
- (121) Johnson, D. M.; Rasmussen, P. G. An Improved Synthesis of 2-Vinyl-4,5-dicyanoimidazole and Characterization of Its Polymers. *Macromolecules* **2000**, *33*, 8597–8603.

CHAPTER II: THEORETICAL BACKGROUND

This chapter is devoted to the theoretical background of the present thesis. In the first section a general overview concerning the Quantum Mechanics (QM) based methods will be presented. Notably, after a general introduction, a detailed description of *Hartree-Fock (HF) theory*, *Møller-Plesset (MP) perturbation theory*, *Coupled Cluster (CC) theory* and *Density Functional Theory (DFT)* will be given. The basic principles of the Molecular Mechanics (MM) will be proposed in the second section together with a description of the MM-based methodologies used in the present work: Molecular Dynamics (MD) simulations at constant temperature and Umbrella Sampling technique.

1. Quantum Mechanics (QM)

1.1. The Schrödinger equation

The study of the properties of a system in Quantum Chemistry relies on the resolution of the Schrödinger equation. The time-independent and non-relativistic form can be expressed as:

$$\hat{H}\Psi = E\Psi \quad (\text{II-1})$$

where \hat{H} is the Hamiltonian operator, Ψ is the wave function and E is the energy of the system. For a system characterized by M nuclei and N electrons, the Hamiltonian operator can be described as:

$$\hat{H} = -\frac{1}{2} \sum_{i=1}^N \nabla_i^2 - \frac{1}{2} \sum_{A=1}^M \frac{1}{M_A} \nabla_A^2 - \sum_{i=1}^N \sum_{A=1}^M \frac{Z_A}{r_{iA}} + \sum_{i=1}^{N-1} \sum_{j>i}^N \frac{1}{r_{ij}} + \sum_{A=1}^{M-1} \sum_{B>A}^M \frac{Z_A Z_B}{r_{AB}} \quad (\text{II-2})$$

where A and B are indexes referring to the nuclei whereas i and j refer to the electrons. The interparticles distances are expressed by the variables r while the masses and the charges by M and Z . Finally, ∇^2 represent the Laplacian operator. Note that, following this definition, the Hamiltonian operator is expressed in atomic units (the numerical values of the electron mass m_e , of the elementary charge e , of the reduced Planck's constant \hbar and of the coulomb constant $1/4\pi\epsilon_0$ are all equal to one).

Furthermore, according to the equation II-2, the operator is divisible in the kinetic part which is expressed by the first two terms (kinetic energy of electrons and nuclei) and the

potential part expressed by the last three terms indicating respectively the Coulomb attraction between electrons and nuclei, the electron-electron repulsion and the nucleus-nucleus repulsion. An exact solution for this equation can be obtained only for systems in which no repulsion between electrons is present (those systems with a single electron). Approximations are therefore necessary in most of the cases.

1.2. The Born-Oppenheimer approximation

The first assumption of the Hamiltonian expression is obtained through the *Born-Oppenheimer approximation*.¹ The momentum (p) of a particle is defined by:

$$p = mv \tag{II-3}$$

Where m and v are respectively the mass and the velocity of the considered particle. Since the momentum p depends on the charge, it is assumed that the p of the electrons and nuclei are of the same order of magnitude. In this case, since the nuclei are so much more massive than the electrons, they must accordingly have much smaller velocities so that the electronic wavefunction depends upon the nuclear positions but not the nuclear motion (which is so much slower than electrons). In addition, it is assumed that the electrons move in a fixed potential due to the nuclei so that the Hamiltonian expression can be simplified to the electronic part as:

$$\hat{H}_{el} = \hat{T}_e + \hat{V}_{Ne} + \hat{V}_{ee} \tag{II-4}$$

or

$$\hat{H}_{el} = -\frac{1}{2} \sum_{i=1}^N \nabla_i^2 - \sum_{i=1}^N \sum_{A=1}^M \frac{Z_A}{r_{iA}} + \sum_{i=1}^{N-1} \sum_{j>i}^N \frac{1}{r_{ij}} \tag{II-5}$$

According to this assumption, the electronic energy E_{el} of a given system is simply the solution of the Schrödinger equation with the electronic Hamiltonian and the electronic wavefunction Ψ_{el} . Finally, by adding the constant contribution of the nuclei repulsion at fixed geometry, the total energy is given by:

$$E_{tot} = E_{el} + \sum_{A=1}^M \sum_{B>A}^M \frac{Z_A Z_B}{r_{AB}} \tag{II-6}$$

1.3. Molecular orbital (MO) approximation and basis functions

Once simplified the Hamiltonian expression, a further approximation is applied to define the functions Ψ . The *orbitals* are definable as the form of the wave-functions describing one of a pair of electrons in a atom. In particular, the *spatial* orbital is definable as a function of the position vector \vec{r} that describes the spatial distribution of a given electron so that $\int |\psi_i(\vec{r}_i)|^2 d\vec{r}$ is the probability to find the particle in a volume $d\vec{r}$. Notably the spatial orbitals are orthonormals:

$$\int \psi_i(\vec{r}_i) \psi_j^*(\vec{r}_j) d\vec{r} = \delta_{ij} \quad (\text{II-7})$$

where δ_{ij} is the symbol of Kronecker ($\delta_{ij} = 1$ if $i = j$ and $\delta_{ij} = 0$ if $i \neq j$).

Nevertheless, the specification of the spin state is also necessary in order to have a complete description of an electron. This condition is obtained through the definition of two orthonormal functions $\alpha(\omega)$ et $\beta(\omega)$ so that two different states of spin are undertaken for each electron. Consequently, for each orbital, two different wave functions (called spin-orbitals) can be defined:

$$\chi(\vec{x}) = \begin{cases} \psi(\vec{r})\alpha(\omega) \\ \psi(\vec{r})\beta(\omega) \end{cases} \quad (\text{II-8})$$

Having the expression of the wavefunction describing one electron, the approximations used for the multi electron wavefunction can be considered. Notably, it can be described as the product of the mono electronic wavefunctions:

$$\Psi^{HP}(\vec{x}_1, \vec{x}_2, \dots, \vec{x}_N) = \chi_1(\vec{x}_1) \chi_2(\vec{x}_2) \dots \chi_N(\vec{x}_N) \quad (\text{II-9})$$

This assumption was proposed by Hartree² and the product of the mono electronic wavefunctions is called *Hartree product*. Nevertheless, according to the *Pauli exclusion principle*, the multi-electrons wavefunction must change its sign with respect to exchange of the electronic coordinates. This anti-symmetric condition is not satisfied by the *Hartree product* so that a better description is necessary. The *Slater determinant* (II-10) is an expression able to describe the multi-electrons wavefunction including the anti-symmetry requirements. For a N -electron system it is definable as:

$$\Psi^{SD}(\vec{x}_1, \vec{x}_2, \dots, \vec{x}_N) = \frac{1}{\sqrt{N!}} \begin{vmatrix} \chi_1(\vec{x}_1) & \chi_2(\vec{x}_1) & \dots & \chi_k(\vec{x}_1) \\ \chi_1(\vec{x}_2) & \chi_2(\vec{x}_2) & \dots & \chi_k(\vec{x}_2) \\ \dots & \dots & \dots & \dots \\ \chi_1(\vec{x}_N) & \chi_2(\vec{x}_N) & \dots & \chi_k(\vec{x}_N) \end{vmatrix} \quad (\text{II-10})$$

where the different ways of placing the electrons in the spin-orbitals is represented by each line whereas the change of the sign of the wavefunction is obtained by the exchange of the lines which correspond to the exchange of two electrons. The symmetric functions are automatically rejected.

A further approximation is used in the so called *LCAO (Linear Combination of Atomic Orbitals)* approach where the molecular orbitals (Ψ) are described as a linear combination of atomic orbitals (φ_i). So, although their exact definition would require an infinite number of basis functions, the orbitals are here represented by a finite number of functions:

$$\Psi = \sum_i^N a_i \chi_i \quad (\text{II-11})$$

where a coefficient a_i is associated to each of the N functions used to create the molecular orbitals. Obviously, their construction needs a mathematical representation of each of the basis orbitals considered. The *STO* (*Slater Type Orbitals*) and *GTO* (*Gaussian Type Orbitals*) represent the two main types of such representation available. The general difference can be appreciated through the following representations for the $1s$ orbital of a hydrogen atom:

$$\chi_{1s}^{STO}(\zeta, r) = \left(\zeta^3/\pi\right)^{1/2} e^{-\zeta r} \quad (\text{II-12})$$

$$\chi_{1s}^{GTO}(\alpha, r) = (2\alpha/\pi)^{3/4} e^{-\alpha r^2} \quad (\text{II-13})$$

Where ζ and α are respectively the exponents of the Slater function and of the Gaussian function. This last is easier to deal with mathematically, since any product of two Gaussian functions can be represented by another Gaussian function. On the other hand, as the atomic orbital approaches to the core an even better description is obtained using the Slater basis function. This shortcoming of GTO can be overcome by reproducing the Slater function behavior using the so called *contracted* Gaussian functions which correspond to the sum of different Gaussian functions called *primitives*. Following this idea, different set of basis functions (called *basis set*) can thus be produced and used. From a more computational point of view, a *basis set* is a mathematical description of the orbitals within a system considered to perform a theoretical calculation. Obviously, larger *basis sets* approximate more accurately the orbitals but on the same time make the calculations more time consuming so that the selection of a *basis set* involves a trade-off between accuracy and computational cost and represents one of the critical parameters for setting a quantum chemistry calculation.

1.4. The Hartree-Fock Theory

One of the simplest approximate theories for solving the Schrödinger equation is the *Hartree-Fock (HF) theory*. It is based on a simple assumption: the single-particle function (orbital) does not depend explicitly on the instantaneous motions of the other particles. In other words, the electrons are subject to an average non-local potential arising from the other electrons. Although this approximation can lead to a poor description of the electronic structure since the correlation among the electrons is neglected, the *HF* theory represent the starting point for most *ab initio* quantum chemistry methods.

The Hartree-Fock Equations

Starting from the time-independent Schrödinger equation (II-1) the energy for an electronic system in the state Ψ is given by:

$$E[\Psi] = \frac{\langle \Psi | \hat{H}_{el} | \Psi \rangle}{\langle \Psi | \Psi \rangle} \quad (\text{II-14})$$

Assuming that the wavefunction can be approximated by a single Slater determinant, and taking into account the normalization condition so that $\langle \Psi_{HF} | \Psi_{HF} \rangle = 1$, the average value of the electronic energy is:

$$E_{HF} = \langle \Psi_{HF} | \hat{H}_{el} | \Psi_{HF} \rangle = \sum_{i=1}^N \langle i | \hat{h} | i \rangle + \sum_{i=1}^{N-1} \sum_{j=1}^N \langle ij | ij \rangle - \langle ij | ji \rangle \quad (\text{II-15})$$

where the information about the kinetic energy and the attraction electron-nucleus of the electron i is given by the first term (II-16) while the second (II-17) and the third (II-18) terms are respectively the *Coulomb* and *Exchange integrals* referring to the interaction between the two electrons i and j .

$$\langle i | \hat{h} | i \rangle = \int \chi_i(\vec{x}_1) \left\{ -\frac{1}{2} \nabla^2 - \sum_A \frac{Z_A}{r_{1A}} \right\} \chi_i^*(\vec{x}_1) d\vec{x}_1 \quad (\text{II-16})$$

$$\langle ii | jj \rangle = \iint |\chi_i(\vec{x}_1)|^2 \frac{1}{r_{12}} |\chi_j(\vec{x}_2)|^2 d\vec{x}_1 d\vec{x}_2 \quad (\text{II-17})$$

$$\langle ij | ji \rangle = \iint \chi_i(\vec{x}_1) \chi_j^*(\vec{x}_1) \frac{1}{r_{12}} \chi_j(\vec{x}_2) \chi_i^*(\vec{x}_2) d\vec{x}_1 d\vec{x}_2 \quad (\text{II-18})$$

The Hartree-Fock method applies the *variational principle*. It consists in choosing a "trial wavefunction" depending on one or more parameters, and finding the values of these parameters for which the expectation value of the energy is the lowest possible. Notably, the principle is applied by minimizing the energy E_{HF} obtained in the equation (II-15) as a functional of the spinorbitals:

$$E_{HF} = E[\{\chi_i\}] \quad (\text{II-19})$$

It can be shown that the obtained energy will be always higher or equal to that of the ground state (E_0):

$$E_{HF} = \langle \Psi_{HF} | \hat{H}_{el} | \Psi_{HF} \rangle \geq E_0 \quad (\text{II-20})$$

Keeping in mind that χ_i are orthonormals, the minimization of E_{HF} allows to obtain the so-called *Hartree-Fock equations*:

$$\hat{f}_i \chi_i = \varepsilon_i \chi_i \quad (\text{II-21})$$

Where ε_i represents the energy of the orbital i and the eigenvalues of the monoelectronic operator \hat{f}_i (*Fock-operator*) which can be expressed as:

$$\hat{f}_i = -\frac{1}{2} \nabla_i^2 - \sum_{A=1}^M \frac{Z_A}{r_{iA}} + V_{HF}(i) \quad (\text{II-22})$$

Where $V_{HF}(i)$ represents the mean potential for the electron i due to the presence of the $N-1$ other electrons. In other words, in the *HF* theory each particle is subjected to the mean field

created by all other particles so that the electron-electron interaction $1/r_{ij}$ in the Hamiltonian is substituted by a mono-electronic operator $V_{HF}(i)$ which is called *Hartree-Fock potential*, given by:

$$V_{HF}(\bar{x}_i) = \sum_j^N (\hat{J}_j(\bar{x}_i) - \hat{K}_j(\bar{x}_i)) \quad (\text{II-23})$$

Where \hat{J}_j is the Coulomb operator (II-24) and \hat{K}_j is the exchange operator (II-25):

$$\hat{J}_j(\bar{x}_1) = \int |\chi_j(\bar{x}_2)|^2 \frac{1}{r_{12}} d\bar{x}_2 \quad (\text{II-24})$$

$$\hat{K}_j(\bar{x}_1) \chi_j(\bar{x}_1) = \int \chi_j^*(\bar{x}_2) \frac{1}{r_{12}} \chi_i(\bar{x}_2) \chi_j(\bar{x}_1) d\bar{x}_2 \quad (\text{II-25})$$

Since the Fock operator depends on the spinorbitals through V_{HF} , the Hartree-Fock equations have to be solved in an iterative way. The general procedure consists of making the orbitals self-consistent with the potential field they generate. This is obtained through an iterative trial-and-error method. The entire procedure is called the *Self Consistent Field (SCF)* method: starting from an initial trial function for the spinorbitals, the mean field felt by each electron is computed to solve the *HF equations* (II-21). The obtained new spinorbitals are then used to compute the new mean fields so that an iterative cycle is established. This procedure lasts until the difference between the energies of the incoming and outgoing orbitals is less than a threshold value (convergence condition).

1.5. The correlation energy

As above described, within the *HF* method the antisymmetric wavefunction is approximated by a single Slater determinant. Nevertheless, single determinants are not able to express the exact wave function since the explicit electron-electron interaction is not taken into account. Notably, following the *HF* method, the multi-electrons wavefunction is definable as sum of the Fock operators:

$$\hat{H}_{HF} \Psi_{SD} = E_{HF} \Psi_{SD} \quad \Rightarrow \quad \sum_i^N \hat{f}_i \Psi_{SD} = \sum_i^N \epsilon_i \Psi_{SD} \quad (\text{II-26})$$

The equation (II-26) describes a system of non-interacting electrons that are effected by a potential V_{HF} . The Fock operator is, in fact, mono-electronic. In other words, the probability of finding an electron at some location around an atom is determined by the distance from the nucleus but not the distance to the other electrons so that the correlation due to the coulomb interaction between the electrons (named *Coulomb correlation*) is completely neglected. Furthermore, within the HF approximation the correlation between electrons of opposite spins

is not taken into account so that the probability of finding two electrons having opposite spins in the same location of space is not equal to zero.

It is worth to underline that although the correlation between electrons of opposite spins is completely neglected in the *HF* approximation, it is fully accounted for electrons of parallel spin. This contribution named *electron exchange* is not part of the *correlation energy* which is by definition the difference between the energy computed with the HF approximation and the exact energy.

$$E_c^{HF} = E_0 - E_{HF} \quad (II-27)$$

The *correlation energy* can be added to the HF theory by using the so-called *post-HF methods* which are able to give more accurate results but requiring more computational time. In the following a brief description of the *post-HF methods* used in the present research will be presented.

1.6. The Møller-Plesset (MP) perturbation theory

In 1934 Møller and Plesset³ proposed a way to tackle the problem of the *correlation energy*. This method is based on the *Rayleigh-Schrödinger (RS) perturbation theory* in which a small perturbation \hat{V} is added to the unperturbed operator \hat{H}_0 to have the "true" operator \hat{H} :

$$\hat{H} = \hat{H}_0 + \lambda \hat{V} \quad (II-28)$$

where λ is a parameter that can vary between 0 and 1. When λ is zero then \hat{H} is equal to the zeroth-order Hamiltonian and when λ is one \hat{H} equals its true value. The perturbed wave function (ψ) and the perturbed energy (E) are expressed in powers of λ :

$$\Psi = \lim_{n \rightarrow \infty} \sum_{i=0}^n \lambda^i \Psi^{(i)} \quad (II-29)$$

$$E = \lim_{n \rightarrow \infty} \sum_{i=0}^n \lambda^i E^{(i)} \quad (II-30)$$

so that by substitution in the time-independent Schrödinger equation (II-1), a new expression is obtained:

$$(\hat{H}_0 + \lambda \hat{V}) \left(\sum_{i=0}^n \lambda^i \Psi^{(i)} \right) = \left(\sum_{i=0}^n \lambda^i E^{(i)} \right) \left(\sum_{i=0}^n \lambda^i \Psi^{(i)} \right) \quad (II-31)$$

The k th-order perturbation equation is given by equating the factors of λ^k in this equation. From *RS perturbation theory* the MP energy correction is obtained by using the following perturbation:

$$\hat{V} = \hat{H} - \left(F + \langle \Phi_0 | \hat{H} - F | \Phi_0 \rangle \right) \quad (\text{II-32})$$

where Φ_0 is the lowest eigenfunction of the Fock-operator:

$$F\Phi_0 = \left(\sum_{k=1}^N \hat{f}(k) \right) \Phi_0 = 2 \left(\sum_{i=1}^{N/2} \varepsilon_i \right) \Phi_0 \quad (\text{II-33})$$

where N is the number of the electrons and ε_i is the orbital energy of the doubly occupied orbital φ_i . The zeroth-order operator can be defined as:

$$\hat{H}_0 = F + \langle \Phi_0 | \hat{H} - F | \Phi_0 \rangle \quad (\text{II-34})$$

The zeroth-order energy is the value of \hat{H} with respect to the Slater determinant Φ_0 which is in turn the eigenfunction of F :

$$F\Phi_0 - \langle \Phi_0 | F | \Phi_0 \rangle \Phi_0 = 0 \Rightarrow \hat{H}_0 \Phi_0 = \langle \Phi_0 | \hat{H} | \Phi_0 \rangle \Phi_0 \quad (\text{II-35})$$

so that

$$E_{MP0} = E_{HF} = \langle \Phi_0 | \hat{H} | \Phi_0 \rangle \quad (\text{II-36})$$

whereas the first-order MP energy is equal to zero:

$$E_{MP1} = \langle \Phi_0 | \hat{V} | \Phi_0 \rangle = 0 \quad (\text{II-37})$$

To obtain an improvement on the Hartree-Fock energy it is therefore necessary the use of the Møller-Plesset perturbation theory to at least second order (MP2)⁴. The energy is given by the second order RS perturbation theory formula written on basis of doubly excited Slater determinants:

$$E_{MP2} = \sum_{i,j,a,b} \langle \varphi_i(1)\varphi_j(2) | r_{12}^{-1} | \varphi_a(1)\varphi_b(2) \rangle \left(\frac{2 \langle \varphi_a(1)\varphi_b(2) | r_{12}^{-1} | \varphi_i(1)\varphi_j(2) \rangle - \langle \varphi_a(1)\varphi_b(2) | r_{12}^{-1} | \varphi_j(1)\varphi_i(2) \rangle}{\varepsilon_i + \varepsilon_j - \varepsilon_a - \varepsilon_b} \right) \quad (\text{II-38})$$

where φ_i and φ_j are the occupied orbitals whereas φ_a and φ_b are the virtual orbitals. The values ε_i , ε_j , ε_a and ε_b are the corresponding orbitals energies.

The MP2 calculation represents the most popular way to incorporate a part of the *correlation energy* in quantum mechanical calculation. Among all the *post-HF methods*, it is the least computationally intensive so assuring a good compromise between accuracy and computational time. Finally, it is worth to underline that the MP perturbation theory is not variational so that energies lower than the exact energy can be obtained.

1.7. The Coupled-Cluster (CC) theory

Another popular perturbation correction method is the *coupled-cluster (CC)* method suggested in 1966 by Cizek⁵. According to this theory the wavefunction can be expressed in an exponential form:

$$\Psi = e^{\hat{T}} \Psi_{HF} \quad (\text{II-39})$$

where \hat{T} is an excitation operator that produces a linear combination of excited Slater determinants. It is named *cluster operator* and it can be written in the following form:

$$\hat{T} = \hat{T}_1 + \hat{T}_2 + \hat{T}_3 + \dots + \hat{T}_n \quad (\text{II-40})$$

where n is the total number of electrons. The \hat{T}_i operators generate all possible determinants having i excitations. For instance:

$$\hat{T}_1 = \sum_i \sum_a t_i^a \hat{a}_i \hat{a}_a^\dagger \quad (\text{II-41})$$

$$\hat{T}_2 = \frac{1}{4} \sum_{i,j} \sum_{a,b} t_{ij}^{ab} \hat{a}_i \hat{a}_j \hat{a}_a^\dagger \hat{a}_b^\dagger \quad (\text{II-42})$$

where i and j indicate the occupied orbitals, a and b the unoccupied ones and \hat{a} and \hat{a}^\dagger are annihilation operators. In order to find the approximate solution of $|\Psi\rangle$ the unknown coefficients t_i^a and t_{ij}^{ab} have to be solved. The exponential operator can be expanded into Taylor series like in the following expression:

$$e^{\hat{T}} = 1 + \hat{T} + \frac{\hat{T}^2}{2!} + \dots = 1 + \hat{T}_1 + \hat{T}_2 + \frac{\hat{T}_1^2}{2} + \hat{T}_1 \hat{T}_2 + \frac{\hat{T}_2^2}{2} + \dots \quad (\text{II-43})$$

Since the number of occupied orbitals as well as the number of excitations are finite, this series is non unlimited. For instance, if we consider the double excitation operator we make the approximation $\hat{T} = \hat{T}_2$ obtaining the CCD energy (coupled cluster with only double excitation operator):

$$\Psi_{CCD} = e^{\hat{T}} \Psi_{HF} = \left(1 + \hat{T}_2 + \frac{\hat{T}_2^2}{2!} + \frac{\hat{T}_2^3}{3!} + \dots \right) \Psi_{HF} \quad (\text{II-44})$$

In a computational point of view, the determination of the coefficients t for all the operators included in the particular approximation represents the main problem. The usual procedure consist of left-multiplying the Schrödinger equation by trial wave functions expressed as determinants of the HF orbitals. The obtained equations are solved iteratively so that the coefficient t are derived and the coupled-cluster energy is computed as:

$$\langle \Psi_{HF} | H | e^{\hat{T}} \Psi_{HF} \rangle = E_{CC} \quad (\text{II-45})$$

The insertion of single excitations in addition to doubles gives the CCSD model whereas the CCSDT one is obtained including triple excitations. This last is computationally very costly and intractable for most of the systems so that several approaches to estimating the effects of the connected triples using perturbation theory have been developed. Among them, CCSD(T)⁶ is the most commonly used. It fully includes singles and doubles whereas triples are computed with perturbation theory.

1.8. The Density Functional Theory

As above discussed, the main approximation of the Hartree-Fock theory is that the *correlation energy* is not taken into account while the *exchange contribution* is exactly computed. Although the post-HF methods are able to partly add this contribution, the computational cost is much higher as confirmed by their different *scaling* (the parameter indicating the time evolution of a calculation with respect to the number n of the basis functions used). Indeed, if the scaling factor for HF method is n^4 , for the post-HF methods is at least n^5 . For instance, scaling values of n^5 and n^8 characterize respectively the methods MP2 and CCSD(T). The correlation energy can be evaluated using an alternative approach given by the *Density Functional Theory* (DFT). The main idea of DFT consists in describing a system not via its many-body wave function but via its electronic density $\rho[\vec{r}]$, a physical observable which is a function of only three spatial coordinates. The first attempt in this direction was made by Thomas and Fermi^{7,8} at about the same time of the work of Hartree (1927-1928). After proposing the full electronic density as the fundamental variable of the many-body problem, they derived a differential equation for the density without reporting the one electron orbitals. Although it set up the basis for the later development of the DFT, the Thomas-Fermi approximation was too crude because of the lack of both exchange and correlation effects.

About 40 years have been necessary before having the formulation of the theorems of Hohenberg and Kohn that put on solid mathematical grounds the idea of Thomas and Fermi and which represent the theoretical basis of the DFT method. The main advantage of this method relies on the low computational cost. Indeed, although the correlation energy is included, the scaling factor is evaluated to n^3 which is lower than the HF method. This gain is due to the specific properties of the electronic density. Indeed, if the HF and post-HF methods are based on the wavefunction which has no physical meaning, the electronic density $\rho(\vec{r})$ used by the DFT is a measurable physical observable depending upon only three spatial variables. Notably, $\rho(\vec{r})$ is definable as the number of electrons per unit volume and can be linked to the wavefunction using the following expression:

$$\rho(\vec{r}) = \Psi^*(\vec{r})\Psi(\vec{r}) = |\Psi^2(\vec{r})| \quad (\text{II-46})$$

The main idea of the DFT is that the ground state energy can be written explicitly as a functional of the electronic density:

$$E_0 = E[\rho] \quad (\text{II-47})$$

The total number of the electrons n is given by the integration of ρ over all space. As above mentioned, following the Born-Oppenheimer approximation, the Hamiltonian can be expressed as:

$$\hat{H}_{el} = \hat{T}_e + \hat{V}_{Ne} + \hat{V}_{ee} = -\frac{1}{2} \sum_{i=1}^N \nabla_i^2 - \sum_{i=1}^N \sum_{A=1}^M \frac{Z_A}{r_{iA}} + \sum_{i=1}^{N-1} \sum_{j>i}^N \frac{1}{r_{ij}} \quad (\text{II-48})$$

where

$$\hat{V}_{Ne} = V_{ext}(\vec{r}) = \sum_{i=1}^N \sum_{A=1}^M \frac{Z_A}{r_{iA}} \quad (\text{II-49})$$

The Hohenberg and Kohn theorems prove that the external potential $V_{ext}(\vec{r})$ is a functional of the electronic density so that the Schrödinger equation can be solved within the Born-Oppenheimer approximation. Furthermore the density that minimizes the total energy is the exact groundstate density. In other words, the ground state energy can be obtained variationally.

The Hohenberg-Kohn theorems

The *first theorem of Hohenberg and Kohn*⁹ proves that for any system of interacting particles in an external potential $V_{ext}(\vec{r})$ the density is uniquely determined. In other words, the external potential and consequently the energy are unique functional of the electronic density:

$$E[\rho] = F_{HK}[\rho] + \int \rho(\vec{r}) V_{ext}(\vec{r}) d\vec{r} \quad (\text{II-50})$$

where F_{HK} represents the so-called *universal functional* of Hohenberg and Kohn. It includes the kinetic and the electron-electron repulsion terms which are indeed independent from the potential and therefore equivalent in all the multielectronic systems:

$$F_{HK}[\rho] = T[\rho] + V_{ee}[\rho] \quad (\text{II-51})$$

According to the second theorem of Hohenberg and Kohn the ground state energy can be obtained variationally: the density that minimizes the total energy is the exact real density. In other words, the energy obtained as functional of an approximate electronic density $\tilde{\rho}$ is higher or equal to the real energy of the system in the ground state.

$$E[\tilde{\rho}] \geq E[\rho] \quad (\text{II-52})$$

Although the Hohenberg-Kohn theorems are extremely powerful, they do not offer a way of solving the Schrödinger equation because of the presence of an electron-electron interaction term in the Hamiltonian. Indeed, if the density ρ for which the energy is minimal is easily obtained from the corresponding wavefunction Ψ using the equation (II-46), an infinite number of wavefunctions can be associated to the same electronic density.

The Kohn-Sham method

A key breakthrough to overcome this problem has been obtained by Kohn and Sham¹⁰. They realized that things would be considerably simpler if the real Hamiltonian is substituted by a fictitious Hamiltonian describing a non-interacting system of N electrons characterized by the same density of the real system where the electrons do interact. For this system, the mono-electronic operator of Kohn and Sham is:

$$\hat{H}_{KS} = -\frac{1}{2}\nabla_i^2 + V_{KS}(\vec{r}) \quad (\text{II-53})$$

where

$$V_{KS}(\vec{r}) = \int \frac{\rho(\vec{r}) - \rho(\vec{r}')}{|\vec{r} - \vec{r}'|} d\vec{r}' + V_{xc}[\rho] + V_{ext}(\vec{r}) \quad (\text{II-54})$$

$V_{xc}[\rho]$ is named exchange-correlation potential. It can be described as the one-electron operator for which the expectation value of the corresponding energy is the exchange-correlation energy E_{xc} :

$$V_{xc}(\vec{r}) = \frac{\delta E_{xc}[\rho]}{\delta \rho} \quad (\text{II-55})$$

The evaluation of this energy contribution represents the main problem of DFT based methods since the exact exchange and correlation functional is still not known. Keeping in mind the definition of the Kohn-Sham one-electron operator, we can undertake now the usual fashion to find orbitals (named *Kohn-Sham orbitals*) that minimize the energy of the system:

$$\hat{H}_{KS}\psi_i = \varepsilon_i\psi_i \quad (\text{II-56})$$

where the total energy can be described as sum of different specific contributions:

$$E_{KS}[\rho] = T_s[\rho] + J[\rho] + E_{xc}[\rho] + \int V_{ext}(\vec{r})\rho(\vec{r})d\vec{r} \quad (\text{II-57})$$

where $T_s[\rho]$ represents the kinetic energy of the non-interacting electrons system, $J[\rho]$ the classical electron-electron repulsion, $E_{xc}[\rho]$ the exchange correlation energy and finally $\int V_{ext}(\vec{r})\rho(\vec{r})d\vec{r}$ the interaction energy with the external potential.

The exchange-correlation energy can be therefore expressed as:

$$E_{xc}[\rho] = (T_{real}[\rho] - T_S[\rho]) + (V_{ee}[\rho] - J[\rho]) = \Delta T - \Delta V_{ee} \quad (\text{II-58})$$

where ΔT represents the correction to the kinetic energy deriving from the interacting nature of the electrons while ΔV_{ee} represents all the non-classical corrections to the electron-electron repulsion energy. So, although E_{xc} is typically referred as the exchange-correlation energy, the term includes also the correction for the classical self-interaction energy and for the difference in kinetic energy between the fictitious non-interacting system and the real one. The differences with the Hartree Fock approximation are evident. Indeed, if HF is a deliberately approximate theory whose development was motivated by the ability to solve the Schrödinger equation, the Kohn-Sham method is in principle a exact theory where the relevant equations must be solved approximately because a key operator has unknown form. So, significant research effort has gone into finding functionals of the density that may be expected to give reasonable E_{xc} in order to make this method more and more accurate.

Exchange-correlation Functionals

The exchange-correlation energy is computed through the so-called exchange-correlation functional F_{xc} :

$$E_{xc}[\rho] = \int F_{xc}[\rho] d\vec{r} \quad (\text{II-59})$$

For matter of clarity, it is opportune to adopt some notations normally used in this field. For instance, the functional dependence of E_{xc} on the electron density is expressed as an interaction between the electron density ρ and the so-called *energy density* ε_{xc} depending on ρ :

$$E_{xc}[\rho] = \int \rho \cdot \varepsilon_{xc}[\rho] d\vec{r} \quad (\text{II-60})$$

where the energy density is treated as a sum of individual exchange and correlation contributions.

Furthermore E_{xc} can be defined as the sum of the exchange and correlation contributions:

$$E_{xc}[\rho] = E_x[\rho] + E_{corr}[\rho] \quad (\text{II-61})$$

Several classes of approximations to the exchange-correlation energy functional have been developed. In the *local density approximation* (LDA)¹¹ the value of the energy density ε_{xc} at some position can be computed only from the value of ρ at that position. In other words, in the LDA approximation the electronic density is assumed locally uniform so that $E_{xc}^{LDA}[\rho]$ is function of the electronic density only. Because of this assumption, the LDA approximation is appropriate only for systems where the electron density is almost spatially uniform, that is typically not true for most of the molecular systems. One way to improve the approximation consist in making the functional dependent not only on the local value of the density but also on the so-called gradient

of the density which is definable as the degree to which the density is locally changing. All the functionals including this gradient correction defines the *generalized gradient approximation* (GGA) family:

$$E_{xc}^{GGA}[\rho] = \int \rho \cdot \varepsilon_{xc}[\rho, \nabla \rho] d\vec{r} \quad (\text{II-62})$$

The first popular GGA exchange functionals have been developed by Becke and are simply abbreviated with B as for instance B88¹² or B97¹³ whereas the most widely used GGA correlation functional was proposed by Lee, Yang and Parr (LYP).¹⁴

A natural development of the GGA approximation is represented by the so-called meta-GGA functionals. Indeed, in addition to the local density and to the gradient of the local density they employ the noninteracting kinetic energy term formed by the Kohn-Sham orbitals ψ_i :

$$T(r) = \frac{1}{2} \sum_i (\nabla \psi_i(r))^2 \quad (\text{II-63})$$

Examples of meta-GGA functionals are the models named VSXC¹⁵ and B97D.¹⁶

Another family consist of the so-called *global hybrids (GH) functionals* that combine a piece of Hartree-Fock exchange in a GGA (or meta-GGA) functional so that the exchange energy is composed by both DFT and HF contributions. Among the large family of functionals used in the present work two hybrid functionals have been proved to be the best characterizing our investigated systems. They are the functional proposed by Boese and Martin¹⁷ for the exploration of reaction mechanisms and named BMK (42% of HF exchange) and the B3LYP model¹⁸ (20% of HF exchange) which is based on the exchange-correlation functionals by Becke¹² and Lee, Yang and Parr¹⁴:

$$E_{xc}^{B3LYP} = (1-a)E_x^{LSDA} + aE_x^{HF} + b\Delta E_x^B + (1-c)E_c^{LSDA} + cE_c^{LYP} \quad (\text{II-64})$$

where the parameters a (0.20), b (0.72) and c (0.81) have been obtained through the computation of atomistic energies, ionization potentials and electronic affinities of a range of appropriately selected molecules¹⁹.

The *Range-Separated hybrids* and the *Doubly hybrids* represents two subcategories of the *hybrid functionals* family. In the *Range-Separated hybrids* the Coulomb potential is separated into a short- and long-ranged part and these contributions are treated separately.^{20,21} Examples are given by the CAM-B3LYP²² and ω -B97X²³ models. The former characterized by 19% (short range) and 65% (long range) of HF exchange while the latter including 16% (short range) and 100% (long range) of such contribution.

Finally, in the so called *Doubly hybrids* models,²⁴ MP2 correlation energy (mixed with a semilocal correlation density functional) is also included. One of the most representative functionals of this family is B2PLYP²⁴ which includes 53% of HF exchange.

1.9. Statistical thermodynamics and partition function

The connection between microscopic and macroscopic properties of a molecular system is assured by the statistical thermodynamic.²⁵⁻²⁷ Just as the microscopic system is described by a fundamental function as the wave-function or the density function, so too the macroscopic properties can be computed by using a fundamental function called *partition function*. For the thermodynamic state in which the number of particles N , the volume V and the temperature T are kept constant (called canonical ensemble) the partition function Q can be defined as:

$$Q(N, V, T) = \sum_i e^{-E_i(N, V)/k_B T} \quad (\text{II-65})$$

where i runs over all the energy states of the system with the energy E_i and k_B is the Boltzmann's constant. The partition function Q can be then used to define all the following macroscopic properties:

$$U = k_B T^2 \left(\frac{\partial \ln Q}{\partial T} \right)_{N, V} \quad (\text{II-66})$$

$$H = U + PV \quad (\text{II-67})$$

$$S = k_B \ln Q + k_B T \left(\frac{\partial \ln Q}{\partial T} \right)_{N, V} \quad (\text{II-68})$$

$$G = H - TS \quad (\text{II-69})$$

where U is the internal energy, H the enthalpy, P is the pressure, S the entropy and G the Gibbs free energy.

Despite these well established relations, the complexity of the partition function Q makes necessary some approximations.

Assuming that the particles do not interact with one another, the partition function can be rewrote as:

$$Q(N, V, T) = \frac{[q(V, T)]^N}{N!} \quad (\text{II-70})$$

where $q(V, T)$ is the partition function of the isolated molecule. In other words, the problem has been simplified from finding the partition function Q for the whole ensemble to finding the simpler molecular partition function q definable as:

$$q(V, T) = \sum_k g_k e^{-\varepsilon_k/k_B T} \quad (\text{II-71})$$

where k refers to all the possible energetic levels, g_k is the degeneration of each level and ε is the molecular energy. This last is assumed to be the sum of electronic, translational, rotational and vibrational terms:

$$\varepsilon = \varepsilon_{elec}(T) + \varepsilon_{trans}(V, T) + \varepsilon_{rot}(T) + \varepsilon_{vib}(T) \quad (\text{II-72})$$

Consequently the molecular partition function q can be now defined as:

$$q = q_{elec}(T)q_{trans}(V,T)q_{rot}(T)q_{vib}(T) \quad (II-73)$$

Therefore, thanks to this approximate treatment, the calculation of the partition function q relies on the computation of their different components.

Electronic partition function

The electronic contribution to the partition function q can be expressed as:

$$q_{elec}(T) = g_0 e^{-\varepsilon_0/k_b T} + g_1 e^{-\varepsilon_1/k_b T} + \dots + g_k e^{-\varepsilon_k/k_b T} \quad (II-74)$$

This expression can be simplified thanks to two approximations. Firstly the energy of the excited states is too high to make a significant contribution in this equation due to the difference between the ground state energy and the excited states energy which is much higher than $k_b T$. Assuming, moreover, that the ground state electronic energy is $\varepsilon_0=0$ we can write:

$$q_{elec} = g_0 \quad (II-75)$$

In other words, the electronic contribution to the partition function is equal to the spin multiplicity of the system and it is assumed to be independent from temperature. The contribution to the entropy can be expressed as :

$$S_{elec} = R \ln q_{elec} \quad (II-76)$$

Translational partition function

The only contribution depending on both temperature and volume is the translational contribution :

$$q_{trans}(V,T) = \left(\frac{2\pi M k_B T}{h^2} \right)^{3/2} V \quad (II-77)$$

where M is the molecular mass and h is the Plank's constant. The translational contributions to entropy and internal energy can be expressed as:

$$S_{trans} = R \left(\ln q_{trans} + \frac{5}{2} \right) \quad (II-78)$$

$$U_{trans} = \frac{3}{2} RT \quad (II-79)$$

Rotational partition function

If I_A , I_B and I_C are the principal moments of inertia and σ is the symmetry number, the rotational contribution can be wrote as:

$$q_{rot}(T) = \frac{\pi^{1/2}}{\sigma} \left(\frac{8\pi^2 k_B T}{h^2} \right)^{3/2} \sqrt{I_a I_b I_c} \quad (II-80)$$

where σ is 1 for asymmetric linear molecules and 2 for symmetric linear molecules. The estimation of the rotational components of the internal energy and entropy is given by:

$$U_{rot} = \frac{3}{2}RT \quad (\text{II-81})$$

$$S_{rot} = R \left(\ln q_{rot} + \frac{3}{2} \right) \quad (\text{II-82})$$

Vibrational partition function

Considering a molecule having N atoms, there are $3N-6$ ($3N-5$ if the molecule is linear) mode of vibrations i and frequencies ν . The main assumption for the vibrational contribution evaluation consist of approximate the modes as harmonic oscillators. In addition, the *zeroth* vibrational level is assumed to be zero so that the individual mode's partition function can be written as:

$$q_{vib,i}(T) = \frac{1}{1 - e^{-h\nu_i/k_B T}} \quad (\text{II-83})$$

whereas focusing on the full vibrational partition function for each mode we have:

$$q_{vib}(T) = \prod_i^{3N-6} \frac{1}{1 - e^{-h\nu_i/k_B T}} \quad (\text{II-84})$$

where the upper limit is $3N-5$ for a linear molecule. The estimation of the vibrational components of the internal energy and entropy gives:

$$S_{vib} = R \sum_i^{3N-6} \left(\frac{h\nu_i}{k_B T (e^{h\nu_i/k_B T} - 1)} \right) - \ln(1 - e^{-h\nu_i/k_B T}) \quad (\text{II-85})$$

$$U_{vib} = R \sum_i^{3N-6} \left(\frac{h\nu_i}{k_B T (e^{h\nu_i/k_B T} - 1)} \right) \quad (\text{II-86})$$

Although the described partition functions allow for an effective connection between the microscopic and the macroscopic properties of a system, it is worth to underline that correction factors are often necessary in order to have a better agreement with the experimental values. This is due to the approximations used to solve the Schrödinger equation and mainly concerns the frequencies values for which a *scaling factor* (constant for a given level of theory) is used. The vibrational contribution has been the unique considered in the present thesis.

2. Molecular Mechanics (MM)

Because of their computational cost, the main limitation of QM methods is the limited size of the system that can be modeled. Larger systems can be studied by using molecular mechanics (MM) based methods²⁸. Thanks to the different way to treat nuclei and electrons in the molecule, they are, in fact, lower computationally expensive. Notably, no wave function or total electron density are taken into account and the energy expression consist of a simple

algebraic equation rather than complex integral evaluations. The molecular mechanical methods are based on the following principles:

- The electrons are not explicitly examined at all but are assumed to find an optimal distribution around the nuclei. Nuclei and electrons lumped together are treated as atom-like particles (spheres).
- Bonds between particles are viewed as harmonic oscillators (springs).
- The different interactions are described through individual potential functions: bond stretching, angle bending, torsional energies and non-bonded interactions.
- The potential energy functions contain parameters which are derived empirically or through highly accurate ab-initio calculations.

2.1. Force Field

In Molecular Mechanics the collection of parameters defining the atoms and the interaction potentials as well as the resulting energy expression is named *force field* (FF). According to its orbital hybridization and bonding connectivity each atom is viewed as a defined type (*atom type*) described by particular parameters which are included in the energy expression. For instance, a sp^3 and a sp^2 carbon are treated differently because of the different hybridization. Furthermore, most of the FF parameterize atoms for specific functional group so that for instance the carbonyl oxygen in a carboxylic acid is described differently than the carbonyl oxygen in a ketone. Although different FF have been developed for different classes of molecules including small organic molecules (MM3),²⁹ biopolymers (AMBER³⁰, GAFF^{31,32}) or organic molecules in condensed phase (OPLS-AA)³³, the same general energy expression is used:

$$E_{tot} = E_s + E_b + E_w + E_{nb} \quad (\text{II-87})$$

Where E_s is the energy contribution for bond stretching, E_b is the energy due to the bond angle bending and E_w is the torsional energy for the twisting about dihedral angles (Figure 1) while E_{nb} is the energy for non bonded interactions such as Van der Waals and electrostatic interactions.

Most of the FF define the stretching and the bending interactions through an harmonic oscillator equations:

$$E_s = \sum_{N_b} \frac{1}{2} k_s (l - l_0)^2 \quad (\text{II-88})$$

$$E_b = \sum_{N_a} \frac{1}{2} k_b (\theta - \theta_0)^2 \quad (\text{II-89})$$

Where N_b and N_a are respectively the total number of bonds and the total number of angles in the molecule, k_s and k_b are the FF force constants assigned to each pair of bonded atoms (k_s) and to each triplet of atoms defining an angle (k_b). The actual bond and angle are expressed respectively by l and θ while the corresponding equilibrium values by the

predetermined parameters l_0 and θ_0 . It is worth to underline that several factors can be taken into account to improve the accuracy of these terms. For instance, some FF include the so-called "cross terms" to account for correlations between stretch and bend components.

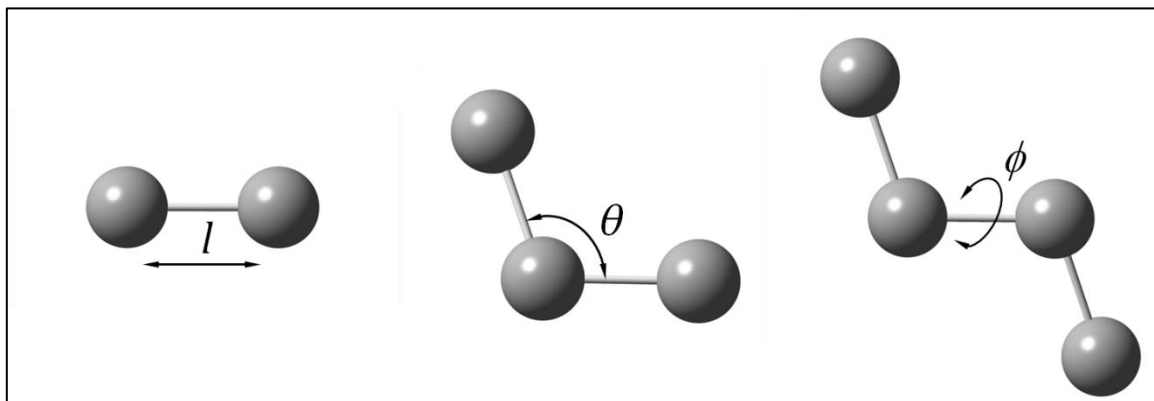


Figure 1: Internal coordinates for molecular mechanics interactions: l governs bond stretching, θ represents the angle term, ϕ gives the dihedral angle.

Differently from stretching and bending contributions, the proper description of the torsional potential requires a form that reflects its inherent periodicity. This is allowed by a cosine expression:

$$E_w = \sum_{N_d} k_d [1 + \cos(n\phi - \phi_0)] \quad (\text{II-90})$$

where N_d is the total number of dihedrals in the molecule, k_d the force constant assigned to each dihedral, n is the periodicity of the rotation (number of cycles in 360°) whereas ϕ and ϕ_0 are respectively the current and the equilibrium value for each dihedral. As with stretch and bend components, other terms may be included depending on the requested accuracy and the availability of data on which to base parameters.

The final term contributing to E_{tot} is the energy given by non bonded interactions which are most often treated as combination of the electrostatic and Van der Waals (VDW) forces. The electrostatic contribution is modeled using a Coulombic potential whereas the VDW interactions are typically described by Leonard-Jones equations:

$$E_{nb} = \sum_{N_{nb}} \left\{ \frac{q_i q_j}{r_{ij}} + 4\epsilon_{ij} \left[\left(\frac{\sigma_{ij}}{r_{ij}} \right)^{12} - \left(\frac{\sigma_{ij}}{r_{ij}} \right)^6 \right] \right\} \quad (\text{II-91})$$

where N_{nb} is the number of pairs of atoms for which the non-bonded interactions are considered, r_{ij} is the distance between the two atoms i and j whereas q_i and q_j are their partial charges that

are treated as a fixed parameters defining all atoms of a given type. ε_{ij} and σ_{ij} are VDW parameters determined following the *Lorentz-Berthelot* mixing rule:

$$\varepsilon_{ij} = \sqrt{\varepsilon_i \varepsilon_j} \quad (\text{II-92})$$

$$\sigma_{ij} = \frac{1}{2}(\sigma_i + \sigma_j) \quad (\text{II-93})$$

where ε_i and ε_j indicate the depth of the potential well created by a pair of atoms i and j respectively whereas σ_i and σ_j refer to the diameter of the sphere approximating such atoms.

Van der Waals and electrostatic contributions are usually not computed for atoms that are at a distance of one or two bonds in a given molecule. This is done in order to overcome numerical problems. Indeed, the potential can become strongly repulsive or attractive because of the small distances involved so that the interactions between such atoms are considered to be already correctly described by the intramolecular terms. The closest interacting centers are separated by at least three bonds and relative to each other in 1-4 position. These types of interactions, often referred as *1,4-vdw* and *1,4-el*, are considered separately with respect to the interactions between atoms separated by more than three bonds which are treated in the same way as if they were intermolecular. *1,4-vdw* and *1,4-el* interactions are, in fact, scaled by a scaling factor depending on the used FF. Finally, it is worth to underline that in order to reduce the computational cost most of the FF use a distance value (named *cutoff*) beyond which all the non-bonded interactions are ignored.

2.2. Molecular Dynamic simulations

Once having a way to compute the total energy of the system, the time-dependent behavior of a molecule can be studied using Molecular Dynamics (MD). By integrating the Newton's laws of motion successive configurations of the system are generated and a trajectory specifying how the positions and velocities of the particles in the system vary with time is obtained.

Basic principle

The trajectory is carried out by solving the differential equations embodied in the Newton's second law which is given by:

$$F_i = m_i a_i \quad (\text{II-94})$$

where F_i is the force exerted on the particle i , whereas m_i and a_i are respectively the mass and the acceleration of the same particle. Considering the simple case where the acceleration is constant:

$$a_i = \frac{dv_i}{dt} = \frac{d^2 x_i}{dt^2} \quad (\text{II-95})$$

where v_i and x_i are respectively the velocity and the position of the particle i . After integration, the velocity of the particle i in the time t can be expressed as:

$$v_i(t) = a_i t + v_i(0) \quad (\text{II-96})$$

there $v_i(0)$ is the initial velocity of the particle i . We can now once again integrate to obtain:

$$x_i(t) = v_i(t)t + x_i(0) \quad (\text{II-97})$$

and combining the (II-96) and (II-97) we obtain the following relation which gives the position of the particle in the time t as a function of the initial position $x_i(0)$, the initial velocity $v_i(0)$ and the acceleration a :

$$x_i(t) = a_i t^2 + v_i(0)t + x_i(0) \quad (\text{II-98})$$

Therefore, to compute a trajectory, together with the initial positions of the atoms and an initial distribution of velocities only the acceleration is necessary that can be determined by the gradient of the potential energy function E :

$$a_i = -\frac{1}{m_i} \frac{dE}{dx_i} \quad (\text{II-99})$$

The Verlet integration algorithm

In a calculation of Molecular Dynamics an algorithm is required for integrating the equations of motion. There are many algorithms commonly used and all of them assume that positions x , velocities v and accelerations a can be approximated by expansions of Taylor series:

$$x(t + \delta t) = x(t) + \delta t v(t) + \frac{1}{2} \delta t^2 a(t) + \frac{1}{6} \delta t^3 b(t) + \dots \quad (\text{II-100})$$

$$v(t + \delta t) = v(t) + \delta t a(t) + \frac{1}{2} \delta t^2 b(t) + \frac{1}{6} \delta t^3 c(t) + \dots \quad (\text{II-101})$$

$$a(t + \delta t) = a(t) + \delta t b(t) + \frac{1}{2} \delta t^2 c(t) + \frac{1}{6} \delta t^3 d(t) + \dots \quad (\text{II-102})$$

where b , c , and d are respectively the third, the fourth and fifth derivative. The most widely used method for integration of motion is the *Verlet algorithm*³⁴ in which the new positions in the time $t + \delta t$ are computed by using positions and accelerations at time t and the positions from the previous step (time $t - \delta t$). Indeed, using the Taylor series expansions we can write:

$$x(t - \delta t) = x(t) - \delta t v(t) + \frac{1}{2} \delta t^2 a(t) - \frac{1}{6} \delta t^3 b(t) + \dots \quad (\text{II-103})$$

adding (II-100) and (II-103):

$$x(t + \delta t) = 2x(t) - x(t - \delta t) + \delta t^2 a(t) \quad (\text{II-104})$$

Note that the velocities do not appear explicitly in the *Verlet algorithm*. Nevertheless they can be calculated in various ways as for instance by dividing the difference in positions in time $t + \delta t$ and $t - \delta t$ by $2\delta t$:

$$v(t) = \frac{x(t + \delta t) - x(t - \delta t)}{2\delta t} \quad (\text{II-105})$$

The Verlet algorithm is widely used because computationally cheap. However, in order to overcome some of its disadvantages, several variations have been developed as for instance the leap-frog algorithm³⁵, the velocity Verlet method³⁶ and the Breeman's algorithm³⁷. In particular, one of its drawback is the lack of an explicitly velocity term in the equations making the velocities not available until the positions at the next step are computed.

Choosing the time step

Once the integration algorithm is selected, a suitable time step δt for the simulation has to be chosen. There are no rigid rules for selecting the most appropriate δt to use in MD. Obviously a time step that is too large will lead atoms to move too far along a given trajectory, thus inadequately simulating the motion whereas a time step too small will make the simulation too time requiring. One general rule is that the time step should be approximately one tenth the time of the shortest motion. For instance in flexible molecules the shortest period of motion is given by bond stretches, especially those involving hydrogen atoms for which the vibration has a repeat period of about 10 fs so that a time step of 1 fs is commonly used.

The thermodynamic ensembles

Molecular Dynamics simulations generate information at the microscopic level such as atomic positions and velocities. The connection between distribution and motion of the atoms and macroscopic properties such as temperature, pressure and energy is made via *statistical mechanics* which is the mathematical means to compute the thermodynamic properties of a material from a molecular description. In *statistical mechanics*²⁶ a small set of parameters as for instance the temperature T , the pressure P and the number of particles N define a *thermodynamic state*. Rather the *microscopic state* is defined by the atomic positions x and momenta p which are viewed as coordinates in a multidimensional space called *phase space* having $6N$ dimensions (where N is the number of the particles of the system). In other words, during a MD simulation a sequence of points in the *phase space* is generated as a function of time. The collection of points in phase space satisfying the conditions of a particular thermodynamic state is called *ensemble*. In the present thesis all the MD simulations have been performed in the *canonical ensemble* (NVT) which correspond to the thermodynamic state characterized by a fix number of atoms (N), a fixed volume (V) and a constant temperature (T). MD simulations can be also carried out in alternative ensemble such as the *microcanonical ensemble* NVE (where the energy is fixed while the temperature varies) and the NVP ensemble (where the pressure is constant and the temperature varies).

Molecular Dynamics at constant temperature

The first step of a MD simulation consist of assigning the initial velocities to the atoms. This is typically obtained through a random selection from a *Maxwell-Boltzmann* distribution providing the probability $p(v_{ix})$ that an atom i of mass m_i has a velocity v_{ix} in the direction x at the temperature of interest T :

$$p(v_{ix}) = \left(\frac{m}{2\pi k_b T} \right)^{1/2} \exp \left[-\frac{1}{2} \frac{m_i v_{ix}^2}{k_b T} \right] \quad (\text{II-106})$$

where k_b is the Boltzmann's constant. In a constant-temperature MD simulation (NVT ensemble) a method (named thermostat) able to prepare the system at the desired temperature (equilibration step) as well as to control the temperature during the simulation is necessary. For instance, this temperature monitoring is obtained scaling the velocity. Indeed, the relation between the imposed temperature T and the time average of the kinetic energy is given by:

$$\langle K \rangle_{NVT} = \frac{3}{2} N k_b T \quad (\text{II-107})$$

where N is the total number of the particles. In particular, the temperature can be controlled simply by multiplying the velocities at each step by a factor λ as in the *Woodcock* thermostat³⁸:

$$\lambda = \sqrt{T_2 / T_1} \quad (\text{II-108})$$

where T_2 is the desired temperature and T_1 the current temperature. The velocities are scaled also in the *Berendsen thermostat*³⁹. Nevertheless, here the temperature is maintained by coupling the system to an external heat bath fixed at the desired temperature. Other thermostats such as the *Langevin*⁴⁰ or the *Andersen*⁴¹ thermostat rely on adding stochastic forces and velocities. In particular, the *Andersen* temperature coupling scheme is a stochastic method in which the velocities are randomized by "imaginary" collisions. Notably, a particle is chosen by random selection at regular intervals and its velocity is randomly reassigned from the *Maxwell-Boltzmann* distribution.

2.3. Free energy calculations: the umbrella sampling technique

One of the limits of the MD simulations is the difficult sampling of regions in the phase space which are statistically less accessible. Indeed, the insufficient sampling of "*rare events*" can make the calculation of a free energy associated to a reaction mechanism or of a conformational change inaccurate because of the loosing of important contributions. One approach for overcoming this limit consists in utilizing a biasing potential (named *umbrella potential*) which is added to the force field energy as a function of the reaction coordinate.⁴² The Potential of Mean Force (PMF) defines the free energy when it is expressed as a function of reaction coordinates and it can be determined as:

$$W(\zeta) = -k_b T \ln[\rho(\zeta)] \quad (\text{II-109})$$

where $W(\zeta)$ is the potential of mean force, ζ the reaction coordinate, k_b the Boltzmann's constant, T the temperature and ρ represents the probability of the coordinate taking on a particular value. The reaction coordinate ζ is a function relating atomic positions x to the state ε :

$$\zeta = \varepsilon(x) \quad (\text{II-110})$$

The calculation of $W(\zeta)$ will be therefore not quite accurate if the sampling is insufficient at several states. The accuracy can be drastically improved dividing the reaction coordinate in several windows on which an "umbrella potential" is applied. Figure II-2 shows how the biasing potential is added: each color is a separate potential for which a different MD simulation is performed.

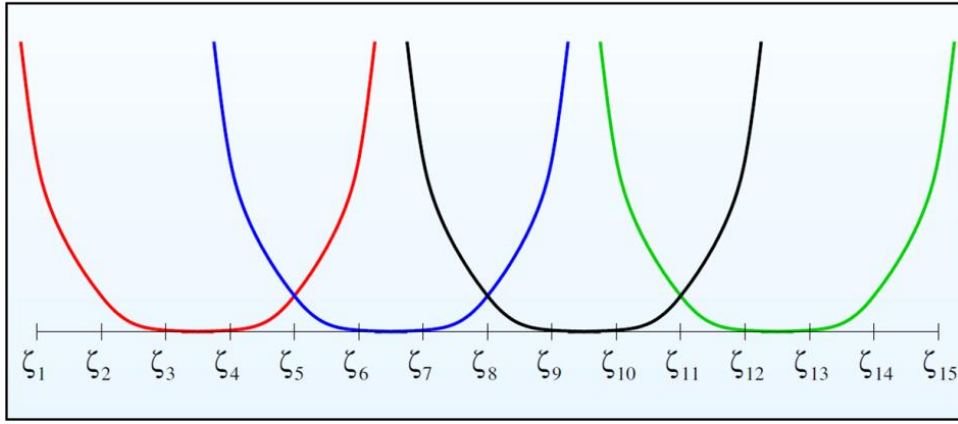


Figure II-1: Picture of umbrella potentials applied to different windows along the reaction coordinate.

The resulting different trajectories (one for each window) are then combined by using an algorithm called Weighted Histogram Analysis Method (WHAM)^{43,44} that allows to convert the biased potential into the unbiased one using all samples taken. Indeed, defining $\rho_i(\zeta)$ the unbiased probability of the i th window we can write:

$$\rho_i(\zeta) = e^{\beta(w_i(\zeta) - f_i)} \rho_i^{(b)}(\zeta) \quad (\text{II-111})$$

where $\beta = 1/(k_b T)$, $w_i(\zeta)$ is the i th biasing potential, $\rho_i^{(b)}(\zeta)$ is the i th biasing probability and f_i is the free energy from adding the biasing potential which is definable as:

$$e^{-\beta f_i} = \int e^{-\beta w_i(\zeta)} \rho(\zeta) d\zeta = \langle e^{-\beta w_i(\zeta)} \rangle \quad (\text{II-112})$$

so using a linear combination of unbiased probabilities:

$$\rho(\zeta) = \sum_{i=1}^N c_i(\zeta) \rho_i(\zeta) = \sum_{i=1}^N c_i(\zeta) (e^{\beta(w_i(\zeta) - f_i)} \rho_i^{(b)}(\zeta)) \quad (\text{II-113})$$

CHAPTER II: Theoretical background

where N is the total number of windows, $\rho(\zeta)$ is the total unbiased probability and $c_i(\zeta)$ are the so called "weights" which have to be defined in order to calculate the biased probabilities in each windows. First the weights are normalized:

$$\sum_{i=1}^N c_i(\zeta) = 1 \tag{II-114}$$

finally they are fully defined by minimizing the variance in $\rho(\zeta)$:

$$\frac{\partial \sigma^2[\rho(\zeta)]}{\partial c_i} = 0 \tag{II-115}$$

3. References

- (1) Born, D.; Oppenheimer J.R. On the Quantum Theory of Molecules. *Anm. Physik* **1927**, *84*, 457-484.
- (2) Hartree D.R. The wave mechanics of an Atom with a Non-Coulomb Central Field. Part II. Some results and Discussion. *Mathematical Proceedings of the Cambridge Philosophical Society* **1928**, *24*, 111-132.
- (3) Møller, C.; Plesset, M. S. Note on an Approximation Treatment for Many-Electron Systems. *Physical Review* **1934**, *46*, 618-622.
- (4) Head-Gordon, M.; Pople, J. A.; Frisch, M. J. MP2 energy evaluation by direct methods. *Chemical Physics Letters* **1988**, *153*, 503-506.
- (5) Cizek, J. On the Correlation Problem in Atomic and Molecular Systems. Calculation of Wavefunction Components in Ursell-Type Expansion Using Quantum-Field Theoretical Methods. *Journal of Chemical Physics* **1966**, *45*, 4256-4266.
- (6) Pople, J. A.; Head-Gordon, M.; Raghavachari, K. Quadratic configuration interaction. A general technique for determining electron correlation energies. *Journal of Chemical Physics* **1987**, *87*, 5968-5975.
- (7) Thomas L.H. The calculation of atomic fields. *Mathematical Proceedings of the Cambridge Philosophical Society* **1927**, *23*, 542-548.
- (8) Fermi E. Un Metodo Statistico per la Determinazione di alcune proprietà dell'atomo. *Rend. Acad. Maz. Lancei* **1927**, *6*, 602-607.
- (9) Hohenberg, P. Inhomogeneous Electron Gas. *Physical Review* **1964**, *136*, B864-B871.
- (10) Kohn, W.; Sham, L. J. Self-Consistent Equations Including Exchange and Correlation Effects. *Physical Review* **1965**, *140*, A1133-A1138.
- (11) Dirac, P.A.M. Note on Exchange phenomena in the Thomas atom. *Mathematical Proceedings of the Cambridge Philosophical Society* **1930**, *26*, 376-385.
- (12) Becke, A. D. Density-functional exchange-energy approximation with correct asymptotic behavior. *Physical Review A* **1988**, *38*, 3098-3100.
- (13) Becke, A. D. Density-functional thermochemistry. V. Systematic optimization of exchange-correlation functionals. *Journal of Chemical Physics* **1997**, *107*, 8554-8560.

CHAPTER II: Theoretical background

- (14) Lee, C.; Yang, W.; Parr, R. G. Development of the Colle-Salvetti correlation-energy formula into a functional of the electron density. *Physical Review B* **1988**, *37*, 785–789.
- (15) Van Voorhis, T.; Scuseria, G. E. A novel form for the exchange-correlation energy functional. *Journal of Chemical Physics* **1998**, *109*, 400–410.
- (16) Grimme, S. Semiempirical GGA-type density functional constructed with a long-range dispersion correction. *Journal of Computational Chemistry* **2006**, *27*, 1787–1799.
- (17) Boese, A. D.; Martin, J. M. L. Development of density functionals for thermochemical kinetics. *Journal of Chemical Physics* **2004**, *121*, 3405–3416.
- (18) Becke, A. D. Density-functional thermochemistry. III. The role of exact exchange. *Journal of Chemical Physics* **1993**, *98*, 5648.
- (19) Curtiss, L. A.; Raghavachari, K.; Trucks, G. W.; Pople, J. A. Gaussian-2 theory for molecular energies of first- and second-row compounds. *Journal of Chemical Physics* **1991**, *94*, 7221.
- (20) Savin, A.; Flad, H.J. Density functionals for the Yukawa electron-electron interaction. *International Journal of Quantum Chemistry* **1995**, *56*, 327–332.
- (21) Leininger, T.; Stoll, H.; Werner, H.J.; Savin, A. Combining long-range configuration interaction with short-range density functionals. *Chemical Physics Letters* **1997**, *275*, 151–160.
- (22) Yanai, T.; Tew, D. P.; Handy, N. C. A new hybrid exchange–correlation functional using the Coulomb-attenuating method (CAM-B3LYP). *Chemical Physics Letters* **2004**, *393*, 51–57.
- (23) Chai, J.D.; Head-Gordon, M. Systematic optimization of long-range corrected hybrid density functionals. *Journal of Chemical Physics* **2008**, *128*, 084106-084121.
- (24) Grimme, S. Semiempirical hybrid density functional with perturbative second-order correlation. *Journal of Chemical Physics* **2006**, *124*, 034108.
- (25) Cramer C. J. *Essential of Computational Chemistry-Theories and Models* (2nd edition). *John Wiley & Sons Ltd* **2004**, Chichester.
- (26) Knox J.H. *Molecular Thermodynamics - An introduction to Statistical Mechanics for Chemists*. *John Wiley & Sons*, **1978**.
- (27) Ochterski J.W. *Thermochemistry in Gaussian*. *Gaussian, Inc, Wallingford, CT*, **2000**, 1-19
- (28) Frenkel D.; Smit B. *Understanding molecular simulation, from algorithm to applications*. *2nd edition*, Academic press **2001**.

CHAPTER II: Theoretical background

- (29) Allinger, N. L.; Yuh, Y. H.; Lii, J. H. Molecular mechanics. The MM3 force field for hydrocarbons. 1. *Journal of the American Chemical Society* **1989**, *111*, 8551–8566.
- (30) Cornell, W. D.; Cieplak, P.; Bayly, C. I.; Gould, I. R.; Merz, K. M.; Ferguson, D. M.; Spellmeyer, D. C.; Fox, T.; Caldwell, J. W.; Kollman, P. A. A Second Generation Force Field for the Simulation of Proteins, Nucleic Acids, and Organic Molecules. *Journal of the American Chemical Society* **1995**, *117*, 5179–5197.
- (31) Wang, J.; Wolf, R. M.; Caldwell, J. W.; Kollman, P. A.; Case, D. A. Development and testing of a general amber force field. *Journal of Computational Chemistry* **2004**, *25*, 1157–1174.
- (32) Wang, J.; Wang, W.; Kollman, P. A.; Case, D. A. Automatic atom type and bond type perception in molecular mechanical calculations. *Journal of Molecular Graphics and Modelling* **2006**, *25*, 247–260.
- (33) Jorgensen, W. L.; Maxwell, D. S.; Tirado-Rives, J. Development and Testing of the OPLS All-Atom Force Field on Conformational Energetics and Properties of Organic Liquids. *Journal of the American Chemical Society* **1996**, *118*, 11225–11236.
- (34) Verlet, L. Computer “Experiments” on Classical Fluids. I. Thermodynamical Properties of Lennard-Jones Molecules. *Physical Review* **1967**, *159*, 98–103.
- (35) Hockney, R. W. The potential calculation and some applications. *Methods in Computational Physics* **1970**, *9*, 135–211.
- (36) Swope, W. C.; Andersen, H. C.; Berens, P. H.; Wilson, K. R. A computer simulation method for the calculation of equilibrium constants for the formation of physical clusters of molecules: Application to small water clusters. *Journal of Chemical Physics* **1982**, *76*, 637–649.
- (37) Beeman, D. Some Multistep Methods for Use in Molecular Dynamics Calculations. *Journal of Computational Physics* **1976**, *20*, 130–139.
- (38) Woodcock, L. V. Isothermal molecular dynamics calculations for liquid salts. *Chemical Physics Letters* **1971**, *10*, 257–261.
- (39) Berendsen, H. J. C.; Postma, J. P. M.; van Gunsteren, W. F.; DiNola, A.; Haak, J. R. Molecular dynamics with coupling to an external bath. *Journal of Chemical Physics* **1984**, *81*, 3684–3690.
- (40) Grest, G. S.; Kremer, K. Molecular dynamics simulation for polymers in the presence of a heat bath. *Physical Review A* **1986**, *33*, 3628–3631.

CHAPTER II: Theoretical background

- (41) Andersen, H. C. Molecular dynamics simulations at constant pressure and/or temperature. *Journal of Chemical Physics* **1980**, *72*, 2384–2393.
- (42) Torrie, G. M.; Valleau, J. P. Monte Carlo free energy estimates using non-Boltzmann sampling: Application to the sub-critical Lennard-Jones fluid. *Chemical Physics Letters* **1974**, *28*, 578–581.
- (43) Kumar, S.; Rosenberg, J. M.; Bouzida, D.; Swendsen, R. H.; Kollman, P. A. THE weighted histogram analysis method for free-energy calculations on biomolecules. I. The method. *Journal of Computational Chemistry* **1992**, *13*, 1011–1021.
- (44) Kumar, S.; Rosenberg, J. M.; Bouzida, D.; Swendsen, R. H.; Kollman, P. A. Multidimensional free-energy calculations using the weighted histogram analysis method. *Journal of Computational Chemistry* **1995**, *16*, 1339–1350.

CHAPTER III: DFT STUDY OF PROTON TRANSFER REACTIONS

In the present chapter the results concerning an in depth theoretical study of proton transfer (PT) reaction in different azolium-azole complexes will be discussed. The final part will be devoted to a brief description of a benchmark study on a set of chosen systems in which different kinds of PT reactions occur. The following results have been object of publications in *Journal of Physical Chemistry A*¹ (section 1) and *Journal of Chemical Theory and Computation*² (section 2).

1. Modeling proton transfer in imidazole-like dimers

1.1. Introduction

As mentioned in chapter I, azoles compounds such as imidazole, triazole and tetrazole have been object of a continued interest in the last years mainly because of their use in the high temperatures PEMFCs. Firstly as viable substitute of water and then as basic component of anhydrous conducting membranes, imidazole has been the first compound extensively studied among the different azoles. More recently, triazole and tetrazole derivatives have been taken into account especially as possible substitutes of imidazole in polymeric membranes. Interestingly, several experimental data have indicated that the imidazole substitution with such alternative azoles significantly improves the conductivity in some polymeric systems.³⁻⁵

As a consequence of the great experimental interest devoted to imidazole and imidazole-like proton conductors, the theoretical analysis of the elementary steps of the proton conduction in these systems has gained more and more attention in the last few years. Notably, PT reactions in imidazole dimers and oligomers have been widely explored mainly using DFT based methods⁶⁻¹⁰ and also considering classical simulations.¹¹ On the contrary, because of their more recent utilize, only few papers have been devoted to PT reactions occurring in triazoles and tetrazoles.^{10,12,13}

The intention of filling this gap and elucidate the differences between such azoles represent only one of the motivations which have driven the DFT investigation described and discussed in the following. The main driven force has been the intent of determining the most suitable approach able to accurately reproduce the energetic and the structural features of this

family of heterocycles in order to apply it for a further DFT investigation on larger systems (azole-based polymers). Indeed, although the performance of DFT for PT reaction has been deeply investigated in literature since many years (see references ^{14,15,16,17,18,19,20}), only a limited number of exchange-correlation functionals have been evaluated so far. Furthermore, these azole systems present some particular features as for instance the coupling between the delocalized π -electrons and the PT reaction so that peculiar effects on the PT energetic can be envisaged.

In the first part of the present chapter the outcomes concerning the application of several DFT approaches to the study of structures and PT mechanisms in imidazole, 1,2,3-triazole and tetrazole (Figure III-1) will be presented.

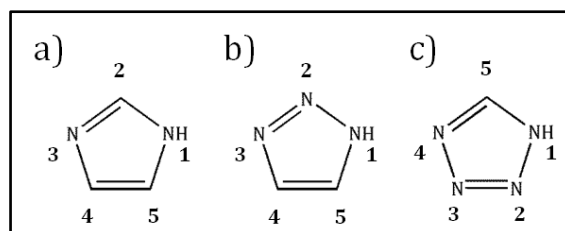


Figure III-1: Sketches and atom numbering of a) imidazole, b) 1,2,3-triazole and c) tetrazole.

1.2. Methodological details

All calculations have been performed using the Gaussian-09 package²¹. Among the large number of exchange correlation functionals present in literature, a representative set, including some of the most used and best performing DFT approaches for PT reaction, has been chosen. Notably, several *global hybrids (GH)* functionals have been selected: B3LYP,²² PBE0,²³ BMK,²⁴ X3LYP,²⁵ mPW1PW91,²⁶ M06HF,²⁷ and M062X.²⁸ To this set, the LC-wPBE model,^{29,30} belonging to the family of the so-called *range separated hybrids (RSH)*, has been added together with a recent exchange-correlation functional developed in our group and included as pure GGA approach (TCA³¹) or casted in a RSH model (LC-TCA³²).

In order to define the best compromise between accuracy and computational cost, three basis sets namely 6-31G(d), 6-311+G(d,p) and 6-311++G(2d,2p) and belonging to the Pople's basis set family have been considered.

Geometry optimizations at MP2 level^{33,34} and single point calculations at CCSD(T) level³⁵ have been also carried out in order to have accurate reference values. Notably, both MP2 and DFT structures have been taken into account for computing CCSD(T) energies.

Finally, harmonic vibrational frequency analysis has been undertaken in order to confirm the nature (minimum or transition state) of the localized stationary states. Such analysis has been performed at both DFT and MP2 levels.

1.3. Identification of the PT reaction mechanisms

In the case of imidazole-like complexes, the PT reaction consist of transferring the proton involved in the H-bond between two moieties, of which one is positive charged. Such a reaction is commonly modeled by means of the simplest models: protonated dimers^{6,10,12,13} (Figure III-2).

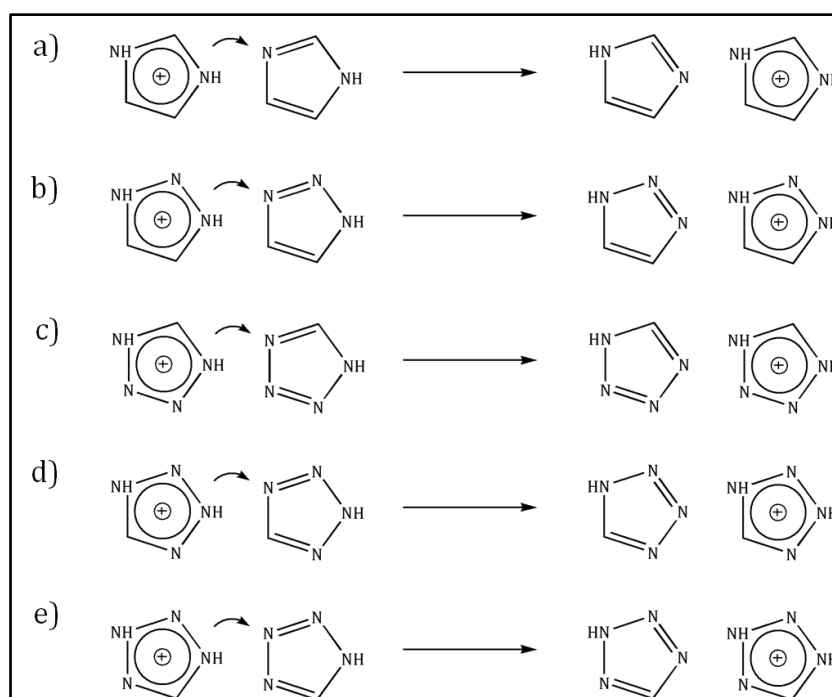


Figure III-2: Sketches of PT mechanisms in protonated dimers of a) imidazole, b) 1,2,3-triazole and c), d), e) tetrazoles.

As shown in figure III-2 (mechanism a), only one PT mechanism can be envisaged for protonated imidazoles ($\text{ImH}^+\text{-Im}$). Notably, the starting and the resulting complexes of such reaction are exactly alike with the two moieties switched/interchanged.

The presence of an additional proton donor/acceptor atom in 1,2,3-triazole (nitrogen atom in position 2) leads to hypothesize different PT reaction mechanisms for the protonated complex ($\text{TrH}^+\text{-Tr}$). Nevertheless, when the excess positive charge is transferred from or to the nitrogen atom in position 2, the complex involved (1,2-diH-1,2,3-triazolium-triazole) is considerably less stable (14.9 kcal/mol at MP2/6-311+G(d,p) level) than that considered when the proton passes from a nitrogen in position 3 to a nitrogen in position 1 (Figure III-2, b). This energy variation is mainly due to the delocalization of the positive charge which is much higher in 1,3-diH-1,2,3-triazolium-triazole than in 1,2-diH-1,2,3-triazolium-triazole. Also in this case, therefore, the PT mechanism is unique and characterized by equal initial and final rearrangements.

On the contrary, the presence of a fourth nitrogen atom in tetrazole leads to different stable tautomeric forms of the protonated complex (TeH⁺-Te). So, even discarding protonated tetrazoles in which the hydrogen atoms are in adjacent positions (because of the lower delocalization as in 1,2,3-triazole), several PT mechanisms can be envisaged (Figure III-2, mechanisms *c*, *d* and *e*). Only 1H-tautomers are involved in the mechanism *c* which is similar to those considered for protonated imidazoles and 1,2,3-triazoles: the final complex is the same of the starting one with the switched positions of the heterocycles. On the contrary, the resulting complex of the PT reaction *d* is different from the initial rearrangement. Indeed, during this PT mechanism the heterocycles change their tautomerism from 2H to 1H tautomer and viceversa if the opposite direction of conduction is considered (mechanism *e*). In other words, mechanisms *d* and *e* refer to two contrary directions of the same PT reaction.

All the reactions depicted in figure III-2 have been analyzed. For each mechanism, the nitrogen atom giving the proton will be referred as N_D (nitrogen donor) while the other nitrogen involved in the H-bond and so accepting the proton as N_A (nitrogen acceptor).

1.4. Basis Set selection

As above mentioned in chapter II, the selection of the *basis set* constitutes one of the critical steps for setting a quantum chemistry calculation with a good compromise between accuracy and speed. In this sense, the values of energetic barriers of proton transfer for mechanisms *a*, *b*, and *c* have been computed using three different basis sets (6-31G(d), 6-311+G(d,p), and 6-311++G(2d,2p)) and using both DFT (B3LYP and PBE0 functionals) and MP2 approaches (Table III-1).

Table III-1: Proton transfer activation energies (kcal/mol) for Imidazolium-Imidazole (ImH⁺-Im), 1,2,3-Triazolium-1,2,3-Triazole (TrH⁺-Tr), and Tetrazolium-Tetrazole (TeH⁺-Te) complexes computed using three different basis sets.

		ImH ⁺ -Im	TrH ⁺ -Tr	TeH ⁺ -Te
mechanism		<i>a</i>	<i>b</i>	<i>c</i>
6-31G(d)	MP2	1.3	1.6	3.4
	B3LYP	1.0	1.0	2.0
	PBE0	0.6	0.6	1.6
6-311+G(d,p)	MP2	0.5	0.4	1.4
	B3LYP	0.7	0.6	1.0
	PBE0	0.3	0.2	0.6
6-311++G(2d,2p)	MP2	0.6	0.7	1.8
	B3LYP	0.9	0.7	1.2
	PBE0	0.4	0.3	0.7

Table III-2: Computed N_D-H (Å), N_A-H (Å) and N_D-N_A (Å) distances for imidazolium-imidazol (ImH^+-Im) complex (mechanism a), 1,2,3-triazolium-1,2,3-triazole complex (mechanism b) and tetrazolium-tetrazole complex (mechanism c) using three different basis sets.

		ImH ⁺ -Im					
		minimum a			transition state		
		N_D-H	N_A-H	N_D-N_A	N_D-H	N_A-H	N_D-N_A
6-31G(d)	MP2	1.094	1.613	2.706	1.286	1.286	2.571
	B3LYP	1.096	1.606	2.702	1.286	1.286	2.572
	PBE0	1.111	1.543	2.655	1.279	1.279	2.558
6-311+G(d,p)	MP2	1.118	1.517	2.634	1.279	1.278	2.557
	B3LYP	1.108	1.562	2.670	1.286	1.286	2.572
	PBE0	1.127	1.501	2.628	1.279	1.279	2.558
6-311++G(2d,2p)	MP2	1.109	1.526	2.635	1.278	1.278	2.555
	B3LYP	1.102	1.569	2.671	1.285	1.285	2.567
	PBE0	1.124	1.499	2.623	1.278	1.278	2.555
		TrH ⁺ -Tr					
		minimum b			transition state		
		N_D-H	N_A-H	N_D-N_A	N_D-H	N_A-H	N_D-N_A
6-31G(d)	MP2	1.082	1.645	2.696	1.283	1.287	2.570
	B3LYP	1.098	1.596	2.686	1.285	1.285	2.571
	PBE0	1.108	1.550	2.651	1.278	1.280	2.557
6-311+G(d,p)	MP2	1.124	1.500	2.620	1.278	1.277	2.554
	B3LYP	1.117	1.539	2.654	1.286	1.286	2.571
	PBE0	1.143	1.465	2.607	1.278	1.280	2.558
6-311++G(2d,2p)	MP2	1.104	1.553	2.629	1.277	1.277	2.554
	B3LYP	1.109	1.551	2.658	1.285	1.285	2.570
	PBE0	1.131	1.485	2.615	1.277	1.277	2.554
		TeH ⁺ -Te					
		minimum c			transition state		
		N_D-H	N_A-H	N_D-N_A	N_D-H	N_A-H	N_D-N_A
6-31G(d)	MP2	1.059	1.747	2.731	1.282	1.283	2.565
	B3LYP	1.065	1.707	2.710	1.283	1.283	2.565
	PBE0	1.068	1.672	2.681	1.276	1.276	2.552
6-311+G(d,p)	MP2	1.072	1.636	2.660	1.275	1.275	2.550
	B3LYP	1.078	1.639	2.678	1.283	1.282	2.565
	PBE0	1.087	1.589	2.639	1.276	1.276	2.551
6-311++G(2d,2p)	MP2	1.065	1.642	2.660	1.275	1.275	2.550
	B3LYP	1.076	1.633	2.678	1.282	1.283	2.565
	PBE0	1.086	1.581	2.639	1.277	1.274	2.551

For all the considered methods, the data show a large variation in going from the smallest to the intermediate basis sets thus indicating that the first one is insufficient to reach converged energies. Regarding the MP2 method, such variation is very large (almost 70%) so confirming as the performances of post-HF methods are stronger influenced by the basis set completeness. On the contrary, only slightly variations are obtained using the largest basis set

Such a trend is confirmed by the analysis of the structural parameters (N_D -H, N_A -H and N_D - N_A distances) involved in the H-bond (Table III-2) where the most significant variations are observed in going from 6-31G(d) to 6-311+G(d,p) basis sets.

In short, this preliminary study indicates that a good level of convergence for the considered systems (considering both energetic and structural features) is achieved using the 6-311+G(d,p) basis set which will be, therefore, the only one considered in further calculations.

1.5. The reference energy values

The second step of this study has been the choice of a appropriate level of theory able to give sufficiently accurate reference values. With this aim, CCSD(T) calculations have been performed on both MP2 and B3LYP optimized structures. The results are shown in table III-3.

Table III-3: Computed single point energies (a.u.) at CCSD(T) level using MP2 and B3LYP structures. All data have been calculated using the 6-311+G(d,p) basis set.

			minimum (a.u)	TS(a.u)
CCSD(T)//MP2	ImH ⁺ -Im	<i>a</i>	-451.733220	-451.730192
	TrH ⁺ -Tr	<i>b</i>	-483.689024	-483.685752
		<i>c</i>	-515.692701	-515.673429
	TeH ⁺ -Te	<i>d</i>	-515.689607	-515.689266
		<i>e</i>	-515.691211	-515.699266
CCSD(T)//B3LYP	ImH ⁺ -Im	<i>a</i>	-451.733775	-451.731609
	TrH ⁺ -Tr	<i>b</i>	-483.690323	-483.688432
		<i>c</i>	-515.694322	-515.690608
	TeH ⁺ -Te	<i>d</i>	-515.691244	-515.691092
		<i>e</i>	-515.693493	-515.691092

Surprisingly, the total energies provided using DFT are lower than those obtained using the post-HF method MP2 in all the considered complexes thus indicating that the B3LYP structures are closer to the optimized CCSD(T) geometries which are too time consuming to be computed. The CCSD(T)/6-311+G(d,p)//B3LYP/6-311+G(d,p) level of theory will be therefore the only used to provide the reference energy values used in the following.

1.6. PT in imidazolium-imidazole complex

The stationary points (minima and transition states) of the complex $\text{ImH}^+\text{-Im}$ have been computed taking into account all the considered functionals. Figure III-3 shows the obtained structures: a perfectly orthogonal rearrangement of the two heterocycles is present in both minimum and TS. Such a conformation takes place at all the considered levels of theory, the planar rearrangement being higher in energy as for instance in the case of the TS computed at B3LYP level (1.5 kcal/mol less stable if the rings are in the same plane). A more detailed analysis of the obtained minimum shows a picture where the distance $\text{N}_\text{D}\text{-H}$ is overestimated by most of the considered functionals while an opposite tendency is observed for the distances $\text{N}_\text{A}\text{-H}$ and $\text{N}_\text{D}\text{-N}_\text{A}$. Exceptions are represented by B3LYP, BMK and LC-wPBE (Table III-4).

Concerning the structure of the TS, the differences among the considered functionals are less significant. Indeed, all the obtained N-H distances are in a small range going from 1.273 Å (LC-TCA0 and M06-HF) to 1.290 Å (TCA) while the $\text{N}_\text{D}\text{-N}_\text{A}$ distance ranges from 2.545 Å to 2.580 Å but with most of the functionals giving values around 2.565 Å. Here, the best agreement with the MP2 data is given by the functionals having 22-25% of HF exchange (PBE0, mPW1PW91, and X3LYP).

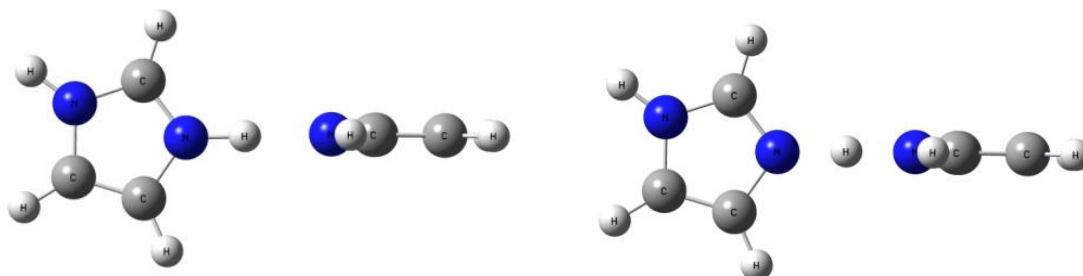


Figure III-3: Structures of minima and transition states of imidazolium-imidazole complex ($\text{ImH}^+\text{-Im}$): minimum (left) and TS (right).

Beyond such small variations concerning the H-bridge parameters, the computed stationary points are predicted to have at any level of theory the structural rearrangement depicted in figure III-3a: in going from the minimum to the TS no significant conformational variation is observed. This is reflected in the low PT energy barrier which is only 1.4 kcal/mol if we consider the reference energy value (Table III-5). As expected, the energetic barrier is underestimated by almost all the functionals being in a range between 0.1 (TCA and M06-2X) and 0.7 (B3LYP) kcal/mol. Interestingly, a value equal to the reference one is computed using the BMK functional while the MP2 method gives a barrier of only 0.5 kcal/mol.

Table III-4: Calculated N_D-H (Å), N_A-H (Å) and N_D-N_A (Å) distances for imidazolium-imidazole complex (ImH^+-Im). All data are computed using the 6-311+G(d,p) basis set.

	ImH ⁺ -Im					
	minimum a			transition state		
	N_D-H	N_A-H	N_D-N_A	N_D-H	N_A-H	N_D-N_A
MP2	1.118	1.517	2.634	1.279	1.278	2.557
B3LYP	1.108	1.562	2.670	1.286	1.286	2.572
PBE0	1.127	1.501	2.628	1.279	1.279	2.558
BMK	1.089	1.611	2.699	1.285	1.285	2.570
X3LYP	1.152	1.455	2.608	1.282	1.282	2.563
mPW1PW91	1.126	1.502	2.628	1.279	1.279	2.558
LC-wPBEE	1.115	1.531	2.646	1.281	1.281	2.561
M06HF	1.174	1.399	2.572	1.273	1.273	2.545
M062X	1.135	1.486	2.621	1.281	1.281	2.562
TCA	1.172	1.444	2.616	1.290	1.290	2.580
LCTCA0	1.136	1.462	2.598	1.273	1.273	2.546

Table III-5: Computed Proton Transfer energy barriers (kcal/mol) for Imidazolium-Imidazole (ImH^+-Im), 1,2,3-Triazolium-1,2,3-Triazole (TrH^+-Tr) and Tetrazolium-Tetrazole (TeH^+-Te) complexes. In parenthesis are reported the imaginary frequencies (cm^{-1}) of the transition states. All the values have been computed with the 6-311+G(d,p) basis set. The CCSD(T)/6-311+G(d,p)//B3LYP/6-311+G(d,p) level of theory has been used for the reference values.

mechanism	ImH ⁺ -Im	TrH ⁺ -Tr	TeH ⁺ -Te		
	<i>a</i>	<i>b</i>	<i>c</i>	<i>d</i>	<i>e</i>
best estim.	1.4	1.2	2.3	0.1	1.5
MP2	0.5 (707i)	0.4 (564i)	1.4 (559i)	0.0 (407i)	0.4 (407i)
B3LYP	0.7 (796i)	0.6 (687i)	1.0 (640i)	0.0 (162i)	1.0 (162i)
PBE0	0.3 (616i)	0.2 (489i)	0.6 (422i)	/	/
BMK	1.4 (989i)	1.3 (911i)	2.9 (875i)	0.2 (696i)	1.8 (696i)
X3LYP	0.2 (532i)	0.1 (364i)	0.6 (278i)	/	/
mPW1PW91	0.4 (652i)	0.2 (534i)	0.5 (473i)	/	/
LC-ωPBE	0.5 (717i)	0.4 (587i)	1.1 (535i)	/	/
M06-HF	0.3 (1374i)	0.2 (1080i)	0.5 (1111.i)	/	/
M06-2X	0.1 (458i)	0.1 (67i)	1.4 (80i)	/	/
TCA	0.1 (432i)	0.0 (239i)	0.1 (140i)	/	/
LC-TCA0	0.2 (548i)	0.1 (360i)	0.8 (270i)	/	/

Taken together, these results show as a direct correlation between HF exchange contribution and the energetic outcomes cannot be done for such complex. For instance, despite the similar percent HF exchange, BMK (42%) and M06-2X (54 %) show very different performances. Indeed, if the first gives a barrier in perfect agreement with the reference one (1.4 kcal/mol), the latter gives a value of only 0.1 kcal/mol. Finally, energy and structure appear as two disconnected features. Indeed, the H-bond distances significantly differ from the MP2 results if functionals providing almost the same barrier are considered.

1.7. PT in 1,2,3-triazolium-1,2,3-triazole complex

The stationary points of the $\text{TrH}^+\text{-Tr}$ complex are characterized at any level of theory by a planar rearrangement of the two rings (figure III-4). The different conformation respect to the $\text{ImH}^+\text{-Im}$ pair could be imputed to the reduced steric effects due to the substitution of the CH group in imidazole with a nitrogen atom. Such a replacement, moreover, is responsible of a different H-bond bridge, the NN length being shorter of about 0.015 Å with respect to the $\text{ImH}^+\text{-Im}$ dimer (table III-6). This leads to shorter $\text{N}_\text{A}\text{-H}$ (about 0.015 Å) and larger $\text{N}_\text{D}\text{-H}$ (about 0.006 Å) distances, a tendency which is confirmed at each level of theory.

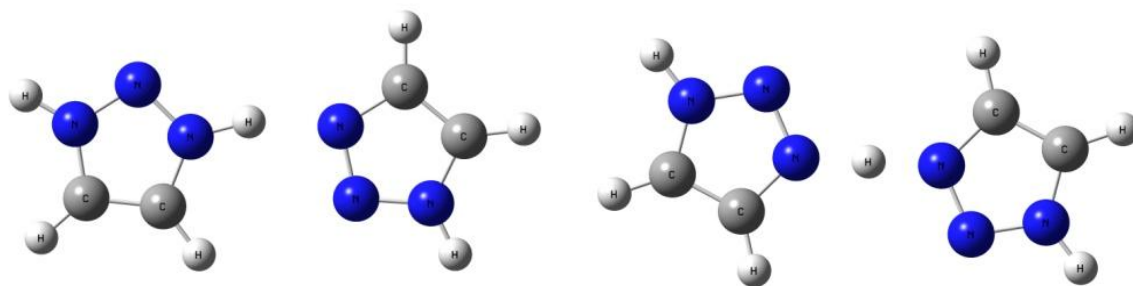


Figure III-4: Structures of minima and transition states of 1,2,3-triazolium-triazole complex ($\text{TrH}^+\text{-Tr}$): minimum (left) and TS (right).

Concerning the performance of the considered functionals, the trend already discussed for the imidazolium-imidazole dimer is here almost respected. Again the $\text{N}_\text{D}\text{-H}$ distances of the minimum are overestimated while the $\text{N}_\text{A}\text{-H}$ and $\text{N}_\text{D}\text{-N}_\text{A}$ lengths underestimated with exception represented in the first case by B3LYP and BMK and in the second one by B3LYP, BMK and LC- ω PBE. The largest deviations for the $\text{N}_\text{D}\text{-H}$ lengths are provided by M06HF and TCA functionals while BMK significantly overestimates both the $\text{N}_\text{A}\text{-H}$ and $\text{N}_\text{D}\text{-N}_\text{A}$ distances. The best estimation is obtained using M06-2X and LC- ω PBE. The trends already discussed in the $\text{ImH}^+\text{-Im}$ system are

confirmed also analyzing the energetic barriers. Indeed, as shown in Table III-5, the best agreement is again given by BMK (1.3 vs. 1.2 kcal/mol) and once again LC-wPBE determines the same results of MP2 (0.4 kcal/mol).

Finally, it is worth to underline that no significant variation has been found between the energetic barriers of the two analyzed complexes. The reference energy value in TrH⁺-Tr pair is only slightly lower (-0.2 kcal/mol) respect to ImH⁺-Im and this trend is confirmed at any level of theory. In short, the analyzed complexes of imidazole and 1,2,3-triazole are characterized by similar structural and energetic features.

Table III-6: Calculated N_D-H (Å), N_A-H (Å) and N_D-N_A (Å) distances for 1,2,3-triazolium-triazole complex (TrH⁺-Tr). All data are computed using the 6-311+G(d,p) basis set.

	TrH ⁺ -Tr					
	minimum b			transition state		
	N_D-H	N_A-H	N_D-N_A	N_D-H	N_A-H	N_D-N_A
MP2	1.124	1.500	2.620	1.278	1.277	2.554
B3LYP	1.117	1.539	2.654	1.286	1.286	2.571
PBE0	1.143	1.465	2.607	1.278	1.280	2.558
BMK	1.081	1.624	2.680	1.285	1.285	2.571
X3LYP	1.166	1.431	2.595	1.282	1.282	2.563
mPW1PW91	1.137	1.477	2.613	1.279	1.279	2.558
LC-wPBEE	1.126	1.505	2.629	1.280	1.280	2.561
M06HF	1.189	1.373	2.559	1.271	1.271	2.542
M062X	1.129	1.497	2.619	1.281	1.281	2.562
TCA	1.196	1.405	2.601	1.289	1.291	2.580
LCTCA0	1.150	1.436	2.584	1.273	1.273	2.546

Finally, it is worth to underline that no significant variation has been found between the energetic barriers of the two analyzed complexes. The reference energy value in TrH⁺-Tr pair is only slightly lower (-0.2 kcal/mol) respect to ImH⁺-Im and this trend is confirmed at any level of theory. In short, the analyzed complexes of imidazole and 1,2,3-triazole are characterized by similar structural and energetic features.

1.8. PT in tetrazolium-tetrazole complex

As above described, because of the different tautomeric forms, three possible PT mechanisms can be envisaged for the TeH⁺-Te complex (Figure III-2). The figure III-5 shows the computed localized structures for the corresponding minima and TSs. Obviously, the same TS is shared by the mechanisms *d* and *e* which present a peculiarity: only two functionals (B3LYP and BMK) are able to characterized all the three structures (minimum *d*, minimum *e* and TS). Indeed,

in contrast with the reference MP2 data, for most of the considered functionals only the minimum *e* is stable so that a TS is not computable. On the contrary, all the considered functionals are able to provide the stationary points of the mechanism *c* which is symmetric as mechanisms *a* and *b*.

The minimum *c* is the highest in energy (+3.5 kcal/mol at MP2 level, table III-7) while the minima *d* and *e* are almost isoenergetic (+0.2 kcal/mol at MP2 level) even if *e* is the most lowest structure and that having the higher interaction energy (33.0 kcal/mol vs. 31.9 and 28.4 kcal/mol at MP2 level). An exception is represented by BMK for which the most stable minimum as well as that characterized by the highest interaction energy is *c*.

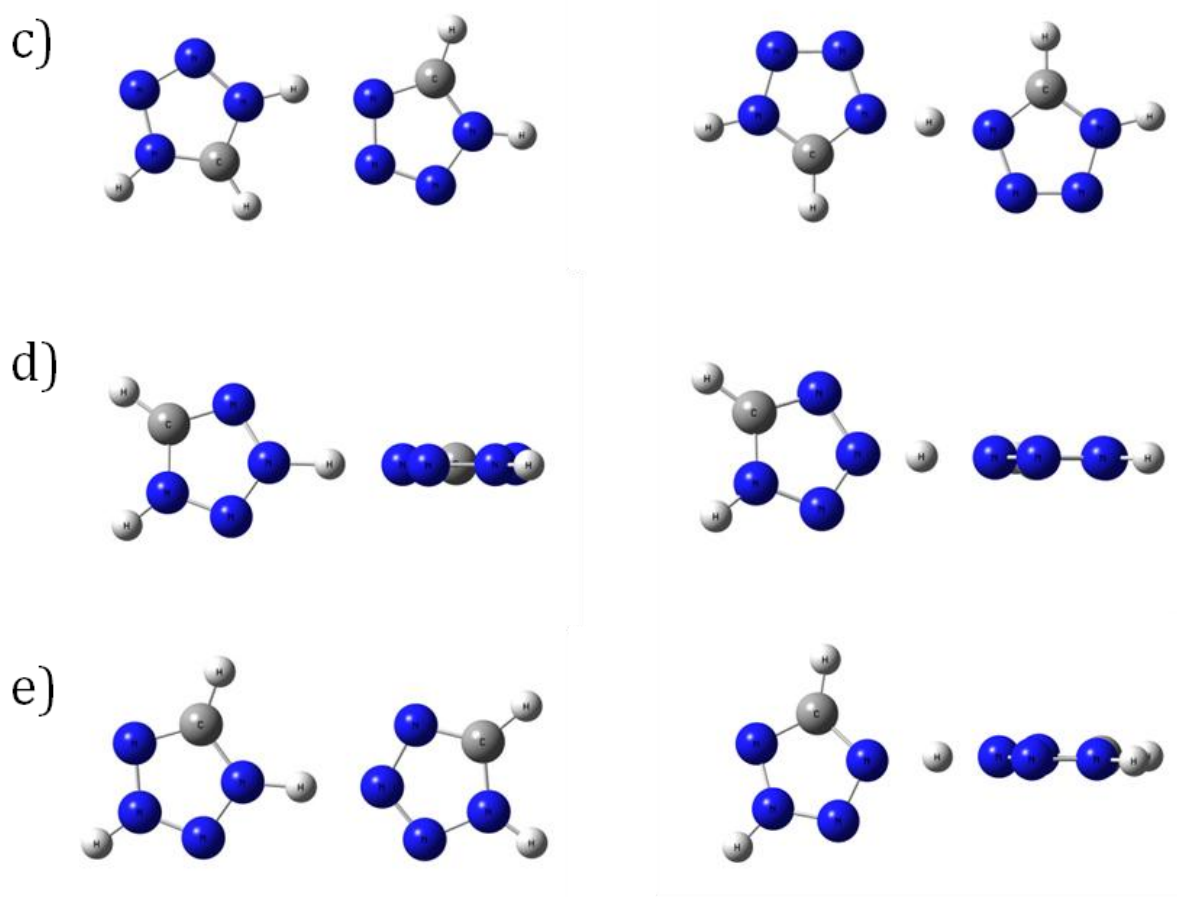


Figure III-5: Structures of minima and transition states of tetrazolium-tetrazole complex ($\text{TeH}^+\text{-Te}$) for all the considered mechanisms: minima (left) and TSs (right).

Different structural rearrangements among the stationary points of the three considered mechanisms have also been computed. Indeed, both minimum and TS of mechanism *c* as well as minimum of mechanism *e* are predicted planar at any level of theory (Figure III-3c and III-3e) in contrast with mechanism *d* where an orthogonal rearrangement of the two rings is detected for

both stationary points, being the planar conformation higher in energy (1.3 kcal/mol at B3LYP level).

Table III-7: Relative energies (ΔE_{rel} , kcal/mol) with respect to the most stable minimum and interaction energies (ΔE_{int} , kcal/mol) of minima c, d and e of the tetrazolium-tetrazole complex. All the values have been computed with the 6-311+G(d,p) basis set.

	minimum	ΔE_{rel}	ΔE_{int}
MP2	c	3.5	31.9
	d	0.3	28.4
	e	0.0	33.0
B3LYP	c	1.3	29.3
	d	1.0	26.4
	e	0.0	30.3
PBE0	c	2.0	30.9
	d	/	/
	e	0.0	32.1
BMK	c	0.0	24.5
	d	2.5	20.8
	e	0.9	24.1
X3LYP	c	1.9	27.4
	d	/	/
	e	0.0	28.1
mPW1PW91	c	1.9	24.9
	d	/	/
	e	0.0	26.0
LC- ω PBE	c	1.4	25.0
	d	/	/
	e	0.0	25.7
M06-HF	c	0.8	27.3
	d	/	/
	e	0.0	27.9
M06-2X	c	0.1	25.8
	d	/	/
	e	0.0	25.7
TCA	c	2.0	25.0
	d	/	/
	e	0.0	26.1
LC-TCA	c	1.6	27.1
	d	/	/
	e	0.0	27.8

This different conformation correlates with their N_D-N_A lengths which are shorter in *d* (2.60 Å at B3LYP level, orthogonal) than in *c* and *e* (2.68 and 2.66 Å, both planar) so suggesting that the final rearrangement could be ruled by the electronic repulsion between the two cycles (see tables III-8 and III-9).

Regarding the minimum *c*, the functionals give results globally respecting the trends already discussed for ImH⁺-Im and TrH⁺-Tr complexes. Indeed, the N_D-H lengths are again overestimated and the N_A-H and N_D-N_A distances underestimated with the exception of BMK and M06-2X following opposite trends (table III-8). TCA, BMK and M06HF provide the largest deviations on N_D-H , N_A-H and N_D-N_A lengths respectively.

Table III-8: Calculated N_D-H (Å), N_A-H (Å) and N_D-N_A (Å) distances for tetrazolium-tetrazole complex (TrH⁺-Tr) involved in mechanism *c*. All data are computed using the 6-311+G(d,p) basis set.

	TeH ⁺ -Te					
	minimum <i>c</i>			transition state		
	N_D-H	N_A-H	N_D-N_A	N_D-H	N_A-H	N_D-N_A
MP2	1.072	1.636	2.660	1.275	1.275	2.550
B3LYP	1.078	1.639	2.678	1.283	1.282	2.565
PBE0	1.087	1.589	2.639	1.276	1.276	2.551
BMK	1.056	1.719	2.707	1.282	1.282	2.564
X3LYP	1.091	1.585	2.628	1.278	1.278	2.557
mPW1PW91	1.099	1.552	2.632	1.276	1.276	2.552
LC-wPBEE	1.073	1.642	2.666	1.271	1.271	2.554
M06HF	1.142	1.443	2.556	1.268	1.268	2.536
M062X	1.066	1.672	2.671	1.278	1.278	2.556
TCA	1.155	1.464	2.615	1.287	1.287	2.574
LCTCA0	1.079	1.590	2.618	1.270	1.270	2.539

As shown in table III-5, the PT energy barrier of mechanism *c* is higher than imidazole and triazole dimers (2.3 vs 1.4 and 1.2 kcal/mol, considering the reference values) and again MP2 and most of the functionals strongly underestimate the barrier (values ranging between 0.1 and 1.4 kcal/mol) with the unique exception represented by BMK (2.9 kcal/mol).

As mentioned, concerning the mechanisms *d* and *e*, only two functionals (BMK and B3LYP) are able to provide all the localizing minima and TS. Notably, as shown in table III-9, the analysis of the H-bond parameters indicates that BMK shows the same trends already discussed for the others mechanisms while B3LYP gives data closer to those used as reference (MP2). Even more interesting is the analysis of the obtained energetic barriers. Indeed, the mechanism *d* is practically barrierless (0.1 kcal/mol at CCSD(T) level) while a larger activation energy has been

found for the opposite direction (1.5 kcal/mol at CCSD(T) level, mechanism *e*). In agreement with the previous cases, BMK slightly overestimates the activation energies while the data closest to MP2 data are provided by B3LYP.

Table III-9: Calculated N_D-H (Å), N_A-H (Å) and N_D-N_A (Å) distances for tetrazolium-tetrazole complex (TrH^+-Tr) involved in mechanism *d* and *e*. All data are computed using the 6-311+G(d,p) basis set

	TeH ⁺ -Te								
	minimum d			transition state			minimum e		
	N_D-H	N_A-H	N_D-N_A	N_D-H	N_A-H	N_D-N_A	N_D-H	N_A-H	N_D-N_A
MP2	1.164	1.424	2.586	1.238	1.319	2.557	1.136	1.473	2.609
B3LYP	1.180	1.417	2.597	1.205	1.380	2.584	1.114	1.544	2.656
PBE0	/	/	/	/	/	/	1.134	1.481	2.613
BMK	1.128	1.511	2.638	1.235	1.339	2.573	1.093	1.596	2.685
X3LYP	/	/	/	/	/	/	1.154	1.451	2.603
mPW1	/	/	/	/	/	/	1.129	1.491	2.619
LC-	/	/	/	/	/	/	1.122	1.513	2.632
M06H	/	/	/	/	/	/	1.171	1.397	2.561
M062	/	/	/	/	/	/	1.132	1.491	2.620
TCA	/	/	/	/	/	/	1.168	1.449	2.616
LCTCA	/	/	/	/	/	/	1.139	1.455	2.591

In short, the BMK model is the only DFT approach able to describe all the three investigated mechanisms and to give barriers which are in agreement with the CCSD(T) data. Nevertheless, the corresponding structures are far from the reference MP2 values in contrast with B3LYP functional which provides structural and energetic results close to the considered post-HF approach.

1.9. Comments

The obtained data point out that the PT reactions occurring in the investigated complexes represent a very difficult playground, even for modern DFT approaches. As above mentioned, this aspect could be related to the coupling between the π -electrons rearrangements of the rings and the PT reaction. However, despite the presence of exceptions represented by some functionals, some direct relationships could be found as for instance between the length of the H-bond and the PT activation energy. The figure III-6 shows the 30 energy barriers (10 functionals for PT mechanisms *a*, *b* and *c*) as function of the N_A-H distance. Even if some data (e.g. BMK) are far from the linear regression, a good correlation ($R^2=0.73$) can be traced between these two quantities.

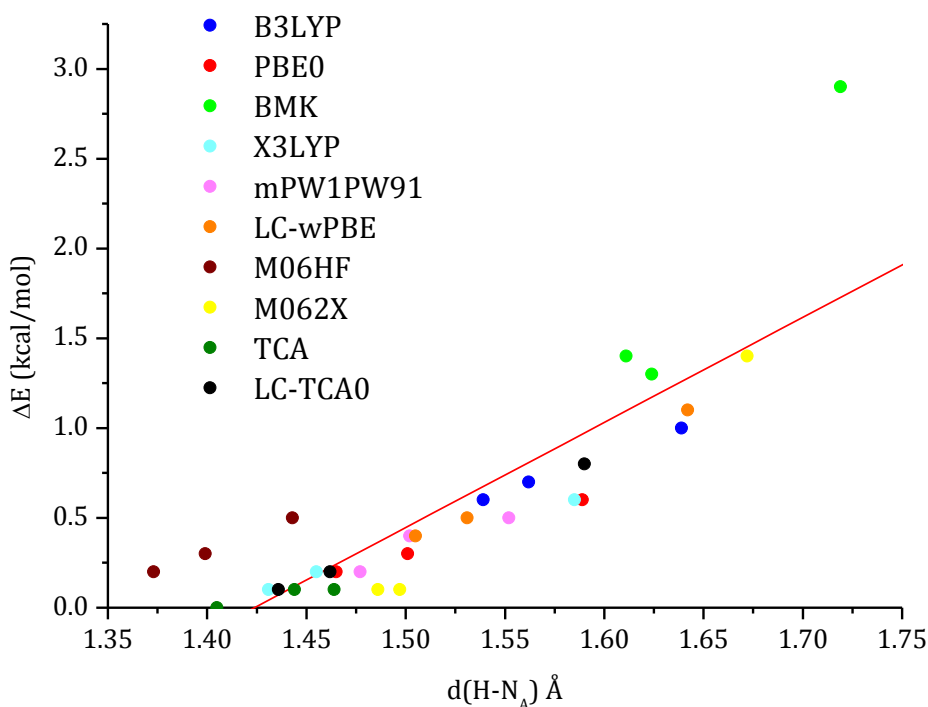


Figure III-6: Plot of 30 DFT proton transfer barriers (ΔE) as function of the $H-N_A$ distances. All points have been included in the linear fitting (red line).

As expected, most of the considered functionals underestimate the barrier with respect to the reference CCSD(T) data with some of them (B3LYP and LC- ω PBE) giving activation energies close to MP2 data. An exception is represented by the BMK model determining values very close to the reference ones.

The obtained barriers are also related to the positive charge localized on the transferred proton. In figure III-7 are reported the reference CCSD(T) values as a function of the Natural Bond Orbitals (NBO) charges³⁶ of the transferring proton computed on the B3LYP structures: the higher is the positive charge, the higher is the computed barrier ($R^2=0.96$). For instance, the lowest charge value (+0.455 [e^-]) corresponds to an energy barrier equal to 0.1 kcal/mol (mechanism *d*) while a value of 2.3 kcal/mol (mechanism *c*) is related to the highest positive charge (+0.480 [e^-]). On the contrary, none direct link can be traced between the imaginary frequencies of the TS and the activation energy, being the curvature of the potential energy surface very different for all the considered functionals (Table III-5). For instance, both BMK and M06HF functionals give high imaginary frequencies but the former determines a significantly lower energy barrier.

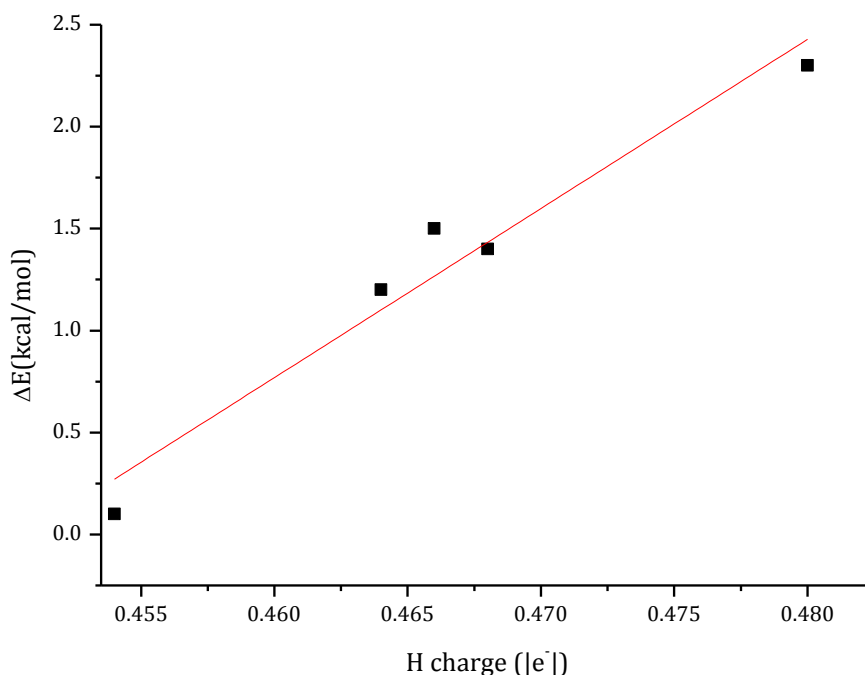


Figure III-7: Proton transfer barriers (ΔE) as function of the NBO charges on the transferred hydrogen in the five considered systems. The red line represent the linear fitting ($R^2=0.956$).

However, despite these evidences, some general considerations can be done. Indeed, most of the considered functionals give energies and frequencies lower than the MP2 data. This indicates that the corresponding energy profile is flatter in proximity of the TS. An exception is represented by the LC-wPBE approach showing a good agreement for both barrier and frequencies but only for three complexes, being unable to characterize the mechanisms *d* and *e*.

From a more chemical point of view, it is worth to underline that PT energies and H-bond parameters are similar for some of the investigated complexes. Indeed imidazole, 1,2,3-triazole as well as complex *e* of tetrazole (the most stable among the three considered) give similar barriers (1.4, 1.2, 1.5 kcal/mol at CCSD(T) level, respectively) and N_D-N_A lengths (2.63, 2.62 and 2.66 Å, respectively). These results are qualitatively consistent with some experiments indicating that imidazole and 1,2,3-triazole, as liquid solvents, show similar proton conductivity^{4,37} while, at the best of our knowledge, no experimental data are available concerning conductivity in liquid tetrazole. The highest computed barrier concerns one of the hypothesized mechanism for PT in tetrazole (mechanism *c*), being the corresponding value equal to 2.3 kcal/mol at CCSD(T) level. This gap can be related to both the higher N_D-N_A distance and the less linear (strong) H-bond (N_D-H-N_A angle= 160°) of the minimum *c* compared to the others.

1.10. The BMK/B3LYP model

The discussed results do not allow the choice of a single functional able to accurately reproduce the structural and energetic features of the investigated complexes so that a combination is necessary. Indeed, although the BMK model shows the best performance from an energetic point of view, the best structures are obtained using the B3LYP approach. Nevertheless, if single point energy refinement is carried out on B3LYP structures using the BMK model, the obtained PT activation energies are in perfect agreement with the reference CCSD(T) values.

Interestingly, the performance of such BMK//B3LYP combined approach is even better than that shown by the pure BMK model (Table III-10). Such a protocol, therefore, has been used for the investigation of larger models, where these N-heterocycles are immobilized in a polymeric matrix (chapters IV, V and VI).

Table III-10: Computed Proton Transfer energy barriers (kcal/mol) for Imidazolium-Imidazole (ImH⁺-Im), 1,2,3-Triazolium-1,2,3-Triazole(TrH⁺-Tr) and Tetrazolium-Tetrazole (TeH⁺-Te) complexes obtained using the combined BMK//B3LYP approach. All the values have been computed with the 6-311+G(d,p) basis set and the reference values using the CCSD(T)/6-311+G(d,p)//B3LYP/6-311+G(d,p) level of theory.

	ImH ⁺ -Im	TrH ⁺ -Tr	TeH ⁺ -Te		
mechanism	<i>a</i>	<i>b</i>	<i>c</i>	<i>d</i>	<i>e</i>
best estim.	1.4	1.2	2.3	0.1	1.5
BMK//B3LYP	1.3	1.1	2.4	0.1	1.7

In summary, the investigated PT reactions occurring on small models of imidazole, 1,2,3-triazole and tetrazole revealed very challenging for the considered DFT approaches. Indeed, despite the use of recent exchange correlation functionals, none of the considered models are able to catch both the structural and energetic features of the investigated complexes so that a combined approach has to be used.

From a broad-spectrum point of view, this first study has confirmed that PT reactions represent a very difficult playground for methods rooted in Density Functional Theory. Nevertheless, it should be argued that PT reactions of interest in chemistry could be significantly different from those occurring in π -conjugated molecules where the energetic can be tuned by the π -electrons reorganization.

Therefore, moved by the aim of finding the best functional(s) for PT reactions and in order to verify if the most recent functionals really represent an improvement with respect to older and more studied approaches, a benchmark study has been realized including a large number of functionals and a representative set of PT reactions.

2. PT reactions: a benchmark study

2.1. Introduction

Beyond the rule in PEMFCs, PT reactions are involved in many chemical processes³⁸⁻⁴¹ so attracting a great interest by both experimentalists and theoreticians since many decades.

From a strictly theoretical point view, the scientific research mainly focused so far on the energetic of such reactions showing that an accurate estimation of both thermodynamics and kinetics can be obtained only including electronic correlation.⁴²

In this context, therefore, a pivotal role can be played by DFT methods which, as already shown in the investigation of imidazole-like dimers, need to go through an assessment step where the performances of the functionals are examined by comparison with available experimental results or higher-level theoretical approaches.

In this sense, the studies performed so far allowed for some general considerations:

- The PT barriers are underestimated by GGA functionals. Such a difference can be partially reduced including HF exchange.^{14-16,43,44}
- This underestimation could be the consequence of the artificial stabilization of the TS made by the self-interaction error (SIE).^{45,46}
- The HF exchange beneficial effects on the barrier estimation can be related to the better electron localization.⁴⁷

Nevertheless, beyond these pioneering works, a systematic benchmark study is still missing in the scientific panorama. The available literature, indeed, concerns only very specific cases where most of the PT reactions of chemical interest are not included.^{48,49} In this context, it could be noted that a recently published benchmark for reactivity (named DBH24/08⁵⁰) also includes hydrogen transfer (HT) reactions. Nevertheless, since they can consist of both intra and inter-molecular reactions with low and high barriers, PT of interest in chemistry can significantly differ from HT reactions.

So, in order to partially fulfill this lack of information, the performances of a large number of functionals (Table III-11) have been tested on a representative set of different PT reactions (Figure III-8). Notably, in contrast with the common trends not only the energetic but also the structural features have been analyzed and compared with coupled cluster data. Furthermore the obtained outcomes have been compared with the DBH24/08 set, standard benchmark for the reaction barrier.

2.2. Methodological details

A locally modified version of the Gaussian 09 package has been used to perform all the calculations. In order to include different rungs of the Perdew's ladder,⁵¹ 27 exchange-correlation functionals have been considered. This representative set include GGAs, Meta-GGAs,

Global and Range Separated Hybrids (GHH and RSH) and double hybrids (DH) (Table III-11). These functionals are among the best performing DFT approaches for chemical applications.

Two basis sets, belonging to the Pople's basis set family and named 6-311+G(2d,p) and 6-311+G(3df,3pd), have been considered. Notably, all the DFT structures have been obtained using the former while, in order to have more accurate barriers, subsequent single point calculations have been performed using the latter. As recently suggested, for the M06 family an "ultrafine" grid corresponding to 96 radial shells around each atom and a spherical product grid having 32 θ points and 64 ϕ points in each shell, has been used.^{52,53}

In order to obtain accurate reference values, geometry optimization at CCSD/cc-pvTZ level have been carried out and single point energies at CCSD(T)/aug-cc-pvTZ have been also computed.

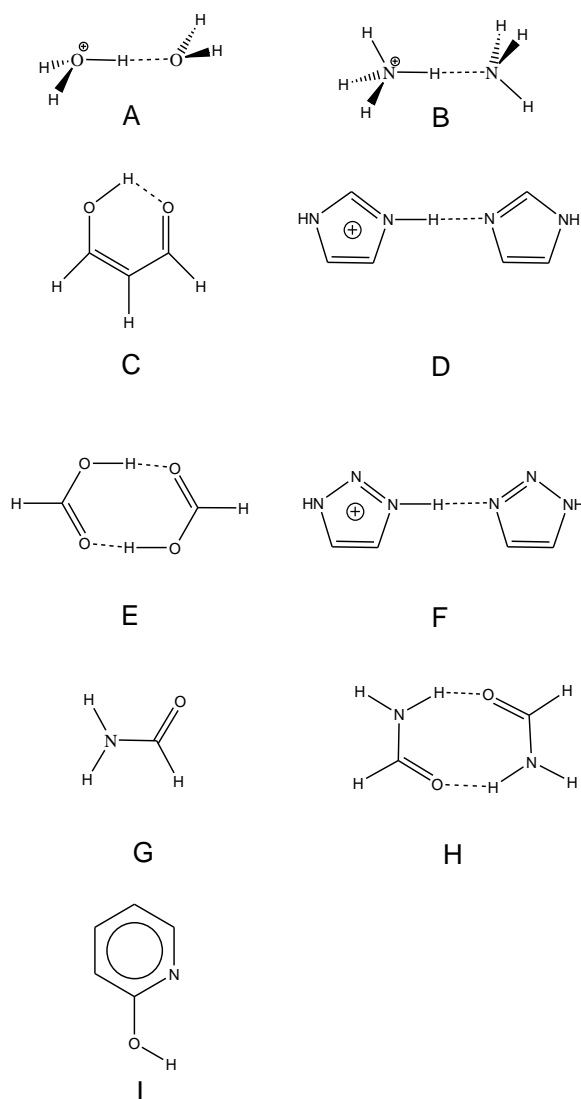


Figure III-8: Sketched of the considered systems: A) protonated water dimer; B) protonated ammonia dimer; C) malonaldehyde; D) protonated imidazole dimer; E) formic acid dimer; F) protonated triazole dimer; H) formamide; G) formamide dimer; I) pyridone.

Table III-11: List of the exchange-correlation functionals considered in the benchmarking study. The HF exchange is expressed as min/max for range separated hybrids.

Functional	%HF exchange ^a	reference
GGA		
GRAC	0	54
BLYP	0	55,56
TCA	0	31
PBEPBE	0	57
Meta-GGA		
VSXC	0	58
B97D	0	59
Global Hybrids		
B972	21	60
B1LYP	25	61
BMK	42	24
X3LYP	21	25
B3LYP	20	22
B3LYP-D	20	22,59
BHandHLYP	50	62
mPW1PW91	25	26
mPW1K	42.8	63
PBE0	25	23
M06-HF	100	27
M06	27	28
M06-2X	54	28
Range-Separated Hybrids		
CAM-B3LYP	19/65	64
LC-PBEPBE	0/100	65
LC- ω PBE	0/100	29,30
ω B97XD	22/100	66
ω B97X	16/100	67
ω B97	0/100	67
Doubly Hybrids		
PBE0-DH	50	68
B2PLYP	53	69

2.3. Results and discussion

The investigated systems are sketched in figure III-8 and labeled from A to I. Since both symmetric (A-F) and non-symmetric (G-I) PT reactions have been taken into account, 12 energy barriers have been considered in total. The used reference values (B3LYP and CCSD values with the corresponding CCSD(T) energies) are reported in Table III-12. Notably four different benchmarks have been carried out: PT energy barriers at B3LYP/6-311+G(2d,p) optimized

structures (1), standard energy barrier evaluations on the DBH24/08 database for kinetics (2), comparison of the PT energy barriers (3) and the optimized H-bond structural parameters (4) for each considered functional with the reference CCSD(T) and CCSD values, respectively.

Table III-12. Reference CCSD/cc-pVTZ values for the H-bond structural parameters (\AA , A=H-acceptor, D=H-donor) and proton transfer barriers (ΔE^\ddagger , kcal/mol) obtained at CCSD(T)/aug-cc-pVTZ//CCSD/cc-pVTZ level. Only the values for the lowest energy minima are reported, while in parenthesis are reported the structural parameters obtained at with the B3LYP/6-311+G(2d,p) approach and the energies computed at CCSD(T)/aug-cc-pVTZ//B3LYP/6-311+G(2d,p) level.

system	d(AD)	d(AH)	d(HD)	ΔE^\ddagger
A ^a	2.750	1.700	1.051	6.71
B	2.719(2.695)	1.620(1.553)	1.100(1.142)	1.02(0.93)
C	2.611(2.571)	1.737(1.674)	0.982(1.001)	3.87(3.85)
D	2.681(2.668)	1.603(1.561)	1.079(1.107)	1.05(1.06)
E	2.689(2.666)	1.702(1.663)	0.988(1.004)	7.90(7.90)
F	2.673(2.655)	1.611(1.543)	1.075(1.114)	1.14(1.03)
G	2.276(2.278)	2.542(2.546)	1.003(1.009)	46.77(46.75)
H	2.888(2.924)	1.874(1.901)	1.018(1.027)	19.10(18.86)
I	2.282(2.290)	2.233(2.255)	0.963(0.969)	38.05(37.96)

a) fixed geometry

Proton transfer barriers at given structure

The performance of the considered functionals has been firstly evaluated by computing PT energy barriers at the B3LYP/6-311+G(2d,p) optimized structures and comparing the obtained outcomes with the corresponding CCSD(T) values. In table III-13 are reported the computed Mean Signed Deviations (MSDs), Root Mean Square Deviations (RMSDs) and Mean Absolute Deviations (MADs). Note that the functionals are listed with respect to the computed MAD. Three RSHs functionals provide the best results, namely ω B97X, ω B97XD and CAM-B3LYP, all containing about 20% of HF exchange at short range. On the contrary, as expected, most of the GGA functionals such as PBEPBE can be found in the bottom of the ranking. Furthermore, it is worthy to note that the dispersion provides a negligible effect on the PT barriers. Indeed the ω B97X and B3LYP models give outcomes very close to those provided by the respective counterparts including empirical dispersion corrections (i.e. ω B97XD and B3LYP-D). Finally, as shown from the close RMSD and MAE values computed for most of the functionals, the obtained results are characterized by a low spreading.

Table III-13. Mean Signed Deviations (MSD), Mean Absolute Deviations (MAD) and Root-Mean Square Deviations (RMSD) for proton transfer barriers obtained at the B3LYP/6-311+G(3d,p) optimized structures. All the single point calculations have been computed using the 6-311+G(3df,3pd) basis set. All the values are in kcal/mol.

	functional	MSD	RMSD	MAD
1	ω B97XD	-0.02	0.85	0.71
2	ω B97X	0.55	1.15	0.75
3	CAM-B3LYP	-0.34	0.95	0.77
4	B1LYP	0.17	1.03	0.78
5	PBE0-DH	-0.66	1.00	0.81
6	BMK	0.46	1.26	0.84
7	X3LYP	-0.47	0.98	0.86
8	B3LYP	-0.52	1.02	0.90
9	M06	-0.69	1.12	0.94
10	B3LYP-D	-0.66	1.17	0.97
11	B972	-0.82	1.14	0.99
12	LC- ω PBE	-0.77	1.19	1.01
13	ω B97	0.88	1.49	1.01
14	mPW1K	0.24	1.27	1.02
15	M06-2X	-0.68	1.33	1.12
16	VSXC	-0.03	1.96	1.30
17	mPW1PW91	-1.32	1.53	1.33
18	PBE0	-1.59	1.77	1.59
19	M06-HF	-1.01	2.71	1.91
20	LC-PBEPBE	-2.16	2.51	2.16
21	BLYP	-2.20	2.65	2.20
22	BHandHLYP	2.32	3.13	2.32
23	B97D	-2.40	2.74	2.40
24	GRAC	-2.52	2.99	2.52
25	B2PLYP	3.05	3.86	3.05
26	TCA	-3.23	3.69	3.23
27	PBEPBE	-3.95	4.42	3.95

Standard energy barrier evaluations on the DBH24/08 database

Composed by 24 barriers and 12 reactions, the DBH24/08 database is nowadays considered as the reference for testing the performances of functionals on kinetics. Notably it includes Hydrogen Transfer (HT), Heavy Atom Transfer (HAT), Nucleophilic Substitution (NS), and Unimolecular and Association (UA) reactions. The table III-14 shows the obtained results. As expected, the functionals expressly designed for kinetics are found on the top of the list, namely M06-2X and BMK. Importantly, high MADs are detected for B1LYP and B3LYP functionals, in contrast with the results obtained for the PT reactions at given structures while only few functionals have comparable relative positions in the two rankings (first and second benchmark). In other words, the performances of most of the functionals differ when taking into account the DBH24/08 (specify designed for kinetics) or PT datasets.

Table III-14. Mean Signed Deviations (MSD), Mean Absolute Deviations (MAD) and Root-Mean Square Deviations (RMSD) for the DBH24/08 benchmark for kinetics. All the value are in kcal/mol. All the single point calculations have been computed using the 6-311+G(3df,3pd) basis set on structures optimized using the 6-311+G(3d,p) basis set.

	functional	MSD	RMSD	MAD
1	M06-2X	0.13	1.45	1.03
2	BMK	0.34	1.82	1.53
3	PBE0-DH	0.84	2.13	1.60
4	mPW1K	0.13	2.10	1.61
5	ω B97XD	0.80	2.41	1.89
6	B2PLYP	1.87	2.42	2.04
7	BHandHLYP	-0.65	2.75	2.10
8	ω B97X	-0.33	2.49	2.10
9	LC- ω PBE	-0.81	2.74	2.18
10	M06	1.80	3.50	2.42
11	M06-HF	-1.41	3.56	2.50
12	ω B97	-1.30	3.19	2.59
13	B972	1.92	3.69	2.74
14	CAM-B3LYP	2.42	3.32	2.78
15	LC-PBEPBE	-0.36	4.40	3.40
16	B1LYP	3.28	3.98	3.43
17	mPW1PW91	3.12	4.19	3.45
18	PBE0	3.53	4.76	3.83
19	B3LYP	4.31	5.14	4.39
20	X3LYP	4.34	5.16	4.44
21	B3LYP-D	4.77	5.62	4.84
22	VSXC	4.25	6.19	4.56
23	B97D	5.97	7.64	6.09
24	GRAC	7.37	8.88	7.38
25	TCA	7.56	9.38	7.56
26	BLYP	7.93	9.23	7.93
27	PBEPBE	8.46	10.45	8.46

Optimized structures: PT barriers & H-bond structural parameters

The structural effects on PT energy barriers have been investigated considering 8 systems (B-I in figure III-8) and a set of 16 functionals, selected among the most representative of the 27 set. Note that having only a stable structure, H_5O_2^+ has not been optimized. Notably, the computed H-bond parameters have been compared with those computed at CCSD level (table III-12). The obtained outcomes are reported in table III-15: the most accurate structures are provided by two global hybrids containing 27 (M06) and 42 (BMK) percent of HF exchange while the largest deviations are given by PBE0, LC-PBE and M06-HF. Interestingly, a different trend is observed when the computed energies are compared with the reference CCSD(T) values. As clearly shown in table III-16, functionals giving accurate geometries such as BMK, M06 or ω B97, provide large errors on energies while an opposite behavior can be detected for approaches giving large errors in geometries (see for instance PBE0-DH and B3LYP).

Table 15. Mean Signed Deviations (MSD), Mean Absolute Deviations (MAD) and Root-Mean Square Deviations for H-bond parameters. In case of asymmetric systems only the values for the lowest energy structure have been considered and the protonated water dimer has not been included. All the values are in Å.

	functional	MSD	RMSD	MAD
1	M06	0.001	0.016	0.012
2	BMK	-0.002	0.017	0.013
3	ω B97X	-0.008	0.019	0.014
4	ω B97	-0.003	0.028	0.017
5	B1LYP	-0.006	0.024	0.018
6	B2PLYP	-0.010	0.032	0.024
7	X3LYP	-0.010	0.035	0.026
8	B3LYP	-0.007	0.035	0.026
9	CAM-B3LYP	-0.018	0.042	0.031
10	LC- ω PBE	-0.023	0.051	0.037
11	PBE0-DH	-0.030	0.057	0.040
12	M06-2X	-0.024	0.057	0.041
13	mPW1PW91	-0.031	0.065	0.047
14	PBE0	-0.028	0.071	0.051
15	LC-PBEPBE	-0.037	0.088	0.066
16	M06-HF	-0.051	0.110	0.079

Table 16. Mean Signed Deviations (MSD), Mean Absolute Deviations (MAD) and Root-Mean Square Deviations (RMSD) for proton transfer barriers obtained using the optimized structures for each functional. All the single point calculations have been computed using the 6-311+G(3df,3pd) basis set on structures optimized using the 6-311+G(3d,p) basis set. All the values are in kcal/mol.

	functional	MD	RMSD	MAD
1	B1LYP	0.25	1.04	0.76
2	ω B97X	0.60	1.17	0.77
3	CAM-B3LYP	-0.33	0.98	0.80
4	X3LYP	-0.42	0.97	0.86
5	B3LYP	-0.51	0.99	0.86
6	BMK	0.50	1.33	0.94
7	PBE0-DH	-0.81	1.12	0.95
8	M06	-0.63	1.23	1.00
9	ω B97	1.01	1.54	1.05
10	LC- ω PBE	-0.88	1.30	1.07
11	M06-2X	-0.70	1.31	1.07
12	mPW1PW91	-1.39	1.62	1.39
13	M06-HF	-0.69	2.50	1.64
14	PBE0	-1.65	1.85	1.65
15	LC-PBEPBE	-0.58	4.79	3.13
16	B2PLYP	3.20	4.02	3.20

Comments

Taken together, the obtained results allow for drawing a final ranking of the considered functionals. Figure III-9 shows the total score, computed for each approach as the sum of the positions obtained in the four benchmarks. Assuming that each trial has the same weight, the

best classified functional is the recent ω B97X model, which provides high ranking in all the four trials. It is followed by BMK, B1LYP and PBE0-DH.

Behind some considerations concerning the positions of each functional, a second general comment concerns the change of the relative ranking in going from one benchmark to another. Concerning the behavior of the functionals in going from PT energy barriers at fixed geometries to those computed at relaxed structures, most of the functionals show a similar ranking (see tables III-13 and III-16) while comparing the ranking on the energy (at fixed geometry) with that on structural parameters, a very different behavior is detected for almost all the functionals. An example, M06 is ranked 1st on structure and 8th on energy. This indicates that functionals providing good structures do not necessarily do the same for energy. Furthermore, from the discussed results, it clearly appears that the DBH24/08 dataset cannot be considered as representative for PT reactions. For instance, the 6th best performing functional on the DBH24/08 (B2LYP) is only in 25th position on the PT barriers at fixed geometry.

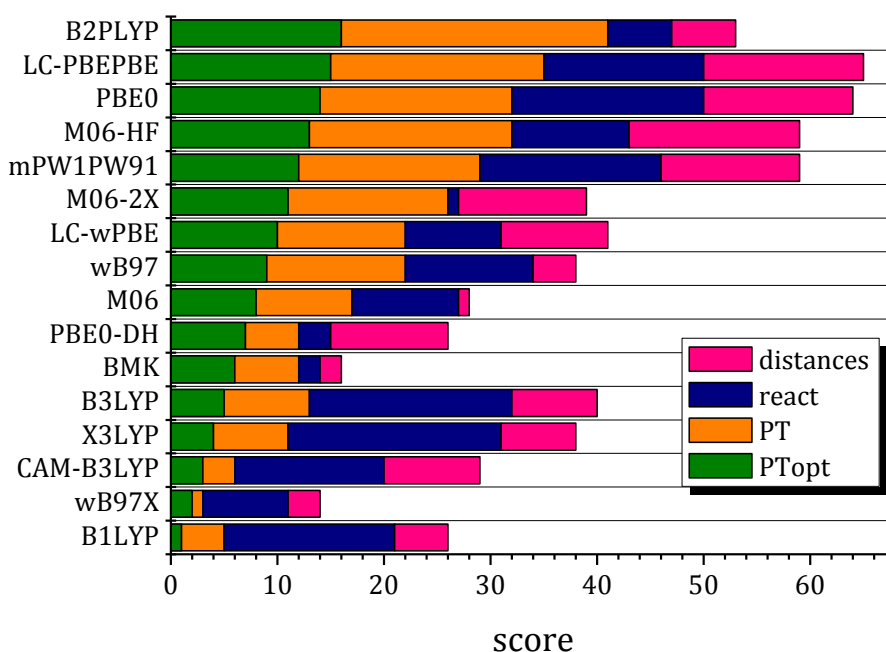


Figure III-9: Summary of the functional score for the four benchmarks: proton transfer barriers at B3LYP geometry (PT), proton transfer barriers at respective optimized geometry (PTopt), standard DBH24/08 test (react) and H-bond structural parameters (distances).

Concerning the rule of the HF exchange in the performances of the considered functionals, it is not possible to get a direct correlation. This is true considering both PT energy barriers and H-bond parameters. As an example, BMK (42% HF exchange) and M06 (0% HF exchange) perform both well on distances and show a similar ranking on PT energies.

3. Conclusions

Despite the use of recent exchange correlation functionals, none of the considered DFT approaches is able to catch both the structural and energetic features of the considered imidazole-like complexes, namely protonated dimers of imidazole, 1,2,3-triazole and tetrazole. Albeit only two functionals (BMK and B3LYP) are able to characterize all the considered PT mechanisms, the use of a combined approach (i.e., BMK single point energy on B3LYP structures), allows to reproduce with a good agreement both structures and proton transfer barriers with respect to the computed reference values. Such a combined BMK/B3LYP model will be the only used in the following where more complex systems (azole-based polymers) will be investigated.

Behind the selection of the best performing approach, some general considerations can be done from the discussed results such as that concerning the strictly relationship between the charge localization on the transferred hydrogen and the computed PT barriers as well as the uncoupling between structural and energetic features. Finally, new mechanisms (*d* and *e*) have been hypothesized for tetrazole-based systems. These lasts are favored with respect to the previously hypothesized in literature³ (mechanism *c*).

In short, the DFT investigation on PT reactions occurring on imidazole-like dimers has shown as such reactions represent a difficult playground even for recent methods rooted in DFT. In order to confirm this evidence from a broad-spectrum point of view, a benchmark study has been realized including a significant number of different exchange correlation functionals and taking into account a representative set of PT reactions. The final ranking, obtained collecting the result provided from four different benchmarks, indicates the best performing functionals, namely wB97X, B1LYP, BMK and PBE0-DH and points out that PT reactions present peculiar characteristics so that benchmarks used for kinetic could be not representative of the functional performances on such class of reactions. Finally, it appears evident from the discussed outcomes that energy and structure for this class of reactions represent two disconnected features, so confirming the picture emerged from the investigation on imidazole-like dimers.

4. References

- (1) Mangiatordi, G. F.; Hermet, J.; Adamo, C. Modeling proton transfer in imidazole-like dimers: a density functional theory study. *Journal of Physical Chemistry A* **2011**, *115*, 2627–2634.
- (2) Mangiatordi, G. F.; Brémond, E.; Adamo, C. DFT and Proton Transfer Reactions: A Benchmark Study on Structure and Kinetics. *Journal of Chemical Theory and Computation* **2012**, *8*, 3082–3088.
- (3) Pu, H.; Wu, J.; Wan, D.; Chang, Z. Synthesis and anhydrous proton conductivity of poly(5-vinyltetrazole) prepared by free radical polymerization. *Journal of Membrane Science* **2008**, *322*, 392–399.
- (4) Zhou, Z.; Li, S.; Zhang, Y.; Liu, M.; Li, W. Promotion of Proton Conduction in Polymer Electrolyte Membranes by 1H-1,2,3-Triazole. *Journal of the American Chemical Society* **2005**, *127*, 10824–10825.
- (5) Çelik, S. Ü.; Aslan, A.; Bozkurt, A. Phosphoric acid-doped poly(1-vinyl-1,2,4-triazole) as water-free proton conducting polymer electrolytes. *Solid State Ionics* **2008**, *179*, 683–688
- (6) Tatara, W.; Wojcik, M. J.; Lindgren, J.; Probst, M. Theoretical study of structures, energies, and vibrational spectra of the imidazole-imidazolium system. *Journal of Physical Chemistry A* *107*, 7827–7831.
- (7) Iannuzzi, M.; Parrinello, M. Proton Transfer in Heterocycle Crystals. *Physical Review Letters* **2004**, *93*, 025901-025904.
- (8) Iannuzzi, M. Proton transfer in imidazole-based molecular crystals. *The Journal of Chemical Physics* **2006**, *124*, 204710–10.
- (9) Münch, W.; Kreuer, K.-D.; Silvestri, W.; Maier, J.; Seifert, G. The diffusion mechanism of an excess proton in imidazole molecule chains: first results of an ab initio molecular dynamics study. *Solid State Ionics* **2001**, *145*, 437–443
- (10) Zhou, Z.; Liu, R.; Wang, J.; Li, S.; Liu, M.; Brédas, J.-L. Intra- and Intermolecular Proton Transfer in 1H(2H)-1,2,3-Triazole Based Systems. *Journal of Physical Chemistry A* **2006**, *110*, 2322–2324.
- (11) Goddard III, W.; Merinov, B.; Duin, A. V.; Jacob, T.; Blanco, M.; Molinero, V.; Jang, S. S.; Jang, Y. H. Multi-paradigm multi-scale simulations for fuel cell catalysts and membranes. *Molecular Simulations* **2005**, *32*, 251-268.

- (12) Subbaraman, R.; Ghassemi, H.; Zawodzinski Jr., T. Triazole and triazole derivatives as proton transport facilitators in polymer electrolyte membrane fuel cells. *Solid State Ionics* **2009**, *180*, 1143–1150.
- (13) Li, A.; Yan, T.; Shen, P. Exploring proton transfer in 1,2,3-triazole-triazolium dimer with ab initio method. *Journal of Power Sources* **2011**, *196*, 905–910.
- (14) Barone, V.; Orlandini, L.; Adamo, C. Proton transfer in model hydrogen-bonded systems by a density functional approach. *Chemical Physics Letters* **1994**, *231*, 295–300.
- (15) Barone, V.; Adamo, C. Proton transfer in the ground and lowest excited states of malonaldehyde: A comparative density functional and post-Hartree–Fock study. *The Journal of Chemical Physics* **1996**, *105*, 11007–11020.
- (16) Sadhukhan, S.; Muñoz, D.; Adamo, C.; Scuseria, G. E. Predicting proton transfer barriers with density functional methods. *Chemical Physics Letters* **1999**, *306*, 83–87.
- (17) Zhao, Y.; Truhlar, D. G. Hybrid Meta Density Functional Theory Methods for Thermochemistry, Thermochemical Kinetics, and Noncovalent Interactions: The MPW1B95 and MPWB1K Models and Comparative Assessments for Hydrogen Bonding and van der Waals Interactions. *Journal of Physical Chemistry A* **2004**, *108*, 6908–6918.
- (18) Proynov, E.; Chermette, H.; Salahub, D. R. New τ -dependent correlation functional combined with a modified Becke exchange. *The Journal of Chemical Physics* **2000**, *113*, 10013–10028.
- (19) Chermette, H.; Razafinjanahary, H.; Carrion, L. A density functional especially designed for hydrogen-only systems. *Journal of Chemical Physics* **1997**, *107*, 10643–10651.
- (20) Tognetti, V.; Adamo, C. Optimized GGA Functional for Proton Transfer Reactions. *Journal of Physical Chemistry A* **2009**, *113*, 14415–14419.
- (21) Frisch, M. J.; Trucks, G. W.; Schlegel, H. B.; Scuseria, G. E.; Robb, M. A.; Cheeseman, J. R.; Scalmani, G.; Barone, V.; Mennucci, B.; Petersson, G. A.; Nakatsuji, H.; Caricato, M.; Li, X.; Hratchian, H. P.; Izmaylov, A. F.; Bloino, J.; Zheng, G.; Sonnenberg, J. L.; Hada, M.; Ehara, M.; Toyota, K.; Fukuda, R.; Hasegawa, J.; Ishida, M.; Nakajima, T.; Honda, Y.; Kitao, O.; Nakai, H.; Vreven, T.; Montgomery, Jr., J. A.; Peralta, J. E.; Ogliaro, F.; Bearpark, M.; Heyd, J. J.; Brothers, E.; Kudin, K. N.; Staroverov, V. N.; Kobayashi, R.; Normand, J.; Raghavachari, K.; Rendell, A.; Burant, J. C.; Iyengar, S. S.; Tomasi, J.; Cossi, M.; Rega, N.; Millam, N. J.; Klene, M.; Knox, J. E.; Cross, J. B.; Bakken, V.; Adamo, C.; Jaramillo, J.; Gomperts, R.; Stratmann, R. E.; Yazyev, O.; Austin, A. J.;

Cammi, R.; Pomelli, C.; Ochterski, J. W.; Martin, R. L.; Morokuma, K.; Zakrzewski, V. G.; Voth, G. A.; Salvador, P.; Dannenberg, J. J.; Dapprich, S.; Daniels, A. D.; Farkas, Ö.; Foresman, J. B.; Ortiz, J. V.; Cioslowski, J.; Fox, D. J. Gaussian, Inc., Wallingford CT, **2009**.

(22) Becke, A. D. Density-functional thermochemistry. III. The role of exact exchange. *Journal of Chemical Physics* **1993**, *98*, 5648-5652.

(23) Adamo, C.; Barone, V. Toward reliable density functional methods without adjustable parameters: The PBE0 model. *Journal of Chemical Physics* **1999**, *110*, 6158-6170.

(24) Boese, A. D.; Martin, J. M. L. Development of density functionals for thermochemical kinetics. *Journal of Chemical Physics* **2004**, *121*, 3405-3416.

(25) Xu, X.; Goddard, W. A. The X3LYP Extended Density Functional for Accurate Descriptions of Nonbond Interactions, Spin States, and Thermochemical Properties. *Proceedings of the National Academy of Sciences* **2004**, *101*, 2673-2677.

(26) Adamo, C.; Barone, V. Exchange functionals with improved long-range behavior and adiabatic connection methods without adjustable parameters: The mPW and mPW1PW models. *Journal of Chemical Physics* **1998**, *108*, 664-675.

(27) Zhao, Y.; Truhlar, D. G. Comparative DFT Study of van der Waals Complexes: Rare-Gas Dimers, Alkaline-Earth Dimers, Zinc Dimer, and Zinc-Rare-Gas Dimers. *Journal of Physical Chemistry A* **2006**, *110*, 5121-5129.

(28) Zhao, Y.; Truhlar, D. G. The M06 suite of density functionals for main group thermochemistry, thermochemical kinetics, noncovalent interactions, excited states, and transition elements: two new functionals and systematic testing of four M06-class functionals and 12 other functionals. *Theoretical Chemistry Accounts* **2007**, *120*, 215-241.

(29) Vydrov, O. A.; Heyd, J.; Krukau, A. V.; Scuseria, G. E. Importance of short-range versus long-range Hartree-Fock exchange for the performance of hybrid density functionals. *Journal of Chemical Physics* **2006**, *125*, 074106-074115.

(30) Vydrov, O. A.; Scuseria, G. E. Assessment of a long-range corrected hybrid functional. *Journal of Chemical Physics* **2006**, *125*, 234109-234118.

(31) Tognetti, V.; Cortona, P.; Adamo, C. A new parameter-free correlation functional based on an average atomic reduced density gradient analysis. *Journal of Chemical Physics* **2008**, *128*, 034101-034109.

- (32) Hermet, J.; Cortona, P.; Adamo, C. New range-separated hybrids based on the TCA density functional. *Chemical Physics Letters* **2012**, 519–520, 145–149.
- (33) Frisch, M. J.; Head-Gordon, M.; Pople, J. A. A direct MP2 gradient method. *Chemical Physics Letters* **1990**, 166, 275–280.
- (34) Head-Gordon, M.; Pople, J. A.; Frisch, M. J. MP2 energy evaluation by direct methods. *Chemical Physics Letters* **1988**, 153, 503–506.
- (35) Pople, J. A.; Head-Gordon, M.; Raghavachari, K. Quadratic configuration interaction. A general technique for determining electron correlation energies. *Journal of Chemical Physics* **1987**, 87, 5968–5975.
- (36) Weinhold, F.; Landis, C. R. Natural bond orbitals and extensions of localized bonding concepts. *Chemistry Education Research and Practice* **2001**, 2, 91–104.
- (37) Kawada, A.; McGhie, A. R.; Labes, M. M. Protonic Conductivity in Imidazole Single Crystal. *Journal of Chemical Physics* **1970**, 52, 3121–3125.
- (38) Rini, M.; Magnes, B.-Z.; Pines, E.; Nibbering, E. T. J. Real-Time Observation of Bimodal Proton Transfer in Acid-Base Pairs in Water. *Science* **2003**, 301, 349–352.
- (39) Sobolewski, A. L.; Domcke, W.; Hättig, C. Tautomeric Selectivity of the Excited-State Lifetime of Guanine/Cytosine Base Pairs: The Role of Electron-Driven Proton-Transfer Processes. *Proceedings of the National Academy of Sciences* **2005**, 102, 17903–17906.
- (40) Duarte, F.; Vöhringer-Martinez, E.; Toro-Labbé, A. Insights on the mechanism of proton transfer reactions in amino acids. *Physical Chemistry Chemical Physics* **2011**, 13, 7773–7782.
- (41) Leopoldini, M.; Russo, N.; Toscano, M. The Preferred Reaction Path for the Oxidation of Methanol by PQQ-Containing Methanol Dehydrogenase: Addition–Elimination versus Hydride-Transfer Mechanism. *Chemistry - A European Journal* **2006**, 13, 2109–2117.
- (42) Matanović, I.; Došlić, N.; Mihalić, Z. Exploring the potential energy surface for proton transfer in acetylacetone. *Chemical Physics* **2004**, 306, 201–207.
- (43) Barone, V.; Orlandini, L.; Adamo, C. Proton transfer in small model systems: A density functional study. *International Journal of Quantum Chemistry* **2004**, 56, 697–705.
- (44) Zhang, Q.; Bell, R.; Truong, T. N. Ab Initio and Density Functional Theory Studies of Proton Transfer Reactions in Multiple Hydrogen Bond Systems. *Journal of Physical Chemistry* **1995**, 99, 592–599.

- (45) Patchkovskii, S.; Ziegler, T. Improving “difficult” reaction barriers with self-interaction corrected density functional theory. *Journal of Chemical Physics* **2002**, *116*, 7806-7813.
- (46) Chermette, H.; Ciofini, I.; Mariotti, F.; Daul, C. A posteriori corrections to systematic failures of standard density functionals: The dissociation of two-center three-electron systems. *Journal of Chemical Physics* **2001**, *115*, 11068-11080.
- (47) Janesko, B. G.; Scuseria, G. E. Hartree-Fock orbitals significantly improve the reaction barrier heights predicted by semilocal density functionals. *Journal of Chemical Physics* **2008**, *128*, 244112-244116.
- (48) Broadbent, S. A.; Burns, L. A.; Chatterjee, C.; Vaccaro, P. H. Investigation of electronic structure and proton transfer in ground state acetylacetone. *Chemical Physics Letters* **2007**, *434*, 31-37.
- (49) Silva, P. J.; Perez, M. A. S.; Brás, N. F.; Fernandes, P. A.; Ramos, M. J. Improving the study of proton transfers between amino acid side chains in solution: choosing appropriate DFT functionals and avoiding hidden pitfalls. *Theoretical Chemistry Accounts* **2012**, *131*, 1-6.
- (50) Zheng, J.; Zhao, Y.; Truhlar, D. G. The DBH24/08 Database and Its Use to Assess Electronic Structure Model Chemistries for Chemical Reaction Barrier Heights. *Journal of Chemical Theory and Computation* **2009**, *5*, 808-821.
- (51) Perdew, J. P.; Ruzsinszky, A.; Constantin, L. A.; Sun, J.; Csonka, G. I. Some Fundamental Issues in Ground-State Density Functional Theory: A Guide for the Perplexed. *Journal of Chemical Theory and Computation* **2009**, *5*, 902-908.
- (52) Wheeler, S. E.; Houk, K. N. Integration Grid Errors for Meta-GGA-Predicted Reaction Energies: Origin of Grid Errors for the M06 Suite of Functionals. *Journal of Chemical Theory and Computation* **2010**, *6*, 395-404.
- (53) Mantina, M.; Valero, R.; Truhlar, D. G. Validation study of the ability of density functionals to predict the planar-to-three-dimensional structural transition in anionic gold clusters. *Journal of Chemical Physics* **2009**, *131*, 064706-064706-5.
- (54) Brémond, E.; Pilard, D.; Ciofini, I.; Chermette, H.; Adamo, C.; Cortona, P. Generalized gradient exchange functionals based on the gradient-regulated connection: a new member of the TCA family. *Theoretical Chemistry Accounts* **2012**, DOI: 10.1007/s00214-012-1184-0.
- (55) Becke, A. D. Density-functional exchange-energy approximation with correct asymptotic behavior. *Physical Review A* **1988**, *38*, 3098-3100.

- (56) Lee, C.; Yang, W.; Parr, R. G. Development of the Colle-Salvetti correlation-energy formula into a functional of the electron density. *Physical Review B* **1988**, *37*, 785–789.
- (57) Perdew, J. P.; Burke, K.; Ernzerhof, M. Generalized Gradient Approximation Made Simple. *Physical Review Letters* **1996**, *77*, 3865–3868.
- (58) Van Voorhis, T.; Scuseria, G. E. A novel form for the exchange-correlation energy functional. *Journal of Chemical Physics* **1998**, *109*, 400–410.
- (59) Grimme, S. Semiempirical GGA-type density functional constructed with a long-range dispersion correction. *Journal of Computational Chemistry* **2006**, *27*, 1787–1799.
- (60) Wilson, P. J.; Bradley, T. J.; Tozer, D. J. Hybrid exchange-correlation functional determined from thermochemical data and ab initio potentials. *Journal of Chemical Physics* **2001**, *115*, 9233–9242.
- (61) Adamo, C.; Barone, V. Toward reliable adiabatic connection models free from adjustable parameters. *Chemical Physics Letters* **1997**, *274*, 242–250.
- (62) Becke, A. D. A new mixing of Hartree-Fock and local density-functional theories. *Journal of Chemical Physics* **1993**, *98*, 1372–1377.
- (63) Lynch, B. J.; Fast, P. L.; Harris, M.; Truhlar, D. G. Adiabatic Connection for Kinetics. *Journal of Physical Chemistry A* **2000**, *104*, 4811–4815.
- (64) Yanai, T.; Tew, D. P.; Handy, N. C. A new hybrid exchange–correlation functional using the Coulomb-attenuating method (CAM-B3LYP). *Chemical Physics Letters* **2004**, *393*, 51–57.
- (65) Iikura, H.; Tsuneda, T.; Yanai, T.; Hirao, K. A long-range correction scheme for generalized-gradient-approximation exchange functionals. *Journal of Chemical Physics* **2001**, *115*, 3540–3544.
- (66) Chai, J.-D.; Head-Gordon, M. Long-range corrected hybrid density functionals with damped atom–atom dispersion corrections. *Physical Chemistry Chemical Physics* **2008**, *10*, 6615–6620.
- (67) Chai, J.-D.; Head-Gordon, M. Systematic optimization of long-range corrected hybrid density functionals. *Journal of Chemical Physics* **2008**, *128*, 084106-084121.
- (68) Brémond, E.; Adamo, C. Seeking for parameter-free double-hybrid functionals: The PBE0-DH model. *Journal of Chemical Physics* **2011**, *135*, 024106–024106–6.

(69) Grimme, S. Semiempirical hybrid density functional with perturbative second-order correlation. *Journal of Chemical Physics* **2006**, *124*, 034108-034124.

CHAPTER IV: PROTON TRANSPORT IN P4VI

As mentioned in the chapter III, the development of a purposely tailored DFT protocol able to catch both the energetic and the structural features of different imidazole-like dimers has been motivated by the interest of having a suitable method to study systems where the azole moieties are immobilized, namely azole-based polymers. This chapter is devoted to an in-depth investigation of the proton conduction mechanism in the first polymeric system considered in the present thesis. Such a system, named poly-(4-vinyl-imidazole), is here investigated as pure polymer while the influence of adding doping acid molecules on the conduction mechanism will be the object of the chapter V. The results discussed in the present chapter have been object of a publication in the journal *Physical Chemistry Chemical Physics*.¹

1. Introduction

1.1. Poly-(4-vinyl-imidazole)

One of the firsts azole-based polymeric systems synthesized and investigated as proton conductors has been the poly-(4-vinyl-imidazole) (P4VI, figure IV-1). Bozkurt at al.² in 2001 reported synthesis, thermal and conduction properties of the pure polymer as well as of blends obtained using different concentration of phosphoric acid (H_3PO_4). In the same year temperature and pressure dependent studies of P4VI blended with several amounts of phosphoric (H_3PO_4) and sulfuric acid (H_2SO_4) were reported by Pu and al.³

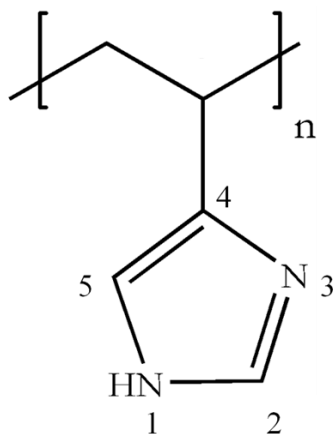


Figure IV-1: Sketches and atom numbering of the poly(4-vinyl-imidazole) chain.

Both the pure polymer and the obtained acid-blended systems showed chemical stability at 150°C and a proton conductivity (σ) depending on the operative conditions such as temperature and pressure. Figure IV-2 shows the temperature dependence of proton conductivities of P4VI and P4VI- $x\text{H}_3\text{PO}_4$ blends, where x refers to the number of H_3PO_4 moles per polymer repeat units. Notably, in all the considered cases, the logarithm of relative proton conductivity increases linearly with increasing the temperature. For instance, concerning the pure polymer ($x=0$), an increment of about 100°K leads to a σ growth of about two order of magnitude (from 10^{-12} to 10^{-10} S/cm).

Although the conductivity of pure P4VI is not at the level requested for fuel cells applications, this system has represented a starting point to develop a series of modified polymers showing better performances.⁴⁻⁷ The poor understanding concerning the explanation of the conductivity differences of these nearly identical polymeric systems is still today considered the main drawback for the design of new azole-based membranes with acceptable level of proton conductivity. This is in part due to the incomplete comprehension of the proton conduction mechanism which is necessary to shed light on how the structure of the proton wire and of the polymer are related to the membrane performance.

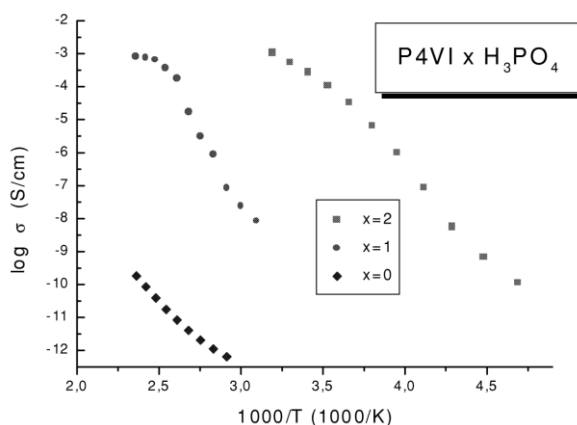


Figure IV-2: Temperature dependence of conductivities of P4VI and P4VI- $x\text{H}_3\text{PO}_4$ blends (adapted from).²

1.2. The Brédas mechanism

As above described in the chapter I, the proton conduction mechanism commonly accepted to explain directional proton molecular transport in azole-based PEMs is the *structural diffusion* also called *Grothuss mechanism*.⁸ Concerning P4VI, a theoretical investigation of such mechanism has been performed by Brédas and coworkers⁹ in order to explain why different values of conductivity are obtained by replacing imidazole with 1,2,3-triazole.⁴ The emerged mechanism (called *Brédas mechanism*¹⁰) relies on the assumption that charge transport occurs through the Grothuss mechanism and is characterized by successive steps (figure IV-3):

- 1) Charge generation: arrival of the proton at one end of the chain of free imidazoles running from one electrode to the other.
- 2) Charge-carrier transport: the excess proton is transferred from the anode to the cathode through a collective proton transfer involving different protons.
- 3) Cooperative rotation: reorientation (or flipping) of the imidazole moieties to recover the starting conformation and to accept a new incoming proton to assure transport in the right direction.
- 4) New charge generation

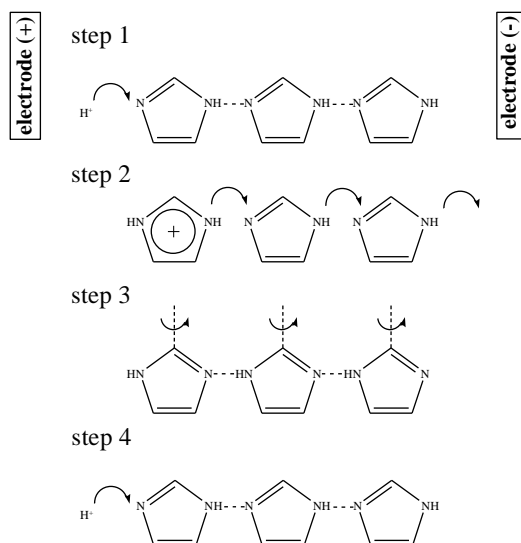


Figure IV-3: The Brédas mechanism for P4VI.

This study has been performed considering models in which the polymeric matrix is not included, an approach which is consistent with other theoretical studies where the conductivity of such polymeric systems is studied focusing on the analysis of proton transfer reactions in dimers, oligomers or chain of free azoles,¹¹⁻¹⁸ therefore in absence of an explicit consideration of the polymer backbone. In these models, nevertheless, some key factors affecting the proton transport mechanism and kinetics in these systems may be missing due to this commonly accepted assumption. For instance, the polymeric constraint could play an important role in the proton conduction since the cooperative rotation (step 3) could be somehow hindered by steric interactions.

Based on these observation and in order to gain more insights into the microscopic mechanism ruling directional charge transport in imidazole-based membranes, in this chapter we present a modeling approach applied both to small (dimer and trimer) and large (oligomer) systems of P4VI. In all the considered models the backbone has been explicitly included. Such an approach relies on the analysis of the electronic structure at DFT level with an explicit description of the dynamical aspects through classical Molecular Dynamics (MD) simulations.

2. Methodological details

All DFT calculations have been performed with the Gaussian-09¹⁹ package and applying the BMK²⁰//B3LYP²¹ protocol described in the chapter III. All the outcomes have been obtained using the 6-311G(d) basis set adding diffuse functions on carbons and nitrogens as well as polarization functions on hydrogens (leading to the 6-311+G(d,p) basis) belonging the heterocycles. Calculations of the harmonic vibrational frequencies have been performed to confirm the nature, minimum or transition state of the localized structures.

Classical Molecular Dynamics simulations were carried out with the AMBER 11 software.²² Based on the DFT outcomes and on a previous work by Voth and collaborators,¹⁸ an improved parameterization of the General Amber Force Field (GAFF)^{23,24} has been carried out. The Restrained ElectroStatic Potential fitting (RESP)^{25,26} procedure has been used to derive the atomic charges. A detailed description of the used F.F. parameters will be given in a following section.

All the MD simulations were carried out in the canonical ensemble, using a time step of 1 fs and sampling the data every 200 fs. The considered model has been first relaxed for 0.5 ns at 393 K, followed by a 4 ns trajectory at the same temperature, this last controlled using the *Andersen* thermostat.²⁷

In order to simulate a locally linear rearrangement as in the real system and minimize spurious model effects arising from the consideration of a single polymer chain (coiling during the MD simulation), the MD simulations have been performed keeping fix the carbons of the backbone to the optimized B3LYP/6-31G(d) structure.

Umbrella sampling calculations²⁸ have been carried out by using dynamics running for 2 ns and a force constant for the harmonic bias potential of $k = 120 \text{ kcal/mol/rad}^2$. The potential of mean force (PMF) has been determined by processing the results with the weighted histogram analysis method (WHAM^{29,30}). In the WHAM equation a bin dimension of 2 degrees has been applied.

3. Results and discussion

3.1. Conduction mechanism in small models: DFT investigation

Protonated dimers

As above mentioned, in the *Brédas mechanism* the polymeric system is represented simply by a free chain ofazole moieties interacting through subsequent hydrogen bonds. Following this model, the excess proton is transferred between two nitrogen atoms which are equivalent at the beginning and at the end of the process (see figure IV-3, step 2). Nevertheless,

as shown in figure IV-1, if the imidazoles are tethered in the polymeric backbone through a covalent binding involving the position 4 (as in P4VI), the positions 1 and 3 of the heterocycles are no longer equivalent so that different PT reactions mechanisms can be envisaged between adjacent imidazoles:

- a) Transfer between nitrogen 1 (N_1) of the first cycle and nitrogen 1 (N_1) of the second cycle
- b) Transfer from N_1 to N_3
- c) Transfer from N_3 to N_1
- d) Transfer from N_3 to N_3

Simple models of protonated dimers which explicitly include the polymeric backbone have been considered to analyze such PT reactions. Figure IV-4 shows the structures of minima and transition states (TS) obtained for all the investigated mechanisms: the proton is transferred from the donor nitrogen atom in position x ($x=1,3$) of the first ring to the acceptor nitrogen atom in position x ($x=1,3$) of the second ring, following the atom numbering listed in figure IV-1. Note that the starting and resulting minima for the PT reactions a (N_1 - N_1) and d (N_3 - N_3) are exactly alike (but with the two imidazoles interchanged) while the product minima by reaction b (N_1 - N_3) is equivalent to the reagent minima of reaction c (N_3 - N_1) and *vice versa*. In other words, mechanisms b and c simply correspond to two opposite directions of the same PT reaction.

Table IV-1: Relative energies (ΔE_{rel} , kcal/mol) with respect to the most stable minimum for all the studied PT mechanisms.

PT mechanism	atoms	ΔE_{rel}	
		minimum	TS
<i>a</i>	N_1 - N_1	16.3	39.8
<i>b</i>	N_1 - N_3	14.3	39.4
<i>c</i>	N_3 - N_1	16.1	39.4
<i>d</i>	N_3 - N_3	0.0	2.5

Table IV-1 shows the relative energies respect to the most stable minima (starting complex of the mechanism d) computed for all the obtained minima and transition states. Starting from these data, the energy barriers corresponding to each PT reaction are simply derivable. Focusing on mechanism d , the obtained activation energy is only slightly higher with respect to that computed for the bare imidazolium-imidazole dimer (1.3 kcal/mol, chapter III), being equal to 2.5 kcal/mol. This indicates that this PT reaction is not significantly affected by the presence of the polymeric matrix. Such a suggestion is confirmed by the analysis of the corresponding structures: in the starting complex a strong hydrogen bond is detected and only a slight rearrangement of the system is necessary to reach the transition state (figure IV-4 *d*).

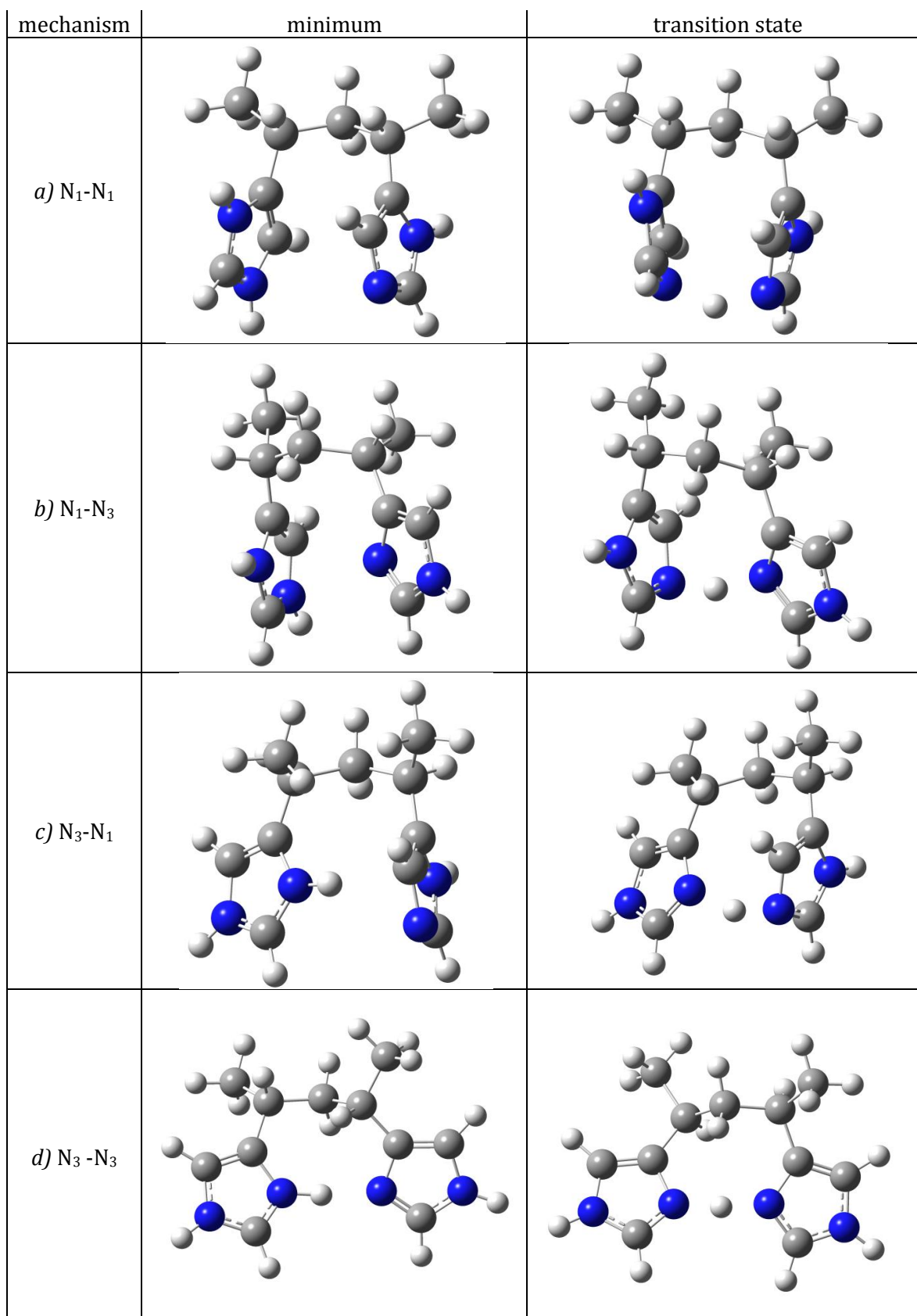


Figure IV-4: Minima and transition states of the protonated dimers involved in the considered PT reactions.

On the contrary, energy barriers greater than 20 kcal/mol are computed for all the other three mechanisms *a*, *b*, *c* so suggesting that the polymeric matrix significantly hinders these PT reactions by imposing strong structural constraints. This is confirmed by the figures IV-4a, 4b, 4c which indicate as for these mechanisms the formation of a strong (linear) H-bond is impeded by the backbone so that an important rearrangement of the system is necessary to reach the transition state. The data itemized in table IV-1 also support this evidence: the relative energies concerning starting minima and transition states of the mechanisms *a*, *b* and *c* are all much higher with respect to the corresponding points of the mechanism *d*.

In short, this first study of the proton conduction in protonated dimers indicates that the polymeric chain energetically rules the conduction in these models making only the mechanism *d* plausible at the operative temperature (energy barrier of about 2.5 kcal/mol).

Protonated trimer

As mentioned, the Grotthuss mechanism in P4VI (*Brédas mechanism*) can take place only if a structural rearrangement involving equivalent and strong hydrogen bonds between the neighboring imidazoles is possible. However, the conclusions drawn from the investigation of protonated dimers indicate that the geometric constraint imposed by the backbone chain excludes the presence of two favorable hydrogen bonds when more than two imidazole moieties are considered. Regarding a trimeric system, for instance, if the central imidazole ring forms a strong N₃-N₃ hydrogen bond with the next imidazole in one direction, it obviously forms an unfavorable hydrogen-bond (between N₁ and N₃ or N₁ and N₁ atoms) with the neighbor imidazole in the other direction so that the structural rearrangement necessary involves a PT energy barrier of as much as 20 kcal/mol. In order to clarify how the proton conduction occurs when more than two imidazole moieties are considered, a trimer system containing one excess proton in the middle has been analyzed (figure IV-5). This model will be referred in the following as *3mer^r* while the three imidazole moieties as *Im_a*, *Im_{b+}* and *Im_c*. By assuming a direction of conduction from *Im_a* to *Im_c*, if the firsts two imidazole moieties are involved in an energetically favored mechanism (H-bond between N₃-N₃, mechanism *d*), the structural rearrangement impedes a linear H-bond between *Im_{b+}* and *Im_c* (N₁-N₃ bridge, mechanism type *b*). Nevertheless, the formation of a new linear (strong) H-bond between *Im_{b+}* and *Im_c* can take place after a flipping (complete rotation of about 180°) of the heterocycle bearing the proton (*Im_{b+}*) around the CC bond (see figure IV-5). The resulting energy barrier obtained through a relaxed scan of the corresponding dihedral angle φ is shown in the figure IV-6 (left). The obtained value of 10.7 kcal/mol indicates that this rotation requires less energy (approximately by a factor of two) than the disfavored PT reactions (*a*, *b*, *c*, table IV-1).

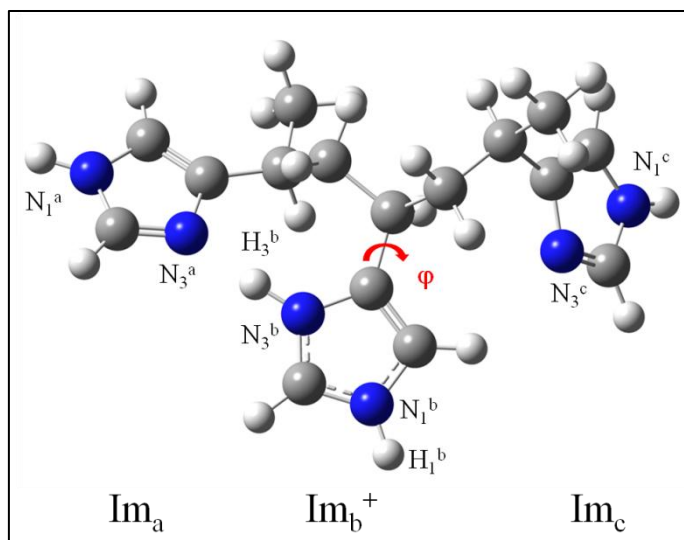


Figure IV-5: Optimized structure of the molecular model 3mer+.

In summary, the results obtained from the DFT investigation on small model systems suggest an alternative conduction mechanism. Indeed, in contrast with the traditional Grotthuss mechanism where different protons are involved in a collective proton transfer (figure IV-3, step 2), here is the same excess proton which is successively transferred from one imidazole to another. Indeed, the first energetically favored PT reaction is followed by a rotation of the protonated heterocycle that causes the formation of a new N₃-N₃ bond with the subsequent imidazole so that a second energetically favored PT can occur. According to this hypothesis, the conduction is the result of a step-by-step PT and the rate-determining step is the rotation of the heterocycle bearing the excess proton.

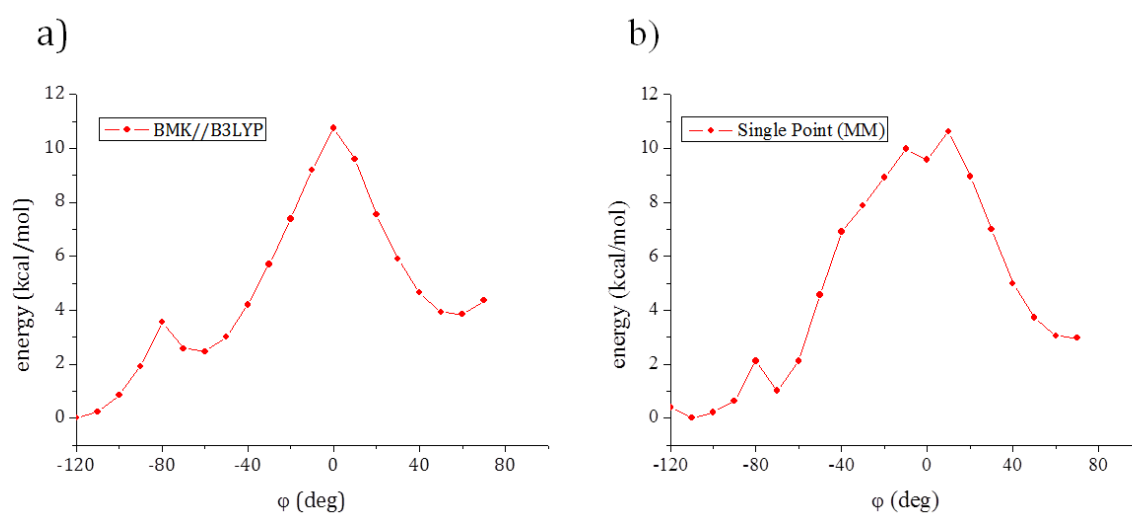


Figure IV-6: Potential energy profile for the torsion around the dihedral angle φ : a) DFT outcomes, b) MM outcomes obtained with the modified GAFF.

3.2. Conduction mechanism in large models: molecular dynamics simulations

According to the picture emerging from the discussed results, proton conductivity in P4VI should not be ruled by the energetic barrier of the PT reaction but by the rotation of the heterocycle bearing the excess proton. Following this hypothesis, the flexibility and in particular the reorientational dynamics of the whole polymeric chain should be crucial aspects in the conduction mechanism which, therefore, can be much better described by including the chemical environment in the investigated model. In order to explore this point, classical MD simulations have been carried out on a larger model system having 15 imidazole moieties. These simulations have been performed using a modified version of the GAFF force field, developed to reproduce the available DFT data.

Force field parametrization

As other force fields, the General Amber Force Field (GAFF^{23,24}) assigns, according to its orbital hybridization and bonding connectivity, to each atom an *atom type* which is described by particular parameters included in the energy expression. The modified version of the GAFF force field used in the present investigation has been obtained through a parameterization performed by considering the DFT data obtained on the model system *3mer⁺*. Table IV-3 shows the atom numbers, the atom types and the relative RESP^{25,26} partial charges computed for *3mer⁺*. The used force field includes all the intramolecular interaction parameters published by Voth and coworkers for imidazole and imidazolium¹⁸ with the exception of two equilibrium angular bending parameters of the central protonated imidazole. These last, in fact, have been replaced by the DFT values (optimized structure) which are considerably different, as shown in the table IV-2.

Table IV-2: Equilibrium bending parameters for the angles c2-na-hn and c2-c2-na.

angle	$\theta_{ijk,o}$ (deg)	
	original	modified
c2-na-hn	119.28	126.35
c2-c2-na	121.38	106.91

A further modification of the GAFF has been performed in order to reproduce the potential energy profile previously obtained using DFT (figure IV-6, left). Notably, a value of the force constant (k_d) referring to the dihedrals describing the torsion around the CC bond and not present in the original FF has been included. Among others, a value of k_d equal to 5.5 kcal/mol has been selected as the best reproducing the DFT data (table IV-4). Notably, for each of the considered k_d value, MM single point calculations have been performed on the DFT structures obtained in the relaxed scan method (one structure for each 10° of φ torsion). As shown in figure IV-6, the rotational barrier obtained using the selected k_d value is in perfect agreement

with the DFT data (10.6 kcal/mol vs. 10.7 kcal/mol) as well as the energy profile which is characterized by a very close shape.

Table IV-3: Atom numbers, GAFF atom types and relative RESP partial charges computed for 3mer⁺.

atom number	GAFF atom type	q (e ⁻)	atom number	GAFF atom type	q (e ⁻)
1	c3	-0.156	24	na	-0.318
2	hc	0.077	25	hn	0.363
3	hc	0.077	26	c3	-0.105
4	c3	-0.005	27	hc	0.032
5	hc	0.052	28	hc	0.032
6	c3	-0.156	29	hc	0.032
7	hc	0.077	30	hn	0.381
8	hc	0.077	31	c3	0.070
9	c3	0.070	32	hc	0.040
10	hc	0.040	33	c3	-0.105
11	c2	-0.101	34	hc	0.032
12	c2	-0.035	35	hc	0.032
13	h4	0.167	36	hc	0.032
14	h5	0.248	37	cd	-0.201
15	cd	-0.201	38	cd	0.164
16	h4	0.196	39	h4	0.196
17	cd	0.164	40	h5	0.143
18	h5	0.143	41	cc	0.155
19	c2	0.076	42	na	-0.318
20	cc	0.155	43	nc	-0.468
21	na	-0.108	44	hn	0.272
22	na	-0.209	45	hn	0.363
23	nc	-0.468			

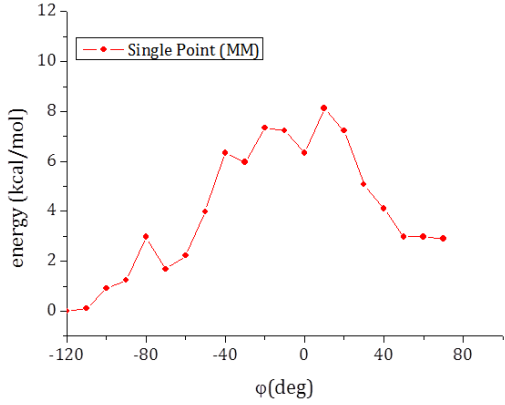
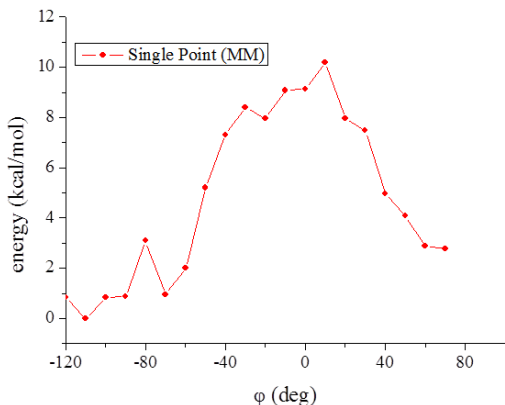
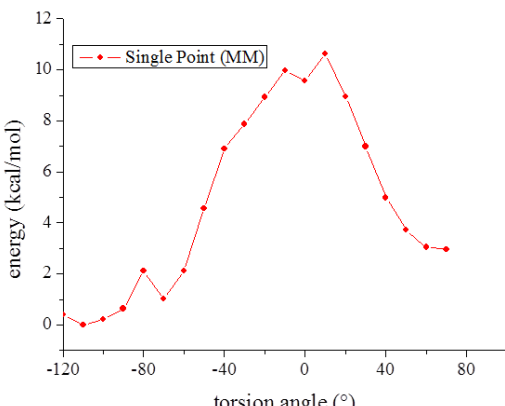
Analysis of the trajectory

The modified version of GAFF has been adopted to perform out MD simulations on a system composed by 15 monomers and containing one excess proton (figure IV-7). In this model, referred in the following as 15mer⁺, all the nitrogen atoms in position 3 are acceptors while the nitrogens in position 1 bear an hydrogen atom. Furthermore, the excess proton has been added to the middle so that the central trimer is similar to the system taken into account for DFT calculations (3mer⁺). Indeed, the charged imidazole (Im_{b+}) is involved in an H-bond with a low PT activation energy (involving two N₃ atoms) and in another one with high PT barrier (involving N₁ and N₃ atoms). For matter of clarity, therefore, the same atom labeling of 3mer⁺ (see figure IV-5) will be used to identify the atoms of the central trimer (see zoom in figure IV-7). For atom numbers, atom types and relative RESP^{25,26} partial charges computed for 15mer⁺ see annex II.

The variation of the dihedral describing the rotation around the covalent C-C bond between the central imidazole Im_{b+} and the backbone (dihedral φ) along the whole 4ns trajectory is shown in the figure IV-8 (a): during the simulation an oscillation of about 80° (from -40° to +40°) is observed thus indicating a large flexibility of the system. Interestingly, the HN lengths relatives to the H-bonds between Im_a-Im_{b+} and Im_{b+}-Im_c are related to this φ motion.

Figure IV-8 shows the time-dependent fluctuations of the H₃^b-N₃^a distance (b) and H₃^b-N₃^c distance (c) along the whole trajectory.

Table IV-4: Energetic profiles obtained using increasing values of k_d . The best agreement with the DFT data is obtained using $K_d=5.5$ kcal/mol (See figure IV-6).

k _d value	corresponding energetic profile
4 kcal/mol	
5 kcal/mol	
5.5 kcal/mol	

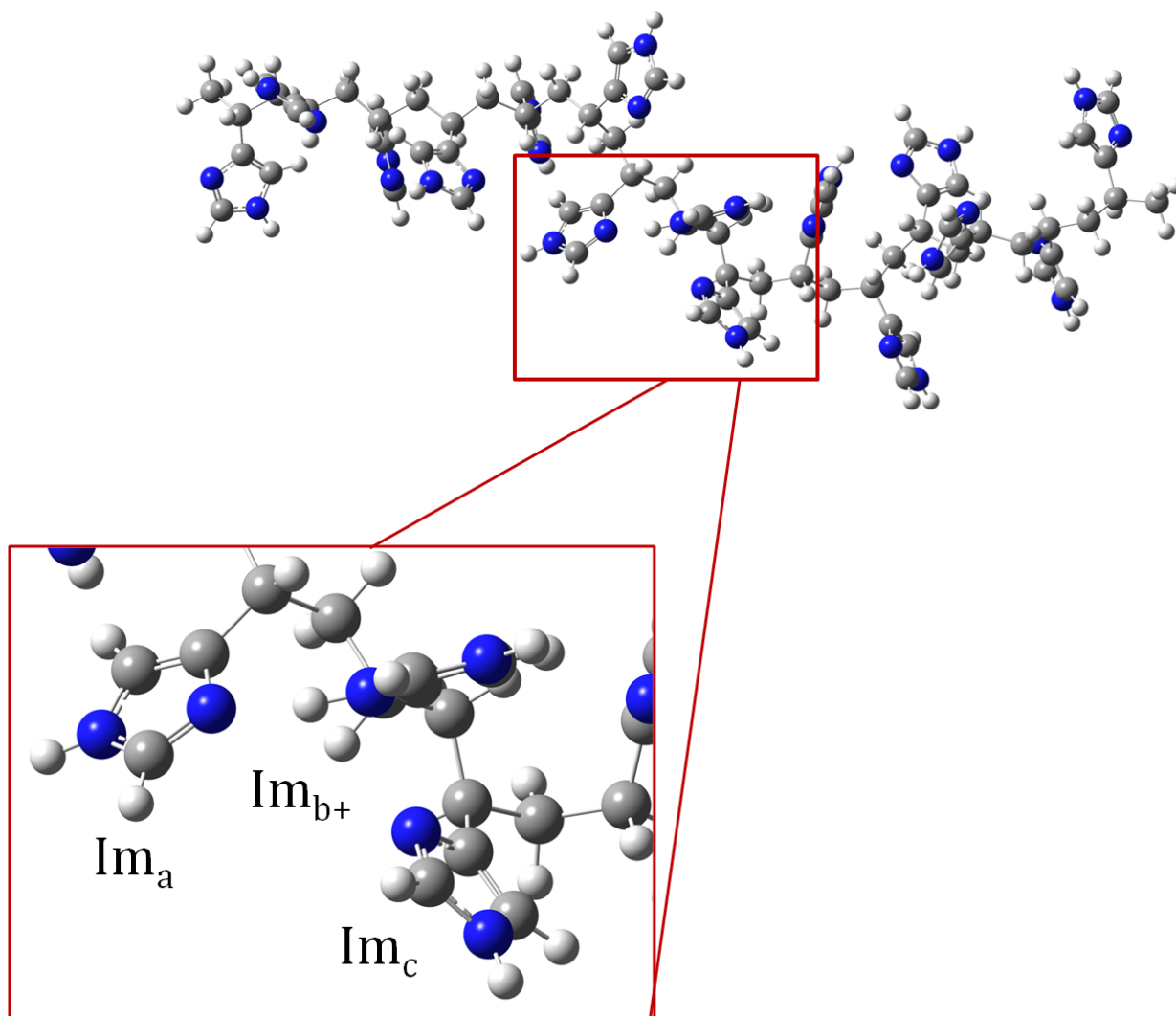


Figure IV-7: Optimized molecular structure of 15mer⁺. The central trimer with the excess proton is shown in the zoom.

Notably, each time that the dihedral φ approaches to 40° , the N_3^a - H_3^b length increases toward about 3 \AA while the H_3^b - N_3^c distance decreases to approximately 2.0 \AA . The φ oscillation is also correlated to an increasing (decreasing) of the NN distances between Im_a and Im_{b^+} (Im_{b^+} and Im_c): N_3^a - N_3^b distance increases up toward 4 \AA and the N_3^b - N_3^c distance goes down to approximately 2.7 \AA . Figure IV-9 shows an extracted (first 100 ps) of the whole trajectory and gives an example of the concomitant variation of NN and HN lengths as a function of the dihedral φ . Focusing on the details of the first part of the trajectory (first 10 ps, see figure IV-10), it appears evident that only few ps are necessary in order to have the first significant imidazolium rotation (from 5.8 ps to 6.0 ps). Such a oscillation occurs very quickly requiring less than 200 fs to take place and an amplitude of only 66° (from $\varphi = -32^\circ$ to $\varphi = +34^\circ$) is associated to an H-bond breaking and forming process, as clearly itemized in figure IV-11. Indeed, the φ oscillation leads

to an increase of about 1.6 Å (from 2.02 to 3.63 Å) of the N_3^a - H_3^b distance, while the H_3^b - N_3^c length decreases by about 1.8 Å (from 4.02 to 2.16 Å).

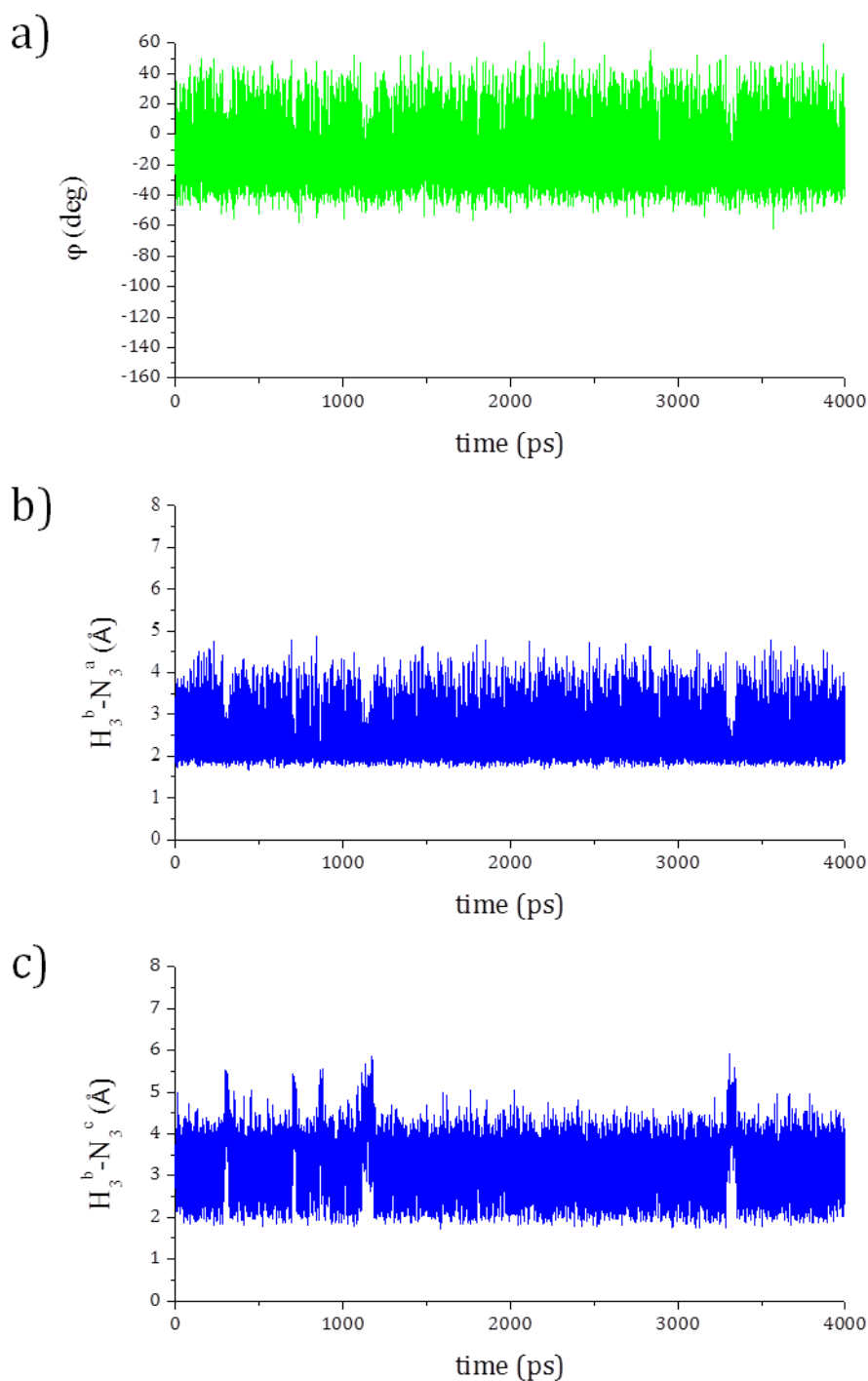


Figure IV-8: Time-dependent fluctuations along the 4-ns trajectory of a) dihedral φ , b) $H_3^b-N_3^a$ distance and c) $H_3^b-N_3^c$ distance.

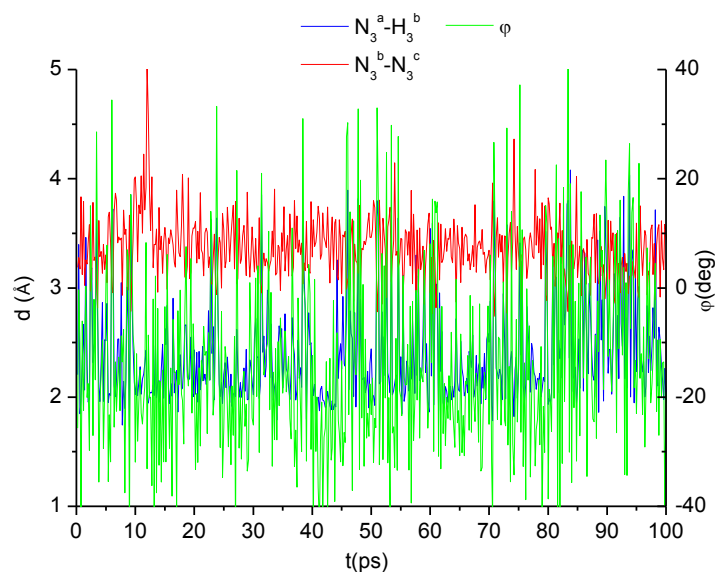


Figure IV-9: Time-dependent evolutions of dihedral ϕ , $H_3^b-N_3^a$ distance and $N_3^b-N_3^c$ distance along the first 100ps of trajectory.

In short, if for the $3mer^+$ system the rate limiting step of the proposed conduction mechanism corresponds to a complete (180°) rotation of the imidazole bearing the excess proton, here the MD simulations suggests that for the more realistic $15mer^+$ polymer such a step consists of a soft motion (frustrated rotation). Indeed, when a large system is considered, a planar rearrangement of the imidazole wires is not permitted due to the polymeric matrix so that a rotation of about 80° is sufficient for the breaking and forming process of H-bond required for subsequent low-barrier PTs.

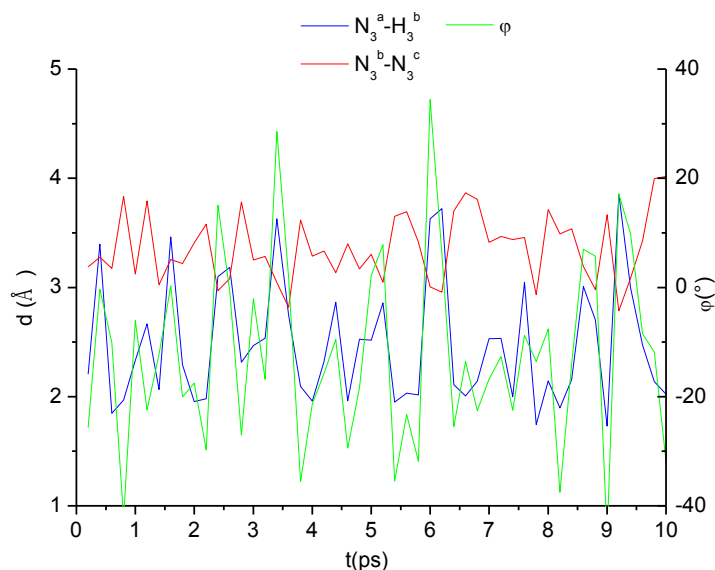


Figure IV-10: Time-dependent evolutions of dihedral ϕ , $H_3^b-N_3^a$ distance and $N_3^b-N_3^c$ distance along the first 10ps of trajectory.

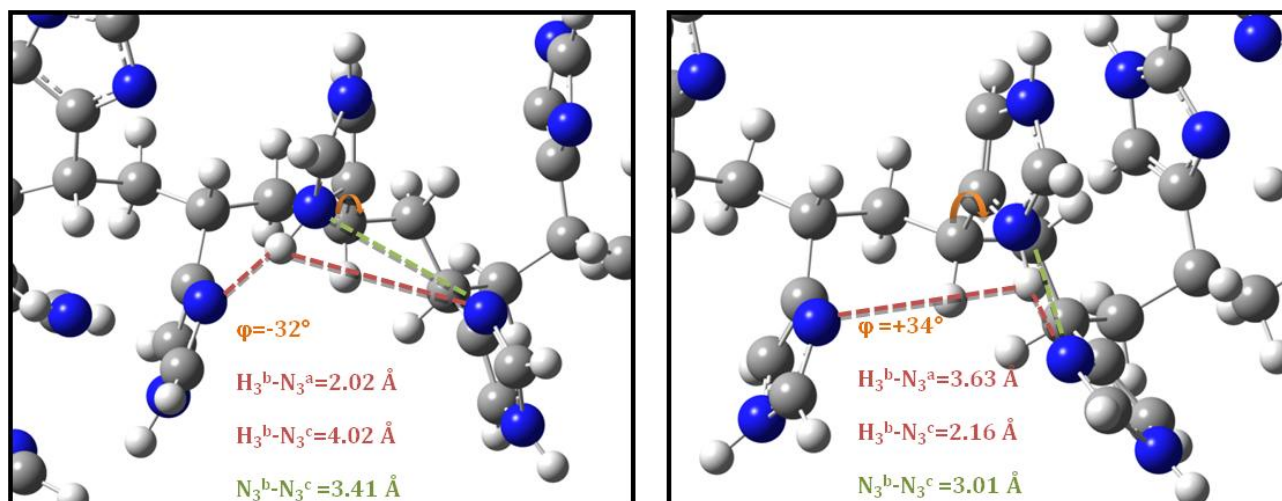


Figure IV-11: Snapshots of the 0.2 ps interval (from 5.8 to 6.0 ps) extracted from the 4-ns trajectory. The considered H-bonds are depicted by a dotted line.

3.3. A new charge-transport mechanism

The discussed results show that the backbone constraint can strongly affect the charge transport in P4VI so that its influence cannot be neglected. In other words, the conclusions obtained in earlier works should be critically revised since these studies are performed on models not including the polymeric matrix and so where the conduction takes place simply along an equivalent H-bonds chain (see figure IV-3, step 2). On the contrary, the present results indicate that when a more realistic system is considered (explicitly including the polymeric matrix) several PTs reactions should be undertaken since the hydrogen bonds between adjacentazole moieties are no longer equivalent. Notably, among the different reaction paths, only one is plausible at operative temperatures having an energy barrier of only 2.5 kcal/mol (vs. values above 20 kcal/mol for the other considered mechanisms). It consists in a PT reaction between two nitrogen atoms in position 3 of the heterocycles. In other words, when the polymeric matrix is included, the presence of more than two imidazole units in the model is sufficient for excluding the existence of an equivalent H-bonds chain. For instance, in a trimeric system, if an imidazole ring is involved in a strong N_3-N_3 hydrogen bond with the neighboring imidazole, it cannot form an H-bond with the ring in the opposite direction (see figure IV-5).

The proton conduction along the chain, therefore, can take place only if an alternative path is considered. It involves the rotation of the protonated imidazole around the CC bond linking this heterocycle with the polymeric chain. Such a rotation, representing the rate limiting step, occurs after each favorable PT and leads to the breaking of the one-hand H-bond and to the formation of the other-hand H-bond. Interestingly, in a trimeric system, this step requires only one half of the energy required for a second direct PT (10 kcal/mol vs. 20kcal/mol).

The MD simulations support this alternative conduction mechanism showing that such rate limiting step occurs quickly at 393K, a typical operational temperature for these systems. Furthermore, such a step is strongly affected by the chemical environment. Indeed, differently from the trimeric system, when a larger oligomer is considered, a partial imidazolium rotation (almost 80° of amplitude) is sufficient to reach $N_3^b-N_3^c$ distances (at least shorter than 2.65 Å) that allow for low energy requiring PT reaction. The figure IV-12 shows the energy of the PT reaction (between Im_b^+ and Im_c) computed at different N-N and H-N distances ($N_3^b-N_3^c$ and $H_3^b-N_3^c$): a PT barrier lower than 3.0 kcal/mol is sufficient when the NN distance decreases to values shorter than 2.65 Å, a threshold which is reached during the simulation (Figure IV-13). Coherently with these evidences, the hypothesized rate limiting step (imidazolium soft motion) is characterized by a low free energy barrier. Figure IV-14 shows the free energy profile along the reaction coordinate (torsion angle φ) computed at different temperatures: the frustrated rotation (from -40° to +40°) requires about 9 kcal/mol at 100K and 6 kcal/mol at 393K. These data, carried out using umbrella sampling technique and weighted histogram analysis method (WHAM), indicates that the temperature dependence of the energy barrier can be assigned to entropic effects.

It is worthy to note, moreover, that together with an adiabatic mechanism which is favored by the low barrier computed along the proton coordinates (3 kcal/mol, comparable to the N-H stretch vibration zero energy); the proton motion could also occur through a non-adiabatic mechanism (tunneling) which becomes possible thanks to the short N-N donor-acceptor distances reached during the simulations. In other words, the quantum mechanical effects are expected to further increase the proton transfer probability relative to the classical description of the proton motion.

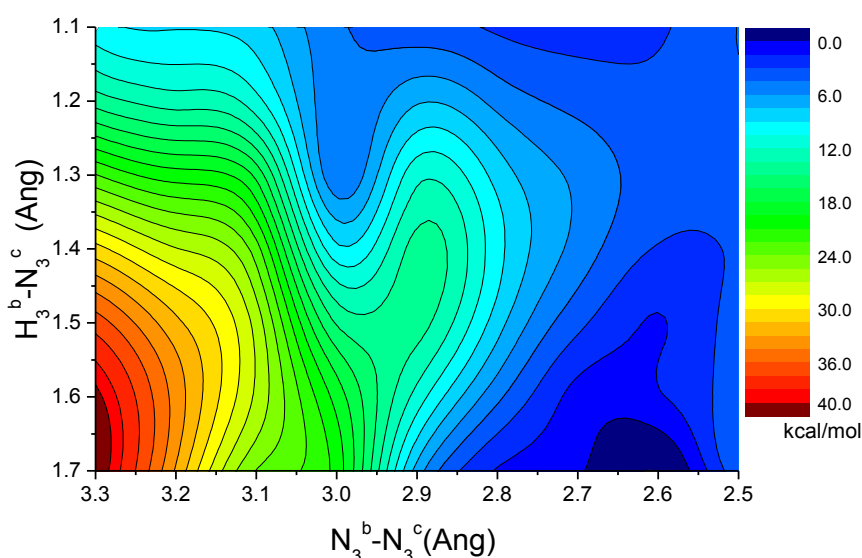


Figure IV-12: 2d plot of the DFT energy landscape for the PT between the second and third imidazole in 3mer⁺ as a function of $H_3^b-N_3^c$ and $N_3^b-N_3^c$ distances.

Taken together, these results allow to hypothesize a new charge transport mechanism where the determining step is a frustrated rotation of the protonated imidazole. Such a mechanism strongly differs from the *Bredas mechanism* sketched in figure IV-3. Indeed, the first step (arrival of the proton at one end of the chain) is here followed by a frustrated rotation (step 2, reorientation) which in turn allows for a second proton transfer (step 3, charge-carrier transport). In other words, the proposed mechanism requires n frustrated rotations of single protonated imidazoles instead of a concerted global rotation for each proton discharged at the electrode (see figure IV-15).

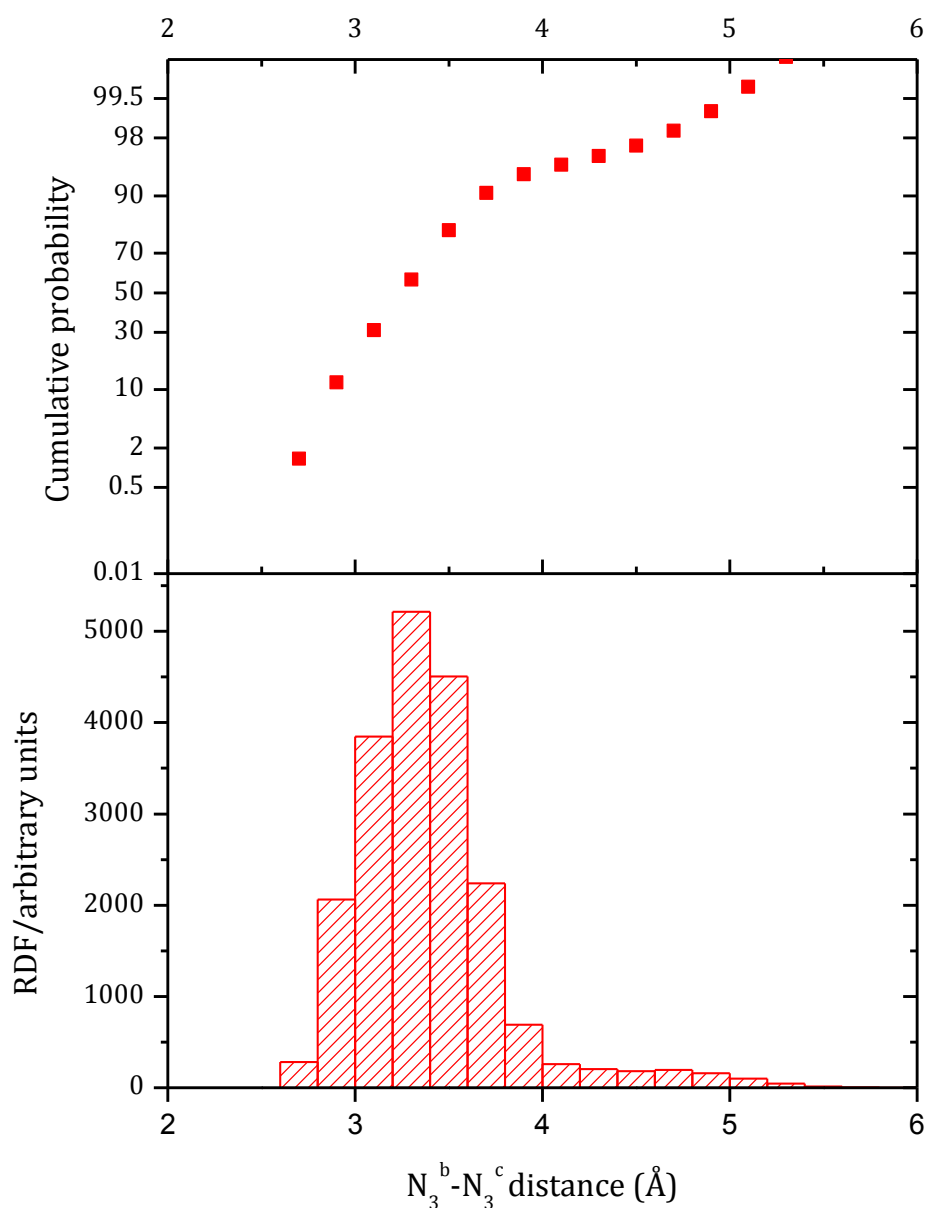


Figure IV-13: Occurrence of the $N_3^b-N_3^c$ distance during the 4ns simulations

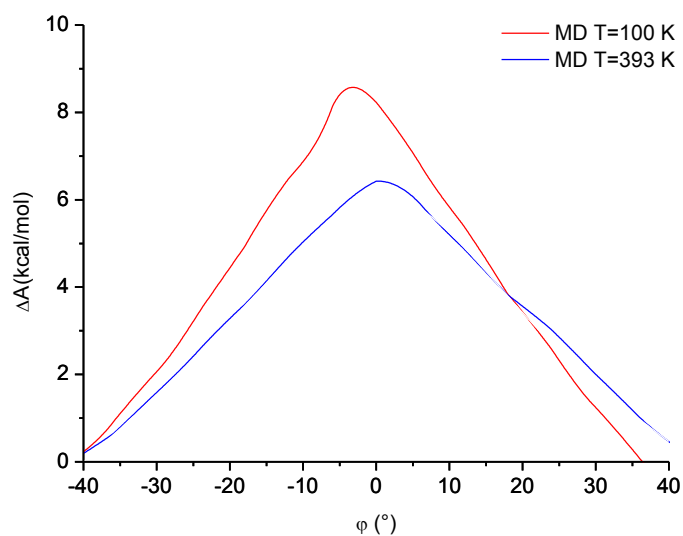


Figure IV-14: Free energy profiles for the 80° amplitude rotation around the dihedral ϕ computed for the model system 3mer⁺ at two different temperatures.

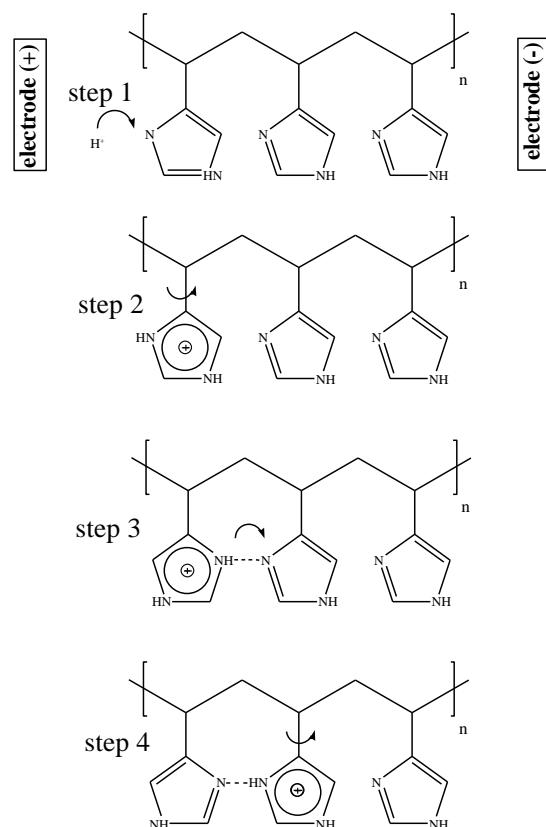


Figure IV-15: Proton conduction mechanism for P4VI proposed in the present research: 1) arrival of a proton at the end of the chain, 2) imidazolium frustrated rotation, 3) single proton transfer reaction, 4) new frustrated rotation.

3.4. Support from experimental evidences

Because of the poor understanding concerning the charge transport in polymer electrolytes, experimental evidences have been often used as indicator for a particular type of conduction mechanism. For instance, the temperature dependence of the conductivity can give an idea of the crucial aspects governing the charge transport in azole-based membranes.^{31,32} Regarding the P4VI itself, it has been found that increasing the temperature, the proton conductivity rises by several order of magnitude.^{2,3} In accordance with this evidence, the computed energy amount required for the rate limiting step of the proposed mechanism decreases as the temperature increases (see figure IV-14). Furthermore, it has been shown that the proton transport in this polymer is strongly promoted by the flexibility of the system.^{2,3} Indeed, proton conductivity increases as the glass transition temperature (T_g) of P4VI decreases (for instance adding acid dopant). Such lower T_g s are the signature of reorientational dynamics in N-heterocyclic polymers due to higher flexibility of the system (for a short discussion on this point see references³³⁻³⁵).

Focusing on the activation energy for the conduction, values of the same order of that found for the proposed mechanism (6 kcal/mol at 393 K) have been estimated for systems comparable to P4VI. For instance values going from 12 to 14 kcal/mol have been found for imidazoles tethered to siloxane backbone. Importantly, the energy requested for the conduction decreases to 6 kcal/mol when an few quantity (10% with respect to the imidazole units) of acid dopant is added³⁶ thanks to the enhanced chain flexibility. In other words, the theoretical value of activation energy issued from our calculations matches well with the experimental estimations so supporting the rule of the ring rotation as rate limiting step in the charge transport. Furthermore, consistently with our proposed mechanism, from NMR data emerges a local picture of the proton conduction where bonds are broken and then reformed as a proton passes along.³⁶

Finally, a further support for the proposed mechanism can be obtained through a qualitative estimation of the proton diffusion coefficient which can be obtained from our calculations. Indeed, such a coefficient can be expressed as:

$$D = \frac{1}{2} v a^2 \exp(-E / RT) \quad (IV-2)$$

where v is the motion frequency, a the proton jump distance and E the required energy for each proton motion.³⁷ Following the proposed mechanism, it can be assumed a proton jump of 4 Å (distance between N_3^a and N_3^c) for each frustrated rotation which in turn require 6 kcal/mol to take place and is characterized by a frequency corresponding to the imaginary frequency computed at the DFT level ($v=4,33 \times 10^{12} \text{ sec}^{-1}$). The resulting value ($D=1.58 \times 10^{-6} \text{ cm}^2 \text{ sec}^{-1}$)

is of the same order to those obtained for other imidazole-based materials³⁸ so further supporting our hypothesis.

3.5. Charges and electrostatic potential: support to the MD simulation quality

Even though the Amber Force Field approach has been largely used in processes involving H-bond breaking and formation as for instance protein-substrate interaction³⁹ or protein conformational changes,^{40,41} it could be argued that the rate-limiting step of the proposed mechanism could be not correctly reproduced by a force field which uses fixed charges. So, in order to further validate the considered theoretical approach, both RESP and NBO⁴² charges have been taken into account for the atoms involved in a formation/breaking process of hydrogen bonds during the investigated soft motion (N_{3^a} , H_{3^b} , N_{3^b} , H-bond between Im_a and Im_{b+}). The obtained data are collected in table IV-5: while small variations (less than 10%) are detected for RESP charges, the NBO model provides charges almost unchanged during the imidazolium rotation. In agreement with this evidence, no significant variation can be observed for the electrostatic potential during such critical step (figure IV-16). Taken together, these results further support the quality of the performed MD simulation.

Table IV-5: NBO and RESP charges computed along the frustrated rotation of the protonated central imidazole in 3mer*.

φ	NBO			Mulliken		
	-30	0	30	-30	0	30
H_{3^b}	0.488	0.487	0.491	0.324	0.315	0.327
N_{3^b}	-0.542	-0.516	-0.536	-0.208	-0.245	-0.220
N_{3^a}	-0.614	-0.601	-0.617	-0.658	-0.620	-0.667

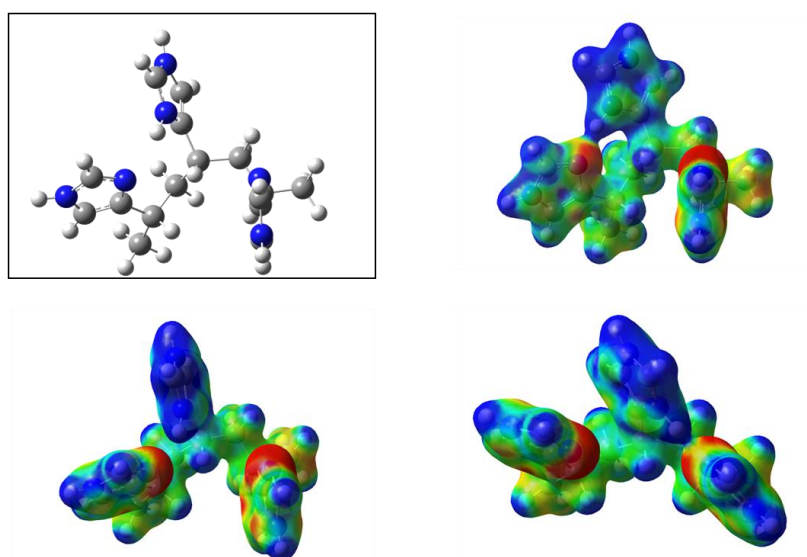


Figure IV-16: Electrostatic potential computed along the frustrated rotation of the dihedral φ : upper right $\varphi=-30^\circ$, lower left $\varphi=0^\circ$, lower right $\varphi=30^\circ$

4. Conclusions

Thanks to the explicit consideration of the polymeric backbone in the investigated models, a new conductivity mechanism has been proposed for a prototype azole-based proton conductors named P4VI. Indeed, the backbone constraint has been proved to be crucial in affecting the charge transport in this system so suggesting that the conclusions drawn from earlier works on chains of free imidazoles should be critically revised.

In particular, the presented theoretical outcomes allow to draw out a mechanism where the frustrated rotation of the imidazole bearing the excess proton is the rate-limiting step. Such a step is necessary before each proton transfer reaction between adjacent azole-moieties can take place. Importantly, the proposed model could be favored respect to the Grotthuss mechanism which is commonly accepted for these systems.

Despite the conductivity of the pure P4VI is far from the level requested for PEMFCs applications (chapter I), the discussed outcomes can represent a useful starting point to shed light on the different conductivity of nearly identical systems. Furthermore, the obtained new insights into the charge-transport can pave the way for the design of new materials with advanced performances. Notably, this last point will be deal with in chapter VI where, based on the suggestions emerged from the present study, an imidazole-base polymer characterized by a different wire tethering will be investigated.

5. References

- (1) Mangiatordi, G. F.; Butera, V.; Russo, N.; Laage, D.; Adamo, C. Charge transport in polyimidazole membranes: a fresh appraisal of the Grotthuss mechanism. *Physical Chemistry Chemical Physics* **2012**, *14*, 10910-10918.
- (2) Bozkurt, A.; Meyer, W. Proton conducting blends of poly(4-vinylimidazole) with phosphoric acid. *Solid State Ionics* **2001**, *138*, 259-265.
- (3) Pu, H.; Meyer, W. H.; Wegner, G. Proton Conductivity in Acid-Blended Poly(4-vinylimidazole). *Macromolecular Chemistry and Physics* **2001**, *202*, 1478-1482.
- (4) Zhou, Z.; Li, S.; Zhang, Y.; Liu, M.; Li, W. Promotion of Proton Conduction in Polymer Electrolyte Membranes by 1H-1,2,3-Triazole. *Journal of American Chemical Society* **2005**, *127*, 10824-10825.
- (5) Johnson, D. M.; Rasmussen, P. G. An Improved Synthesis of 2-Vinyl-4,5-dicyanoimidazole and Characterization of Its Polymers. *Macromolecules* **2000**, *33*, 8597-8603.
- (6) Pu, H.; Wu, J.; Wan, D.; Chang, Z. Synthesis and anhydrous proton conductivity of poly(5-vinyltetrazole) prepared by free radical polymerization. *Journal of Membrane Science* **2008**, *322*, 392-399.
- (7) Çelik, S. Ü.; Aslan, A.; Bozkurt, A. Phosphoric acid-doped poly(1-vinyl-1,2,4-triazole) as water-free proton conducting polymer electrolytes. *Solid State Ionics* **2008**, *179*, 683-688.
- (8) Agmon, N. The Grotthuss mechanism. *Chemical Physics Letters* **1995**, *244*, 456-462.
- (9) Zhou, Z.; Liu, R.; Wang, J.; Li, S.; Liu, M.; Brédas, J.-L. Intra- and Intermolecular Proton Transfer in 1H(2H)-1,2,3-Triazole Based Systems. *Journal of Physical Chemistry A* **2006**, *110*, 2322-2324.
- (10) Alkorta, I.; Elguero, J. Theoretical models of directional proton molecular transport. *Organic & Biomolecular Chemistry* **2006**, *4*, 3096-3101.
- (11) Tatara, W.; Wojcik, M. J.; Lindgren, J.; Probst, M. Theoretical study of structures, energies, and vibrational spectra of the imidazole-imidazolium system. *The Journal of Physical Chemistry. A* *107*, 7827-7831.
- (12) Iannuzzi, M.; Parrinello, M. Proton Transfer in Heterocycle Crystals. *Physical Review Letters* **2004**, *93*.

- (13) Iannuzzi, M. Proton transfer in imidazole-based molecular crystals. *The Journal of Chemical Physics* **2006**, *124*, 204710–204710–10.
- (14) Deng, W.-Q.; Molinero, V.; Goddard, W. A., 3rd Fluorinated imidazoles as proton carriers for water-free fuel cell membranes. *Journal of American Chemical Society* **2004**, *126*, 15644–15645.
- (15) Goddard, W.; Merinov, B.; Duin, A. V.; Jacob, T.; Blanco, M.; Molinero, V.; Jang, S. S.; Jang, Y. H., Multi-paradigm multi-scale simulations for fuel cell catalysts and membranes. *Molecular simulations* **2006**, *32*, 351-268.
- (16) Subbaraman, R.; Ghassemi, H.; Zawodzinski Jr., T. Triazole and triazole derivatives as proton transport facilitators in polymer electrolyte membrane fuel cells. *Solid State Ionics* **2009**, *180*, 1143–1150.
- (17) Li, A.; Yan, T.; Shen, P. Exploring proton transfer in 1,2,3-triazole-triazolium dimer with ab initio method. *Journal of power sources* *196*, 905–910.
- (18) Chen, H.; Yan, T.; Voth, G. A. A computer simulation model for proton transport in liquid imidazole. *Journal of Physical Chemistry A* **2009**, *113*, 4507–4517.
- (19) Frisch, M. J.; Trucks, G. W.; Schlegel, H. B.; Scuseria, G. E.; Robb, M. A.; Cheeseman, J. R.; Scalmani, G.; Barone, V.; Mennucci, B.; Petersson, G. A.; Nakatsuji, H.; Caricato, M.; Li, X.; Hratchian, H. P.; Izmaylov, A. F.; Bloino, J.; Zheng, G.; Sonnenberg, J. L.; Hada, M.; Ehara, M.; Toyota, K.; Fukuda, R.; Hasegawa, J.; Ishida, M.; Nakajima, T.; Honda, Y.; Kitao, O.; Nakai, H.; Vreven, T.; Montgomery, Jr., J. A.; Peralta, J. E.; Ogliaro, F.; Bearpark, M.; Heyd, J. J.; Brothers, E.; Kudin, K. N.; Staroverov, V. N.; Kobayashi, R.; Normand, J.; Raghavachari, K.; Rendell, A.; Burant, J. C.; Iyengar, S. S.; Tomasi, J.; Cossi, M.; Rega, N.; Millam, N. J.; Klene, M.; Knox, J. E.; Cross, J. B.; Bakken, V.; Adamo, C.; Jaramillo, J.; Gomperts, R.; Stratmann, R. E.; Yazyev, O.; Austin, A. J.; Cammi, R.; Pomelli, C.; Ochterski, J. W.; Martin, R. L.; Morokuma, K.; Zakrzewski, V. G.; Voth, G. A.; Salvador, P.; Dannenberg, J. J.; Dapprich, S.; Daniels, A. D.; Farkas, Ö.; Foresman, J. B.; Ortiz, J. V.; Cioslowski, J.; Fox, D. J. Gaussian, Inc., Wallingford CT, **2009**.
- (20) Boese, A. D.; Martin, J. M. L. Development of density functionals for thermochemical kinetics. *The Journal of Chemical Physics* **2004**, *121*, 3405–3416.
- (21) Becke, A. D. Density-functional thermochemistry. III. The role of exact exchange. *The Journal of Chemical Physics* **1993**, *98*, 5648.

- (22) Case D. A.; Darden T. A.; Cheatham T. E.; Simmerling C. L.; Wang J.; Duke R. E.; Luo R.; Walker, R. C.; Zhang W.; Merz K. M.; Roberts B.; Wang B.; Hayik S.; Roitberg A.; Seabra G.; Kolossvary I.; Wong K. F.; Paesani F.; Vanicek J.; Liu J.; Wu X.; Brozell S. R.; Steinbrecher T.; Gohlke H.; Cai Q.; Ye X.; Wang J.; Hsieh M. J.; Cui G.; Roe D. R.; Mathews D. H.; Seetin M. G.; Sagui C.; Babin V.; Luchko T.; Gusarov S.; Kovalenko A. and Kollman P. A., AMBER 11; University of California: San Francisco, **2010**.
- (23) Wang, J.; Wolf, R. M.; Caldwell, J. W.; Kollman, P. A.; Case, D. A. Development and testing of a general amber force field. *Journal of Computational Chemistry* **2004**, *25*, 1157–1174.
- (24) Wang, J.; Wang, W.; Kollman, P. A.; Case, D. A. Automatic atom type and bond type perception in molecular mechanical calculations. *Journal of Molecular Graphics and Modeling* **2006**, *25*, 247–260.
- (25) Bayly, C. I.; Cieplak, P.; Cornell, W.; Kollman, P. A. A well-behaved electrostatic potential based method using charge restraints for deriving atomic charges: the RESP model. *The Journal of Physical Chemistry* **1993**, *97*, 10269–10280.
- (26) Cornell, W. D.; Cieplak, P.; Bayly, C. I.; Kollman, P. A. Application of RESP charges to calculate conformational energies, hydrogen bond energies, and free energies of solvation. *Journal of the American Chemical Society* **1993**, *115*, 9620–9631.
- (27) Andersen, H. C. Molecular dynamics simulations at constant pressure and/or temperature. *The Journal of Chemical Physics* **1980**, *72*, 2384–2393.
- (28) Torrie, G. M.; Valleau, J. P. Monte Carlo free energy estimates using non-Boltzmann sampling: Application to the sub-critical Lennard-Jones fluid. *Chemical Physics Letters* **1974**, *28*, 578–581.
- (29) Kumar, S.; Rosenberg, J. M.; Bouzida, D.; Swendsen, R. H.; Kollman, P. A. THE weighted histogram analysis method for free-energy calculations on biomolecules. I. The method. *Journal of Computational Chemistry* **1992**, *13*, 1011–1021.
- (30) Kumar, S.; Rosenberg, J. M.; Bouzida, D.; Swendsen, R. H.; Kollman, P. A. Multidimensional free-energy calculations using the weighted histogram analysis method. *Journal of Computational Chemistry* **1995**, *16*, 1339–1350.
- (31) Armand, M. Polymer solid electrolytes - an overview. *Solid State Ionics* **1983**, *9–10*, 745–754.

- (32) Ratner, M. A.; Mac-Callum, J. R.; Vincent, C. A.; Polymer Electrolyte Review-1. *Elsevier Applied Science*, New York **1987**, 173.
- (33) Nagamani, C.; Viswanathan, U.; Versek, C.; Tuominen, M. T.; Auerbach, S. M.; Thayumanavan, S. Importance of dynamic hydrogen bonds and reorientation barriers in proton transport. *Chemical Communications* **2011**, 47, 6638–6640.
- (34) Schuster, M. F. H.; Meyer, W. H.; Schuster, M.; Kreuer, K. D. Toward a New Type of Anhydrous Organic Proton Conductor Based on Immobilized Imidazole†. *Chemistry of Materials* **2003**, 16, 329–337.
- (35) Persson, J. C.; Jannasch, P. Intrinsically Proton-Conducting Benzimidazole Units Tethered to Polysiloxanes. *Macromolecules* **2005**, 38, 3283–3289.
- (36) Benhabbour, S. R.; Chapman, R. P.; Scharfenberger, G.; Meyer, W. H.; Goward, G. R. Study of Imidazole-Based Proton-Conducting Composite Materials Using Solid-State NMR. *Chemistry of Materials* **2005**, 17, 1605–1612.
- (37) O’Keeffe, M.; Perrino, C. T. Proton conductivity in pure and doped KH₂PO₄. *Journal of Physics and Chemistry of Solids* **1967**, 28, 211–218.
- (38) Schuster, M.; Meyer, W. .; Wegner, G.; Herz, H. .; Ise, M.; Schuster, M.; Kreuer, K. .; Maier, J. Proton mobility in oligomer-bound proton solvents: imidazole immobilization via flexible spacers. *Solid State Ionics* **2001**, 145, 85–92.
- (39) Rosen, S. A. J.; Gaffney, P. R. J.; Spiess, B.; Gould, I. R. Understanding the relative affinity and specificity of the pleckstrin homology domain of protein kinase B for inositol phosphates. *Physical Chemistry Chemical Physics* **2011**, 14, 929–936.
- (40) Wang, L.; Berne, B. J.; Friesner, R. A. On Achieving High Accuracy and Reliability in the Calculation of Relative Protein–Ligand Binding Affinities. *Proceedings of the National Academy of Sciences* **2012**, 109, 1937–1942.
- (41) Xue, Y.; Ward, J. M.; Yuwen, T.; Podkorytov, I. S.; Skrynnikov, N. R. Microsecond Time-Scale Conformational Exchange in Proteins: Using Long Molecular Dynamics Trajectory To Simulate NMR Relaxation Dispersion Data. *Journal of the American Chemical Society* **2011**, 134, 2555–2562.
- (42) Weinhold, F.; Landis, C. R. Natural bond orbitals and extensions of localized bonding concepts. *Chemistry Education Research and Practice* **2001**, 2, 91-104.

CHAPTER V: PROTON TRANSPORT IN H₃PO₄-DOPED P4VI

The present chapter is devoted to the investigation of the role of phosphoric acid (H₃PO₄) in the conductivity mechanism of P4VI, the azole-based system previously investigated as pure polymer (chapter IV). Such an investigation has been performed by using a molecular model where together to a protonated trimer of P4VI, two molecules of H₃PO₄ have been taken into account. The obtained data, object of a manuscript in preparation,¹ can be considered as very preliminary, being the result of a first crude effort to model the effect of acid doping on charge transport of P4VI.

1. Introduction

As above mentioned, the levels of conductivity reached by pure azole-based polymers are far from those requested for PEMFCs applications.²⁻⁵ However, such a gap can be partially reduced by doping the pure polymer with strong acids able to 1) increase the polymer backbone mobility acting as plasticizer and 2) introduce extrinsic charge carriers acting as protons source.^{2,3,5-7} Notably, the interaction between the N-heterocycles polymer and the doping acid is supposed to occur via hydrogen bond^{2,8,9} while two different situations can be envisaged for the mechanism of conduction:

- doping with small amount of acid (< 15 mol % with respect to the azole units)
- blending with molar excess of acid

The increasing of the conductivity obtained in the first case is mainly related to the observed decreasing of glass transition temperature (T_g), hence leading to an enhanced polymer flexibility. It is commonly accepted that in systems where a molar excess of acid is used, the conductivity of the blends is mainly based on proton transfer between acid moieties as well as on their self diffusion (vehicular mechanism), the observed values being equal to those of the pure acid.^{2,3} Among the different doping acids, the most common is phosphoric acid (H₃PO₄) which has the highest intrinsic proton conductivity of any known substance.^{10,11}

Based on these evidences, several azole-based systems blended with H₃PO₄ have been prepared and studied as proton conductors in the last years and such a materials have shown conductivity levels several order of magnitude higher with respect to the corresponding pure polymers.^{2-7,9,12} In this context, an important example is represented by the H₃PO₄-blended P4VI which shows levels of conductivity which are significantly higher than P4VI alone. Interestingly,

this happens also after doping with amounts of H₃PO₄ much lower than those of saturation.^{2,3} In this regard, it is worth to note that, albeit the conductivity of the system becomes higher in saturated systems, the presence of high acid quantity is a drawback that leads to leaching problems as well as to negative effects especially concerning the chemical and mechanical stability of the membrane.^{5,13,14} In other words, from a technical point of view, the use of low quantity of phosphoric acid is preferred. In this sense, maximizing the acid effect on the proton conductivity could be crucial to allow the use of lower quantities of dopant. However, this goal can be achieved only if a better understanding of its role on the mechanism of conduction is obtained. In this context, the literature reports some examples of studied mainly focused on the interactions between dopant and polymer. Concerning the P4VI itself, Bozkurt and coworkers showed, through IR spectra, that the "addition of H₃PO₄ to P4VI results in protonation of the free nitrogen on the imidazole rings" hypothesizing a polysalt formation,² suggested, some years later, also for benzimidazole polymers doped with the same dopant.⁹ More recently, insights into the poly-benzimidazole (PBI)- phosphoric acid interactions have been obtained through a Raman study¹⁵ while Pahari and coworkers⁸ have carried out MD simulations on monomer of polybenzimidazole doped with H₃PO₄ to investigate its structural and dynamical properties at varying temperature and acid content. Albeit interesting in order to shed light on the interactions polymer-acid, these studies are still far from giving insights into the mechanism of conduction of the H₃PO₄-doped materials, to which no specific study has been still devoted at the best of our knowledge.

Based on these evidences and background, in this chapter we present a DFT based investigation of the role of phosphoric acid in the conduction mechanism of P4VI for which a mechanism of conduction alternative to Grotthuss has been hypothesized for the acid-free system (chapter IV). Notably, a molecular model characterized by a protonated trimer of P4VI and two molecules of phosphoric acid has been taken into account and the obtained results compared with those obtained with the pure polymer. For this purpose, the DFT investigation described in the present chapter has been performed following the computational details reported in chapter IV (Section 2).

2. Results and discussion

As shown in chapter IV, the main reason why the Grotthuss mechanism could be impeded in pure P4VI is the impossibility to get an H-bond network along the chain because of the polymeric matrix constraint so that an alternative path has to be taken into account in order to transfer the excess proton in the considered acid-free model systems. Based on these results, the first step of the present study has been the evaluation of a possible H-bond network

(hereafter defined as Grotthuss chain) in the considered H_3PO_4 -included model system (Section 2.1) followed by an investigation on the energy involved in the proton transfer reactions considered (Section 2.2) and finally on the rate determining step of the emerged mechanism (Section 2.3).

2.1. Identification of a Grotthuss chain in the starting complex

As already mentioned, the present investigation has been carried out by using a molecular model characterized by two molecules of phosphoric acid added to a trimeric system of P4VI. Figure V-1 shows the optimized structure of the starting complex (before the arrival of the first excess proton and hypothesizing a direction of conduction from left to right). As in chapter IV, the polymeric system has been built in order to have a linear (strong) hydrogen bond (involving nitrogen atoms in position 3) between the first (Im_a) and the second (Im_b) imidazole and bonding the hydrogen of the third imidazole (Im_c) to the position 3 in order to have the nitrogen in position 1 as acceptor. As expected, in the lowest energy structure the acid molecules interact with all the imidazole wires through hydrogen bonds. However, the protons (H_1^a and H^b) involved in the H-bond between the dopant and the imidazole wires do not transfer spontaneously to form a salt. Nevertheless, a further analysis of the energetic concerning the H_1^a transfer from O^a to N_1^a reveals how such a proton transfer reaction is energetically allowed requiring only 1.04 kcal/mol to occur. This transfer can be (ideally) considered as the first step of the charge transport in the considered model, since it is required (making O_a acceptor) in order to accept the incoming excess proton. Note that the second dopant molecule (PA_b) simultaneously interacts with two proton wires (Im_b and Im_c) donating and accepting an hydrogen bond at the same time.

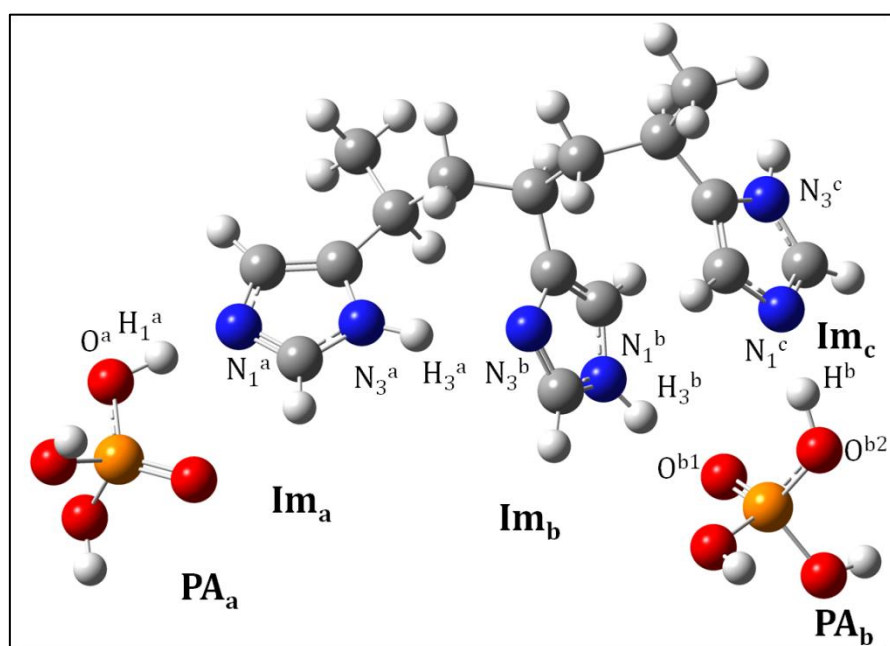


Figure V-1: Optimized structure of the starting neutral complex.

In other words, thanks to the presence of two molecules of H_3PO_4 into the model, together with the interaction between Im_a and Im_b (as in the corresponding acid-free model), a new H-bond network is established as shown in table V-1 where the distances between the considered hydrogens and the corresponding atom acceptors (A_A) as well as the angles among the atom donors (A_D), the hydrogens and the atom acceptors are reported.

Table V-1: Atom acceptor-hydrogen distances (A_A-H , Å) and atom donor-hydrogen - atom acceptor angles (A_D-H-A_A , deg) in the optimized structure of the starting neutral minimum. See figure V-1 for atom labeling.

H-bond	distance A_A-H	angle $A_D-H---A_A$
O ^a - H _{1^a} --- N _{1^a}	1.53	175
N _{3^a} - H _{3^a} --- N _{3^b}	1.94	156
N _{1^b} - H _{3^b} --- O ^{b1}	1.82	158
O ^{b2} - H ^b ---N _{3^c}	1.57	176

Taken together, these data indicates the presence of a Grotthuss chain in the considered model, differently from the corresponding acid-free model where the presence of two successive strong H-bonds is impeded by the polymeric constraint.

2.2. Proton transfer reactions in the protonated model

As already mentioned, in order to trigger the conduction an excess positive charge has to be added to the considered model. Figure V-2 shows the optimized structure of the protonated molecular system obtained adding a proton to PA_a in order to study the conduction from the left to the right side. Indeed, as the excess proton (H_1^e) arrives, H_1^a transfers from O_a to N_{1^a} so determining the starting complex for subsequent proton transfers along the chain (see the arrows in figure V-2).

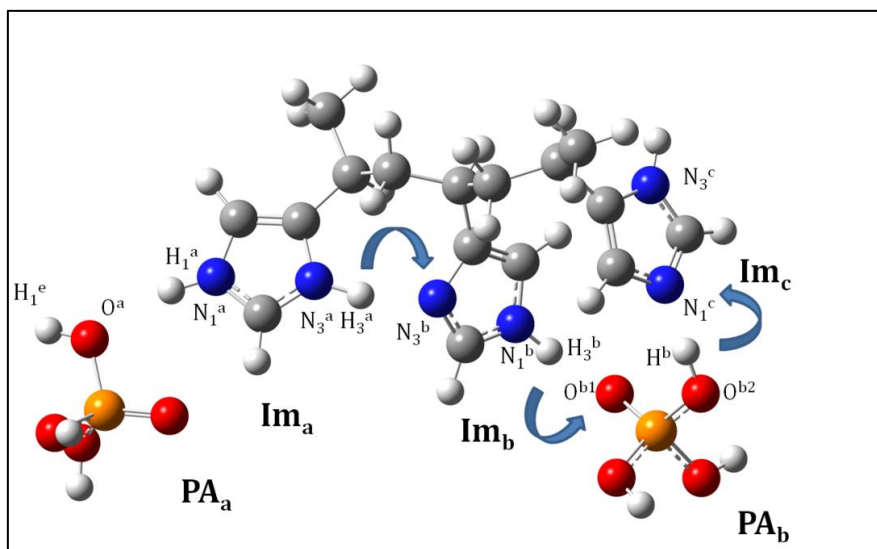
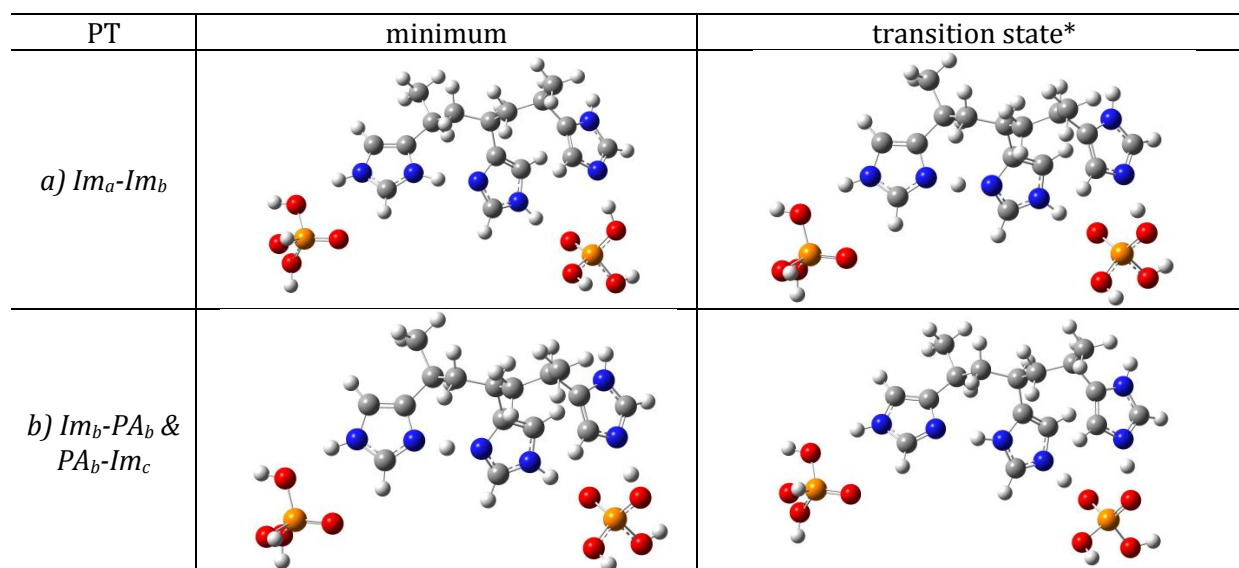


Figure V-2: Optimized structure of the starting protonated complex.

The obtained conformation, in fact, is characterized by a protonated imidazole (Im_a) which establishes an H-bond with a neutral one (Im_b) through two nitrogen atoms in position 3, a condition which favors an energetically allowed proton transfer (chapter IV). In addition, once H_3^a is transferred from Im_a to Im_b , one proton can be conducted from Im_b to Im_c by means of the H-bonding bridge obtained thanks to the presence of PA_b .

Figure V-3 shows the minima and transition states referring to the PT reactions occurring in the considered model: *a)* transfer from Im_a to Im_b , *b)* transfer from Im_b to PA_b and from PA_b to Im_c . Note that only one transition state is considered for the transfer reaction involving both H_3^b and H^b , this last occurring spontaneously as H_3^b approaches to O_b^1 . Concerning the transfer from protonated Im_a to Im_b (PT reaction *a*), only 2.5 kcal/mol are required (Table V-2). Such a value is equal to that computed for an acid-free protonated dimer where the same PT mechanism occurs (involving nitrogen atoms in position three) so indicating that such a proton transfer reaction is not affected by the presence of dopant molecules in the system. The resulting complex is in turn starting conformation for a concerted proton transfer from Im_b to Im_c requiring about 5 kcal/mol (estimated through relaxed scan calculation) to take place. Such a value is much lower with respect to that computed (23.5 kcal/mol) for a proton transfer between nitrogen atoms in position 1 (as between Im_b and Im_c) in absence of acid. The presence of PA_b therefore promotes the transfer from Im_b and Im_c which otherwise would occur by requiring an energy barrier too high due to the inability of the proton wires to establish a strong (linear) H-bond between nitrogen atoms in position 1.



*: In case of PT *b)* the transition state is hypothesized considering the highest energy structure of the relaxed scan calculation.

Figure V-3: Minima and transition states of the PT reactions occurring in the protonated model.

Table V-2: Proton transfer energy barriers computed in the acid-included model system and in the corresponding mechanism of the acid-free system. All values are in kcal/mol.

	acid-included model	acid-free model
PT	ΔE	ΔE
a) Im_a - Im_b	2.5	2.5 (N_3 - N_3)
b) Im_b - PA_b & PA_b - Im_c	5.2	23.5 (N_1 - N_1)

Note that the resulting complex of PT *b*) will be characterized by a protonated Im_c which can be considered as the starting minimum for a new transfer N_3 - N_3 (as between Im_a and Im_b). In other words, the resulting complex after the conduction of the first proton (from the left to the right side) is a neutral system where an H-bond network is established in the opposite direction with respect to the starting model (figure V-4 vs. figure V-1) so that a reorientation becomes necessary for subsequent intermolecular proton transfer in the same direction.

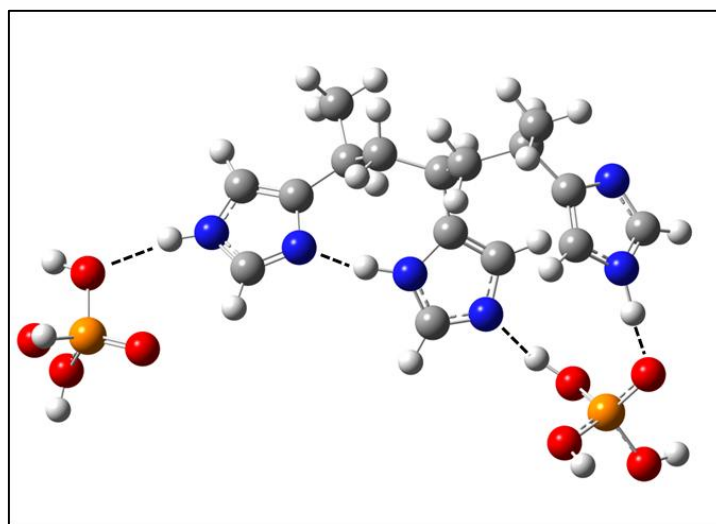


Figure V-4: Optimized structure of the resulting complex after the first proton shuttling along the chain. The H-bonds are depicted by a dotted line.

2.3. Investigation of the rate-limiting step

Because of the presence of no-equivalent nitrogen atoms in the system (as a consequence of the casting in position 4 of the heterocycles), a cooperative rotation involving only the imidazole moieties would not be able to give a suitable conformation for a new proton shuttling along the chain. Indeed, since the involved nitrogen atoms would be those in position 1, an H-bond between Im_a and Im_b would not be possible in absence of an acid molecule between these heterocycles. In the considered molecular model, therefore, the flipping process must also involve one doping molecule, namely PA_b which, at the end of the process, must be located between Im_a and Im_b . For this reason, a relaxed scan calculation of the dihedral corresponding to the rotation of the central imidazole around the C-C bond (bond between Im_b and the backbone) has been realized by keeping fix the interaction between Im_b and PA_b (H_3^b - O_b^1 distance). Note

that, in order to have an reasonable computational time, the molecule of dopant not directly involved in such a reorientation process (PA_a) has been excluded in the investigated model. Figure V-5 *b* shows the optimized structure of the complex obtained after a complete rotation of the central proton wire while in figure V-5 *a* an intermediate structure (corresponding to almost half rotation) is shown.

Interestingly, during the rotational process, PA_b establishes hydrogen bonds with all the proton wires of the considered model (figure V-4 *a*). Such interactions, together with the weak dispersion forces due to the quasi-parallel rearrangement of the imidazoles, contribute to reduce the energy required for the whole process. Indeed, the highest energy structure of the performed relaxed calculation (figure V-5 *b*) has an energy only 6.5 kcal/mol higher with respect to the starting conformation.

In short, a new proton shuttling along the chain can happens in the considered model after almost 6.5 kcal/mol, involved in the necessary rearrangement necessary to restore an H-bond network for a new proton conduction in the same direction.

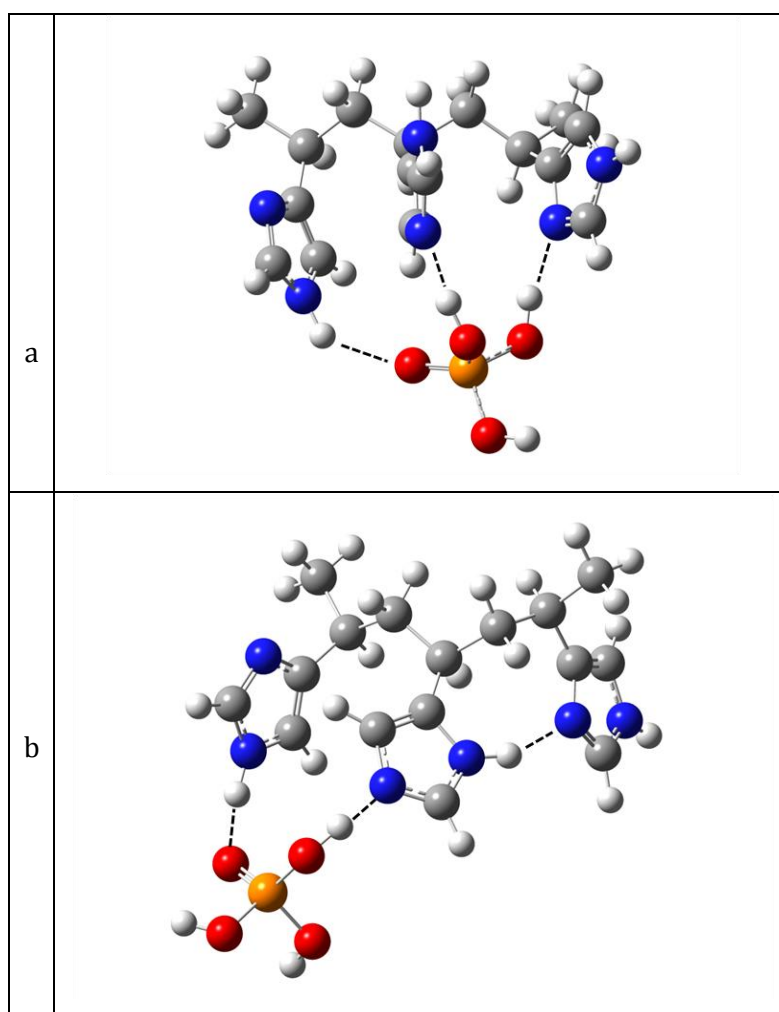


Figure V-5: Optimized molecular structure of the investigated model to study the rate-limiting step: a) highest energy structure of the relaxed scan calculation, b) resulting complex.

2.4. Comments

The discussed results show as the inclusion of molecules of phosphoric acid can strongly affect the mechanism of conduction in P4VI. Indeed, while in the pure polymer the presence of two successive hydrogen bonds (necessary condition for a Grotthuss mechanism) is impeded due to the polymeric constraint, an H-bond network can be detected in the acid-included model here investigated and characterized by two molecules of H_3PO_4 , added to a trimer of P4VI.

In particular, the preliminary study on the neutral system (here representing the starting complex before the arrival of the first excess proton) shows as a strong (linear) H-bond can be established between the proton wires and the dopant molecules. Importantly, the protons involved in such interactions are delocalized between the two moieties allowing the first acid molecule (PA_a) to act as acceptor of the incoming excess proton. Furthermore, the optimized molecular structure shows as a dopant molecule added within the chain (instead of at one end) establishes two simultaneous interactions, one with Im_b (as H-bond acceptor), the other with Im_c (as H-bond donor), in contrast with Bozcurt et al.² according to whom H_3PO_4 interacts with a single molecule of heterocycle forming a salt. In other words, thanks to the obtained minimized conformation, H_3PO_4 acts as hydrogen bonding bridge between two proton wires among which a hydrogen bond (involving nitrogen atoms in position 1) would not otherwise be possible (chapter IV).

This is confirmed by a further analysis of the energies involved in the first proton shuttling along the chain, performed on a protonated model system (after the arrival of the excess proton transfer on PA_a). If more than 20 kcal/mol are required to transfer the proton between two adjacent imidazoles through nitrogen atoms in position 1 (chapter IV), here about 5 kcal/mol are enough to transfer the excess charge from Im_b to Im_c thanks to the presence of PA_b which is involved in a simultaneous double proton transfer.

Taken together, all these results suggest that a Grotthuss mechanism could be not impeded by the polymeric constraint in the considered model. However, in order to better investigate this hypothesis, a further investigation has been performed focusing the attention on the rate-limiting step (reorientation) of the hypothesized mechanism. Notably, following the Grotthuss hypothesis a neutral system has been taken into account assuming that such a process occurs after the discharge at the electrode (step 2,) and before the arrival of a new incoming excess proton (new step 1, see figure IV-3). Albeit a detailed energetic profile has not still been obtained, due to the complexity of the investigated model (such a point is under present investigation), the analysis of the highest energy conformation (after a relaxed scan calculation) indicated that the molecule of H_3PO_4 which is involved in that flipping process is able to establish interactions with all the three heterocycles of the system so contrasting the energy necessary to break the hydrogen bonds during the reorientation. The estimated value (6.5

kcal/mol) is close to the proton conduction activation energy obtained for similar N-heterocycles systems doped with phosphoric acid.¹⁶

In summary, from all the investigated outcomes emerges a Grotthuss-like mechanism characterized by different steps: 1) establishment of strong H-bond interactions between dopant and polymer, 2) arrival of the excess positive charge on the first acid molecule and consequent collective proton transfer along the Grotthuss chain, 3) reorientation of all the imidazoles with the simultaneous transfer of the phosphoric acid molecules within the chain, 4) formation of a new H-bond network in order to conduct a new proton in the same direction.

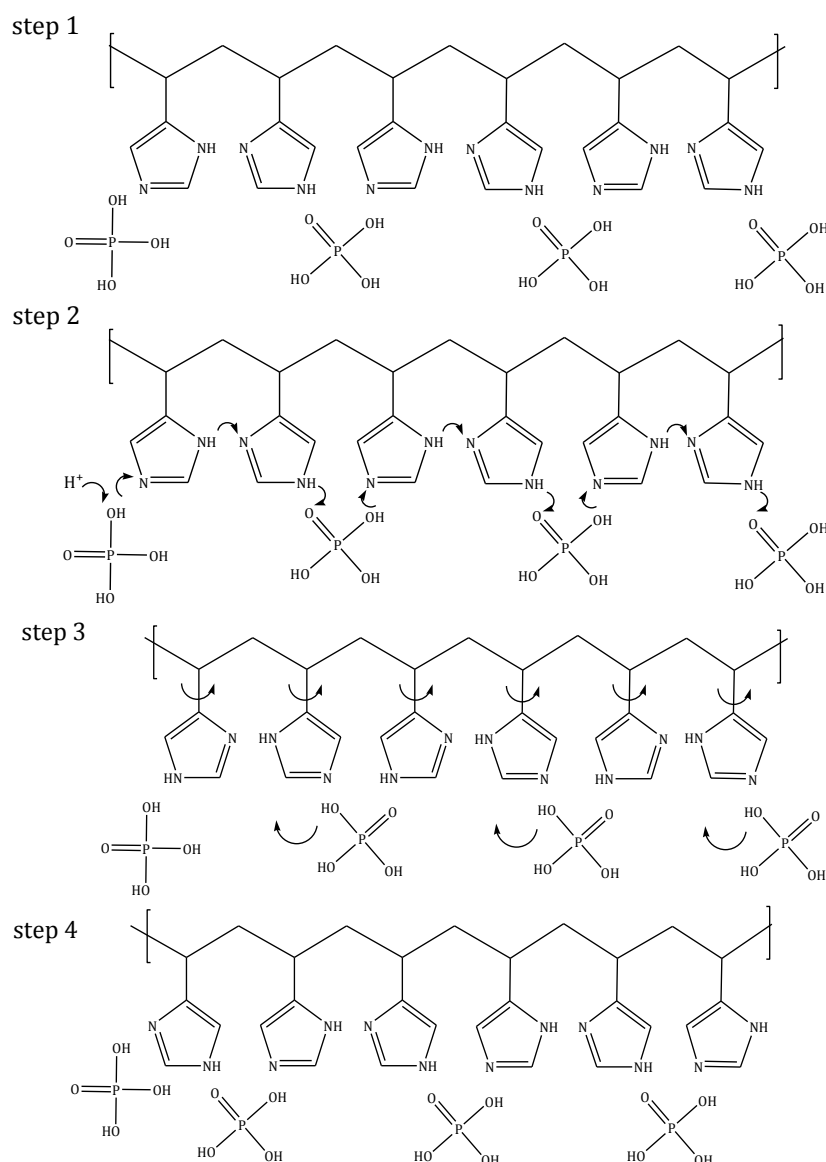


Figure V-6: Directional proton conduction mechanism hypothesized for the P4VI doped with an acid amount equal to $x=0.5$ (x =moles of acid for each P4VI repeat unit).

From a more chemical point of view, it is worth underlining that such a proposed mechanism refers to a condition where the polymer is blended with levels of H_3PO_4 much lower

than those of saturation, in particular corresponding to an acid amount equal to $x=0.5$ (where x refers to is the moles of acid for each P4VI repeat unit). Indeed, as shown in figure V-6, in the emerged model one molecule of acid is required within the chain for each pair of imidazoles.

3. Conclusions

The performed DFT investigation provides insights into how the interactions between an acid dopant (in this case H₃PO₄) and a poly-imidazole membrane (here P4VI) can affect the mechanism of conduction in blends where less than a molar excess of acid is used. Interestingly, from the discussed outcomes, it appears evident that molecules of phosphoric acid within the chain can interact simultaneously with two or threeazole moieties allowing for a Grotthuss path, impeded in the corresponding pure polymer because of the polymeric matrix constraint.

Albeit these findings are far from giving an accurate picture of the charge transport in H₃PO₄-blended systems, being necessary an investigation on more larger (realistic) systems, they can represent the starting point for a more detailed investigation with the aim to shed light on the effect of acid dopant on proton conduction of these systems that cannot be related to the only enhanced backbone mobility.

4. References

- (1) Butera, V.; Mangiatordi, G. F.; Sicilia, E.; Russo, N.; Adamo, C. On the phosphoric acid rule on charge transport in blends of poly(4-vinylimidazole): a theoretical investigation. *In preparation*.
- (2) Bozkurt, A.; Meyer, W. Proton conducting blends of poly(4-vinylimidazole) with phosphoric acid. *Solid State Ionics* **2001**, *138*, 259–265.
- (3) Pu, H.; Meyer, W. H.; Wegner, G. Proton Conductivity in Acid-Blended Poly(4-vinylimidazole). *Macromolecular Chemistry and Physics* **2001**, *202*, 1478–1482.
- (4) Pu, H.; Wu, J.; Wan, D.; Chang, Z. Synthesis and anhydrous proton conductivity of poly(5-vinyltetrazole) prepared by free radical polymerization. *Journal of Membrane Science* **2008**, *322*, 392–399.
- (5) Çelik, S. Ü.; Bozkurt, A.; Hosseini, S. S. Alternatives toward proton conductive anhydrous membranes for fuel cells: Heterocyclic protogenic solvents comprising polymer electrolytes. *Progress in Polymer Science* **2012**, *37*, 1265–1291.
- (6) Çelik, S. Ü.; Aslan, A.; Bozkurt, A. Phosphoric acid-doped poly(1-vinyl-1,2,4-triazole) as water-free proton conducting polymer electrolytes. *Solid State Ionics* **2008**, *179*, 683–688.
- (7) Qingfeng, L.; Hjuler, H. A.; Bjerrum, N. J. Phosphoric acid doped polybenzimidazole membranes: Physicochemical characterization and fuel cell applications. *Journal of Applied Electrochemistry* **2001**, *31*, 773–779.
- (8) Pahari, S.; Choudhury, C. K.; Pandey, P. R.; More, M.; Venkatnathan, A.; Roy, S. Molecular Dynamics Simulation of Phosphoric Acid Doped Monomer of Polybenzimidazole: A Potential Component Polymer Electrolyte Membrane of Fuel Cell. *Journal of Physical Chemistry B* **2012**, *116*, 7357–7366.
- (9) Asensio, J. A.; Borros, S.; Gomez-Romero, P. Proton-conducting polymers based on benzimidazoles and sulfonated benzimidazoles. *Journal of polymer science. Part A. Polymer chemistry* **2002**, *40*, 3703–3710.
- (10) Dippel, T.; Kreuer, K. D.; Lassègues, J. C.; Rodriguez, D. Proton conductivity in fused phosphoric acid; A ¹H/³¹P PFG-NMR and QNS study. *Solid State Ionics* **1993**, *61*, 41–46.
- (11) Vilčiauskas, L.; Tuckerman, M. E.; Bester, G.; Paddison, S. J.; Kreuer, K.-D. The mechanism of proton conduction in phosphoric acid. *Nature Chemistry* **2012**, *4*, 461–466.

- (12) Di Noto, V.; Piga, M.; Giffin, G. A.; Quartarone, E.; Righetti, P.; Mustarelli, P.; Magistris, A. Structure-property interplay of proton conducting membranes based on PBI5N, SiO₂-Im and H₃PO₄ for high temperature fuel cells. *Physical Chemistry Chemical Physics* **2011**, *13*, 12146–12154.
- (13) Mustarelli, P.; Quartarone, E.; Grandi, S.; Angioni, S.; Magistris, A. Increasing the permanent conductivity of PBI membranes for HT-PEMs. *Solid State Ionics*. **2012**, *225*, 228-231.
- (14) Zhang, H.; Shen, P. K. Recent development of polymer electrolyte membranes for fuel cells. *Chemical Reviews* **2012**, *112*, 2780–2832.
- (15) Conti, F.; Majerus, A.; Di Noto, V.; Korte, C.; Lehnert, W.; Stolten, D. Raman study of the polybenzimidazole-phosphoric acid interactions in membranes for fuel cells. *Physical Chemistry Chemical Physics* **2012**, *14*, 10022–10026.
- (16) Narayanan, S. R.; Yen, S.-P.; Liu, L.; Greenbaum, S. G. Anhydrous Proton-Conducting Polymeric Electrolytes for Fuel Cells. *Journal of Physical Chemistry B* **2006**, *110*, 3942–3948.

CHAPTER VI: PROTON TRANSPORT IN 2-TETHERED SYSTEMS

Starting from the conclusions drawn out in chapter IV where the backbone constraint has been proved to be crucial in effecting the charge transport in P4VI, in this chapter the effect of a different wire tethering (position 2 instead of 4) will be explored in order to get more insights into how the structure of the proton wire and of the polymer are related to proton conductivity. The results discussed in the present chapter have been object of a paper recently submitted.¹

1. Introduction

As described in chapter IV, when imidazoles are casted in a polymer backbone through the position 4, the positions 1 and 3 in the heterocycles (nitrogen atoms) are no longer equivalent and the geometric constraint imposed by the backbone excludes the presence of two successive favorable hydrogen bonds leading to an alternative mechanism of conduction. In other words, because of the polymeric matrix, a necessary condition for the Grotthuss mechanism is not verified, namely the H-bond network along the chain. This leads to an alternative reaction path requiring n frustrated rotations of single protonated imidazoles instead of a collective proton transfer along the chain (figure VI-1).

However, following the proposed mechanism, only few protons can be transferred along the chain at the same time even if these frustrated rotations are uncoupled since the concentration gradient of charged particles (in this case protons) in condensed matter cannot be high in absence of counterions (because of the proton-proton repulsion). Nevertheless, the investigation on P4VI suggests that the tethering position of the proton wires is a critical factor in determining such alternative-to-Grotthuss path. Indeed, as a consequence of a different casting (position 2 instead of 4) the nitrogen atoms in position 1 and 3 of the heterocycles are equivalent as in free chain of imidazoles thus suggesting that a Grotthuss-like mechanism could be allowed in 2-tethered systems (figure VI-2).

Such an hypothesis is based on the available experimental literature. Rasmussen and coworkers, for instance, have investigated in depth the Poly(2-vinyl-4,5-dicyanoimidazole) (see figure VI-3)

through infrared, solid-state NMR spectroscopy and polymer viscosity studies.² Importantly, the decreasing of the viscosity in the 1-methylated system (Poly(1-methyl-2-vinyl-4,5-dicyanoimidazole)) has been explained as the presence of a strong hydrogen-bonded motif, as confirmed by the solid-state NMR. The same polymer has been also object of a patent by Wixom and al.³ where a Grotthuss mechanism based on a collective proton transfer involving a single chain for both pure and acid doped system is hypothesized. Notably, the authors points out on "the high hydrogen bonding characteristics of the material of the present invention". The properties of the corresponding cyano-free polymer (Poly(2-vinyl-imidazole)) doped with phosphoric and sulfuric acid have been investigated by Narayanan and coworkers⁴ which found that this system is a stable proton-conducting up to 200°C.

To gain more insights into the mechanism of conduction of these systems, in this chapter we present an in-depth investigation performed on model systems where the imidazole wires are casted through the position 2. Notably, as for P4VI, the analysis of the electronic structure at DFT level has been combined with MD simulations for an explicit description of the dynamical aspects related to the investigated systems. The effect of the different imidazole casting on the proton conduction mechanism has been evaluated by considering models nearly identical to those investigated in chapter IV but characterized by a different tethering.

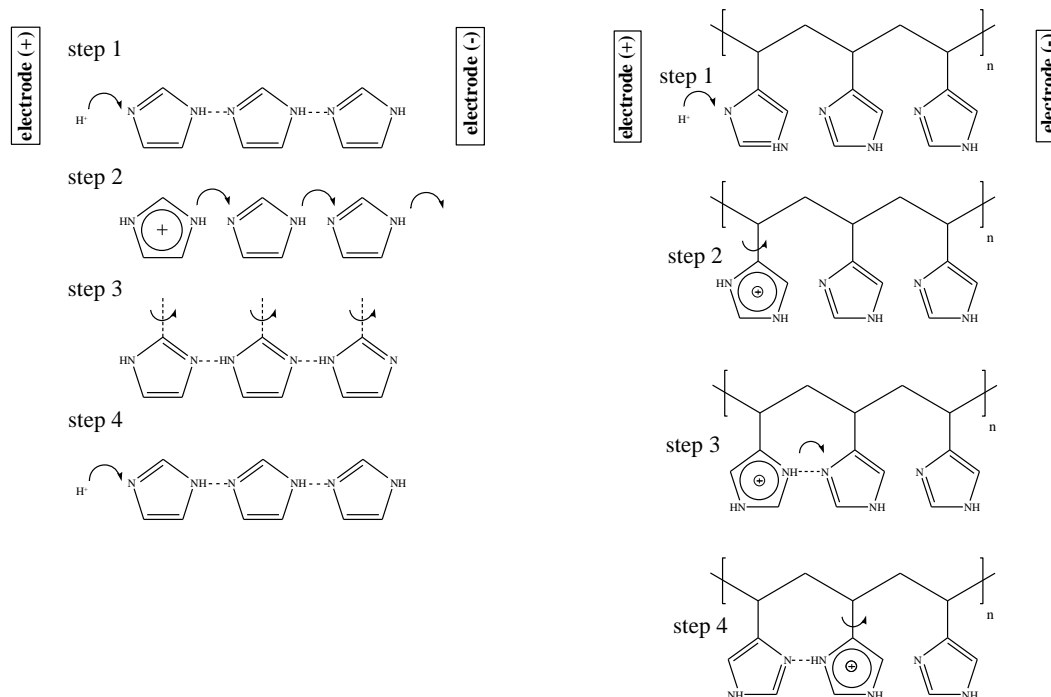


Figure VI-1: Directional proton transport mechanisms. Left: Grotthuss-like mechanism, involving 1) arrival of a proton at the end of the chain; 2) proton transfers along the chain; 3) flipping of all imidazoles; 4) arrival of a second proton. Right: mechanism proposed in the previous investigation on P4VI (chapter IV), involving 1) arrival of a proton at the end of the chain; 2) frustrated rotation of the protonated imidazole; 3) single proton transfer; 4) frustrated rotation of the protonated imidazole.

2. Methodological details

In order to compare the results with those obtained for P4VI⁵, all the calculations have been carried out following the computational details reported in chapter IV (Section 2). Concerning the MD simulations, a new parameterization of the General Amber Force Field (GAFF^{6,7}) has been performed in order to adapt it to the investigated models (details given in the following sections). Furthermore, after an equilibration of 0.5 ns, 80 ns of MD simulations have been performed taking into account two different temperatures (393 and 453 K). Finally, in order to explore the obtained trajectories, data were sampled every 500 fs.

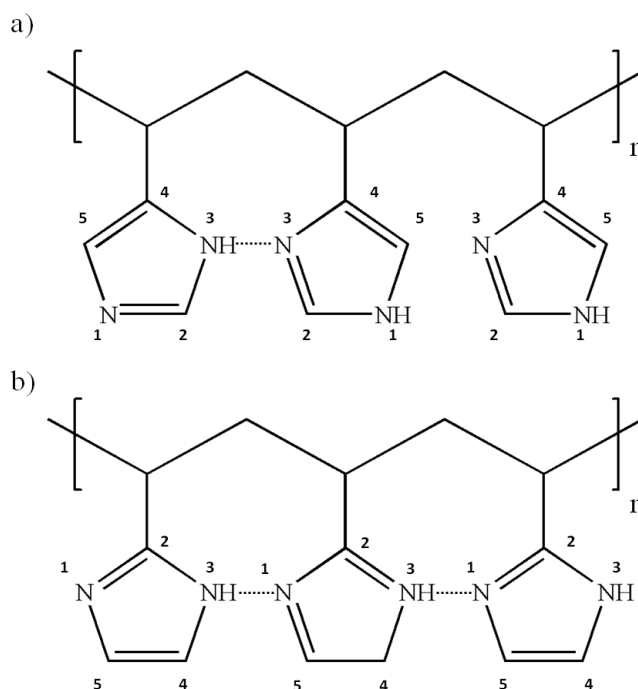


Figure VI-2: Schematic representation and atom numbering of one chain of a) P4VI and b) corresponding 2-tethered system. The H-bonds are depicted by a dotted line.

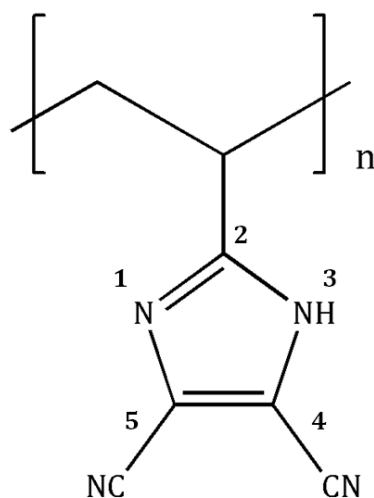


Figure VI-3: Sketches and atom numbering of the poly(2-vinyl-4,5-dicyanoimidazole) chain.

3. Results and discussion

3.1. Conduction mechanism in small models: DFT investigation

PT in protonated dimers

As shown in figure VI-2, when the imidazole wires are casted through the position 2 of the heterocycles, the nitrogen atoms are still equivalent as in free-chain models so that an H-bond network along the chain can be favored, differently from P4VI. In other words, because of the different tethering, only one kind of PT reaction can be envisaged between two adjacent imidazoles. Such a reaction has been analyzed by considering the simplest systems, namely protonated dimers. Notably, in order to evaluate the influence of both the backbone constraint and the cyano substituents, different models have been taken into account, namely imidazolium-imidazole dimer with a) an explicit consideration of the polymeric matrix, b) CN substituents in positions 4 and 5 and c) both polymeric matrix and CN groups. Note that this last corresponds to the protonated dimer of the Poly (2-vinyl-4,5-dicyanoimidazole) while the model *a*, except for the tethering position, corresponds to the protonated dimer of the same polymer investigated in chapter IV (P4VI).

Figure VI-4 shows the structures of minima and transition states (TS) computed for all the investigated models: for all the considered systems the initial and final rearrangements (reactants and products) are exactly alike with the two moieties switched/interchanged (symmetric PTs). As shown in table VI-1 which reports the energy barriers computed for each model, the activation energy for the PT reaction occurring in model *a* is only slightly higher than that computed for the bare imidazolium-imidazole dimer using the same DFT protocol (1.7 vs 1.3 kcal/mol, see chapter III). This result indicates not only that such a PT reaction is only slightly affected by the polymeric backbone constraint, but also that it is energetically favored with respect to the most favorable PT mechanism for the corresponding 4-tethered model (chapter IV) (1.7 vs 2.5 kcal/mol, respectively). An higher value of the energy barrier is computed for model *b*: the presence of the cyano substituents leads to an higher PT reaction energy (3.2 kcal/mol).

Surprisingly, when both polymeric constraint and cyano groups are included into the system (model *c*) the computed energy barrier is almost equal to that obtained for model *a* (about 1.7 kcal/mol, see Table VI-1). In other words, when the imidazole moieties are casted in a polymeric backbone, the cyano groups do not affect the activation energy thus suggesting that the increasing of the barrier in model *b* is not the result of an electronic but rather of a geometric effect. This is further supported by the analysis of the obtained structures (figure VI-4). Indeed, despite minimum and transition state of model *b* are characterized by theazole moieties in same plane as in models *b* and *c*, the proton wires are here rotated of 180° each other

with the consequent orientation of the cyano groups in two opposite directions (figure VI-4, b). Such a different reorientation leads to a longer length between nitrogen donor (N_D) and nitrogen acceptor (N_A) in the starting minimum (Table VI-1) so that a stronger rearrangement of the system (and consequently an highest amount of energy) is necessary to reach the transition state. Interestingly, this conformation is impeded when the backbone chain is added to the model b (model c). In other words, in presence of cyano substituents the geometrical constraint of the polymeric matrix favors the considered PT reaction.

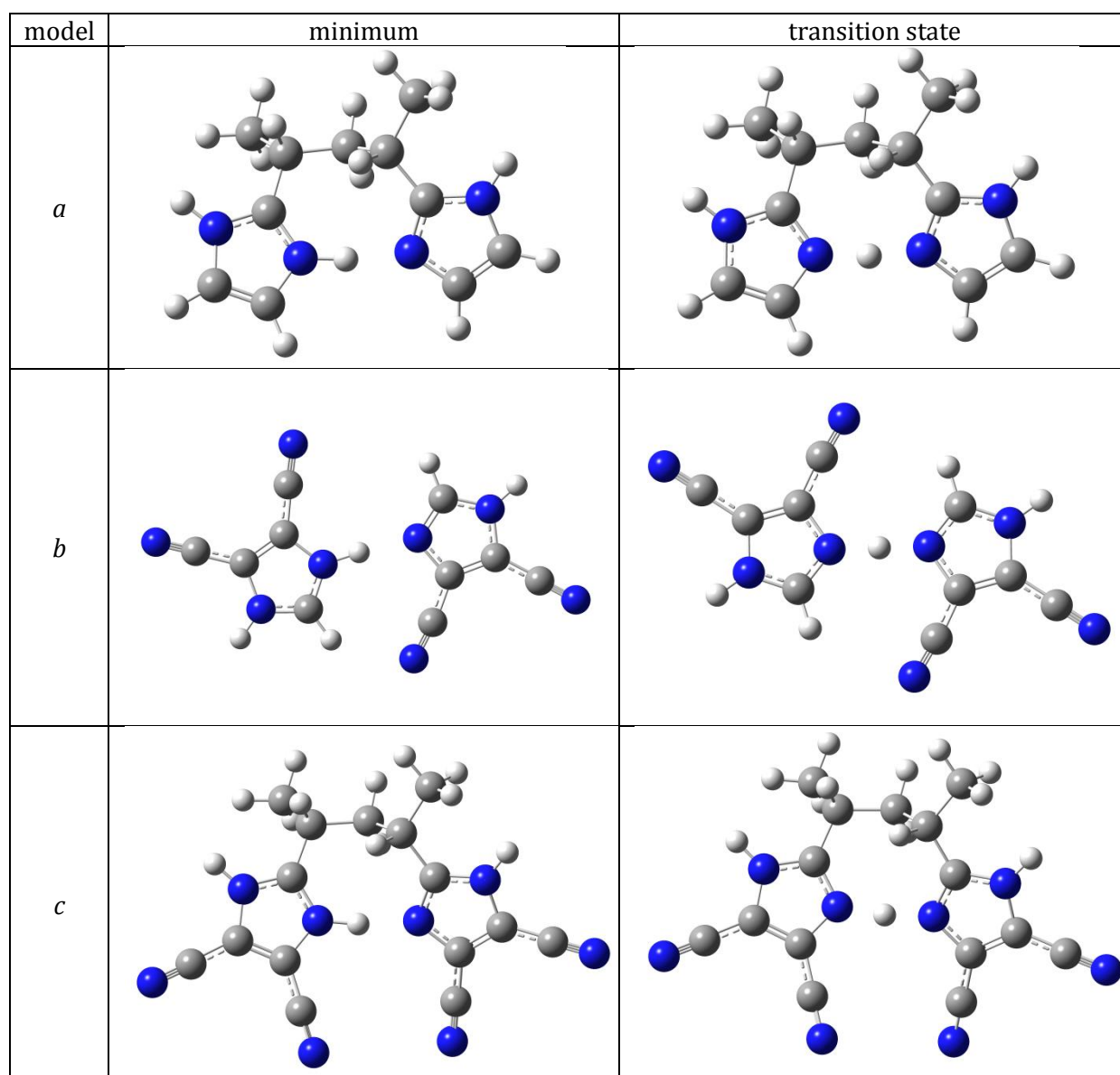


Figure VI-4: Structures of the stationary points (minima and transition states) of different protonated dimeric systems involved in the investigated proton transfer reactions.

In summary, in all the considered 2-tethered models, the PT reaction occurring between adjacent imidazoles is energetically allowed in spite of the geometrical effect of the cyano substituents which increases the energy barrier in absence of the polymeric matrix.

Table VI-1: N_D -H (Å), H- N_A (Å) and N_D - N_A (Å) distances for both minima and transition states of PT reactions occurring in the investigated models. The corresponding energy barriers (kcal/mol) are also reported.

model	minimum			transition state			ΔE
	N_D -H	H- N_A	N_D - N_A	N_D -H	H- N_A	N_D - N_A	
a)	1.09	1.60	2.67	1.27	1.30	2.56	1.68
b)	1.07	1.70	2.77	1.29	1.29	2.58	3.20
c)	1.09	1.61	2.69	1.27	1.30	2.56	1.69

Cooperative reorientation in a trimeric model

Although it is a necessary condition, the presence of an H-bond network along the chain is not sufficient to assume the Grotthuss mechanism which can take place only if a cooperative rearrangement involving the breaking and the formation of a series of H-bond occurs. Indeed, as above discussed in the introduction of chapter IV, once a proton is transferred from one imidazole ring to an adjacent one, reorientation (or flipping) of the imidazole moieties becomes necessary (rate-limiting step) for subsequent intermolecular proton transfer in the same direction. To verify that a Grotthuss-like mechanism is allowed in 2-tethered systems and in order to gain more insights into this rate-limiting process, a trimeric model has been analyzed. Based on the previous outcomes on protonated dimers indicating that the effect of the cyano substituents can be neglected when the polymeric matrix is included and in order to directly compare the obtained results with those obtained investigating P4VI where no substituent is present, a model of the bare poly-(2-vinyl-imidazole) has been considered (figure VI-5 a).

Such a trimeric model will be referred in the following as *3mer* and the three heterocycles as Im_a , Im_b and Im_c . Note that, differently from the trimeric model of P4VI analyzed in chapter IV, here a neutral system is considered. Indeed, following the Grotthuss hypothesis it is assumed that the reorientation step occurs after the discharge at the electrode (step 2) and before a new charge generation (new step 1, see figure VI-1 left). Therefore, by construction of the model, the starting conformation (Figure VI-5 a) corresponds to the resulting complex after the first proton shuttling through the hydrogen-bonded network assuming a direction of conduction from Im_a to Im_c .

Potential energy analysis for rotation around the covalent bond between Im_b and the polymeric matrix has been performed scanning the corresponding dihedral φ_2 (figure VI-5 a). The resulting energetic profile has been computed relaxing the molecular structure at each scan step (10° along the reaction coordinates). As shown in figure VI-6 a, the obtained potential energy curve is

characterized by a two-fold barrier. Notably, about 8 kcal/mol are required to break the two starting H-bonds. This amount of energy is then regained through the formation of a new H-bond network in the opposite direction (from 60° to $+120^\circ$) as depicted in figure VI-5 *b* showing the resulting complex ($\varphi_2 = 120^\circ$). From -60° to $+60^\circ$ no H-bond is observed and the obtained local minimum at 0° corresponds to a conformation able to maximize the aromatic-aromatic interactions (π stacking) between the heterocycles. Such a interactions leads to a energy gain of about 2 kcal/mol.

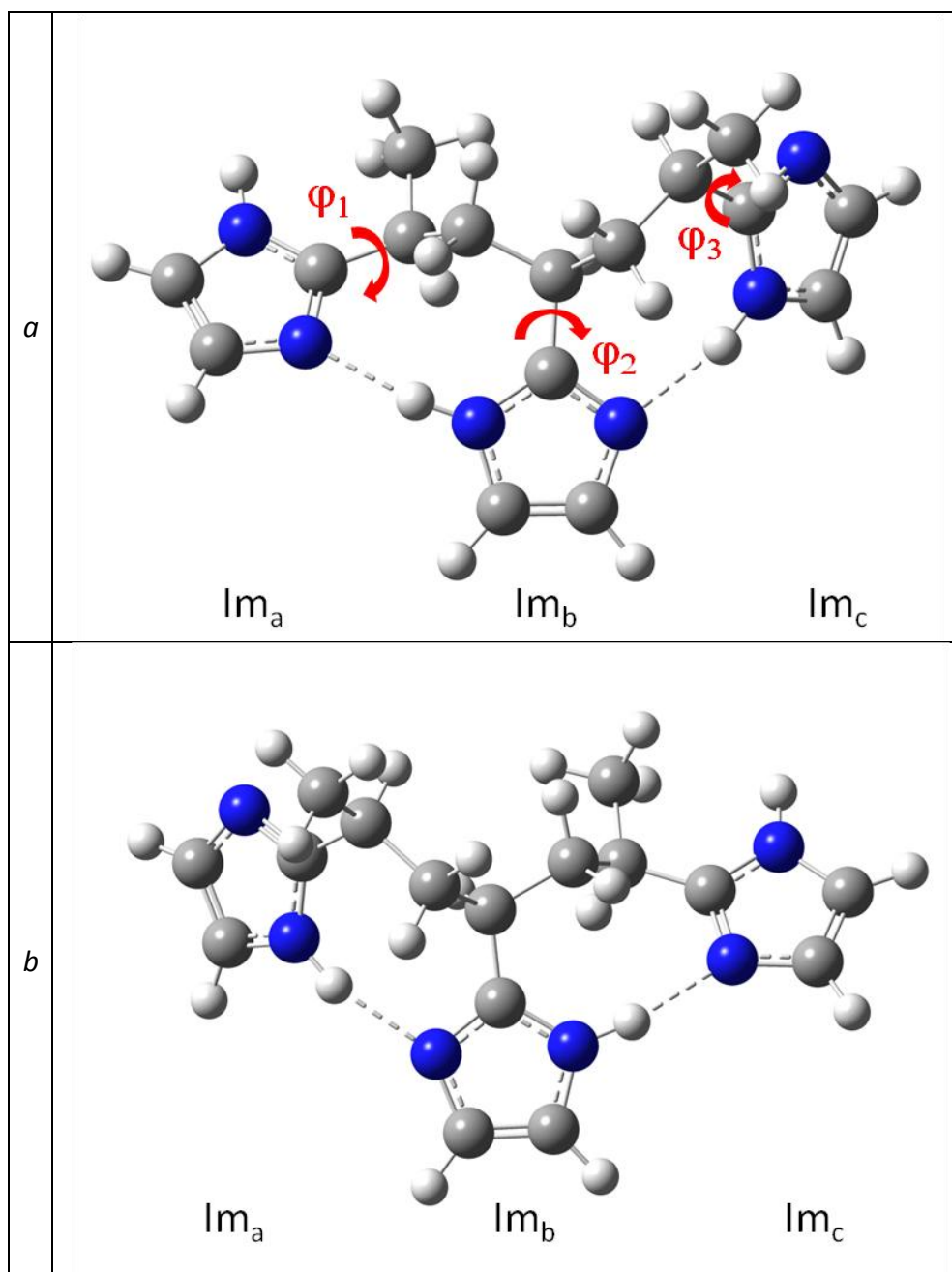


Figure VI-5: Optimized molecular structure of protonated imidazole trimer (3mer) before (a) and after (b) the flipping of all the imidazoles. The H-bonds are depicted by a dotted line.

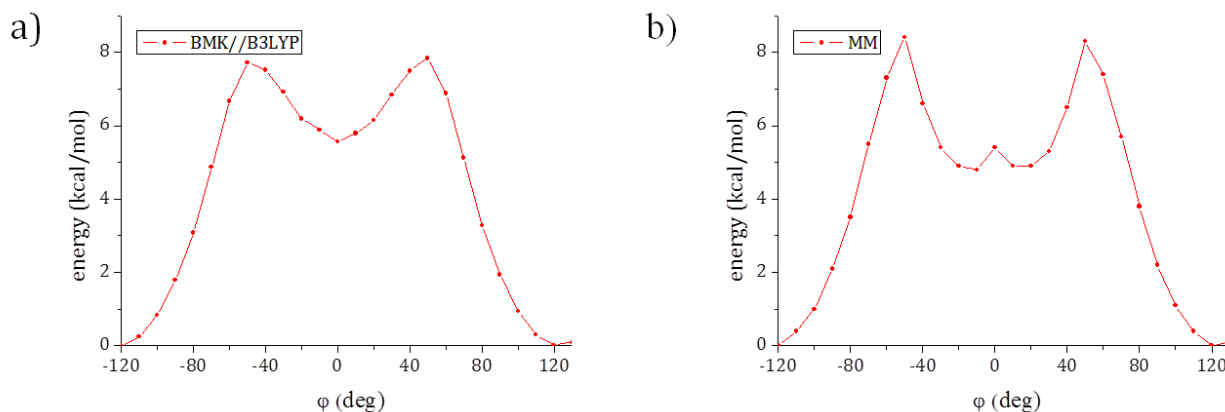


Figure VI-6: Potential energy profile for the torsion around the dihedral angle ϕ_2 : a) DFT outcomes, b) MM outcomes obtained with the modified GAFF.

In summary, the rotation of the central heterocycle (Im_b) in the investigated model leads to a subsequent rotation of the adjacent imidazoles (Im_a and Im_c) so that the formation of a new H-bond network in the opposite direction (necessary condition for a new proton conduction form Im_a to Im_c) can take place.

3.2. Conduction mechanism in large models: Molecular Dynamics simulations

The study performed on P4VI (chapter IV) revealed as the effect of the geometric constraint due to the presence of the polymeric matrix inazole-based polymers can depend on the size of the considered model. Indeed, when a large oligomer is considered (15 imidazoles linked to the corresponding polymeric backbone), a planar rearrangement of the proton wires is not allowed, differently from dimeric and trimeric models. This indicates that the H-bond network hypothesized for the investigated 2-tethered systems in small models could be compromised in a larger model. Furthermore, the hypothesized determining step (cooperative reorientation of all the imidazoles) could be strongly affected by the chemical environment. In order to explore these points, an oligomer composed by 15 monomers and including the polymeric matrix (referred in the following as 15mer) has been considered. The corresponding structure optimized at B3LYP/6-31G(d) level is depicted in figure VI-7. As expected, a planar rearrangement of the imidazoles is impeded in 15mer, differently from the previously investigated small models. Nevertheless, the H-bond network is preserved thanks to a spiral-like conformation as clearly shown in the zoomed figure. In other words, according to our calculations an H-bond network is allowed along the chain of a 2-tethered poly-imidazole system.

As for *3mer* (figure VI-5 b), the considered model represents the resulting complex after the first proton shuttling through the H-bond network and before the cooperative rotation, following the Grotthuss hypothesis and assuming again a direction of conduction from the left to the right side. Of course, a necessary condition to accept a new incoming proton is that the first proton wire of the chain (Im_1) acts once again as acceptor and a new H-bond network is established in the opposite direction, a step which is expected to be the rate determining step. Such a process has been investigated performing out MD simulations on 15mer. Notably, as for P4VI, the GAFF has been adapted to the investigated system by using the available DFT data as reference values.

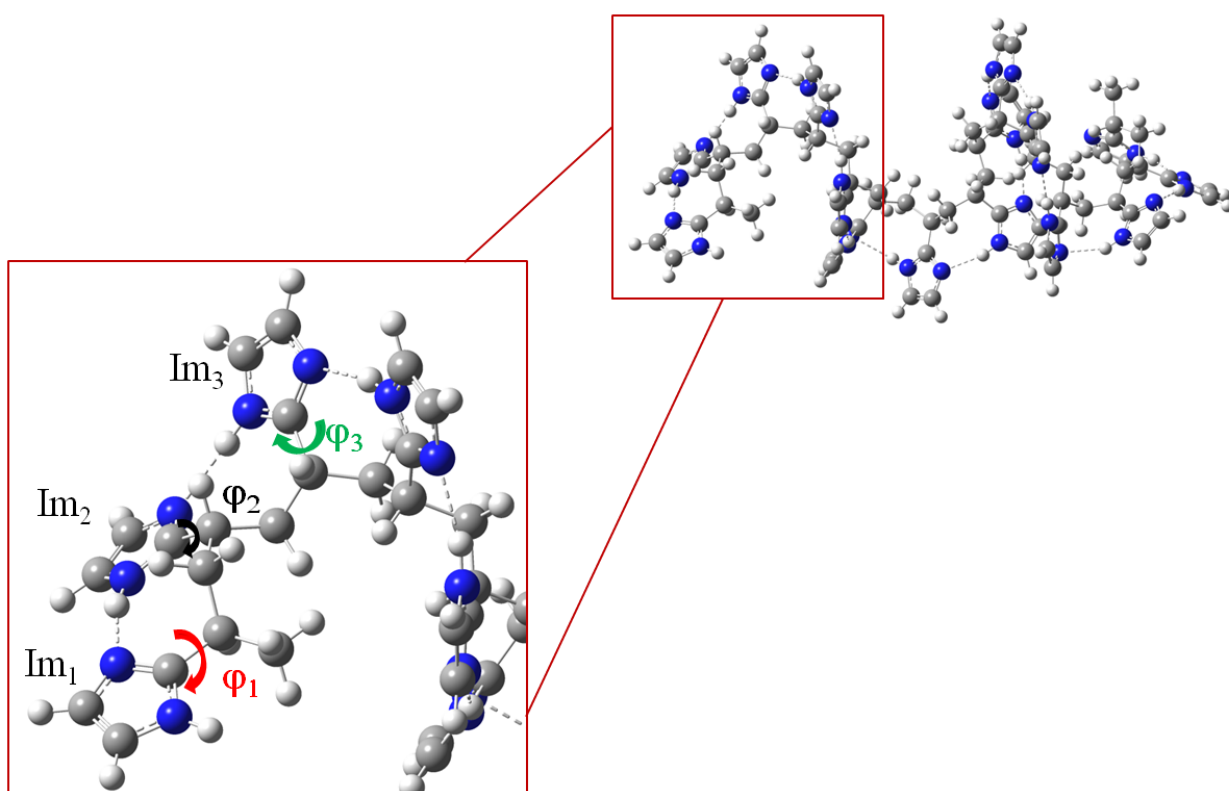


Figure VI-7: Optimized molecular structure of the imidazole oligomer containing 15 residues (15mer). The zoom shows the first imidazoles of the chain. The H-bonded are depicted by a dotted line.

Force Field calibration

In analogy with the previous investigation on P4VI, the GAFF parameterization has been carried out by means of the DFT data obtained for the trimeric model and including all the intramolecular interaction parameters published by Voth and coworkers for imidazole and imidazolium.⁸ Table VI-2 shows the atom numbers, the atom types and the relative RESP partial charges computed for *3mer*. Different scaling factors with respect to the GAFF default values

have been applied to the 1-4 non bonded interactions. Notably, the best agreement has been achieved scaling by a factor of 0.667 and 0.100 the 1-4 electrostatic and VDW interactions respectively (Table VI-3). The effect on such modification on the potential energy barrier is depicted in Table VI-4.

Table VI-2: Atom numbers, GAFF atom types and relative RESP partial charges computed for 3mer.

atom number	GAFF atom type	q (e ⁻)	atom number	GAFF atom type	q (e ⁻)
1	c3	0.060	23	c3	-0.308
2	hc	0.033	24	hc	0.092
3	hc	0.033	25	hc	0.092
4	c3	-0.473	26	hc	0.092
5	hc	0.131	27	cd	-0.457
6	c3	0.060	28	cd	0.445
7	hc	0.033	29	na	-0.189
8	hc	0.033	30	na	-0.189
9	c3	-0.108	31	nc	-0.656
10	hc	0.098	32	nc	-0.633
11	cd	-0.428	33	cd	-0.457
12	cc	0.162	34	cc	0.145
13	cd	0.649	35	cc	0.162
14	cd	0.445	36	hn	0.330
15	na	-0.365	37	hn	0.428
16	nc	-0.633	38	hn	0.330
17	c3	-0.308	39	h4	0.247
18	hc	0.092	40	h4	0.113
19	hc	0.092	41	h4	0.250
20	Hc	0.092	42	h4	0.115
21	c3	-0.108	43	h4	0.247
22	hc	0.098	44	h4	0.113

Table VI-3: Scaling factors for 1-4 electrostatic and 1-4 van der Waals interactions.

Interaction	Scaling factors	
	default	modified
1-4 electrostatic	0.833	0.667
1-4 van der Waals	0.500	0.100

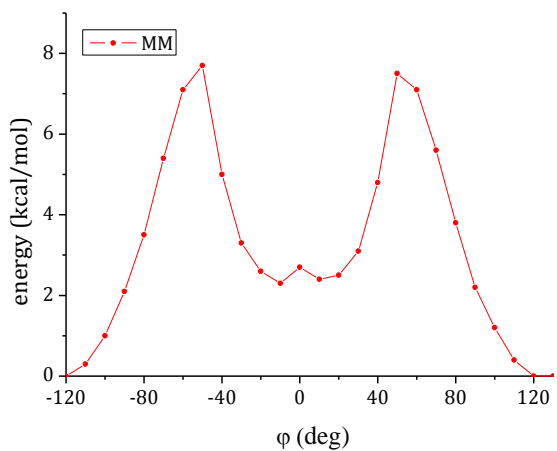
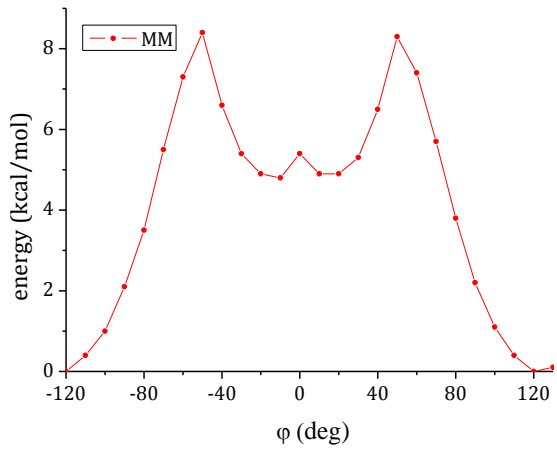
Figure VI- 6 *b* shows the resulting energetic profile provided using the modified GAFF version (MM single point calculations on the relaxed DFT structures): the obtained data are in good agreement with the DFT results (Figure VI-6 *a*).

Analysis of trajectory

In order to investigate the cooperative rearrangement of the proton wires, the analysis of the obtained trajectories has been carried out focusing the attention on the dihedral angles able to describe the rotation of the heterocycles. All the dihedral values have been normalized so that the DFT optimized value will be referred as $\varphi=0$. This enabled us a straightforward analysis of

the time dependent evolution by means of the variations with respect to the starting conformation. Figure VI-8 shows the evolution of the torsion angle φ_1 (rotation of Im₁) during an extracted of the 80ns trajectory at 393 K: after the first 72.6 ns where φ_1 oscillates almost around the starting equilibrium value, a change of conformation is observed. Interestingly, such a variation is preserved in the following nanoseconds so indicating that a new stable conformation with the first imidazole rotated ($\varphi_1=-150$) is obtained.

Table VI-4: Energetic profiles obtained using a) default, b) modified scaling factors of 1-4 electrostatic and 1-4 van der Waals interactions (the values are reported in table VI-3).

scaling factors	corresponding energetic profile
a)default	
b)modified	

As expected, such a rotation is related to the conformational variation of the successive imidazoles (Im₂ and Im₃) as clearly shown in Figure VI-8 a where the time dependent variations of φ_1 , φ_2 , and φ_3 are depicted. In other words, after about 72.6 ns of simulation on *15mer* the cooperative imidazoles rotation takes place and a new H-bond network in the opposite direction can be established. A detailed picture of this process is given in figure VI-9 that illustrates some selected snapshots while in the figure VI-8 b a more detailed extract of the trajectory

corresponding to this cooperative rotation is shown. Notably, during the first 72.5545 ns of simulation, φ_1 , φ_2 and φ_3 show values close to these obtained in the DFT optimized structure (see figure VI-8 b). In other words, during this time interval, the starting H-bond network is kept so that a new incoming proton cannot be accepted by the first imidazole. Going from 72.5545 to 72.5550 ns (after 0.5 ps of simulation), the rotation of Im₁ leads to the breaking of the H-bond between Im₁ and Im₂ (see figure VI-9 b). Such a event triggers a process which rapidly (after 0.5 ps) leads to the breaking of the second H-bond (between Im₂ and Im₃, figure VI-9 c) and to the successive rotation of Im₃ occurring at 72.5620 ps (figure VI-9 d). In other words, thanks to the breaking of the first hydrogen bond a cascade process takes place so that a new hydrogen bond in the opposite direction is established.

In short, albeit about 72 ns are necessary at 393K to observe the rate limiting step of the hypothesized Grotthuss mechanism, such a process occurs very quickly once triggered by the rotation of the first imidazole of the chain. Notably, less than 10 ps are required for the reorientation of the first three imidazoles, a quasi-concerted process.

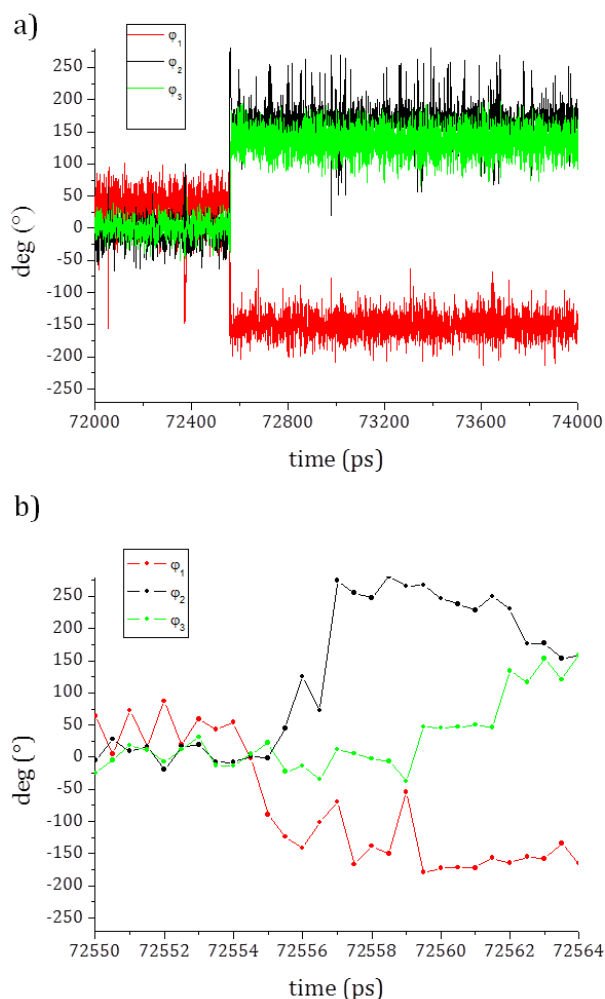


Figure VI-8: Time-dependent fluctuations of dihedral φ_1 , φ_2 , φ_3 extracted from the 80-ns trajectory obtained for the 15mer at 393K: a) From 72 to 74 ns, b) 14-ps interval depicting the flipping process

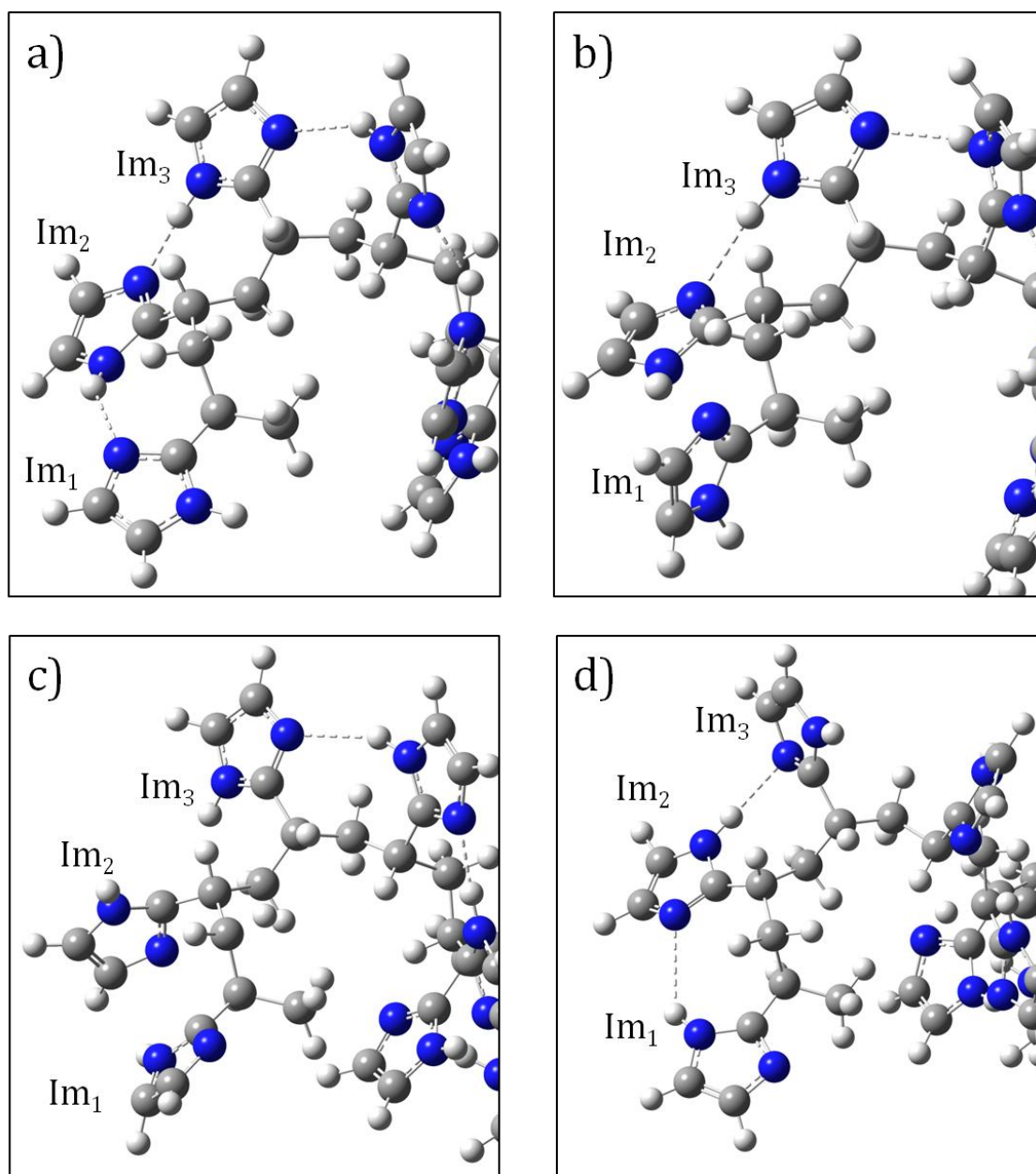


Figure VI-9. Images of some snapshots of the 80-ns MD trajectory obtained for 15mer at 393K: a) at 72.5545 ns, b) at 72.5550 ns, c) at 72.5555 and d) 72.5620 ns. The H-bonds are depicted by a dotted line.

4. Comments and experimental evidences

Taken together, these results further support the idea emerged by the investigation of P4VI (chapter IV): the tethering position of the proton wires can strongly affect the mechanism of conduction in N-heterocycles polymers. Indeed, in spite of the backbone constraint, in a 2-tethered model system the presence of two successive linear (strong) H-bonds is permitted when more than two monomeric units are considered (i.e. 3mer, see figure VI-5 a), in contrast

with the outcomes obtained for the corresponding 4-tethered polymer. The study carried out on small 2-tethered models suggests that the Grotthuss mechanism can be a plausible hypothesis. Indeed, the analysis of the electronic structure by means of DFT indicates that the unique possible PT reaction between adjacent imidazoles is energetically favored for all the investigated systems. Interestingly such a barrier is not influenced by the presence in position 4 and 5 of the heterocycles of cyano substituents, in contrast with the common assumption according to which withdrawing groups in position 4 and 5 would increase proton conductivity by making the protons more labile (as the result of the increasing of the acidity of the imidazole).^{3,9}

The Grotthuss hypothesis is strongly supported by the further analysis on larger oligomers (3mer and 15mer) of a 2-tethered model system, performed focusing the attention on the rate-limiting step (flipping of the imidazoles) of such hypothesized mechanism. Indeed, a relaxed scan calculation on 3mer indicates that the cooperative rotation of the proton wires is not energetically prohibitive requiring only 8 kcal/mol to take place. In addition, when a larger oligomer is considered (15mer), an H-bond network (necessary condition for the Grotthuss mechanism) is observed albeit the strong backbone constraint impedes the planarity of the system, as in P4VI. This is achieved thanks to a helix-like conformation (see figure VI-7). Importantly, the rate limiting step occurs during the MD simulations after 72 ns at 393K, the minimum temperature of the expected operative range forazole-based polymers (393-453 K).

The obtained simulations are consistent with some experimental evidences. Indeed, variable-temperature (VT) ¹H MAS spectra show that the increasing of the temperature strongly favor the molecular motion so determining an higher proton mobility,² as suggested by the obtained MD results. Indeed, as depicted in figure VI-10, a temperature increasing equal to 60 K is sufficient to observe the rate limiting step of the hypothesized mechanism after only 3 ns of simulation (vs. 72 ns at 393K).

In short, the main conclusion provided from the experimental literature according to which "imidazoles with substituents at the 2-position favor the 1,3-chain motif" depicting a picture where the Grotthuss mechanism is a "plausible hypothesis".² Furthermore, the DFT data indicate that the activation energy for the PT reaction is much lower with respect to the energy involved in the cooperative rotation of the proton wires (1.7 Vs. 8.3 kcal/mol), so further supporting that such a process can be considered as the rate-determining step of the conduction mechanism. Consistent with these results, the sulfonated derivatives of Poly(2-vinyl-4,5-dicyanoimidazole) have shown higher proton mobility with respect to the polymer itself⁹ thus indicating that the interruption of ordered hydrogen bond between the azoles moieties can promote the proton conduction. Indeed, lower is the H-bond strength, lower can be expected the energy involved in the cooperative rotation, this last requiring the breaking of such hydrogen bonds to take place.

Finally, from a broad-spectrum point of view, the fact that the charge transport is promoted in 2-tethered poly-imidazole systems is also confirmed by the high values of proton conductivities (up to 10^{-4} S/cm) detected in some fully polymeric proton solvents where imidazole is covalently bounded to flexible spacer through its position 2.¹⁰

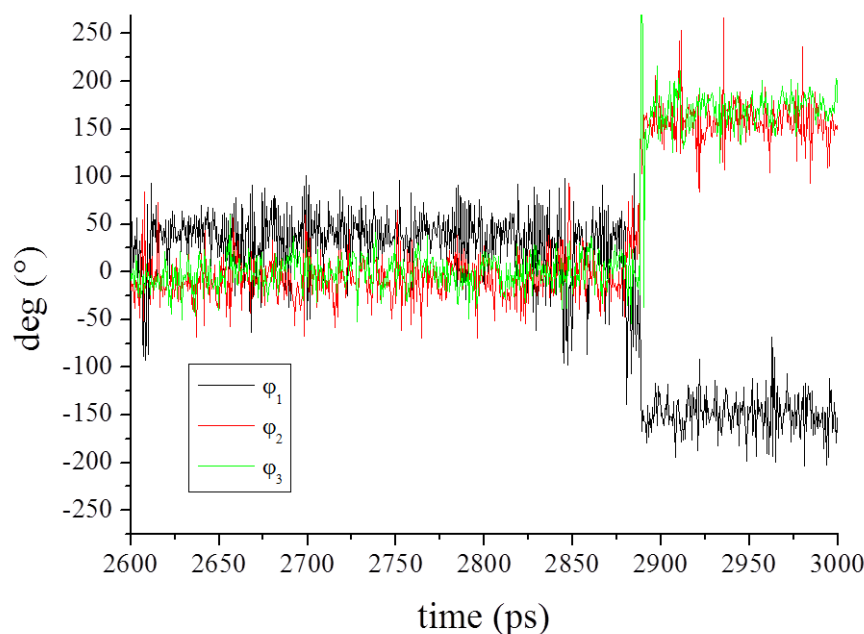


Figure VI-10. Time-dependent fluctuations of dihedral φ_1 , φ_2 and φ_3 extracted from the 80-ns trajectory obtained for 15mer at 453K.

5. Conclusions

In this chapter, the outcomes obtained through a combined DFT/MD approach applied on a 2-tethered poly-imidazole model system have been presented. The discussed results show as in poly-imidazole membranes the proton conduction mechanism can directly depend on the tethering position of the imidazole wires. Indeed, in contrast with the conclusions drawn from the investigation of proton conduction in P4VI (chapter IV), in the considered 2-tethered model the Grotthuss mechanism is not impeded by the polymeric constraint.

The obtained data, taken together with those already discussed in the chapter IV, point out for the first time the influence of the heterocycle tethering position on the conductivity of poly-imidazole membranes so representing a promising starting point for a further study focused on the rational design of such systems.

CHAPTER VI: Proton transport in 2-tethered systems

Hopefully, these findings can pave the way for the design of new and performing materials where an ideal compromise between H-bond strength and H-bond network flexibility can be realized in the Grotthuss hypothesis scenario.

6. References

- (1) Mangiatordi, G. F.; Adamo, C. Can the wire tethering directs the charge trasport in polyimidazole membranes? A theoretical study. *Submitted*.
- (2) Densmore, C. G.; Rasmussen, P. G.; Goward, G. R. Probing Hydrogen Bonding and Proton Mobility in Dicyanoimidazole Monomers and Polymers. *Macromolecules* **2004**, *38*, 416–421.
- (3) Wixom, M.; Lei, H.; Zhang, P.; Ma, J. *United States patent, T/J Technologies, Inc., Ann Arbor, MI (US)*, **2005**, no. 6,878,475 B2.
- (4) Narayanan, S. R.; Yen, S.-P.; Liu, L.; Greenbaum, S. G. Anhydrous Proton-Conducting Polymeric Electrolytes for Fuel Cells. *Journal of Physical Chemistry B* **2006**, *110*, 3942–3948.
- (5) Mangiatordi, G. F.; Butera, V.; Russo, N.; Laage, D.; Adamo, C. Charge transport in polyimidazole membranes: a fresh appraisal of the Grotthuss mechanism. *Physical Chemistry Chemical Physics* **2012** *14*, 10910-10918.
- (6) Wang, J.; Wolf, R. M.; Caldwell, J. W.; Kollman, P. A.; Case, D. A. Development and testing of a general amber force field. *Journal of Computational Chemistry* **2004**, *25*, 1157–1174.
- (7) Wang, J.; Wang, W.; Kollman, P. A.; Case, D. A. Automatic atom type and bond type perception in molecular mechanical calculations. *Journal of Molecular Graphics and Modeling* **2006**, *25*, 247–260.
- (8) Chen, H.; Yan, T.; Voth, G. A. A computer simulation model for proton transport in liquid imidazole. *Journal of Physical Chemistry A* **2009**, *113*, 4507–4517.
- (9) Ye, G.; Fortier-McGill, B.; Traer, J. W.; Czardybon, A.; Goward, G. R. Probing Proton Mobility in Polyvinazene and its Sulfonated Derivatives Using ¹H Solid-State NMR. *Macromolecular Chemistry and Physics* **2007**, *208*, 2076–2084.
- (10) Herz, H. G.; Kreuer, K. D.; Maier, J.; Scharfenberger, G.; Schuster, M. F. H.; Meyer, W. H. New fully polymeric proton solvents with high proton mobility. *Electrochimica Acta* **2003**, *48*, 2165–2171.

GENERAL CONCLUSIONS

Proton Exchange Membrane Fuel Cells (PEMFCs) have increasingly received attention in the last years as a clean and promising technology for energy conversion especially in portable electronics. Nevertheless, such a technology still doesn't provide adequate costs and performances to be competitive with less environmental friendly devices. Most of the challenges arise from the need for solid electrolytes, key component of the system, having better operating characteristics. Indeed, albeit they suffer of important drawbacks, only perfluorosulfonic membranes such as Nafion are today commercialized for PEMFCs applications. Such a materials, being water-dependent systems, do not allow for all the important technical advantages of working at temperatures above 100°C. The consequent intense research performed in the last years has permitted the identification of promising alternative systems such as theazole-based polymers. However, despite the recent progresses, the performances obtained from these new generation membranes are still far from the level requested for PEMFCs applications mainly because of the absence of a thorough understanding concerning the mechanistic aspects governing their proton conductivity.

Based on these experimental evidences and background, the aim of this PhD thesis was to provide insights into the mechanism of conduction of such proton exchange membranes in order to pave the way for a rational design of materials with enhanced performances. In contrast with the common trend, the present theoretical investigation has been realized by including the effect of the backbone constraint which has been proved to be crucial in affecting the mechanism of conduction. Previous studies, indeed, focused on the analysis of proton transport in liquid imidazole and the obtained findings have been also extended to the polymeric systems. In other words, models with an explicit consideration of the polymer matrix had never been studied, taking for granted, also for polymers, the common accepted mechanism of conduction for liquid azoles, namely the Grotthuss mechanism. Since this latter is based on the collective proton transfer among the proton wires (here N-heterocycles), a necessary prerequisite to take place consists of the presence of an hydrogen bond network along the polymeric chain. However, albeit indispensable, such a condition is not sufficient to assert that the structural diffusion happens in the polymer, being necessary the cooperative reorientation of all the proton wires in order to restore the starting conformation, a process which is supposed to be the rate limiting step.

General conclusions

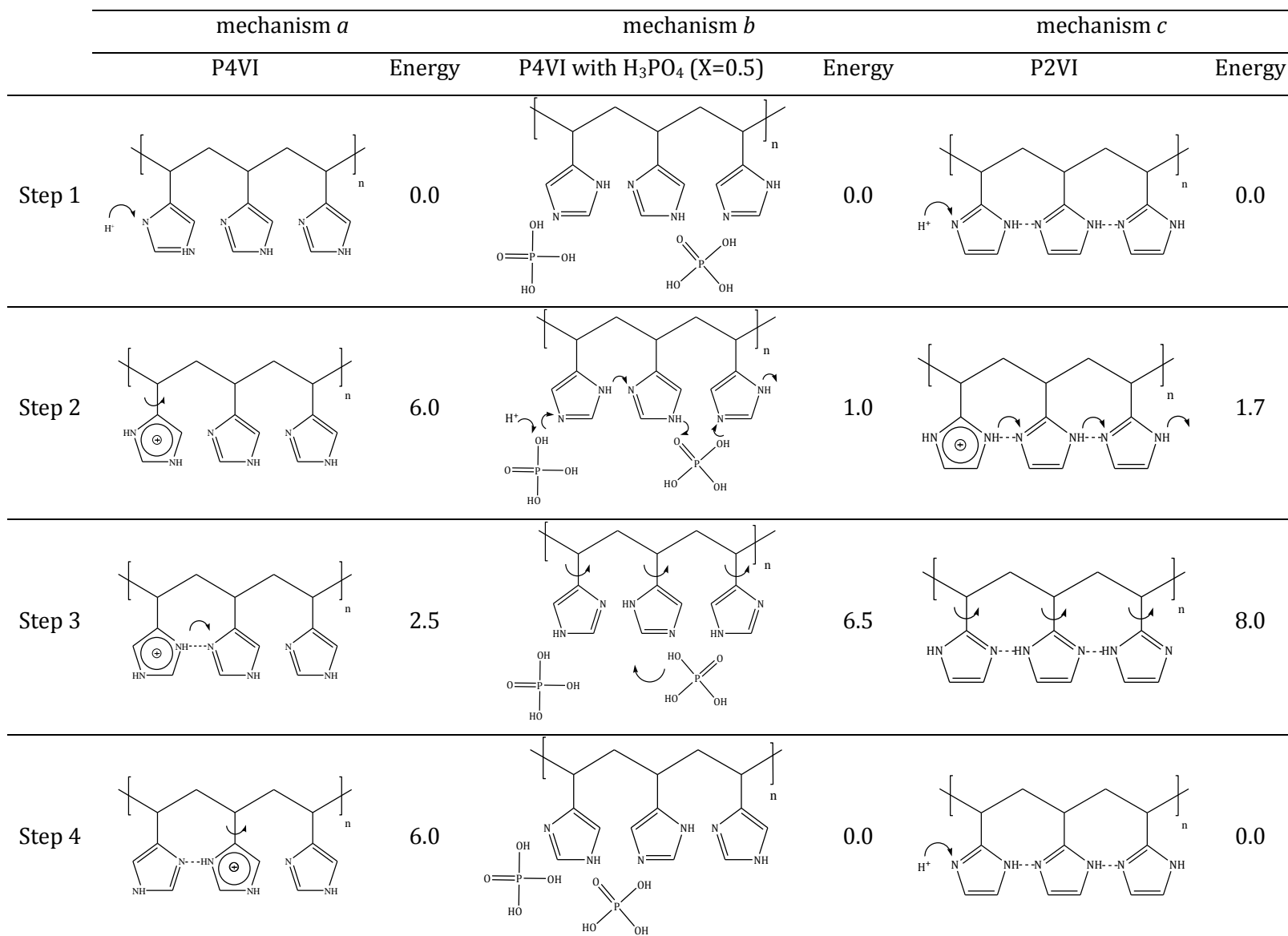


Figure C-1: Schematic representation of the mechanisms proposed in the present thesis. All the energy values are reported in kcal/mol.

General conclusions

The present research, therefore, focused not only on the evaluation the existence of such a fundamental prerequisite in different systems but also on the estimation of the energy involved in the hypothesized rate-determining step leading to a critical revision of the conclusions obtained in earlier works and to different models of mechanism on which it is worth now come back for a final overview.

The investigation of the proton transport on the first considered polymeric system, namely Poly(4-vinyl-imidazole) (P4VI), has revealed as the backbone constraint could impede the H-bond network leading to an alternative mechanism of conduction where the rate limiting step is represented by the frustrated rotation of the imidazole carrying the transferred proton, necessary before each proton transfer reaction can take place. Despite the energy involved in such a step is equal to only 6 kcal/mol, as shown in figure C-1 (step 2, mechanism *a*), the obtained alternative path can fully explain the low conductivity observed in such polymer. In fact, there are two major reasons why such a mechanism can be considered as less efficient than the common structural diffusion. First and foremost, the energy involved in the rate limiting step is requested before each single proton transfer between adjacent imidazoles, while in the Grotthuss mechanism the cooperative rotation allows for a new proton shuttling along the whole chain. In other words, in order to conduct one excess proton along one chain of P4VI, it is necessary that the limiting step occurs n times, where n refers to the number of monomeric units on the considered chain. Secondly, albeit the frustrated rotations are uncoupled, only one proton can be transferred along the chain at the same time due to the proton-proton repulsion that would otherwise occur.

Importantly, if the H-bond network along the chain cannot be reached in the pure system, it can be observed after adding an acid dopant such as phosphoric acid (H_3PO_4). In other words, the presence of dopant cancels the negative effect due to the backbone topology. Indeed, the picture emerged from the investigation of a model corresponding to P4VI doped with low quantity of H_3PO_4 (about one-half the amount of saturation) indicates that a collective proton transfer can take place along the chain due to the H_3PO_4 ability to act as hydrogen bonding bridge between imidazoles among which an H-bond would not otherwise be possible. Furthermore, as shown in figure C-1, about 6.5 kcal/mol are for the reorientational process necessary for a new proton shuttling along the chain. Note that, despite such a process requires a energy higher respect to the rate determining step of the mechanism hypothesized for the pure polymer (mechanism *a*); the emerged model gives a possible explanation of the increased conductivity reported in literature as a consequence of the H_3PO_4 doping. Indeed, the hypothesized path can be considered as a Grotthuss-like mechanism, more efficient for the reasons above mentioned.

In this regard, it is worth to note that in spite of the positive effect on the proton conductivity, the presence of a dopant acid can compromise the membrane stability and, as a

General conclusions

consequence, its permanent conductivity. For these reasons, the development of solid electrolytes able to conduct protons not only in anhydrous but also in acid-free conditions is highly desirable. Interestingly, the present research has shown as a greater ease in obtaining the indispensable requisite of the Grothuss mechanism, namely the H-bond network can be achieved also acting on the backbone topology. This is clearly shown by the mechanism emerged for the Poly(2-vinyl-imidazole) (P2VI) system (figure C-1, mechanism *c*) indicating that the Grothuss mechanism is not impeded by the polymeric constraint if the proton wires are casted through the position 2 instead of 4 (as in P4VI). Notably, only 8 kcal/mol are estimated for the cooperative rotation of all the imidazoles, a process observed through molecular dynamics simulations at the operative temperature of this system.

Despite the relevant findings achieved through the considered molecular models, it is worthy to note that larger models (such as systems including more than one polymeric chain) should be considered to have a more accurate picture of the mechanism of conduction of the considered polymers. This could be readily carried out due to the availability of the modified versions of the General Amber Force Field (GAFF) which have been proved to be able to accurately describe the investigated materials. Such a study, therefore, can be considered as the natural evolution of the present thesis.

It could be also argued that the considered polymers show levels of conductivity far from those requested for PEMFCs applications and that new and better performing materials have been prepared in the last years.¹⁻⁴ However, thanks to the investigated systems, the present research allowed to point out as the different conductivity of the azole-based systems could not be depend only on the efficiency of transport between the proton wires but also by their ability to form an H-bond network, taken for granted so far in literature.

Interestingly, an experimental work recently published by Basak et al⁴ is consistent with the conclusions of the present thesis. The authors investigated the anhydrous proton conductivity of two compounds, one based on imidazole and the other on 1,2,3-triazole showing that the conductivity of this latter is three orders of magnitude lower than that of the imidazole-based systems because of the different ability to form an extended hydrogen bond network (figure C-2). Such a different behavior cannot be explained by the previously theoretical investigations neglecting the influence of the backbone topology and according to which enhanced proton conductivity can be achieved by the substitution of imidazole with 1,2,3-triazole (see for instance the work by Bredas and collaborators⁵). On the contrary, based on the results of the present research, the greater difficulty to get an H-bond network in the 1,2,3-triazole based system can be related on the absence of equivalent nitrogen atoms in positions 1-3 which are instead present in the imidazole-based material, being a 2-tethered system. In other words, the obtained insights into the mechanism of proton transport in P4VI and P2VI are

General conclusions

extendable to more recent and better performing polymers providing a *rationale* of the different conductivity of different systems. This, as mentioned in chapter I, is crucial to design new Proton Exchange Membranes (PEMs) able to efficiently conduct protons in anhydrous and acid-free conditions, a challenge which was not yet overcome and that appears as the only way to produce systems characterized by a permanent conductivity and high durability, two properties which must be achieved before having azole-based marketable membranes.

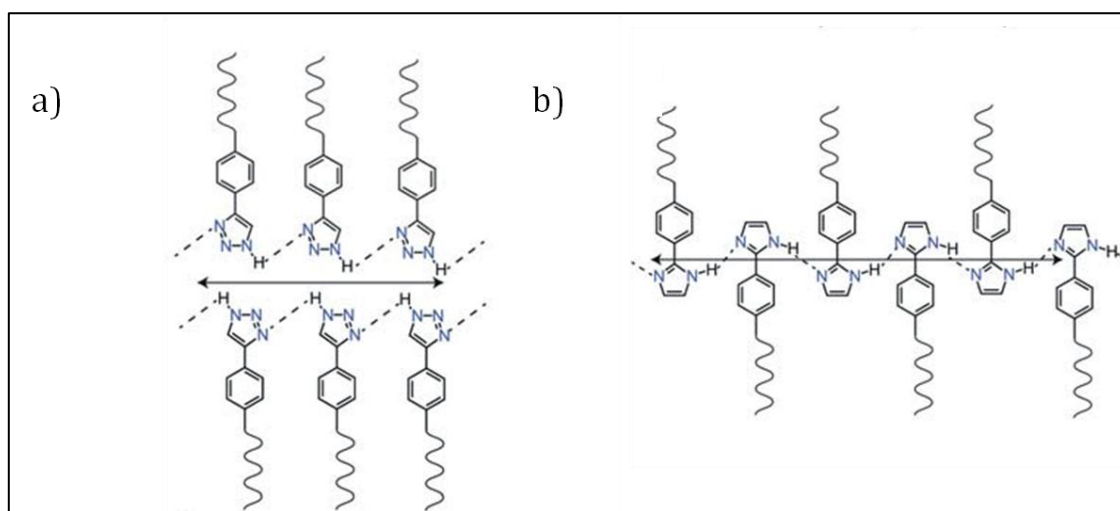


Figure C-2: Hypothetical proton conduction pathways for the 1,2,3-triazole (a) and imidazole (b) based systems investigated by Basak et al. Note the better H-bond directionality in b) (adapted from⁴).

References

- (1) Çelik, S. Ü.; Bozkurt, A.; Hosseini, S. S. Alternatives toward proton conductive anhydrous membranes for fuel cells: Heterocyclic protogenic solvents comprising polymer electrolytes. *Progress in Polymer Science* **2012**, *37*, 1265–1291.
- (2) Mustarelli, P.; Quartarone, E.; Grandi, S.; Angioni, S.; Magistris, A. Increasing the permanent conductivity of PBI membranes for HT-PEMs. *Solid State Ionics*, in press.
- (3) Zhang, H.; Shen, P. K. Recent development of polymer electrolyte membranes for fuel cells. *Chemical Reviews* **2012**, *112*, 2780–2832.
- (4) Basak, D.; Versek, C.; Harvey, J. A.; Christensen, S.; Hillen, J.; Auerbach, S. M.; Tuominen, M. T.; Venkataraman, D. Enhanced anhydrous proton conduction in binary mixtures of 1H-imidazole–1H-1,2,3-triazole based compounds. *Journal of Materials Chemistry* **2012**, *22*, 20410–20417.
- (5) Zhou, Z.; Liu, R.; Wang, J.; Li, S.; Liu, M.; Brédas, J.-L. Intra- and Intermolecular Proton Transfer in 1H(2H)-1,2,3-Triazole Based Systems. *Journal of Physical Chemistry A* **2006**, *110*, 2322–2324.

ANNEXES

ANNEX I: Supplementary information for chapter III

Annexes

Table A1. Proton transfer barriers obtained with the 6-311+G(3df,3pd) basis set. All the value are in kcal/mol and have been obtained using the B3LYP/6-311+G(2d,p) optimized structures. In case of asymmetric structures the PT barrier has been computed in the two opposite directions here labeled as X_1 (forward) and X_2 (reverse) where X identifies the system. (see figure III-8).

functional	system											
	A	B	C	D	E	F	G ₁	G ₂	H ₁	H ₂	I ₁	I ₂
w-B97XD	6.11	0.58	3.65	0.78	7.39	0.77	48.28	35.74	20.40	1.62	37.54	37.97
wB97X	6.21	0.82	4.08	1.20	8.05	1.09	48.86	36.42	21.55	2.21	38.51	38.74
CAM-B3LYP	5.52	0.53	3.05	0.90	6.14	0.74	48.14	35.94	19.23	1.22	37.84	37.80
B1LYP	5.46	0.64	3.52	1.08	7.29	0.89	48.87	36.60	20.57	1.75	38.07	38.37
PBE0-DH	6.55	0.39	2.61	0.58	5.94	0.47	47.68	35.42	18.39	0.90	37.44	36.85
BMK	6.27	0.96	4.15	1.49	8.00	1.31	48.73	35.65	22.26	2.13	37.45	38.26
X3LYP	5.10	0.49	3.04	0.87	6.47	0.71	47.89	35.60	19.57	1.22	37.07	37.48
B3LYP	4.96	0.48	3.01	0.87	6.51	0.70	47.75	35.42	19.70	1.21	36.81	37.36
M06	6.26	0.05	3.05	0.55	6.92	0.65	46.89	34.37	20.10	1.05	36.29	36.70
B3LYP-D	4.46	0.28	3.39	0.71	6.37	0.60	47.91	35.47	18.84	0.87	36.63	37.64
B972	5.56	0.33	2.58	0.64	6.18	0.48	47.35	34.89	19.29	0.90	36.37	36.71
LC-wPBE	5.75	0.37	2.68	0.66	5.83	0.49	47.37	34.54	19.46	0.76	36.75	37.15
w-B97	6.09	1.02	4.43	1.47	8.63	1.32	49.11	36.51	22.60	2.62	38.62	39.21
mPW1K	7.07	0.49	3.20	0.80	6.44	0.65	49.68	37.32	19.21	1.31	38.58	39.30
M062X	5.40	0.00	3.14	0.33	5.59	0.29	47.44	37.03	16.05	1.48	38.91	37.19
VSXC	5.28	0.66	3.87	1.18	10.02	1.21	46.16	33.71	23.99	2.49	35.60	36.53
mPW1PW91	5.36	0.20	2.20	0.44	5.23	0.31	46.77	34.39	17.84	0.38	36.02	36.11
PBE0	5.23	0.13	2.03	0.35	4.99	0.24	46.25	33.93	17.45	0.21	35.61	35.63
M06HF	5.35	0.06	3.36	-0.20	4.45	-0.40	47.23	38.48	11.51	1.42	40.76	36.93
LC-PBEPBE	5.57	0.00	1.39	0.14	2.90	0.02	45.81	33.17	15.71	-0.74	35.72	35.47
BLYP	2.85	0.20	2.08	0.54	5.48	0.39	44.50	32.10	18.63	0.31	32.97	34.70
BHandHLYP	7.84	1.06	4.89	1.59	8.88	1.37	52.89	40.64	22.37	3.00	42.59	41.82
B97D	2.88	-0.11	2.23	0.23	5.02	0.13	44.80	32.25	17.23	-0.19	32.88	34.93
GRAC	3.14	0.01	1.67	0.24	5.28	0.20	43.97	31.35	18.63	0.07	32.29	33.99
B2PLYP	8.02	1.27	5.56	1.87	10.12	1.61	53.80	41.60	23.89	3.77	43.49	42.72
TCA	2.91	-0.16	0.96	-0.07	4.24	0.11	42.92	30.19	17.33	-0.51	31.44	33.02
PBEPBE	2.63	-0.29	0.59	-0.18	3.15	-0.24	41.86	29.42	15.45	-1.22	30.52	31.97

Annexes

Table A2. Details on the statistics of the DBH24/08 dataset

functional	Heavy Metal Transfer			Nucleophilic Transfer			Unimolecular and Association			Hydrogen Transfer			Total		
	MD	RMSD	MAD	MD	RMSD	MAD	MD	RMSD	MAD	MD	RMSD	MAD	MD	RMSD	MAD
M062X	0.54	0.94	0.68	-0.74	1.04	1.92	-0.13	1.12	1.37	0.85	1.28	1.40	0.13	1.45	1.03
BMK	1.52	1.93	1.52	-0.93	1.11	1.42	-0.75	1.98	2.05	1.52	1.52	1.84	0.34	1.82	1.53
PBE0-DH	1.73	2.61	1.90	-0.15	0.56	0.73	-0.45	1.70	2.18	2.24	2.24	2.46	0.84	2.13	1.60
mPW1K	0.70	1.22	1.32	-1.03	1.20	1.64	-0.69	2.45	2.93	1.53	1.59	1.76	0.13	1.61	2.01
w-B97XD	1.83	2.88	2.20	-0.32	0.75	0.79	-0.78	1.99	2.25	2.48	2.61	3.05	0.80	2.41	1.89
B2PLYP	2.89	3.33	2.89	2.25	2.25	2.29	-0.02	0.65	0.89	2.37	2.37	2.51	1.87	2.42	2.04
BHandHLYP	-1.19	3.99	2.88	-0.87	1.44	1.84	-0.80	2.34	2.65	0.26	1.73	2.00	-0.65	2.75	2.10
w-B97X	-0.28	2.41	2.35	-1.07	1.46	1.75	-1.62	2.32	2.94	1.66	2.28	2.71	-0.33	2.49	2.10
LC-wPBE	-0.59	2.54	2.10	-3.03	3.03	3.27	-1.05	2.06	2.76	1.44	1.51	2.28	-0.81	2.74	2.18
M06	4.16	6.04	4.47	1.27	1.27	1.39	-0.34	1.85	2.13	2.10	2.10	2.45	1.80	3.50	2.42
M06HF	-4.20	6.10	4.70	0.72	1.72	2.13	-0.93	1.72	1.99	-1.22	1.84	2.27	-1.41	3.56	2.50
PBEPBE	14.16	16.28	14.16	6.85	6.85	6.99	3.10	3.10	4.11	9.72	9.72	10.29	-1.30	3.19	2.59
B972	3.56	5.60	4.14	1.53	1.53	1.66	-0.67	1.79	2.00	3.27	3.50	4.02	1.92	3.69	2.74
CAM-B3LYP	4.02	4.11	4.02	0.89	0.97	1.10	0.64	2.00	2.52	4.14	4.14	4.45	2.42	3.32	2.78
LC-PBEPBE	0.25	4.96	3.29	-4.24	4.24	4.52	-0.89	2.42	3.00	3.43	3.67	4.84	-0.36	4.40	3.40
B1LYP	5.45	5.55	5.45	2.78	2.78	2.87	1.04	1.62	2.51	3.86	3.86	4.23	3.28	3.98	3.43
mPW1PW91	5.63	6.25	5.63	1.88	1.88	1.95	0.65	1.95	2.64	4.32	4.32	4.50	3.12	4.19	3.45
PBE0	6.36	7.21	6.36	1.87	1.87	1.92	0.88	2.07	2.73	5.00	5.00	5.26	3.53	4.76	3.83
B3LYP	7.25	7.47	7.25	3.51	3.51	3.55	1.41	1.72	2.91	5.07	5.07	5.38	4.31	5.14	4.39
X3LYP	7.23	7.43	7.23	3.48	3.48	3.52	1.40	1.78	2.92	5.25	5.25	5.52	4.34	5.16	4.44
VSXC	7.41	9.67	7.41	3.83	3.83	4.55	0.29	1.53	2.05	5.45	5.45	5.91	4.25	6.19	4.56
B3LYP-D	7.79	8.09	7.79	3.99	3.99	4.06	1.64	1.93	3.09	5.64	5.64	5.90	4.77	5.62	4.84
B97D	9.91	11.56	9.91	6.02	6.02	6.07	1.49	1.90	2.91	6.45	6.54	7.39	5.97	7.64	6.09
GRAC	12.74	13.73	12.74	6.19	6.19	6.28	2.63	2.68	4.14	7.90	7.90	8.38	7.37	8.88	7.38
TCA	12.62	14.68	12.62	6.61	6.61	6.72	2.69	2.69	3.49	8.31	8.31	8.88	7.56	9.38	7.56
BLYP	12.88	13.86	12.88	7.43	7.43	7.50	3.24	3.24	4.22	8.17	8.17	8.65	7.93	9.23	7.93
w-B97	-1.96	3.54	2.82	-1.78	2.29	2.73	-2.26	3.00	3.73	0.81	2.26	2.62	8.46	10.45	8.46

Table A3. Proton transfer barriers obtained using the optimized structures for each functional. All the values are in kcal/mol. In case of asymmetric structures the PT barrier has been computed in the two opposite directions here labeled as X_1 (forward) and X_2 (reverse) where X identifies the system (see figure III-8).

functional	system										
	B	C	D	E	F	G ₁	G ₂	H ₁	H ₂	I ₁	I ₂
M06	0.09	3.07	1.64	6.94	1.15	46.78	34.25	20.53	1.19	36.19	36.64
BMK	1.04	4.21	1.58	8.11	1.44	48.58	35.54	22.60	2.26	37.33	38.18
wB97X	0.87	4.11	1.25	8.10	1.26	48.76	36.34	21.79	2.36	38.42	38.71
w-B97	1.14	4.50	1.59	8.70	1.69	49.00	36.42	22.85	2.88	38.51	39.22
B1LYP	0.66	3.54	1.10	7.32	0.92	48.87	36.60	20.89	1.81	38.07	38.37
B2PLYP	1.38	5.54	1.86	10.11	1.62	53.86	41.66	24.29	3.94	43.55	42.73
X3LYP	0.49	3.04	0.87	6.47	0.72	47.89	35.60	19.88	1.25	37.07	37.48
B3LYP	0.48	3.01	0.87	6.51	0.70	47.75	35.42	19.70	1.21	36.81	37.36
CAM-B3LYP	0.54	3.05	0.91	6.16	0.75	48.11	35.92	19.52	1.22	37.82	37.80
LC-wPBE	0.37	2.66	0.66	5.83	0.49	47.21	34.42	19.59	0.77	36.60	37.09
PBE0-DH	0.39	2.59	0.59	5.93	0.49	47.56	35.36	18.54	0.91	37.37	36.77
M062X	0.11	3.15	0.30	5.63	0.34	47.34	36.91	16.33	1.55	38.87	37.15
mPW1PW91	0.23	2.23	0.46	5.25	0.34	46.71	34.34	18.07	0.45	35.98	36.06
PBE0	0.18	2.07	0.39	5.02	0.29	46.17	33.88	17.70	0.33	35.57	35.58
LC-PBEPBE	0.11	1.54	0.25	3.35	0.16	45.52	33.01	17.12	17.12	35.51	35.34
M06HF	0.34	3.54	0.50	5.34	0.25	47.15	38.44	12.16	2.26	40.76	37.08

Table A4. Distances between H-acceptor and H-donor for the optimized structures for each functional. In case of asymmetric systems only the values for the lowest energy structure (reported in figure III-8) have been considered and the protonated water dimer has not been included. All the values are in Å.

functional	system								
	B	C	D	E	F	G	H	I	
M06	2.726	2.594	2.705	2.700	2.696	2.268	2.884	2.277	
BMK	2.723	2.587	2.696	2.695	2.682	2.266	2.926	2.278	
wB97X	2.715	2.581	2.683	2.669	2.674	2.270	2.880	2.280	
w-B97	2.731	2.593	2.700	2.681	2.688	2.281	2.886	2.285	
B1LYP	2.707	2.584	2.679	2.679	2.667	2.276	2.908	2.288	
B2PLYP	2.701	2.571	2.660	2.665	2.647	2.281	2.890	2.283	
X3LYP	2.694	2.568	2.666	2.660	2.653	2.276	2.884	2.287	
B3LYP	2.695	2.571	2.668	2.666	2.655	2.278	2.896	2.290	
CAM-B3LYP	2.689	2.549	2.661	2.636	2.640	2.268	2.864	2.279	
LC-wPBE	2.672	2.538	2.644	2.640	2.632	2.266	2.895	2.273	
PBE0-DH	2.661	2.529	2.623	2.618	2.615	2.262	2.850	2.270	
M062X	2.647	2.582	2.618	2.650	2.620	2.268	2.857	2.282	
mPW1PW91	2.656	2.526	2.626	2.622	2.615	2.269	2.863	2.277	
PBE0	2.650	2.522	2.619	2.618	2.610	2.269	2.857	2.278	
LC-PBEPBE	2.627	2.466	2.597	2.548	2.586	2.250	2.796	2.254	
M06HF	2.632	2.460	2.572	2.500	2.561	2.257	2.832	2.276	

Table A5. Distances between H and H-donor for the optimized structures for each functional. In case of asymmetric systems only the values for the lowest energy structure (reported in III-8) have been considered and the protonated water dimer has not been included. All the values are in Å.

functional	system							
	B	C	D	E	F	G	H	I
M06	1.114	0.994	1.088	0.996	1.078	1.009	1.028	0.967
BMK	1.116	0.990	1.088	0.994	1.093	1.009	1.023	0.964
wB97X	1.115	0.992	1.090	0.997	1.085	1.007	1.025	0.965
w-B97	1.109	0.992	1,085	0,998	1,075	1,007	1,026	0,967
B1LYP	1,130	0,996	1,098	0,999	1,104	1,007	1,024	0,967
B2PLYP	1.127	1.000	1.105	1.001	1.110	1.007	1.025	0.968
X3LYP	1.140	1.000	1.107	1.003	1.113	1.008	1.027	0.968
B3LYP	1.142	1.001	1.107	1.004	1.114	1.009	1.027	0.969
CAM-B3LYP	1.136	1.000	1.105	1.004	1.110	1.008	1.027	0.967
LC-wPBE	1.144	1.001	1.114	1.003	1.121	1.007	1.025	0.966
PBE0-DH	1.137	0.997	1.113	0.999	1.116	1.003	1.023	0.962
M062X	1.175	0.990	1.135	0.999	1.126	1.008	1.024	0.966
mPW1PW91	1.159	1.005	1.124	1.005	1.133	1.006	1.026	0.965
PBE0	1.166	1.008	1.130	1.007	1.138	1.007	1.028	0.966
LC-PBEPBE	1.180	1.017	1.146	1.021	1.157	1.008	1.034	0.966
M06HF	1.179	1.014	1.167	1.035	1.174	1.006	1.027	0.963

Table A6. Distances between H and H-acceptor for the optimized structures for each functional. In case of asymmetric systems only the values for the lowest energy structure (reported in figure 1) have been considered and the protonated water dimer has not been included. All the values are in Å

functional	system							
	B	C	D	E	F	G	H	I
M06	1.612	1.715	1.617	1.705	1.643	2.534	1.861	2.241
BMK	1.606	1.711	1.609	1.702	1.593	2.532	1.909	2.253
wB97X	1.599	1.700	1.594	1.672	1.604	2.532	1.859	2.245
w-B97	1.622	1.713	1.616	1.683	1.645	2.535	1.864	2.248
B1LYP	1.576	1.697	1.582	1.680	1.566	2.544	1.889	2.256
B2PLYP	1.574	1.671	1.555	1.663	1.540	2.546	1.869	2.251
X3LYP	1.554	1.671	1.560	1.656	1.542	2.544	1.862	2.253
B3LYP	1.553	1.673	1.561	1.663	1.543	2.547	1.874	2.290
CAM-B3LYP	1.553	1.634	1.556	1.632	1.540	2.532	1.842	2.248
LC-wPBE	1.528	1.635	1.530	1.637	1.513	2.527	1.871	2.235
PBE0-DH	1.523	1.626	1.510	1.620	1.501	2.526	1.831	2.230
M062X	1.471	1.706	1.484	1.651	1.501	2.530	1.879	2.251
mPW1PW91	1.497	1.612	1.502	1.616	1.484	2.535	1.840	2.236
PBE0	1.483	1.604	1.489	1.611	1.473	2.536	1.833	2.233
LC-PBEPBE	1.448	1.535	1.451	1.527	1.430	2.507	1.766	2.220
M06HF	1.454	1.534	1.405	1.465	1.392	2.509	1.809	2.267

Optimized CCSD/cc-pVTZ structures of the systems B-I (see figure III-8 for labeling).

System B

Minimum

N	-1.36620400	0.00000200	-0.00001600
H	-1.76236400	-0.00285400	-0.93457700
H	-1.76212300	0.81083400	0.46491800
H	-1.76206900	-0.80800900	0.46984800
N	1.35314500	0.00000100	-0.00000900
H	0.25353300	0.00000400	-0.00021600
H	1.70795300	-0.06146500	0.95159600
H	1.70824900	-0.79332300	-0.52892700
H	1.70823000	0.85478900	-0.42246500

TS

N	1.29702400	0.00000000	0.00000000
H	1.67346300	0.76041800	-0.55881300
H	1.67346000	-0.86415800	-0.37913300
H	1.67345700	0.10373800	0.93795000
N	-1.29702400	0.00000000	0.00000000
H	0.00000400	0.00000000	0.00000000
H	-1.67346300	-0.76020600	0.55910100
H	-1.67346000	0.86430100	0.37880600
H	-1.67345800	-0.10409300	-0.93791000

System C

Minimum

C	0.00922700	1.09470900	-0.00003500
H	0.03214500	2.17174700	-0.00001000
C	1.24597200	0.34069600	-0.00001900
O	1.29579400	-0.88626800	-0.00001000
H	2.18244100	0.91522700	-0.00009700

Annexes

C	-1.17746600	0.44255600	-0.00003400
O	-1.31503500	-0.87406600	-0.00002600
H	-2.12257300	0.96988500	0.00105400
H	-0.40447400	-1.24195200	-0.00013300

TS

C	-0.00001300	1.12824500	0.00010200
H	-0.00002100	2.20342600	0.00018500
C	-1.18169900	0.38415800	0.00013000
O	-1.17552200	-0.88824100	0.00002600
H	-2.15451500	0.87411900	0.00024000
C	1.18167200	0.38421400	-0.00007200
O	1.17551600	-0.88822500	-0.00017500
H	2.15450500	0.87410100	-0.00012900
H	0.00030900	-1.11962700	-0.00006000

System D

Minimum

C	-2.10687200	-0.62331600	0.90236100
C	-3.42517900	-0.42266600	0.62771800
N	-3.44941600	0.35337400	-0.50829700
H	-4.26914100	0.68675000	-0.98223000
H	-1.67109100	-1.17888400	1.71257600
H	-4.32049100	-0.75011600	1.12123000
N	-1.33030300	0.01685300	-0.04681300
C	3.44460700	0.58308500	0.40354900
C	2.15476100	0.95816100	0.60425100
N	1.35085500	0.03144400	-0.02569600
H	4.37085400	1.02272600	0.72087500
H	1.74756700	1.79630400	1.13723900
N	3.39461400	-0.57282300	-0.34967500
H	0.27223800	0.03664100	-0.05280200

Annexes

C	-2.17706000	0.59211700	-0.87603000
H	-1.91515800	1.17987400	-1.73790900
C	2.11966600	-0.88062800	-0.59226700
H	1.77929600	-1.73078100	-1.15478200
H	4.18613900	-1.10496900	-0.66832400

TS

C	-2.07244700	-0.80529600	0.77312000
C	-3.37521400	-0.51404800	0.51439000
N	-3.35449300	0.47230000	-0.44795900
H	-4.15696700	0.91362000	-0.86120500
H	-1.65679800	-1.51712400	1.46175400
H	-4.28975300	-0.90696800	0.91612000
N	-1.27452200	-0.00622400	-0.02231200
C	3.37521900	0.51411700	0.51431600
C	2.07245500	0.80541900	0.77300000
N	1.27452200	0.00623300	-0.02231000
H	4.28976100	0.90708900	0.91598600
H	1.65681300	1.51735700	1.46152400
N	3.35448800	-0.47237900	-0.44788100
H	-0.00000300	0.00000700	-0.03874900
C	-2.07803600	0.75082900	-0.74415500
H	-1.77150000	1.48673500	-1.46559200
C	2.07802800	-0.75093900	-0.74403500
H	1.77148600	-1.48695300	-1.46536000
H	4.15695800	-0.91377100	-0.86105900

System E

minimum

C	1.89939200	0.17115500	0.00004200
O	1.50597400	-1.07898800	-0.00005500

Annexes

O	1.18249100	1.15000600	0.00008700
H	2.98799700	0.25068600	0.00025400
H	0.51913600	-1.11635200	-0.00021200
C	-1.89942600	-0.17116000	0.00005100
O	-1.18250900	-1.14999300	-0.00012700
O	-1.50593300	1.07897200	0.00002400
H	-2.98803900	-0.25070900	0.00000300
H	-0.51907300	1.11643800	-0.00003300

TS

C	-1.76022500	0.00002300	-0.00002600
O	-1.19776000	-1.12329100	0.00008600
O	-1.19772200	1.12330200	-0.00013600
H	-2.85101800	0.00003100	-0.00003100
H	-0.00006000	-1.09575100	0.00006900
C	1.76022500	-0.00002200	0.00003300
O	1.19772000	-1.12330200	0.00005300
O	1.19776200	1.12329100	-0.00000900
H	2.85101700	-0.00003200	0.00005300
H	0.00006300	1.09575300	-0.00008500

System F

Minimum

C	-2.42281000	-1.16379300	-0.00005600
C	-3.54068000	-0.37238400	0.00020300
N	-3.04791600	0.88523400	0.00004500
H	-3.54906000	1.75726600	0.00008800
H	-2.33337500	-2.23344000	-0.00011400
H	-4.59158300	-0.59116900	0.00039200
N	-1.72596700	0.90191200	-0.00018300
N	-1.34044200	-0.34182700	-0.00010300
C	3.26957700	0.79990100	-0.00000500

Annexes

C	1.92660100	1.06020900	0.00010600
N	1.32632800	-0.15472600	-0.00014000
H	0.27078100	-0.35843100	-0.00028700
H	4.13280900	1.43820600	-0.00000600
H	1.36995200	1.97834800	0.00016000
N	2.17523300	-1.13712900	0.00001900
N	3.34630300	-0.55326600	0.00009500
H	4.16957000	-1.13576200	0.00015400

TS

C	2.11863900	1.13140500	0.00017300
C	3.38701300	0.61752000	0.00016600
N	3.19761800	-0.72208000	0.00003600
H	3.88855400	-1.45486600	-0.00001000
H	1.77221000	2.14753200	0.00025600
H	4.35859700	1.07409000	0.00023900
N	1.92574600	-1.05463700	-0.00003600
N	1.27266800	0.06933500	0.00004700
C	-3.38701300	-0.61752100	-0.00016000
C	-2.11863800	-1.13140500	-0.00016200
N	-1.27266800	-0.06933400	-0.00004700
H	0.00000000	0.00000100	0.00000000
H	-4.35859600	-1.07409100	-0.00023000
H	-1.77220900	-2.14753100	-0.00023600
N	-1.92574600	1.05463800	0.00002600
N	-3.19761900	0.72207900	-0.00004300
H	-3.88855500	1.45486500	-0.00000400

System G

Minimum

C	0.16209400	0.38550500	0.00002000
O	1.19230900	-0.24519200	0.00004800

Annexes

H	0.13832200	1.48527200	-0.00000500
N	-1.08153200	-0.15745200	-0.00029900
H	-1.89751900	0.42056000	0.00098600
H	-1.18111800	-1.15516300	0.00060600

TS

C	0.03744900	0.50916400	0.00000000
O	1.08301400	-0.22456400	0.00000000
H	0.07220200	1.59308500	0.00000000
N	-1.00635600	-0.26353300	-0.00000100
H	-1.96372000	0.04610600	0.00000200
H	0.04720200	-1.05293300	0.00000100

System H

Minimum

C	-2.02527000	-0.14229200	0.00049700
O	-1.40817900	-1.19704300	-0.00030000
H	-3.12354700	-0.13144200	0.00085300
N	-1.47731800	1.07954700	-0.00000900
H	-2.07188100	1.88449100	0.00041400
H	-0.46609500	1.19486200	-0.00053000
C	2.02529500	0.14227500	0.00046800
N	1.47727800	-1.07953200	-0.00021600
H	3.12357000	0.13140100	0.00222400
O	1.40821600	1.19703300	-0.00051200
H	2.07175400	-1.88453800	0.00094500
H	0.46603700	-1.19469500	-0.00162900

TS

C	1.83371800	-0.01483200	-0.00001000
O	1.33521600	1.16066200	0.00002900
H	2.92384300	-0.06029100	-0.00001300
N	1.14530500	-1.11276500	-0.00004500

Annexes

H	1.71962100	-1.94060900	-0.00007200
H	-0.17430200	-1.14678200	-0.00004900
C	-1.83371800	0.01483200	0.00001300
N	-1.14530600	1.11276500	0.00005800
H	-2.92384300	0.06029000	0.00002800
O	-1.33521500	-1.16066200	-0.00004900
H	-1.71962300	1.94060800	0.00010800
H	0.17430400	1.14678200	0.00004200

System I

Minimum

C	0.99824700	-1.22292500	0.00000400
C	1.81066000	-0.10404500	0.00000100
C	1.19532200	1.15127300	0.00000100
C	-0.18315500	1.23127700	-0.00000200
C	-0.89869600	0.02861400	-0.00000800
H	1.42711900	-2.21617300	0.00000300
H	2.88468600	-0.20648300	0.00000200
H	1.78941300	2.05429600	0.00000200
H	-0.71126700	2.17171000	0.00000000
N	-0.34229400	-1.16897100	-0.00000200
O	-2.24740800	0.08760700	0.00000300
H	-2.54889300	-0.82656400	0.00000500

TS

C	-0.89268600	-1.28202000	0.00001600
C	-1.77018000	-0.22131400	0.00000700
C	-1.24371100	1.08862000	-0.00001200
C	0.11261100	1.33213100	-0.00001800
C	0.95462900	0.20026300	-0.00000500
H	-1.21288700	-2.31309700	0.00002800

Annexes

H	-2.83416200	-0.39317100	0.00001200
H	-1.92772600	1.92654000	-0.00002000
H	0.52607700	2.32738100	-0.00003000
N	0.42576600	-1.04344800	0.00000800
O	2.22676600	0.03348100	0.00000100
H	1.69022800	-1.21745500	0.00001500

ANNEX II: Supplementary information for chapter IV

Annexes

Table A7: Atom numbers, GAFF atom types and relative RESP partial charges obtained for 15mer⁺.

atom number	GAFF atom type	q (e ⁻)
1	c3	0.186
2	c3	-0.379
3	hc	0.099
4	hc	0.099
5	c3	0.104
6	hc	0.067
7	c3	-0.007
8	hc	0.014
9	hc	0.014
10	c3	0.021
11	c3	-0.353
12	hc	0.074
13	hc	0.074
14	c3	-0.036
15	hc	0.106
16	c3	0.035
17	hc	0.043
18	hc	0.043
19	c3	-0.363
20	c3	-0.620
21	hc	0.185
22	hc	0.185
23	c3	0.079
24	c3	-0.056
25	hc	0.031
26	hc	0.031
27	c3	-0.152
28	c3	-0.075
29	hc	0.022
30	hc	0.022
31	c3	-0.048
32	hc	0.085
33	c3	-0.218
34	hc	0.060
35	hc	0.060
36	hc	0.060
37	cd	-0.092
38	cd	0.331
39	h4	0.138
40	h5	0.096
41	cd	-0.253
42	h4	0.190
43	cd	0.250
44	h5	0.113
45	cd	-0.177
46	h4	0.170
47	cd	0.358
48	h5	0.088
49	cd	-0.233
50	h4	0.194
51	cd	0.329

Annexes

52	h5	0.089
53	cc	0.383
54	cc	0.382
55	cc	0.406
56	cc	0.249
57	na	-0.444
58	nc	-0.658
59	na	-0.452
60	nc	-0.598
61	na	-0.410
62	nc	-0.674
63	na	-0.499
64	nc	-0.642
65	c3	-0.075
66	hc	0.022
67	hc	0.022
68	c3	-0.152
69	c3	-0.056
70	hc	0.031
71	hc	0.031
72	c3	0.079
73	hc	0.066
74	c3	-0.620
75	hc	0.185
76	hc	0.185
77	c3	-0.363
78	c3	0.035
79	hc	0.043
80	hc	0.043
81	c3	-0.036
82	hc	0.106
83	c3	-0.353
84	hc	0.074
85	hc	0.074
86	c3	0.021
87	c3	-0.007
88	hc	0.014
89	hc	0.014
90	c3	0.104
91	c3	-0.379
92	hc	0.099
93	hc	0.099
94	cd	-0.233
95	cd	0.329
96	h4	0.194
97	h5	0.089
98	cd	-0.177
99	h4	0.170
100	cd	0.358
101	h5	0.088
102	cd	-0.253
103	h4	0.190
104	cd	0.250
105	h5	0.113
106	cc	0.406

Annexes

107	cc	0.382
108	cc	0.383
109	nc	-0.642
110	na	-0.444
111	nc	-0.674
112	na	-0.499
113	nc	-0.598
114	na	-0.410
115	hn	0.363
116	hn	0.367
117	hn	0.369
118	hn	0.367
119	hn	0.376
120	hn	0.363
121	cd	-0.264
122	h4	0.207
123	cd	0.231
124	h5	0.111
125	cd	-0.166
126	h4	0.164
127	cd	0.187
128	h5	0.122
129	cd	-0.253
130	cd	0.298
131	h4	0.207
132	h5	0.097
133	c2	-0.118
134	c2	0.073
135	h4	0.182
136	h5	0.216
137	cd	-0.253
138	cd	0.298
139	h4	0.207
140	h5	0.097
141	cd	-0.166
142	cd	0.187
143	h4	0.164
144	h5	0.122
145	cd	-0.264
146	cd	0.231
147	h4	0.207
148	h5	0.111
149	cc	0.351
150	cc	0.421
151	cc	0.329
152	c2	0.119
153	cc	0.329
154	cc	0.421
155	cc	0.351
156	nc	-0.533
157	na	-0.425
158	nc	-0.546
159	na	-0.379
160	nc	-0.640
161	na	-0.397

Annexes

162	na	-0.208
163	na	-0.299
164	nc	-0.640
165	na	-0.397
166	nc	-0.533
167	na	-0.425
168	nc	-0.546
169	na	-0.379
170	hn	0.355
171	hn	0.372
172	hn	0.352
173	hn	0.382
174	hn	0.352
175	hn	0.372
176	hn	0.355
177	hc	0.078
178	hc	0.066
179	hc	0.225
180	hc	0.045
181	hc	0.081
182	c3	-0.048
183	hc	0.085
184	c3	-0.218
185	hc	0.060
186	hc	0.060
187	hc	0.060
188	hc	0.045
189	hc	0.225
190	hc	0.078
191	hn	0.324
192	hn	0.376
193	hc	0.067
194	cd	-0.092
195	cd	0.331
196	h4	0.138
197	h5	0.096
198	cc	0.249
199	nc	-0.658
200	na	-0.452
201	hn	0.369

ANNEX III: Supplementary information for chapter VI

Annexes

Table A8: Atom numbers, GAFF atom types and relative RESP partial charges obtained for 15mer.

atom number	GAFF atom type	q (e ⁻)
1	c3	-0.010
2	hc	0.026
3	hc	0.026
4	c3	-0.232
5	hc	0.088
6	c3	0.025
7	hc	0.043
8	hc	0.043
9	c3	-0.34
10	hc	0.112
11	cd	-0.375
12	cc	-0.0149
13	cd	0.425
14	cd	0.406
15	nc	-0.453
16	c3	0.153
17	hc	0.002
18	hc	0.002
19	c3	-0.008
20	hc	0.039
21	c3	-0.092
22	hc	0.021
23	hc	0.021
24	hc	0.021
25	cd	0.009
26	cd	0.385
27	nc	-0.479
28	cd	-0.314
29	cd	-0.312
30	na	-0.200
31	na	-0.155
32	nc	-0.546
33	na	-0.222
34	cc	0.0548
35	hn	0.299
36	hn	0.298
37	hn	0.271
38	c3	-0.198

Annexes

39	c3	0.222
40	hc	0.117
41	cd	0.326
42	hc	-0.042
43	hc	-0.042
44	c3	-0.305
45	nc	-0.538
46	na	-0.084
47	hc	0.094
48	c3	0.073
49	cd	0.420
50	cc	0.076
51	cd	-0.380
52	hn	0.215
53	hc	0.033
54	hc	0.033
55	c3	-0.091
56	na	-0.206
57	nc	-0.467
58	hc	0.089
59	cd	0.315
60	cd	-0.318
61	hn	0.288
62	cc	-0.015
63	nc	-0.585
64	na	0.021
65	cc	0.130
66	cd	-0.469
67	hn	0.188
68	c3	-0.174
69	c3	-0.158
70	hc	0.087
71	hc	0.087
72	c3	0.260
73	hc	0.098
74	cd	0.278
75	hc	-0.034
76	hc	-0.034
77	c3	-0.537
78	nc	-0.471
79	na	-0.152

Annexes

80	hc	0.140
81	c3	0.260
82	cd	0.472
83	cc	0.007
84	cd	-0.281
85	hn	0.286
86	hc	-0.034
87	hc	-0.034
88	c3	-0.158
89	na	-0.189
90	nc	-0.534
91	hc	0.098
92	cd	0.278
93	c3	-0.174
94	cd	-0.319
95	hn	0.288
96	cc	0.013
97	nc	-0.471
98	na	-0.152
99	hc	0.087
100	hc	0.087
101	cc	0.007
102	cd	-0.281
103	hn	0.286
104	c3	-0.091
105	c3	0.073
106	hc	0.089
107	cd	0.315
108	hc	0.033
109	hc	0.033
110	c3	-0.305
111	nc	-0.585
112	na	0.021
113	hc	0.094
114	c3	0.222
115	cd	0.420
116	cc	0.130
117	cd	-0.469
118	hn	0.188
119	hc	-0.042
120	hc	-0.042

Annexes

121	c3	-0.198
122	na	-0.206
123	nc	-0.467
124	hc	0.117
125	cd	0.326
126	c3	0.153
127	cd	-0.318
128	hn	0.288
129	cc	-0.015
130	nc	-0.538
131	na	-0.084
132	hc	0.002
133	hc	0.002
134	cc	0.076
135	cd	-0.380
136	hn	0.215
137	c3	-0.337
138	c3	0.025
139	hc	0.112
140	cd	0.406
141	hc	0.043
142	hc	0.043
143	c3	-0.232
144	nc	-0.453
145	na	-0.200
146	hc	0.089
147	c3	-0.010
148	cd	0.425
149	cc	-0.015
150	cd	-0.314
151	hn	0.299
152	hc	0.026
153	hc	0.026
154	c3	-0.008
155	na	-0.155
156	nc	-0.546
157	cd	0.385
158	cd	-0.375
159	hn	0.271
160	cc	0.055
161	nc	-0.479

Annexes

162	na	-0.222
163	cc	0.009
164	cd	-0.313
165	hn	0.298
166	hc	0.039
167	c3	-0.092
168	hc	0.021
169	hc	0.021
170	hc	0.021
171	h4	0.211
172	h4	0.134
173	h4	0.229
174	h4	0.125
175	h4	0.215
176	h4	0.138
177	h4	0.227
178	h4	0.116
179	h4	0.220
180	h4	0.140
181	h4	0.246
182	h4	0.113
183	h4	0.188
184	h4	0.136
185	h4	0.216
186	h4	0.138
187	h4	0.188
188	h4	0.136
189	h4	0.246
190	h4	0.113
191	h4	0.220
192	h4	0.140
193	h4	0.227
194	h4	0.116
195	h4	0.215
196	h4	0.138
197	h4	0.229
198	h4	0.125
199	h4	0.211
200	h4	0.134

Synthèse générale

1. Contexte et objectifs

L'*Economie Hydrogène* (une hypothétique future société basée sur l'utilisation de l'hydrogène moléculaire H₂ comme vecteur d'énergie) est aujourd'hui considérée comme l'une des solutions les plus efficaces pour pallier la plupart des problèmes environnementaux de la planète comme le réchauffement global, problème fortement dépendant des émissions de gaz à effet de serre.¹ Elle repose sur un réseau composé de trois étapes fonctionnelles : la production, le stockage et l'utilisation.²

L'hydrogène peut être produit en utilisant différentes méthodes. Actuellement, environ 50% de la demande mondiale de H₂ est produite par reformage à la vapeur du gaz naturel,³ un processus qui n'est pas considéré comme durable car conduisant à des émissions de gaz à effet de serre. Heureusement, grâce aux progrès concernant la production d'hydrogène de manière biologique, une diminution de ce pourcentage est prévue dans un futur proche.⁴ Actuellement, l'absence d'une technologie sûre pour le stockage d'hydrogène à température ambiante est considérée comme l'un des principaux obstacles à l'économie de l'hydrogène. La mise au point de nouveaux matériaux ayant de meilleures performances⁵, grâce au développement de la recherche scientifique, est l'une des pistes envisagées pour surmonter ce problème. En ce qui concerne l'utilisation de l'hydrogène, il ya deux principales façons de produire de l'énergie : la combustion et l'utilisation de piles à combustible.^{6,7} La seconde est considérée comme la plus prometteuse pour une future *Economie Hydrogène* parce que plus appropriée pour un large éventail d'applications et capable d'assurer un meilleur rendement.⁷

1.1. Les piles à combustible

Les piles à combustible sont des dispositifs utilisés pour produire l'électricité à partir de différents combustibles. Elles sont constituées par deux électrodes et un électrolyte. Même si différents types de piles ont été développés, le principe de fonctionnement est commun : le combustible est oxydé à l'électrode négative (anode) et l'oxygène est réduit à l'électrode positive (cathode). Ces réactions électrochimiques ont lieu grâce à l'utilisation d'un catalyseur, généralement du platine⁸. Les ions sont transportés d'une électrode à l'autre à travers l'électrolyte, considéré comme l'élément clé du système. En effet, il détermine la fenêtre de température de fonctionnement des piles à combustible qui, pour cette raison, sont appelées en fonction du type d'électrolyte utilisé. Elles sont notamment classées en deux principaux groupes :

Synthèse générale

- Les piles à combustible à basse température, qui fonctionnent à des températures $< 250\text{ C}^\circ$. A cette catégorie appartiennent les piles alcalines (AFC), à méthanol direct (DMFC), à membrane d'échange de protons (PEMFC) et à acide phosphorique (PAFC).
- Les piles à combustible à haute température, fonctionnant à des températures $> 500\text{ C}^\circ$ comme les piles à oxyde solide (SOFC) et à carbonate fondu (MCFC).

Parmi les différents types de piles, les PEMFC ont attiré le plus grande intérêt parce que ces dispositifs sont les plus appropriés pour les applications mobiles comme les voitures électriques et ordinateurs portables⁹.

La membrane d'échange de protons (PEM)

Les particularités d'une PEMFC sont l'utilisation d'une membrane polymérique (PEM) comme électrolyte et la basse température de fonctionnement ($50\text{-}100\text{ C}^\circ$). Les réactions ayant lieu peuvent être exprimées de la manière suivante :

- Réaction à l'anode : $2\text{H}_2 \rightarrow 4\text{H}^+ + 4\text{e}^-$
- Réaction à la cathode : $\text{O}_2 + 4\text{H}^+ + 4\text{e}^- \rightarrow 2\text{H}_2\text{O}$
- Réaction globale : $2\text{H}_2 + \text{O}_2 \rightarrow 2\text{H}_2\text{O}$

La PEMFC est principalement composée de i) plaques bipolaires ii) catalyseur iii) PEM. Les protons sont les porteurs de charge du système : ils traversent la membrane polymérique de l'anode à la cathode (Figure S-1).

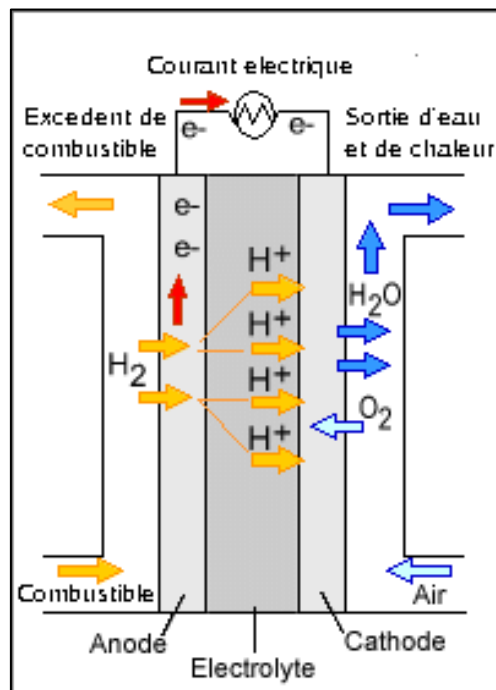


Figure S-1 : Diagramme d'une PEMFC¹⁰

Malgré les efforts fournis ces dernières années tant de la part de la recherche académique qu'industrielle, des obstacles à la commercialisation des piles à combustible existent encore,

principalement en raison de la faible durabilité et du coût élevé.¹¹ Une amélioration de ce dispositif peut se faire à travers l'amélioration et l'innovation continue de sa composante clé : la membrane d'échange de protons.¹²⁻¹⁴ En effet, même si les membranes actuellement utilisées présentent la plupart des propriétés requises comme la stabilité mécanique, chimique et thermique ainsi qu'une haute conductivité protonique, elles ont encore un coût trop élevé pour une commercialisation à grande échelle.

L'état de l'art est représenté par les polymères perfluorés comme le Nafion,¹⁵ la première PEM de cette classe à être commercialisée. Ce matériau peut atteindre des niveaux de conductivité élevés ($7,8 \times 10^{-2}$ S/cm à température ambiante) et il est également caractérisé par une haute stabilité à différentes températures et pressions.¹⁶ Cependant, en plus de son coût élevé,¹⁷ il présente une conductivité protonique régie par le degré d'hydratation,^{16,18} propriété qui ne lui permet pas d'être utilisé à des températures supérieures à 80° C, car se produirait alors une évaporation substantielle de l'eau. Toutefois, plusieurs avantages techniques peuvent être obtenus en augmentant le température de fonctionnement.¹² En effet, au-dessus de 100°C l'empoisonnement du catalyseur par le monoxyde de carbone (un des inconvénients de ce dispositif) est fortement réduite.¹⁹ De plus, les températures élevées permettent une meilleure gestion de l'eau²⁰ et de la chaleur²¹ pendant le processus et améliorent également la cinétique des réactions électrochimiques¹² en permettant d'utiliser moins de platine,^{22,23} catalyseur très coûteux.

Compte tenu de ces avantages, l'accent a dernièrement été mis sur le développement de membranes capables de travailler à faible taux d'humidité et à températures plus élevées.^{14,24} Les stratégies utilisées peuvent être divisées en deux sous-catégories principales : i) utilisation de Nafion modifié,²⁵⁻²⁷ ii) utilisation de matériaux de départ différents.²⁸⁻³¹ En ce qui concerne la deuxième approche, le rôle le plus important a été joué par des hétérocycles aromatiques contenant des atomes d'azote, comme l'imidazole ou le 1,2,3-triazole.

1.2. Les azoles et les polymères à base d'azoles comme conducteurs de protons

L'incapacité des membranes perfluorées à conduire des protons à des températures élevées repose sur le mécanisme de conduction. Celui-ci doit nécessairement être assisté par l'eau¹⁶ et implique à la fois le mouvement d'ions hydroniums (transport véhiculaire³²) et la diffusion structurale (mécanisme de Grotthuss).^{33,34} Dans ce contexte, le remplacement de l'eau par des azoles a suscité beaucoup d'enthousiasme durant les dernières années.³⁵⁻³⁷ En effet, la migration des protons dans ces composés se produit, comme dans l'eau, à travers le mécanisme véhiculaire et le mécanisme de Grotthuss mais leurs points d'ébullition sont plus élevés, permettant ainsi des températures de fonctionnement supérieures (> 100 °C).^{35,38} Toutefois, ces solvants alternatifs présentent un grand inconvénient. En effet, au vu de leur petite taille, ils peuvent lessiver progressivement au cours du processus, conduisant ainsi à un déclin progressif de la performance du système.³⁹ Pour cette raison,

une stratégie plus prometteuse consiste à incorporer de façon covalente ces composés hétérocycliques dans les membranes polymériques afin qu'ils ne puissent être traînés hors de la membrane, tandis que leur mobilité locale est maintenue. Notamment, le travail de Schuster et ses collaborateurs, publié en 2001,⁴⁰ a introduit le concept de base selon lequel les azoles immobilisés peuvent participer directement au mécanisme de conduction protonique. Comme le mécanisme de transport véhiculaire ne peut avoir lieu après l'immobilisation des hétérocycles, les auteurs ont également suggéré que la conductivité protonique de ces systèmes était sûrement le résultat d'un mécanisme de Grotthuss.

Sur la base de ces évidences, plusieurs polymères contenant des azoles immobilisés ont été synthétisés.^{38,41-46} (Tableau S-1). Parmi eux, les systèmes ayant une structure de base de polyéthylène ont été largement étudiés, à la fois en tant que polymères purs ou dopés par l'acide phosphorique ou sulfurique. En effet, ces acides forts sont capables d'améliorer la conductivité en augmentant la flexibilité du système ou grâce à la participation directe au mécanisme de la conduction protonique.

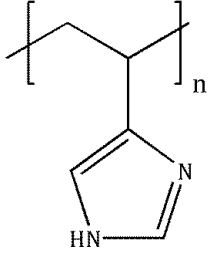
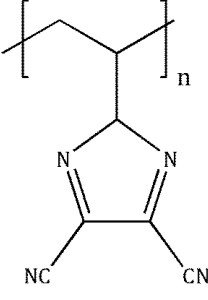
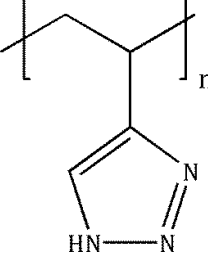
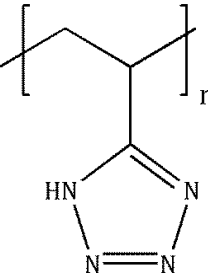
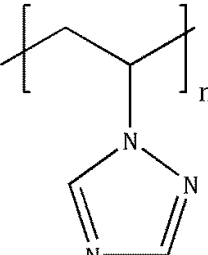
1.3. Objectifs de la thèse

Malgré les progrès réalisés, la conductivité montrée par les polymères à base d'azole (valeurs maximales dans la gamme de 10^{-5} à 10^{-4} S/cm) est encore inférieure à celle prévue pour les membranes d'acide fluorosulfoniques (10^{-1} S/cm). Ceci est principalement dû à la mauvaise compréhension des aspects mécanistiques impliqués dans le transport de charge de ces systèmes. Dans ce contexte, la chimie théorique et computationnelle peut jouer un rôle important. Notamment, les méthodes théoriques basées sur la théorie de la fonctionnelle de la densité (DFT) permettent d'effectuer une étude approfondie des réactions de transfert de proton à travers une approche quantique. Dans le même temps, les processus dynamiques complexes qui se produisent dans les systèmes polymères peuvent être étudiés par des simulations de Dynamique Moléculaire classique (MD).

Le présent travail de thèse propose, dans le contexte scientifique décrit, une étude théorique des processus liés à la conductivité des protons dans les polymères à base d'azole afin de fournir des indications pour une conception rationnelle de nouveaux matériaux avec de meilleures performances. Cette étude est réalisée grâce à une approche combinée, fondée à la fois sur l'application de méthodes DFT et sur l'utilisation de la dynamique moléculaire.

Synthèse générale

Tableau S-1 : Conducteurs de protons présentant des azoles immobilisés et une structure de base de polyéthylène.

polymère	structure	référence	année
a) poly-(4-vinyl-imidazole)		Bozkurt et al. ⁴²	2001
b) poly-(2-vinyl-4,5-dicyanoimidazole)		Densmore et al. ⁴⁶	2004
c) poly-(4-vinyl-1,2,3-triazole)		Zhou et al. ³⁸	2005
d) poly-(5-vinyl-1,2,3,4-tetrazole)		Pu at al. ⁴⁴	2008
e) poly-(1-vinyl-1,2,4-triazole)		Çelik et al. ⁴⁵	2008

2. Étude DFT des réactions de transfert de proton dans les azoles

Comme mentionné ci-dessus, l'imidazole, le 1,2,3-triazole et le tétrazole (Figure S-2) représentent les éléments fondamentaux de la plupart des membranes à base d'azole. Afin de déterminer l'approche DFT la plus appropriée, c'est à dire capable de reproduire avec précision

l'énergie et les caractéristiques structurales de cette famille d'hétérocycles, une analyse théorique des réactions de transfert de proton (PT) se produisant dans ces systèmes a été effectuée.

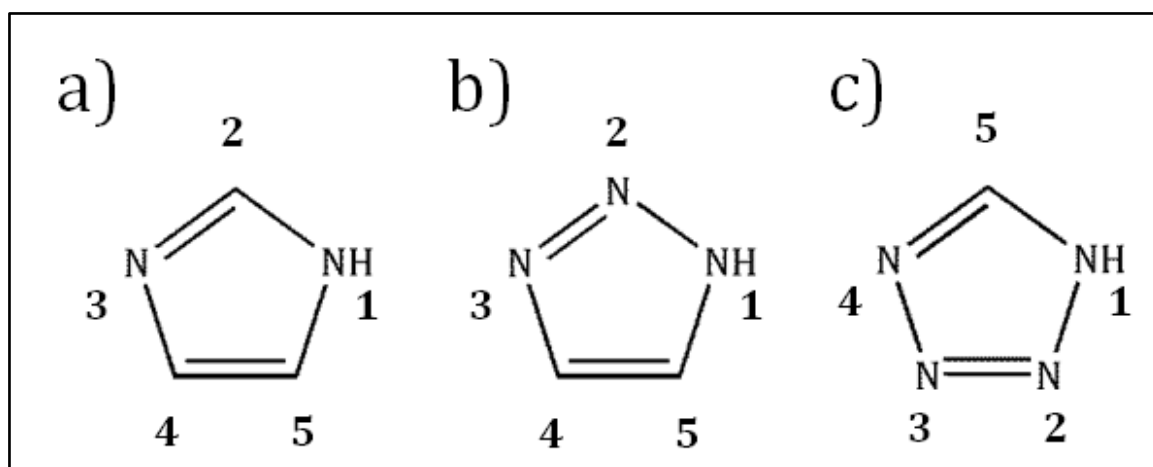


Figure S-2. Structure moléculaire et numérotation des atomes : a)imidazole b) 1,2,3-triazole and c) tétrazole.

Cette étude a été réalisée en utilisant les fonctionnelles DFT les plus utilisées et les plus performantes pour les réactions de transfert de proton : B3LYP,⁴⁸ PBE0,⁴⁹ BMK,⁵⁰ X3LYP,⁵¹ mPW1PW91,⁵² M06HF,⁵³ M062X,⁵⁴ LC-wPBE,^{55,56} TCA⁵⁷ et LC-TCA.⁵⁸ Les résultats obtenus ont été comparés avec des valeurs de références données par des calculs CCSD(T)⁵⁹ pour l'énergie et MP2^{60,61} pour la structure.

Dans ces composés, la réaction de transfert de proton consiste à transférer le proton impliqué dans la liaison hydrogène entre deux moitiés, dont l'une est chargée positivement. Une telle réaction est généralement étudiée en prenant en compte les systèmes les plus simples, c'est-à-dire des dimères protonés.⁶²⁻⁶⁵

Si, pour l'imidazole (ImH⁺-Im, mécanisme *a*) et le 1,2,3-triazole (TrH⁺-Tr, mécanisme *b*) un seul type de PT peut être détecté, trois mécanismes différents sont envisagés pour le tétrazole (TeH⁺-Te, mécanismes *c*, *d* et *e*) en raison de la tautomérie (Figure S-3).

Après la sélection des fonctions de base (6-311+G(d,p)) capables d'assurer un bon compromis entre la précision et le temps de calcul et d'une méthode appropriée (CCSD(T)//B3LYP) pour les valeurs de référence de l'énergie, les barrières énergétiques correspondant aux cinq mécanismes de transfert de proton ont été calculées, avec chacune des fonctionnelles DFT considérées. Comme indiqué dans le tableau S-2, seules deux fonctionnelles (B3LYP et BMK) sont capables de fournir les énergies d'activation pour les cinq mécanismes. En effet, les mécanismes *d* et *e* se réfèrent aux deux directions contraires de la même réaction PT (Figure S-3) et pour la plupart des fonctionnelles, seul le minimum de départ du mécanisme *e* est stable, de sorte qu'un état de transition n'est pas calculable. En outre, la plupart des fonctionnelles considérées sous-estiment la barrière par rapport à des

données des référence CCSD(T). Notamment, certaines d'entre elles (B3LYP et LC-wPBE) donnent des énergies d'activation proches des données MP2. Une exception est donnée par le modèle BMK qui détermine des valeurs très proches de celles de référence.

D'un point de vue géométrique, l'analyse de la performance des fonctionnelles a été effectuée sur les paramètres concernant la liaison hydrogène entre les deux moitiés de la structure de minimum et de l'état de transition calculé : les distances N_D-H , $H-N_D$ et N_D-N_A où N_D se réfère à l'atome d'azote qui donne l'hydrogène et N_A à l'atome d'azote qu'il accepte. A l'inverse de l'analyse énergétique, les meilleures performances sont obtenues en utilisant l'approche B3LYP (écart absolu moyen de 0.02 Å)

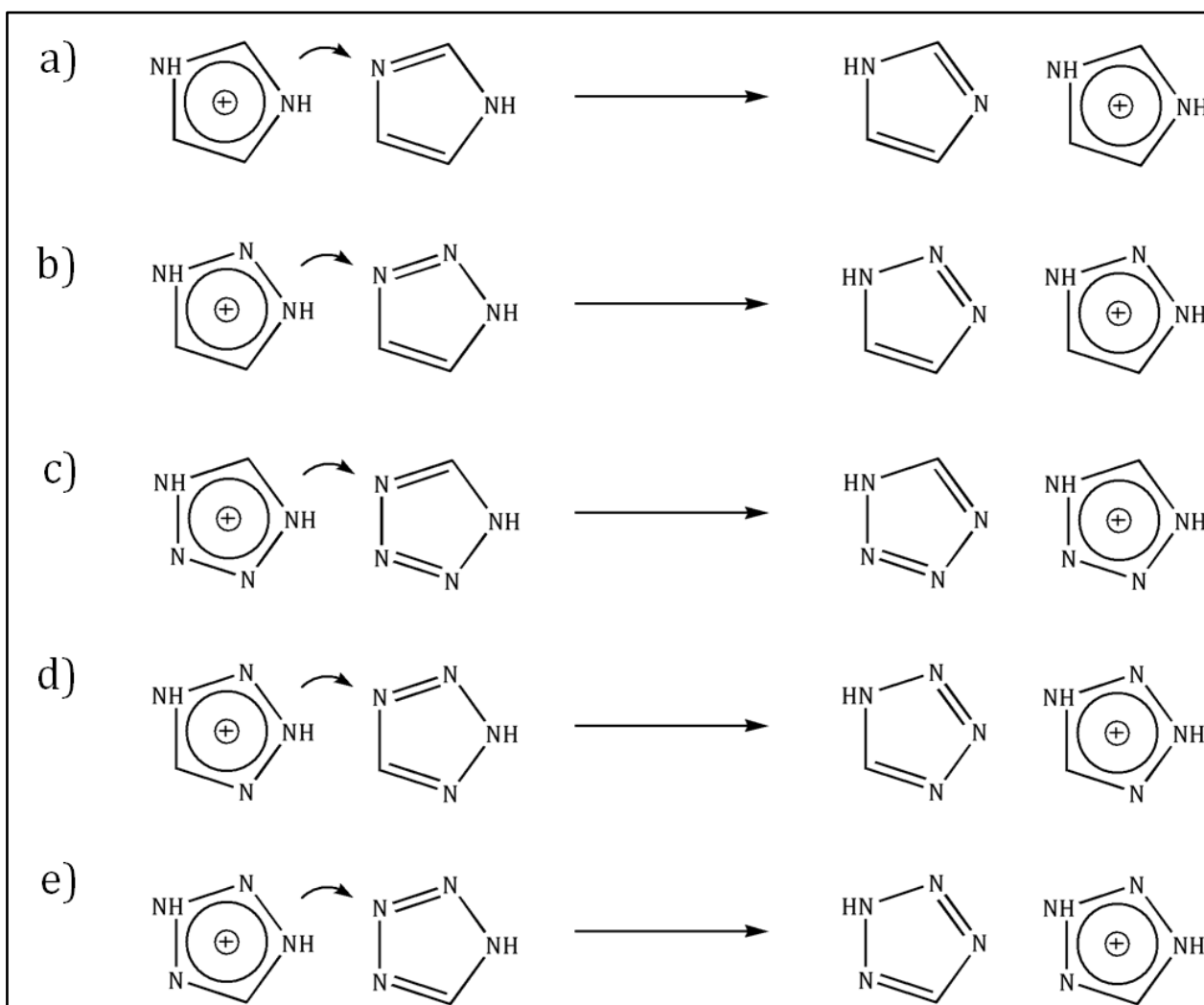


Figure S-3. Mécanismes de transfert de proton dans a) imidazole, b) 1,2,3-triazole et c), d), e) tétrazole.

Tableau S-2 : Barrières d'énergie (kcal/mol) calculées pour le transfert de proton dans les complexes Imidazolium-Imidazole (ImH⁺-Im), 1,2,3-Triazolium-1,2,3-Triazole(TrH⁺-Tr) et Tetrazolium-Tetrazole (TeH⁺-Te). Toutes les valeurs ont été calculées en utilisant les fonctions de base 6-311+G(d,p). Le niveau de théorie CCSD(T)/6-311+G(d,p)//B3LYP/6-311+G(d,p) a été utilisé pour les valeurs de référence.

mécanisme	ImH ⁺ -Im	TrH ⁺ -Tr	TeH ⁺ -Te		
	<i>a</i>	<i>b</i>	<i>c</i>	<i>d</i>	<i>e</i>
best estim.	1,4	1,2	2,3	0,1	1,5
MP2	0,5	0,4	1,4	0,0	0,4
B3LYP	0,7	0,6	1,0	0,0	1,0
PBE0	0,3	0,2	0,6	/	/
BMK	1,4	1,3	2,9	0,2	1,8
X3LYP	0,2	0,1	0,6	/	/
mPW1PW91	0,4	0,2	0,5	/	/
LC-wPBE	0,5	0,4	1,1	/	/
M06HF	0,3	0,2	0,5	/	/
M062X	0,1	0,1	1,4	/	/
TCA	0,1	0,0	0,1	/	/
LC-TCA0	0,2	0,1	0,8	/	/

2.1. Le modèle BMK/B3LYP

Les résultats présentés ici ne permettent pas le choix d'une fonctionnelle unique pour reproduire fidèlement les caractéristiques structurales et énergétiques des complexes étudiés. En effet, les meilleures énergies sont données par BMK, tandis que les meilleures structures sont obtenues par B3LYP, d'où la nécessité de combiner les deux approches. Notamment, si des calculs d'énergie à un seul point sont effectués sur les structures B3LYP en utilisant le modèle BMK, les énergies d'activation obtenues (1.3, 1.1, 2.4, 0.1 et 1.7 kcal/mol) sont en parfait accord avec les données de référence CCSD(T), et fournissent de meilleures valeurs que celles fournies par le pur modèle BMK. Ce protocole BMK/B3LYP⁶⁶ a donc été utilisé pour une étude plus approfondie des systèmes où ces hétérocycles sont immobilisés, à savoir les polymères à base d'azoles.

3. Une étude de référence de réactions PT

L'Étude des réactions de transfert de proton dans les azoles a indiqué que ces réactions représentent un domaine assez délicat pour les méthodes ancrées dans la théorie de la fonctionnelle de la densité, puisque les caractéristiques structurales et énergétiques sont découplées, et que les résultats discutés ne permettent pas le choix d'une fonctionnelle unique. Afin d'avoir plus d'informations concernant la performance de la DFT dans ce genre de réactions, une étude de référence a été réalisée. Elle comprend un ensemble représentatif des réactions de transfert de proton ainsi qu'un grand nombre de fonctionnelles allant de celles utilisant l'approximation du gradient généralisé (GGA) aux hybrides doubles (DH). Les systèmes étudiés sont esquissés dans la figure S-4 et étiquetés de A à I. Des réactions à la fois symétriques et non-symétriques ont été prises en compte, et 12 barrières d'énergie ont été considérées. En outre, afin d'obtenir des valeurs de référence précises, des optimisations de géométrie au niveau CCDS/cc-pvTZ ont été menées et des énergies en CCSD(T)/aug-cc-pvTZ ont également été calculées. Le classement obtenu pour ces fonctionnelles a été comparé à ceux émis par le test standard pour la cinétique, représenté par le DHB 24/08 *database*. Ainsi, quatre *benchmark* différents ont été effectués : énergies d'activation de transfert de proton calculés avec des structures optimisées au niveau B3LYP/6-311+G(2d,p) (1), évaluations standards de la barrière d'énergie avec le DBH 24/08 *database* (2), comparaison des barrières d'énergie du transfert de proton (3), paramètres optimisés de la liaison hydrogène (4), pour chaque fonctionnelle considérée avec les valeurs de référence CCSD(T) et CCSD, respectivement. Sur la base de l'écart absolu moyen par rapport aux valeurs de référence, un classement des fonctionnelles a été obtenu pour chaque *benchmark*. En supposant que chaque essai a le même poids, un score total a été attribué à chaque fonctionnelle en vue d'obtenir un classement final. Le score correspond à la position relative dans le classement, sachant que le score le plus petit est donné pour les meilleures performances. Comme indiqué dans la figure S-5, la fonctionnelle la mieux classée est le modèle récent ω B97X, qui obtient un classement élevé dans chacun des quatre essais. Elle est suivie par BMK, B1LYP et PBE0-DH. En plus des considérations concernant les positions de chaque fonctionnelle, une deuxième observation générale prend en compte le changement de classement relatif pour aller d'un *benchmark* à l'autre. En ce qui concerne le comportement des fonctionnelles lorsque l'on passe des barrières d'énergie à géométries fixes à celles calculées sur les structures optimisées avec chaque fonctionnelle, la plupart des fonctionnelles montrent un classement similaire. Au contraire, en comparant le classement de l'énergie (à géométrie fixe) avec celui correspondant aux paramètres structurels, un comportement très différent est détecté pour la quasi-totalité des fonctionnelles.

Synthèse générale

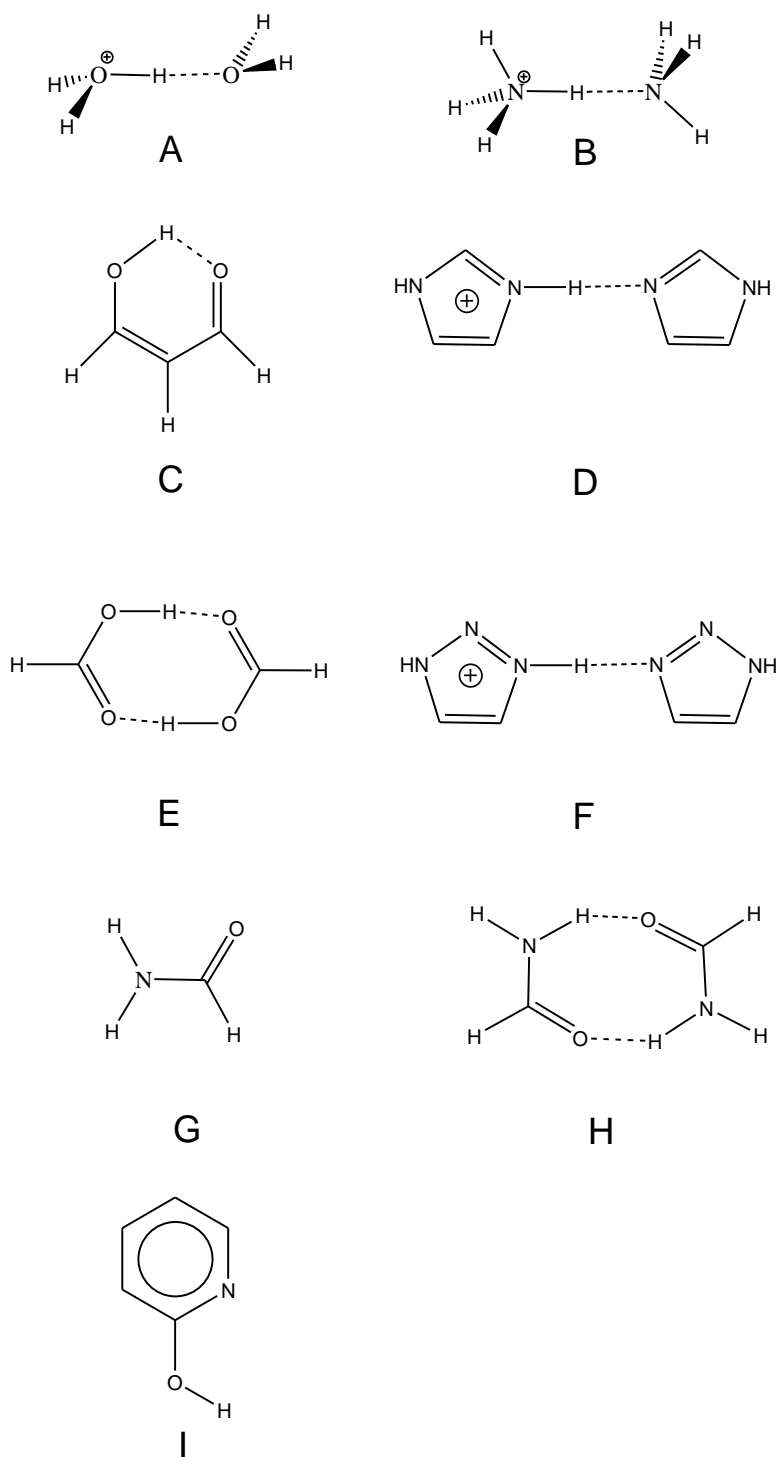


Figure S-4. Sketches des systèmes pris en compte : Dimère protoné d'eau ; B) dimère protoné d'ammoniac ; C) malonaldéhyde; D) dimère protoné d'imidazole E) dimère d'acide formique; F) dimère protoné du triazole, H) formamide; G) dimère de la formamide; I) pyridone.

Par exemple, M06 est classé 1^{ère} pour la structure et 8^{ème} pour l'énergie. Cet aspect indique que les fonctionnelles offrant de bonnes structures ne permettent pas nécessairement d'obtenir des valeurs correctes pour l'énergie. En outre, à partir des résultats obtenus, il apparaît clairement que la *database* DBH24/08 ne peut pas être considérée comme représentative de réactions de transfert de proton. Par exemple, la fonctionnelle classée 6^{ème} sur la DBH24/08 (B2LYP) est seulement en 25^{ème}

Synthèse générale

position en ce qui concerne les barrières à géométrie fixe. Enfin, en ce qui concerne la règle de l'échange HF dans les performances des fonctionnelles considérées, il n'est pas possible d'obtenir une corrélation directe. Cela est vrai à la fois pour les barrières d'énergie et pour les paramètres géométriques. A titre d'exemple, BMK (42% d'échange HF) et M06 (0% d'échange HF) montrent un comportement similaire concernant les caractéristiques à la fois structurales et énergétiques.

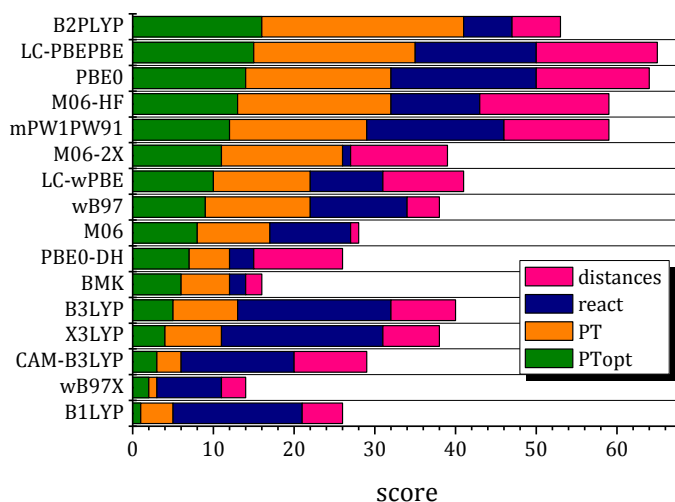


Figure S-5. Score final de chaque fonctionnelle pour les quatre benchmarks : barrières de transfert de proton à la géométrie B3LYP (PT), barrières de transfert de proton à la géométrie optimisée correspondante (PTopt), évaluations standards de la barrière d'énergie sur la DHB 24/08 database (react) et comparaison des paramètres optimisés pour la liaison hydrogène (distances).

En bref, cette étude de référence a confirmé que les réactions de transfert de proton ont certaines caractéristiques particulières, de sorte que les *benchmarks* utilisés pour la cinétique pourraient ne être pas représentatifs des performances des fonctionnelles et, comme suggéré par l'enquête sur les azoles, l'énergie et la structure représentent deux caractéristiques déconnectées pour les méthode DFT.

4. Étude du transport de protons dans P4VI

Le mécanisme communément admis pour expliquer le transport de protons dans les systèmes polymériques à base d'azoles est le mécanisme de Grotthuss.^{33,34} Ce mécanisme est basé sur un transfert de proton collectif parmi les azoles, suivi d'une rotation contemporaine de tous les hétérocycles, nécessaire pour rétablir la conformation de départ (Figure S-6). Ce mécanisme a été proposé par Bredàs⁶³ pour la conduction protonique du poly-(4-vinylimidazole) (P4VI), un prototype conducteur de protons.^{41,42}

Synthèse générale

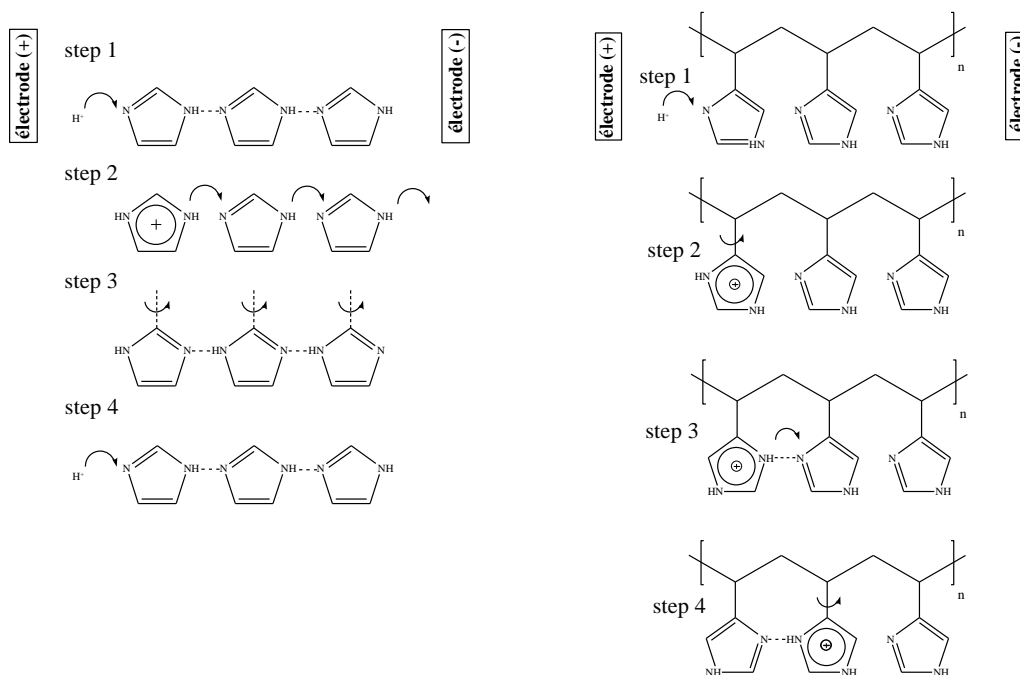


Figure S-6 : mécanismes de transfert de proton pour P4VI. Gauche : mécanisme de Grotthuss, Droite : mécanisme proposé dans la présente thèse.

L'étude théorique du mécanisme de conduction protonique dans P4VI ainsi que dans d'autres systèmes basés sur les azoles, a été réalisée en utilisant des modèles ne comprenant pas la matrice polymérique.^{62,64,65,67-71} Ceci donne une compréhension incomplète de la structure des azoles et du polymère, qui sont liés à la conductivité protonique. Pour obtenir de plus amples informations concernant le mécanisme microscopique régissant le transport de charge dans ces systèmes, une approche combinant DFT et simulations de dynamique moléculaire (MD) a été appliquée sur de petits (dimères et trimères) et grands modèles (oligomères large) du P4VI, avec une considération explicite de la matrice polymérique.

4.1. Étude DFT du mécanisme de conduction dans les petits modèles

Comme vu sur la Figure S-7, l'utilisation de modèles avec la chaîne polyéthylène a pour premier effet de rendre non équivalentes les positions 1 et 3 dans les hétérocycles. Par conséquent, quatre mécanismes différents peuvent être proposés pour le transfert du proton sur des dimères protonés (entre deux imidazoles adjacents) : a) transfert à partir de l'azote 1 (N_1) du premier cycle à l'azote 1 (N_1) du deuxième cycle, b) de N_1 à N_3 , c) de N_3 à N_1 , d) de N_3 à N_3 . Les barrières d'énergie correspondantes, calculées en utilisant le protocole BMK/B3LYP,⁶⁶ sont présentées dans le tableau S-3 : le seul mécanisme énergétiquement possible aux températures de fonctionnement de ce système (393 K) est le mécanisme *d*.

Synthèse générale

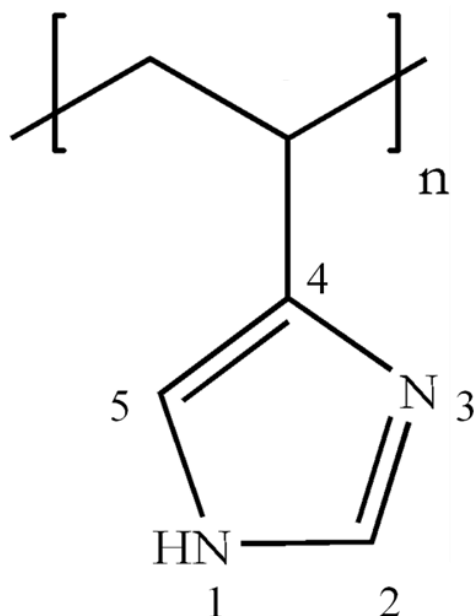


Figure S-7 : Structure moléculaire et numérotation des atomes des hétérocycles dans la chaîne du P4VI

Tableau S-3 : énergies d'activation (kcal/mol) pour le mécanisme de transfert de proton étudié.

PT mechanism	atoms	ΔE
<i>a</i>	N ₁ -N ₁	23,5
<i>b</i>	N ₁ -N ₃	25,1
<i>c</i>	N ₃ -N ₁	23,3
<i>d</i>	N ₃ -N ₃	2,5

En effet, la formation d'une forte liaison hydrogène (linéaire) impliquant les atomes N₁-N₁, N₁-N₃ and N₃-N₁ est entravée par la présence de la matrice polymérique, de sorte qu'un réarrangement important du système est nécessaire pour atteindre l'état de transition pour les mécanismes *a*, *b*, *c*. En d'autres termes, lorsque plus de deux moitiés des imidazoles sont considérées, la présence de la matrice polymère ne permet pas la formation d'un réseau de liaisons hydrogènes dans la chaîne. En effet, si l'imidazole central forme une forte liaison hydrogène (N₃-N₃) avec l'imidazole adjacent dans une direction, il forme une liaison hydrogène défavorable (entre N₁ et N₃ ou N₁ et atomes N₁) avec l'imidazole voisin dans l'autre direction, de sorte que le réarrangement structurel nécessaire implique une barrière d'énergie pour le transfert du proton de 20 kcal/mol. Afin de clarifier la façon dont la conduction protonique se produit lorsque plus de deux unités monomériques sont considérées, un trimère contenant un proton en excès dans le milieu a été analysé (*3mer*⁺, figure S-8).

La conduction de Im_a à Im_c sur ce modèle peut se produire uniquement si la rotation de l'hétérocycle central (Im_b⁺) a lieu. En effet, cela permet une nouvelle liaison hydrogène forte N₃-N₃ entre Im_b⁺ and Im_c de sorte que le transfert du proton entre ces deux hétérocycles peut avoir lieu. Comme cette rotation n'est pas énergétiquement prohibitive (environ 10 kcal/mol au niveau DFT), un

nouveau mécanisme de conduction a été supposé pour le modèle considéré. En effet, si le mécanisme de Grotthuss est basé sur un transfert de proton collectif parmi les azoles, selon la nouvelle hypothèse, une rotation de l'imidazole protoné est nécessaire avant chaque transfert de proton.

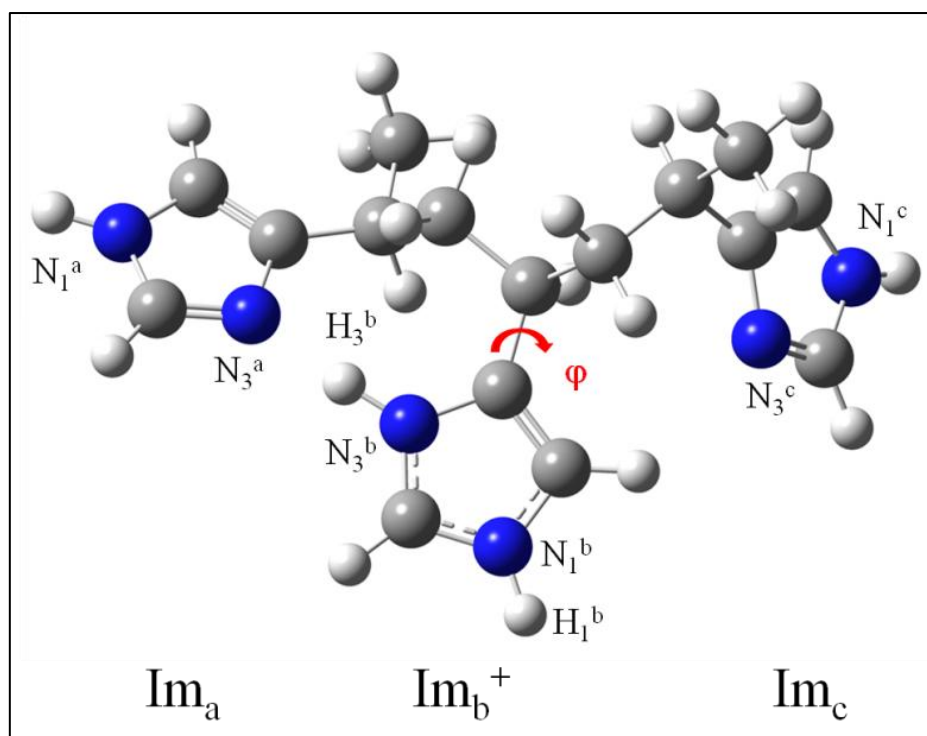


Figure S-8 : Structure moléculaire optimisée du modèle $3mer^+$.

4.2. Étude MD du mécanisme de conduction dans les grands modèles

Afin de confirmer le mécanisme émergent de l'étude DFT, l'effet de l'environnement chimique sur l'étape limitante va être considéré. Pour cela, une étude de dynamique moléculaire a été réalisée sur un système plus large composé de 15 monomères et contenant un proton en excès lié à l'hétérocycle central.

Pendant la simulation de 4 nanosecondes effectuée en utilisant un champ de force (GAFF^{72,73}) calibré sur les résultats DFT, l'étape limitante se produit rapidement et continuellement à la température de fonctionnement de 393 K. En outre, les simulations obtenues indiquent qu'en raison de la contrainte polymérique, qui, dans un grand système, ne permet pas un réarrangement planaire des hétérocycles, une rotation d'environ 80° (vs. 180° dans $3mer^+$) est suffisante pour le processus de rupture et de formation des liaisons hydrogènes requises pour les subséquents transferts de proton avec faibles barrières (N_3-N_3 , mécanisme *d*). Ceci est clairement montré par la Figure S-9 où deux instantanés extraits de la trajectoire obtenue sont représentés. Ainsi, lorsque l'on passe de 5,8 à 6,0 picosecondes, une oscillation de seulement 66° est associée à la rupture de la liaison hydrogène entre

le premier et le second imidazole (variation de la distance $H_3^b-N_3^a$ de 2,02 à 3,63 Å) et à la formation contemporaine d'une nouvelle liaison hydrogène entre le deuxième et le troisième imidazole (variation de la distance $H_3^b-N_3^c$ de 4,02 à 2,16 Å).

En d'autres termes, les simulations de dynamique moléculaire non seulement soutiennent le nouveau mécanisme émergé des calculs DFT, mais ils indiquent aussi que, si un model plus grand qu'un trimère est pris en compte, l'étape limitante correspond à un mouvement doux de l'imidazole protoné (rotation frustrée) au lieu d'une rotation complète de 180°.

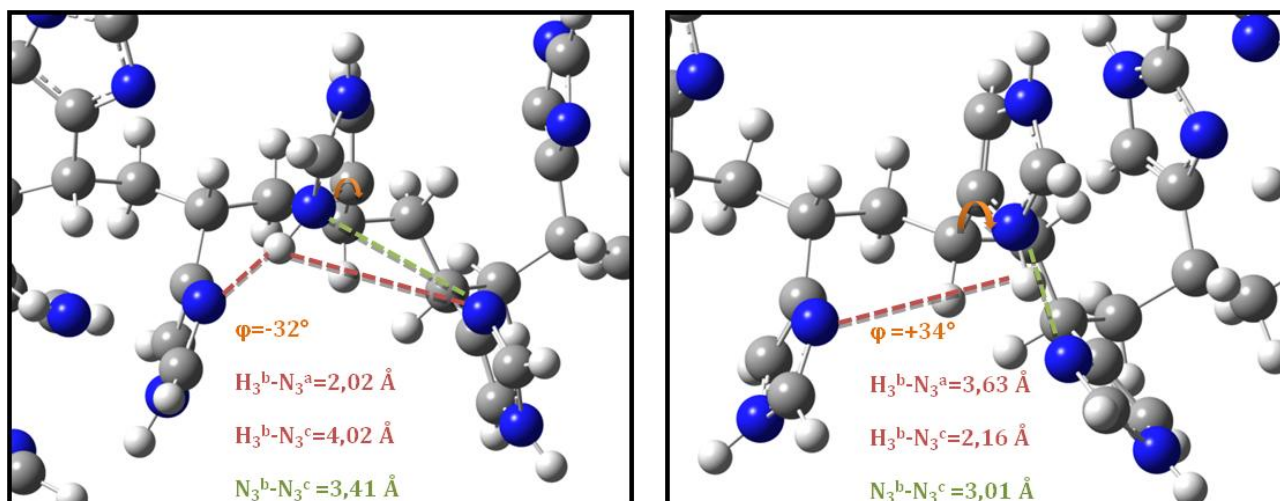


Figure S-9 : Instantanés de l'intervalle de 0,2 picosecondes (de 5,8 à 6,0) extraits de la trajectoire obtenue. Les liaisons hydrogènes sont représentées par une ligne pointillée.

4.3. Un nouveau mécanisme de transport de charge

Pris dans leur ensemble, ces résultats permettent de supposer un nouveau mécanisme de transport de charge⁷⁴ où l'étape limitante est une rotation frustrée de l'imidazole protoné. Un tel mécanisme diffère fortement du mécanisme de Grotthuss esquissé dans la figure S-6 (gauche). En effet, la première étape (arrivée du proton à une extrémité de la chaîne) est ici suivie d'une rotation frustrée (étape 2, réorientation) qui permet un second transfert de proton (étape 3). En d'autres termes, pour chaque proton libéré à l'électrode, le mécanisme proposé nécessite n rotations frustrées des imidazoles seuls au lieu d'une rotation globale et concertée (Figure S-6, droite).

Comme il sera montré dans la section 6, ces résultats pourraient ouvrir la voie à la conception de nouveaux polymères pour un transport de proton plus efficace, menant ainsi à des matériaux avec de meilleures performances.

5. Conduction protonique des P4VI dopés avec du H₃PO₄

Les niveaux de conductivité atteints par les polymères à base d'azoles sont loin d'approcher ceux demandés pour les PEMFC. Cependant, un tel écart peut être partiellement réduit par dopage du polymère pur avec des acides forts capables de 1) augmenter la mobilité de la matrice polymérique agissant comme plastifiant et 2) introduire des porteurs de charge extrinsèques agissant comme source de protons.^{41,42,45} En ce qui concerne le deuxième point, la plupart des aspects liés à l'influence d'un tel dopant sur le mécanisme de conduction sont encore inconnus.^{75,76}

À partir de ces données, une étude DFT sur le rôle de l'acide phosphorique dans le mécanisme de conduction du P4VI a été réalisée. Notamment, un modèle moléculaire caractérisé par un trimère protoné de P4VI et deux molécules de l'acide phosphorique a été mis en place (Figure S-10).

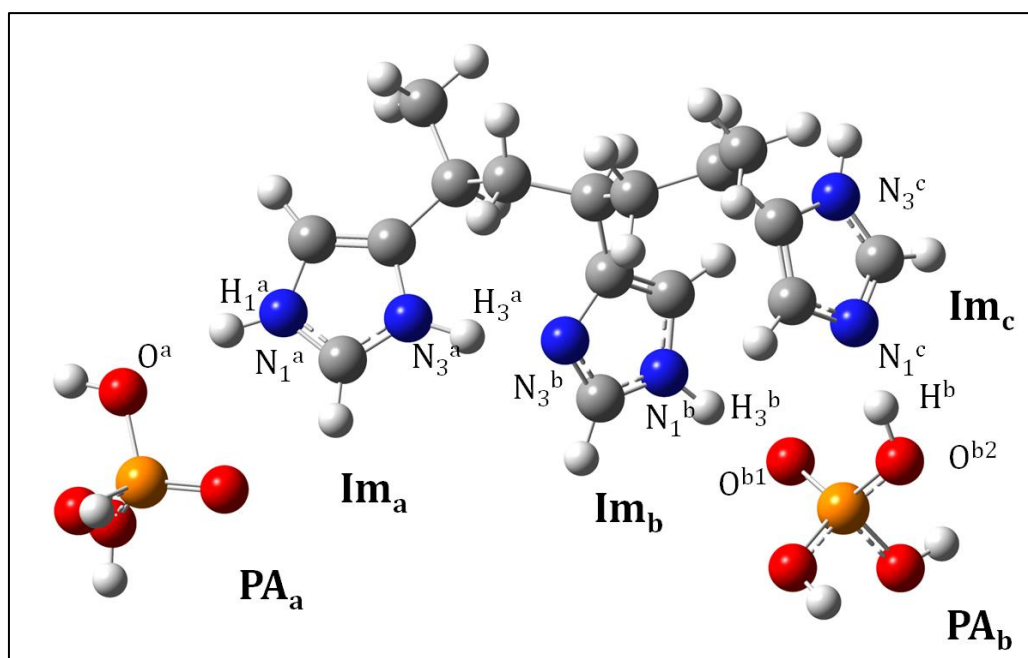


Figure S-10 : Structure optimisée du complexe protoné considéré

Cette étude a montré que l'ajout de deux molécules d'acide dans le modèle permet un mécanisme de Grotthuss. En effet, grâce à l'acide phosphorique dans la chaîne (PA_b) un pont de liaison hydrogène entre deux hétérocycles (Im_b et Im_c), impossible en temps normal, peut être établi. Ceci est confirmé par une analyse approfondie des énergies impliquées dans la conduction du premier proton en excès sur la chaîne. En effet, si plus de 20 kcal/mol sont nécessaires pour transférer le proton entre deux imidazoles adjacents par des atomes d'azote en position 1 sans dopant (voir section 4), près de 5 kcal/mol sont suffisants pour transférer la charge de Im_b à Im_c, grâce à la présence de PA_b, impliqué dans un double transfert de proton simultané. Enfin, grâce à un *scan* à géométrie relaxée, une estimation de l'étape limitante (une rotation simultanée de tous les imidazoles, et dans le même temps, le transfert de toutes les molécules de H₃PO₄) a été obtenue. Une telle valeur (6,5 kcal/mol)

n'est pas énergiquement prohibitive, et confirme donc que le mécanisme de Grotthuss pourrait être favorisé dans le modèle considéré, contrairement à ce qui se passe dans le système pur.

6. Transport des protons dans les systèmes avec attache en position 2

Dans la littérature expérimentale,^{46,77} il a été proposé que les systèmes dans lesquels les imidazoles sont liés en position 2 sont caractérisés par un extensif réseau de liaisons hydrogène, ce qui supposerait un mécanisme de Grotthuss. Pour vérifier ces assertions, une étude théorique de modèles avec attache en position 2 a été menée. L'approche de modélisation (étude combinée DFT/MD) utilisée pour P4VI a été à nouveau considérée. Des modèles correspondants à l'étude antérieure sur P4VI (mais caractérisés par une attache par la position 2 au lieu de 4) ont été étudiés afin de vérifier si le seul effet d'une attache sur une position différente pourrait permettre un réseau de liaisons hydrogène dans la chaîne, contrairement à ce qui a été montré pour le système précédemment étudié (Figure S-11).

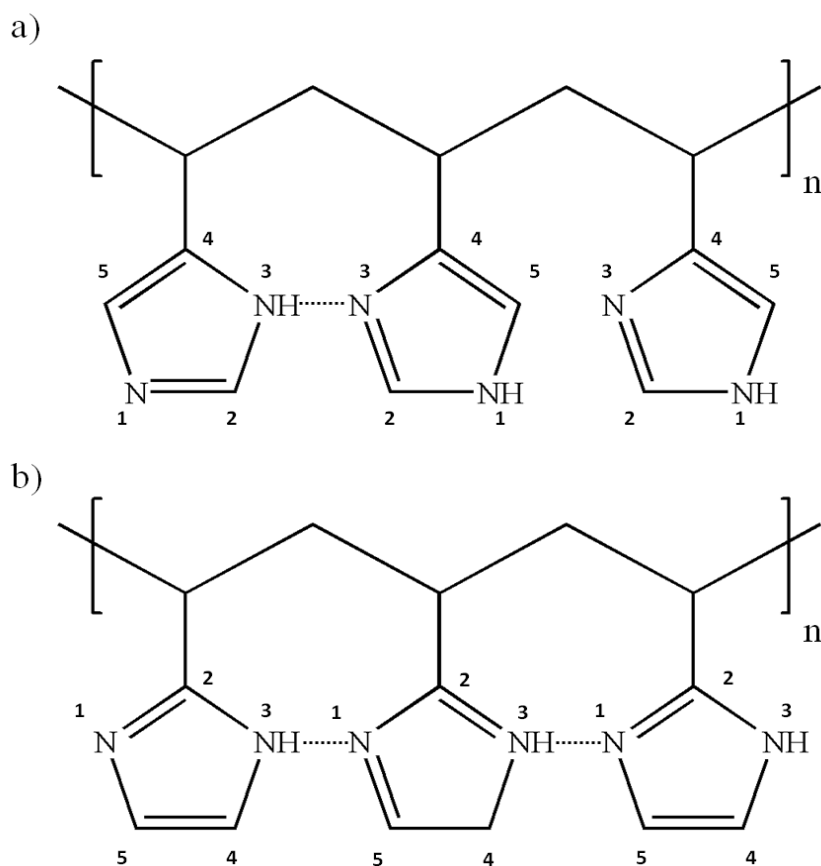


Figure S-11 : Représentation schématique et numérotation des atomes d'une chaîne a) de P4VI et b) correspondant au système où l'imidazole est attaché en position 2.

6.1. Étude DFT du mécanisme de conduction dans les petits modèles

Le premier effet de la liaison avec la matrice polymérique en position 2 des hétérocycles est la présence de deux atomes d'azote équivalents, comme vu dans la figure S-12, qui représente la structure moléculaire d'un des systèmes avec attache en position 2 les plus étudiés, à savoir le (Poly(2-vinyl-4,5-dicyanoimidazole)).^{46,77}

En conséquence, une seule réaction de transfert de proton peut être envisagée entre imidazoles adjacents. L'étude DFT de cette réaction a été effectuée sur deux modèles différents, en utilisant le protocole BMK/B3LYP⁶⁶. Cette étude indique qu'un tel transfert de charge est énergétiquement favorisé pour les deux systèmes étudiés (figure S-13). Notamment, les groupes cyano n'ont aucun effet électronique observable sur la barrière du transfert de proton. Bien entendu, une fois qu'un proton est transféré d'un imidazole à l'autre imidazole adjacent, une réorientation (ou retournement) de tous les imidazoles est nécessaire (étape limitante) pour permettre un transfert ultérieur intermoléculaire de proton dans la même direction. Cette rotation n'est pas énergétiquement prohibée (environ 8 kcal/mol au niveau DFT sur un model trimérique) ce qui indique que le mécanisme de Grotthuss pourrait être favorisé dans ces systèmes.

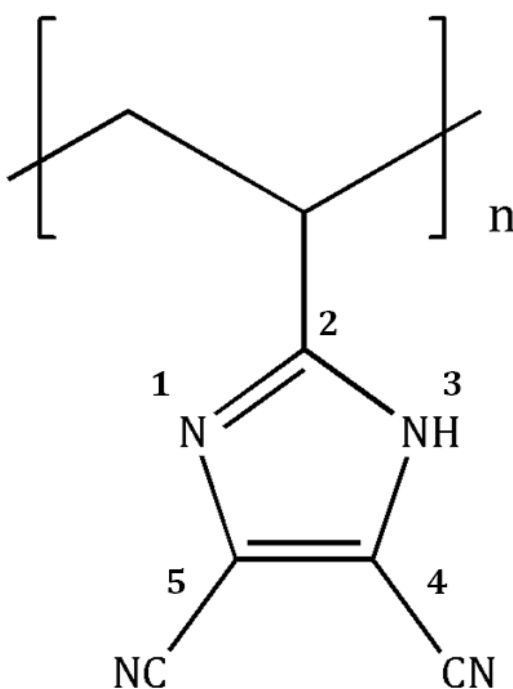


Figure S-12 : Structure moléculaire et numérotation des atomes des hétérocycles dans la chaîne du Poly(2-vinyl-4,5-dicyanoimidazole).

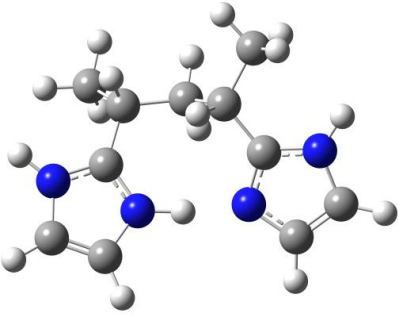
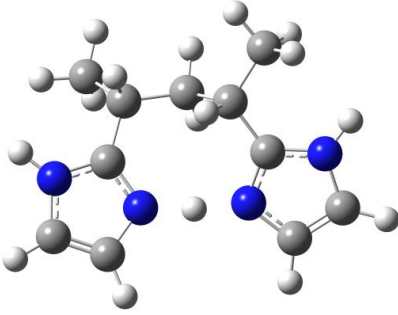
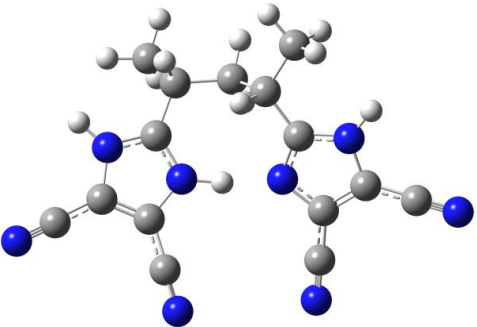
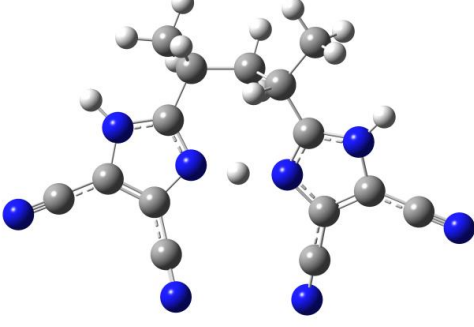
modèle	ΔE (kcal/mol)	minimum	état de transition
<i>a</i>	1,68		
<i>b</i>	1,69		

Figure S-13. Structures des points stationnaires (minima et états de transition) des deux systèmes de dimères impliqués dans les réactions de transfert de proton étudiés.

6.2. Étude MD du mécanisme de conduction dans les grands modèles

L'étude MD effectuée sur un système plus vaste soutient fermement les suggestions formulées à partir des résultats DFT. En effet, quand un oligomère plus grand est considéré (caractérisé par 15 monomères), un réseau de liaisons hydrogène (condition nécessaire pour le mécanisme de Grotthuss) est observé, bien que, comme dans le P4VI, la matrice polymérique empêche le réarrangement planaire des hétérocycles. Ce résultat est obtenu grâce à une conformation en forme de spirale. Surtout, l'étape limitante du mécanisme hypothétique (rotation simultanée des imidazoles) se produit au cours de la simulation MD après 72 ns à 393K, la température minimale d'intervalle de fonctionnement prévue pour les polymères à base d'azoles (Figure S-14).

Pris ensemble, ces résultats confirment l'idée émergée de l'étude du P4VI : la position d'attache des imidazoles peut fortement affecter le mécanisme de conduction dans les polymères N-hétérocycles. En effet, à la différence de P4VI, pour le système examiné, avec attache en position 2, le mécanisme de Grotthuss n'est pas entravé par la matrice polymérique.

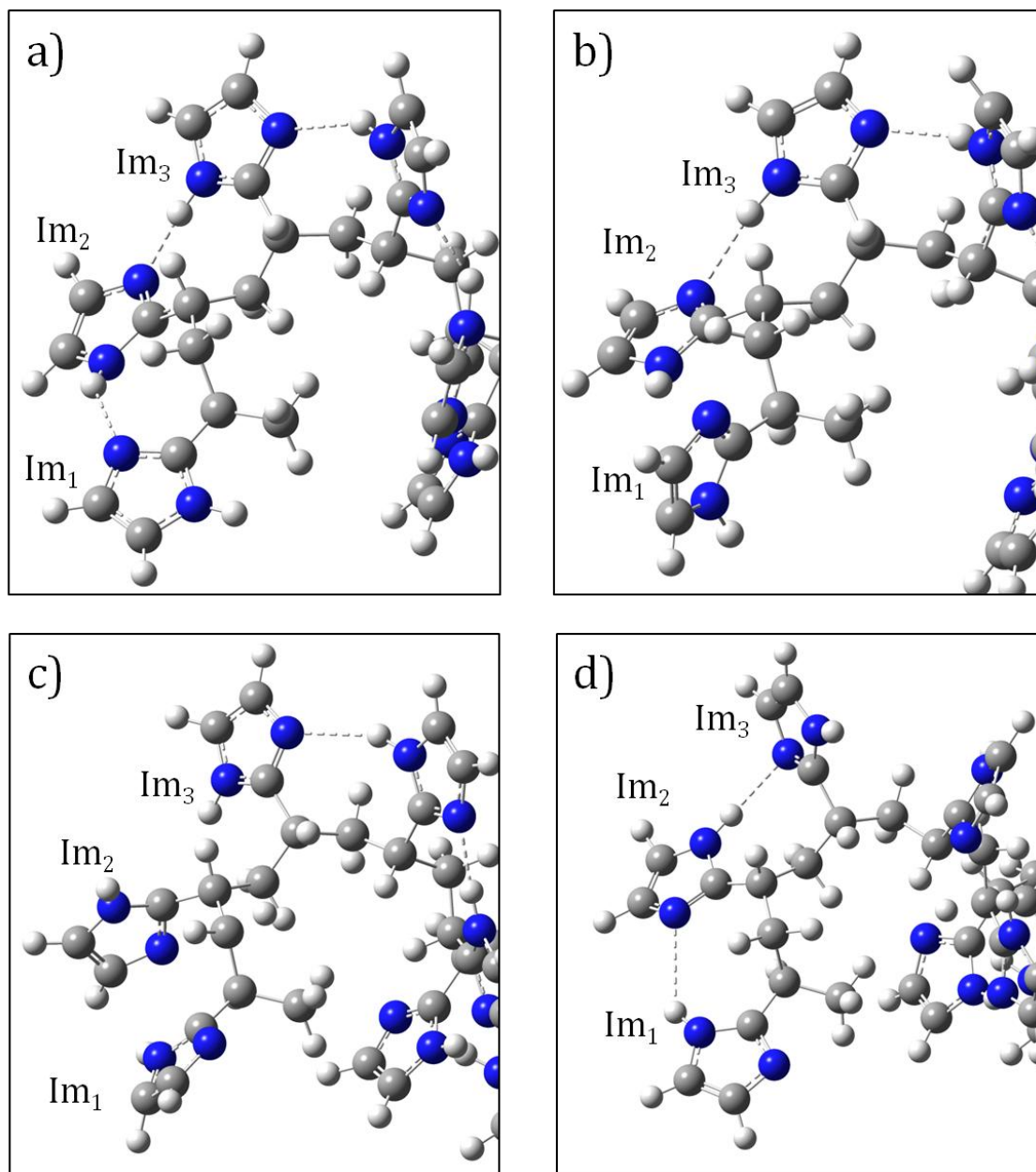


Figure S-14. Images de quelques instantanés de la trajectoire MD obtenue pour le grand oligomère à 393 K : a) à 72,5545 ns, b) à 72,5550 ns, c) à 72,5555 et d) 72.5620 ns. Les liaisons hydrogène sont représentées par une ligne pointillée.

7. Conclusion générale

Ce travail a permis :

- l'élaboration d'un protocole DFT capable de reproduire les caractéristiques énergétiques et structurales des réactions de transfert de proton qui se produisent dans des dimères protonés d'imidazole, 1,2,3-triazole et tétrazole, les composants clés des membranes polymériques, objets de la présente recherche.

Synthèse générale

- la réalisation d'une étude de référence des réactions de transfert de proton, ce qui a permis d'obtenir quelques considérations générales à propos du rôle de l'échange Hartree-Fock sur les barrières d'énergie du transfert du proton et la relation entre l'énergie et la structure.
- l'hypothèse d'un nouveau mécanisme de conduction pour P4VI, capable d'expliquer sa faible conductivité protonique.
- d'obtenir de nouveaux résultats concernant le rôle de l'acide phosphorique dans le mécanisme de conduction de P4VI.
- de souligner que la manière d'attacher les hétérocycles dans la membrane peut déterminer le mécanisme de conduction dans les membranes à base d'azoles.

En bref, grâce à une approche novatrice basée sur l'utilisation combinée de la DFT et de la MD, ce travail a permis d'améliorer la compréhension du mécanisme de la conduction dans les systèmes à base d'azoles, donnant ainsi des indications importantes pour la conception de nouveaux et meilleurs matériaux.

8. Références

- (1) Eckaus, R. S. Comparing the Effects of Greenhouse Gas Emissions on Global Warming. *The Energy Journal* **1992**, *13*, 25–36.
- (2) Crabtree, G. W.; Dresselhaus, M. S.; Buchanan, M. V. The Hydrogen Economy. *Physics Today* **2004**, *57*, 39–44.
- (3) Muradov, N. Z.; Veziroğlu, T. N. From hydrocarbon to hydrogen–carbon to hydrogen economy. *International Journal of Hydrogen Energy* **2005**, *30*, 225–237.
- (4) Gust, D.; Moore, T. A.; Moore, A. L. Mimicking Photosynthetic Solar Energy Transduction. *Accounts of Chemical Research* **2000**, *34*, 40–48.
- (5) Jain, I. P.; Lal, C.; Jain, A. Hydrogen storage in Mg: A most promising material. *International Journal of Hydrogen Energy* **2010**, *35*, 5133–5144.
- (6) Schäfer, A.; Heywood, J. B.; Weiss, M. A. Future fuel cell and internal combustion engine automobile technologies: A 25-year life cycle and fleet impact assessment. *Energy* **2006**, *31*, 2064–2087.
- (7) Prospects for a hydrogen economy, *Parliamentary Office of Science and Technology* **2002**, number 186.
- (8) Carrette, L.; Friedrich, K. A.; Stimming, U. Fuel Cells – Fundamentals and Applications. *Fuel Cells* **2001**, *1*, 5–39.
- (9) Ralph, T. R. Proton Exchange Membrane Fuel Cells. *Platinum Metals Review* **1997**, *41*, 102–113.
- (10) US Department of energy, Types of fuel cells, http://www1.eere.energy.gov/hydrogenandfuelcells/fuelcells/fc_types.html (accessed May 13, 2012).
- (11) Gittleman C.; Masten D.; Jorgensen S. Automotive fuel cell R&D needs. DOE Fuel Cell Pre-Solicitation Workshop March 16, **2010**.
- (12) Zhang, J.; Xie, Z.; Zhang, J.; Tang, Y.; Song, C.; Navessin, T.; Shi, Z.; Song, D.; Wang, H.; Wilkinson, D. P.; Liu, Z.-S.; Holdcroft, S. High temperature PEM fuel cells. *Journal of Power Sources* **2006**, *160*, 872–891.
- (13) Bose, S.; Kuila, T.; Nguyen, T. X. H.; Kim, N. H.; Lau, K.; Lee, J. H. Polymer membranes for high temperature proton exchange membrane fuel cell: Recent advances and challenges. *Progress in Polymeric Science* **2011**, *36*, 813–843.

- (14) Hickner, M. A.; Ghassemi, H.; Kim, Y. S.; Einsla, B. R.; McGrath, J. E. Alternative Polymer Systems for Proton Exchange Membranes (PEMs). *ChemInform* **2004**, *35*, no.
- (15) Steck A. E. New Materials for Fuel Cell Systems. *Proc. 1st International Symposium Montreal* **1995**, 74.
- (16) Sone, Y.; Ekdunge, P.; Simonsson, D. Proton Conductivity of Nafion 117 as Measured by a Four-Electrode AC Impedance Method. *Journal of Electrochemical Society* **1996**, *143*, 1254–1259.
- (17) Rikukawa, M.; Sanui, K. Proton-conducting polymer electrolyte membranes based on hydrocarbon polymers. *Progress in Polymeric Science* **2000**, *25*, 1463–1502.
- (18) Casciola, M.; Alberti, G.; Sganappa, M.; Narducci, R. On the decay of Nafion proton conductivity at high temperature and relative humidity. *Journal of Power Sources* **2006**, *162*, 141–145.
- (19) Baschuk, J. J.; Li, X. Carbon monoxide poisoning of proton exchange membrane fuel cells. *International Journal of Energy Research* **2001**, *25*, 695–713.
- (20) Hogarth, W. H. J.; Diniz da Costa, J. C.; Lu, G. Q. (Max). Solid acid membranes for high temperature ($i_{140^\circ\text{C}}$) proton exchange membrane fuel cells. *Journal of Power Sources* **2005**, *142*, 223–237.
- (21) Li, Q.; He, R.; Jensen, J. O.; Bjerrum, N. J. Approaches and Recent Development of Polymer Electrolyte Membranes for Fuel Cells Operating above 100 °C. *Chemistry of Materials* **2003**, *15*, 4896–4915.
- (22) Zhang, L.; Zhang, J.; Wilkinson, D. P.; Wang, H. Progress in preparation of non-noble electrocatalysts for PEM fuel cell reactions. *Journal of Power Sources* **2006**, *156*, 171–182.
- (23) Wang, B. Recent development of non-platinum catalysts for oxygen reduction reaction. *Journal of Power Sources* **2005**, *152*, 1–15.
- (24) Zhang, H.; Shen, P. K. Advances in the high performance polymer electrolyte membranes for fuel cells. *Chemical Society Reviews* **2012**, *41*, 2382–2394.
- (25) Choi, Y.; Kim, Y.; Kim, H. K.; Lee, J. S. Direct synthesis of sulfonated mesoporous silica as inorganic fillers of proton-conducting organic–inorganic composite membranes. *Journal of Membrane Science* **2010**, *357*, 199–205.
- (26) Pereira, F.; Vallé, K.; Belleville, P.; Morin, A.; Lambert, S.; Sanchez, C. Advanced Mesostructured Hybrid Silica–Nafion Membranes for High-Performance PEM Fuel Cell. *Chemistry of Materials* **2008**, *20*, 1710–1718.

- (27) Lin, Y.-F.; Yen, C.-Y.; Ma, C.-C. M.; Liao, S.-H.; Lee, C.-H.; Hsiao, Y.-H.; Lin, H.-P. High proton-conducting Nafion®/–SO₃H functionalized mesoporous silica composite membranes. *Journal of Power Sources* **2007**, *171*, 388–395.
- (28) Poppe, D.; Frey, H.; Kreuer, K. D.; Heinzl, A.; Mülhaupt, R. Carboxylated and Sulfonated Poly(arylene-co-arylene sulfone)s: Thermostable Polyelectrolytes for Fuel Cell Applications. *Macromolecules* **2002**, *35*, 7936–7941.
- (29) Lafitte, B.; Karlsson, L. E.; Jannasch, P. Sulfophenylation of Polysulfones for Proton-Conducting Fuel Cell Membranes. *Macromolecular Rapid Communications* **2002**, *23*, 896–900.
- (30) Asensio, J. A.; Borros, S.; Gomez-Romero, P. Proton-conducting polymers based on benzimidazoles and sulfonated benzimidazoles. *Journal of Polymer science. Part A. Polymer chemistry* **2002**, *40*, 3703–3710.
- (31) Hofmann, M. A.; Ambler, C. M.; Maher, A. E.; Chalkova, E.; Zhou, X. Y.; Lvov, S. N.; Allcock, H. R. Synthesis of polyphosphazenes with sulfonimide side groups. *Macromolecules* **2002**, *35*, 6490–6493.
- (32) Kreuer, K.-D.; Rabenau, A.; Weppner, W. Vehicle Mechanism, A New Model for the Interpretation of the Conductivity of Fast Proton Conductors. *Angewandte Chemie International Edition in English* **1982**, *21*, 208–209.
- (33) De Grotthuss, C. J. Memoir upon the decomposition of water, and of the bodies which it holds in solution, by means of galvanic electricity. *Philosophical Magazine Series 1* **1806**, *25*, 330–339.
- (34) Agmon, N. The Grotthuss mechanism. *Chemical Physics Letters* **1995**, *244*, 456–462.
- (35) Kreuer, K. D.; Fuchs, A.; Ise, M.; Spaeth, M.; Maier, J. Imidazole and pyrazole-based proton conducting polymers and liquids. *Electrochimica Acta* **1998**, *43*, 1281–1288.
- (36) Münch, W.; Kreuer, K.-D.; Silvestri, W.; Maier, J.; Seifert, G. The diffusion mechanism of an excess proton in imidazole molecule chains: first results of an ab initio molecular dynamics study. *Solid State Ionics* **2001**, *145*, 437–443.
- (37) Noda, A.; Susan, M. A. B. H.; Kudo, K.; Mitsushima, S.; Hayamizu, K.; Watanabe, M. Brønsted Acid–Base Ionic Liquids as Proton-Conducting Nonaqueous Electrolytes. *Journal of Physical Chemistry B* **2003**, *107*, 4024–4033.
- (38) Zhou, Z.; Li, S.; Zhang, Y.; Liu, M.; Li, W. Promotion of Proton Conduction in Polymer Electrolyte Membranes by 1H-1,2,3-Triazole. *Journal of the American Chemical Society* **2005**, *127*, 10824–10825.

- (39) Fernicola, A.; Panero, S.; Scrosati, B. Proton-conducting membranes based on protic ionic liquids. *Journal of Power Sources* **2008**, *178*, 591–595.
- (40) Schuster, M.; Meyer, W. .; Wegner, G.; Herz, H. .; Ise, M.; Schuster, M.; Kreuer, K. .; Maier, J. Proton mobility in oligomer-bound proton solvents: imidazole immobilization via flexible spacers. *Solid State Ionics* **2001**, *145*, 85–92.
- (41) Pu, H.; Meyer, W. H.; Wegner, G. Proton Conductivity in Acid-Blended Poly(4-vinylimidazole). *Macromolecular Chemistry and Physics* **2001**, *202*, 1478–1482.
- (42) Bozkurt, A.; Meyer, W. Proton conducting blends of poly(4-vinylimidazole) with phosphoric acid. *Solid State Ionics* **2001**, *138*, 259–265.
- (43) Martwiset, S.; Woudenberg, R. C.; Granados-Focil, S.; Yavuzcetin, O.; Tuominen, M. T.; Coughlin, E. B. Intrinsically conducting polymers and copolymers containing triazole moieties. *Solid state ionics* *178*, 1398–1403.
- (44) Pu, H.; Wu, J.; Wan, D.; Chang, Z. Synthesis and anhydrous proton conductivity of poly(5-vinyltetrazole) prepared by free radical polymerization. *Journal of Membrane Science* **2008**, *322*, 392–399.
- (45) Çelik, S. Ü.; Aslan, A.; Bozkurt, A. Phosphoric acid-doped poly(1-vinyl-1,2,4-triazole) as water-free proton conducting polymer electrolytes. *Solid State Ionics* **2008**, *179*, 683–688.
- (46) Densmore, C. G.; Rasmussen, P. G.; Goward, G. R. Probing Hydrogen Bonding and Proton Mobility in Dicyanoimidazole Monomers and Polymers. *Macromolecules* **2004**, *38*, 416–421.
- (47) Johnson, D. M.; Rasmussen, P. G. An Improved Synthesis of 2-Vinyl-4,5-dicyanoimidazole and Characterization of Its Polymers. *Macromolecules* **2000**, *33*, 8597–8603.
- (48) Becke, A. D. Density-functional thermochemistry. III. The role of exact exchange. *Journal of Chemical Physics* **1993**, *98*, 5648-5652.
- (49) Adamo, C.; Barone, V. Toward reliable density functional methods without adjustable parameters: The PBE0 model. *Journal of Chemical Physics* **1999**, *110*, 6158–6170.
- (50) Boese, A. D.; Martin, J. M. L. Development of density functionals for thermochemical kinetics. *Journal of Chemical Physics* **2004**, *121*, 3405–3416.
- (51) Xu, X.; Goddard, W. A. The X3LYP Extended Density Functional for Accurate Descriptions of Nonbond Interactions, Spin States, and Thermochemical Properties. *Proceedings of the National Academy of Sciences* **2004**, *101*, 2673–2677.

- (52) Adamo, C.; Barone, V. Exchange functionals with improved long-range behavior and adiabatic connection methods without adjustable parameters: The mPW and mPW1PW models. *Journal of Chemical Physics* **1998**, *108*, 664-675.
- (53) Zhao, Y.; Truhlar, D. G. Comparative DFT Study of van der Waals Complexes: Rare-Gas Dimers, Alkaline-Earth Dimers, Zinc Dimer, and Zinc-Rare-Gas Dimers. *Journal of Physical Chemistry A* **2006**, *110*, 5121-5129.
- (54) Zhao, Y.; Truhlar, D. G. The M06 suite of density functionals for main group thermochemistry, thermochemical kinetics, noncovalent interactions, excited states, and transition elements: two new functionals and systematic testing of four M06-class functionals and 12 other functionals. *Theoretical Chemistry Accounts* **2007**, *120*, 215-241.
- (55) Vydrov, O. A.; Heyd, J.; Krukau, A. V.; Scuseria, G. E. Importance of short-range versus long-range Hartree-Fock exchange for the performance of hybrid density functionals. *Journal of Chemical Physics* **2006**, *125*, 074106-074115.
- (56) Vydrov, O. A.; Scuseria, G. E. Assessment of a long-range corrected hybrid functional. *Journal of Chemical Physics* **2006**, *125*, 234109-234118.
- (57) Tognetti, V.; Cortona, P.; Adamo, C. A new parameter-free correlation functional based on an average atomic reduced density gradient analysis. *Journal of Chemical Physics* **2008**, *128*, 0034101-034109.
- (58) Hermet, J.; Cortona, P.; Adamo, C. New range-separated hybrids based on the TCA density functional. *Chemical Physics Letters* **2012**, *519-520*, 145-149.
- (59) Pople, J. A.; Head-Gordon, M.; Raghavachari, K. Quadratic configuration interaction. A general technique for determining electron correlation energies. *Journal of Chemical Physics* **1987**, *87*, 5968-5975.
- (60) Frisch, M. J.; Head-Gordon, M.; Pople, J. A. A direct MP2 gradient method. *Chemical Physics Letters* **1990**, *166*, 275-280.
- (61) Head-Gordon, M.; Pople, J. A.; Frisch, M. J. MP2 energy evaluation by direct methods. *Chemical Physics Letters* **1988**, *153*, 503-506.
- (62) Tatara, W.; Wojcik, M. J.; Lindgren, J.; Probst, M. Theoretical study of structures, energies, and vibrational spectra of the imidazole-imidazolium system. *Journal of Physical Chemistry A* **2003**, *107*, 7827-7831.

- (63) Zhou, Z.; Liu, R.; Wang, J.; Li, S.; Liu, M.; Brédas, J.-L. Intra- and Intermolecular Proton Transfer in 1H(2H)-1,2,3-Triazole Based Systems. *Journal of Physical Chemistry A* **2006**, *110*, 2322–2324.
- (64) Subbaraman, R.; Ghassemi, H.; Zawodzinski Jr., T. Triazole and triazole derivatives as proton transport facilitators in polymer electrolyte membrane fuel cells. *Solid State Ionics* **2009**, *180*, 1143–1150.
- (65) Li, A.; Yan, T.; Shen, P. Exploring proton transfer in 1,2,3-triazole-triazolium dimer with ab initio method. *Journal of Power Sources* **2011**, *196*, 905–910.
- (66) Mangiatordi, G. F.; Hermet, J.; Adamo, C. Modeling proton transfer in imidazole-like dimers: a density functional theory study. *Journal of Physical Chemistry A* **2011**, *115*, 2627–2634.
- (67) Iannuzzi, M.; Parrinello, M. Proton Transfer in Heterocycle Crystals. *Physical Review Letters* **2004**, *93*, 025901- 025910-4.
- (68) Iannuzzi, M. Proton transfer in imidazole-based molecular crystals. *Journal of Chemical Physics* **2006**, *124*, 204710– 204710–10.
- (69) Deng, W.-Q.; Molinero, V.; Goddard, W. A., 3rd Fluorinated imidazoles as proton carriers for water-free fuel cell membranes. *Journal of the American Chemical Society* **2004**, *126*, 15644–15645.
- (70) Goddard III, W.; Merinov, B.; Duin, A. V.; Jacob, T.; Blanco, M.; Molinero, V.; Jang, S. S.; Jang, Y. H. Multi-paradigm multi-scale simulations for fuel cell catalysts and membranes. *Molecular Simulations* **2005**, *32*, 251-268.
- (71) Chen, H.; Yan, T.; Voth, G. A. A computer simulation model for proton transport in liquid imidazole. *Journal of Physical Chemistry A* **2009**, *113*, 4507–4517.
- (72) Wang, J.; Wolf, R. M.; Caldwell, J. W.; Kollman, P. A.; Case, D. A. Development and testing of a general amber force field. *Journal of Computational Chemistry* **2004**, *25*, 1157–1174.
- (73) Wang, J.; Wang, W.; Kollman, P. A.; Case, D. A. Automatic atom type and bond type perception in molecular mechanical calculations. *Journal of Molecular Graphics and Modeling* **2006**, *25*, 247–260.
- (74) Mangiatordi, G. F.; Butera, V.; Russo, N.; Laage, D.; Adamo, C. Charge transport in poly-imidazole membranes: a fresh appraisal of the Grotthuss mechanism. *Physical Chemistry Chemical Physics* **2012**, *14*, 10910-10918.
- (75) Çelik, S. Ü.; Bozkurt, A.; Hosseini, S. S. Alternatives toward proton conductive anhydrous membranes for fuel cells: Heterocyclic protogenic solvents comprising polymer electrolytes. *Progress in Polymeric Science* **2012**, *37*, 1265–1291.

Synthèse générale

(76) Lee, S.-I.; Yoon, K.-H.; Song, M.; Peng, H.; Page, K. A.; Soles, C. L.; Yoon, D. Y. Structure and Properties of Polymer Electrolyte Membranes Containing Phosphonic Acids for Anhydrous Fuel Cells. *Chemistry of Materials* **2012**, *24*, 115–122.

(77) Wixom, M.; Lei, H.; Zhang, P.; Ma, J. *United States patent, T/J Technologies, Inc., Ann Arbor, MI (US)*, **2005**, no. 6,878,475 B2.

List of publications

Mangiatordi, G. F.; Hermet, J.; Adamo, C. Modeling proton transfer in imidazole-like dimers: a density functional theory study. *Journal of Physical Chemistry A* **2011**, *115*, 2627–2634.

Mangiatordi, G. F.; Butera, V.; Russo, N.; Laage, D.; Adamo, C. Charge transport in poly-imidazole membranes: a fresh appraisal of the Grothuss mechanism. *Physical Chemistry Chemical Physics* **2012**, *14*, 10910-10918.

Mangiatordi, G. F.; Brémond, E.; Adamo, C. DFT and proton transfer reactions: a benchmark study on the structure and kinetics, *Journal of Chemical Theory and Computation* **2012**, *8*, 3082-3088.

Publication submitted

Mangiatordi, G. F.; Adamo, C. Can the wire tethering directs the charge trasport in poly-imidazole membranes? A theoretical study, *submitted*.

Publication in preparation

Butera, V.; **Mangiatordi, G. F.;** Sicilia, E.; Russo, N.; Adamo, C. On the phosphoric acid rule on charge transport in blends of poly(4-vinylimidazole): a theoretical investigation, *manuscript in preparation*.

Oral communications

Mangiatordi G. F.; "Azoles as proton transport facilitators in PEMFCs: a theoretical investigation" Hypomap M12 meeting, **05.06.2010-07.06.2010**, Stockholm (Sweden).

Mangiatordi G. F.; "Modeling proton transfer in poly(4-vinyl-imidazole): a density functional theory study." Hypomap M12 meeting, **28.10.2010-31.10.2010**, Bremen (Germany).

Mangiatordi G. F.; "Modeling proton transfer in fuel cells" Journée Chimie Théorique et Modélisation de l'Ecole Doctorale de Chimie Physique et Chimie Analytique de Paris Centre, **04.02.2011**, Paris (France).

Mangiatordi G. F.; "Proton transfer in fuel cells: a combined DFT-MD approach" Journées Modélisation de Paris, **18.05.2011-19-05-2011**, Paris (France).

Mangiatordi G. F.; "Proton Transfer in fuel cells: a combined DFT-MD approach" XXIV Congresso Nazionale della Società Chimica Italiana, **11.09.2011-16.09.2011**, Lecce (Italy).

Mangiatordi G. F.;"Proton Transfer in fuel cells: a combined DFT-MD approach" Università degli studi di Bari "Aldo Moro", **16-09-2011** Bari (Italy).

Mangiatordi G. F.;"Charge transport in poly-imidazole membranes: a fresch appraisal of the Grothhuss mechanism" Final Hypomap M12 meeting, **07.05.2012-10.05.2012**, Goa (India).

Mangiatordi G. F.;"Charge transport in poly-imidazole membranes: a fresch appraisal of the Grothhuss mechanism", The Energy and Materials Research Conference, **20.06.2012-22.06.2012**, Torremolinos (Spain)

Mangiatordi G. F.;"Charge transport in poly-imidazole membranes: a fresch appraisal of the Grothhuss mechanism", Solid State Proton Conductors Conference, **10.09.2012-14.09.2012**, Grenoble (France).

Mangiatordi G. F.;"Charge transport in poly-imidazole membranes: a fresch appraisal of the Grothhuss mechanism", Italian Institute of Technology, **20.09.2012**, Genova (Italy).

Abstract

Modeling charge transfer in fuel cells

The performances of Proton Exchange Membrane Fuel Cells (PEMFCs) are strongly influenced by the proton conductivity of the solid electrolyte. The azole-based polymers are among the most promising materials to improve the effectiveness of these systems. A detailed theoretical study of proton transfer (PT) reaction in protonated imidazole, 1,2,3-triazole, and tetrazole dimers has been performed. In particular, several approaches based on Density Functional Theory (DFT) have been considered and their results compared with those provided by post Hartree-Fock (post-HF) methods. Starting from this first investigation, a benchmark study has been realized including a significant number of different exchange correlation functionals and taking into account a representative set of PT reactions.

The developed DFT protocol has been applied on more complex systems. In particular, the results obtained from the investigation performed on Poly(4-vinyl-imidazole) (P4VI) suggest that the commonly accepted (Grotthuss) conduction mechanism, based on a sequential proton transfer between imidazole moieties, could be impeded in this system because of the backbone constraint. Such a study, performed through a combined Density Functional Theory (DFT) / Molecular Dynamics simulations (MD) approach, allowed to hypothesize an alternative mechanism of conduction. This latter involves a rotation of the protonated imidazole, constituting the rate-limiting step, before each PT reaction between adjacent azoles can take place. Importantly, a further study performed on phosphoric-acid (H_3PO_4) included models has revealed as low concentrations of H_3PO_4 could allow for the Grotthuss mechanism despite the polymeric constraint so giving a possible explanation of the higher conductivity of the acid-blended systems respect to the pure ones.

The underpinning role played by the backbone topology on the conductivity has been then confirmed by the investigation carried out on a second polymer. Indeed, the outcomes obtained following the same DFT/MD protocol used for P4VI, have revealed as the wire tethering position can strongly affect the mechanism of conduction, the Grotthuss path being favored in the investigated 2-tethered poly-imidazole system.

In short, the obtained simulations show how the polymeric matrix play a crucial role in the conductivity mechanism, thus indicating that models including the polymeric constraint are necessary to investigate theoretically these systems, in contrast with what has been done so far. From a more chemical point of view, the present research represents a first effort for a more systematic study of the relationship between backbone connectivity and efficiency of the charge transport, necessary in order to design new and better performing azole-based materials.

Résumé

Modélisation du transfert de charge dans les piles à combustible

Les performances des piles à combustible à échange de protons (PEMFC) sont fortement influencées par la conductivité protonique de l'électrolyte solide. Les polymères à base d'azole sont parmi les matériaux les plus prometteurs pour améliorer l'efficacité de ces systèmes. Une étude théorique détaillée de réaction du transfert de protons (PT) en dimères protonée du imidazole, 1,2,3-triazole et tétrazole a été effectuée. En particulier, plusieurs approches basées sur la théorie du fonctionnelle de la densité (DFT) ont été envisagées et leurs résultats ont été comparés avec ceux fournis par post-Hartree-Fock (post-HF) méthodes. A partir de ce premier travail, une étude de référence a été réalisé, y compris un nombre important de différents fonctionnelles et en tenant compte d'un ensemble représentatif de réactions du PT.

Le protocole DFT mis au point a été appliqué sur des systèmes plus complexes. Notamment, les résultats obtenus à partir de l'étude réalisée sur le poly(4-vinyl-imidazole) (P4VI) suggèrent que le mécanisme de conduction communément admis (Grotthuss), basé sur un transfert de proton séquentielle entre les imidazoles, pourrait être entravé dans ce système en raison de l'effet de la matrice polymérique. Cette étude, réalisée par le biais d'une approche combinée théorie du fonctionnelle de la densité (DFT) / simulations de Dynamique Moléculaire (MD), a permis de proposer un mécanisme alternatif de conduction. Celle-ci implique une rotation de l'imidazole protoné, constituant l'étape limitante, avant que chaque PT peut avoir lieu entre les azoles adjacentes. Une étude supplémentaire réalisée sur des modèles avec du acide phosphorique (H_3PO_4) a révélé que faibles concentrations de H_3PO_4 pourrait permettre le mécanisme de Grotthuss malgré la matrice polymérique, donnant ainsi une explication possible de la conductivité plus élevée des systèmes dopée avec de l'acide par rapport à les purs.

Le rôle crucial joué par la matrice polymérique sur la conductivité a été ensuite confirmée par l'étude menée sur un second polymère. En effet, les résultats obtenus à la suite de la même DFT/MD protocole utilisé pour P4VI ont révélé que la position d'attache du imidazole peut fortement affecter le mécanisme de conduction, le transport de charge de type Grotthuss étant favorisée dans le système étudié avec attache en position 2.

En bref, les simulations obtenus montrent comment la matrice polymérique jouent un rôle crucial dans le mécanisme de la conductivité indiquant ainsi que les modèles comprenant la matrice polymère sont nécessaires pour étudier théoriquement ces systèmes, en contraste avec ce qui a été fait jusqu'à présent. Du point de vue plus chimique, la présente recherche représente une première tentative pour une étude plus systématique de la relation entre la connectivité de la matrice polymère et l'efficacité du transport de charge, nécessaire pour concevoir de nouveaux et plus performants matériaux à base d'azole.